LAKE HISTORY IN THE PALEO-OWENS RIVER SYSTEM, CA FOR THE PAST 2.0 MYR BASED ON ^{36}Cl DATING OF EVAPORITES FROM SEARLES LAKE

By

Nancy Olga Jannik

Submitted in Partial Fulfillment of the
Requirements for the Degree of
Doctor of Philosophy

New Mexico Institute of Mining and Technology
Socorro, New Mexico
May, 1989

ABSTRACT

Chlorine-36 is used to date climatically-sensitive saline lake sediments from hydrologically closed basins in southeastern California -- primarily sediments from Searles and Panamint basins. During wet periods of the past 2.0 Ma, lakes that formed in the closed basins fluctuated in size in direct response to the balance between runoff and evaporation. Therefore, evidence of the fluctuations such as elevated shorelines and alternating sedimentological sequences are indicators of past hydrologic conditions. A chronology for the KM-3 core from Searles Lake is compiled, based on ages determined by ^{36}Cl for the evaporites, together with those determined by ^{14}C and U-Th series for younger sediments, and by magnetostratigraphy for older sediments. This chronology, along with other criteria such as correlations between Searles and Panamint basins, the chloride budget and sedimentology, is used to reconstruct the history of lake fluctuations in the paleo-Owens River system. It is inferred that Searles Lake desiccated at most twice during the past 600 ka -- during the interval around 286 ka, and from 10 ka to the present. The lake history curve shows that the Holocene is anomalously arid. Major overflows from Searles to Panamint occurred during the intervals from 1.3 Ma to 1.0 ka, 750 to 600 ka, 500 to 400 ka, and 150 to 120 ka. The oldest overflow is correlated with the Sherwin glaciation and the youngest with the Tahoe glaciation. Comparing the lake-fluctuation chronology to the $\delta^{18}O$ record of marine foraminifera, it is noted that the strongest similarity is in the periodicities of the cycles -- 40 to 50 kyr before the Jaramillo magnetic reversal (730 ka) and 100 kyr after. However, at

Searles Lake, this fluctuation in the lake chronology is modulated by longer-term cycles of aridity and humidity. Thus, although the mid-latitude Quaternary climate record reflects the high-latitude ice volume fluctuations that dominate the marine ^{18}O record, it also contains evidence for climatic forcing of a different type.

ACKNOWLEDGEMENTS

Funds in support of this research were provided by NSF grant EAR 8313745.

The author would like to extend her gratititude to Fred M. Phillips for his guidance, support, editorial expertise, patience and endless discussions. Most of all I appreciated the opportunity to work with Fred on a truly exciting interdisciplinary project. Within the realms of hydrology, glacial geology, isotope geochemistry, physics, statistics and climatology I was allowed to grow as a scientist and remain a Friend of the Pleistocene. Many thanks are extended to G. I. Smith (who will always be fondly remembered as Mr. Searles Lake) for his support, sampling assistance and helpful comments on the manuscript. G. I. willingly shared his work and continued interest and enthusiasm for the study area and the new discoveries coming forth. Special thanks go to David Elmore for sharing accelerator mass spectrometry with hydrogeologists. I appreciated David's support, interest and patience as a fledgling geologist attempted to enter the physicist's world of isotope measurements. I would also like to thank Janet Elmore for her hospitality and friendship as she tried to make Rochester, NY seem warm even on New Year's Eve in The Lab. I gratefully acknowledge the other members of my committee, John Hawley, Andy Campbell, and David Love, who contributed invaluable comments and advice.

The following deserve thanks for providing samples: Ihor Kunasz - Clayton Valley samples, Donald Curry - historical Great Salt Lake samples and Bonneville Basin core samples, Robert Hale - basalt samples, Fraser Goff - Long Valley water samples, and Larry Benson - access to the Walker Lake core. Special thanks to the Kerr-McGee Corporation, particularly Gale Moulton, for access to the KM-3 core and other Searles cores.

To the many who helped with lab and field work, I offer my appreciation. Special gratitude to Nick Conard and Peter Kubik who helped gather ^{36}Cl data, to Melitta Rorty and Julie Mattick for their friendship and invaluable help in the field and lab, and to the boys in Eaton Hall for their support and the James Mason impressions that kept me awake through the night.

There are special people without which this work would not have been completed. Thanks seems so trivial at this time, and my heartfelt gratitude cannot be sufficiently expressed. To my friends on Fifth Street - thanks for those "special thoughts". I would like to thank Barb Ramer for her support and for typing most of the manuscript. I thank Claire Carlson for editing and other helpful suggestions. Special gratitude is offered to Catherine Carlson for drafting, editing, encouragement, and yes, I'll admit, making me aware of some type of "mystery" in all of this.

Endless appreciation is extended to Shirley Schmitz, who unselfishly gave of herself in so many ways. She sat with me through the long nights and provided encouragement when most needed. This work is completed because of her support. Thank you, my friend.

To Mom, what can I say? The continuous supply of encouragement and chicken soup got us through this. Thank you for your faith in me.

To the rest of my family and friends who were so patient and involved in countless other ways - yes, I can come out and play now.

I would like to dedicate this work to my Father. He did not live to see its completion, but he knows that it is done. It is because of him that I will go on seeking. This one is for you Dad. We miss you so very much.

TABLE OF CONTENTS

CONTENTS (continued)

CONTENTS (continued)

LIST OF FIGURES

FIGURES (continued)

LIST OF TABLES

Now I conceive that as all these Lakes do receive Rivers and have no Exits or Discharge, so 'twill be necessary that their Waters rise and cover the Land, until such time as their Surfaces are sufficiently extended, so as to exhale in Vapour that Water that is poured in by the Rivers; and consequently that Lakes must be bigger or lesser according to the Quantity of the Fresh they receive. †

†E. Halley, "On the cause of the saltness of the ocean, and of the several lakes that emit no rivers; with a proposal, by help thereof, to discover the age of the world," Philos. Trans. R. Soc. London, 29, 296-300 (1715).

the discovery continues...

CHAPTER I

INTRODUCTION

DEFINING THE PROBLEM

Up to the present time, the best record of Quaternary climatic history has been found in deep-sea sediment cores, particularly in the ^{18}O content of foraminiferal tests. Time-series analysis of ^{18}O data for the past 700 kyr[1] has indicated a strong 100-kyr periodicity in global ice volume, corresponding to one of the frequencies in the orbital insolation variations predicted by the Milankovitch theory (Hays and others, 1976). This insight has proven to be a key in understanding the nature and origins of Quaternary climatic change.

Deep-sea sediment cores are most informative with regard to climatic phenomena that directly affect the ocean (for example, ice volume, water temperature, carbonate content of ocean water). Ice volume, the above parameter most strongly related to events on land, is predominately a reflection of climatic events at high northern and southern latitudes. Thus, deep-sea sediment cores provide limited understanding of past climatic changes in mid-latitude continental environments.

One reason for the lack of data in this crucial area is that there are very few accumulations of continental sediments that are continuous, climatically informative and capable of being absolutely dated. One mid-latitude continental environment

[1]In this study, kyr and Myr are used for time spans, and ka and Ma are used for ages.

that could potentially provide sediment accumulations with these qualities is closed-basin lakes. Closed-basin lakes, which lack surface outlets, respond very sensitively to fluctuations in climate, most significantly, the amount of precipitation falling on the drainage basin (Smith and Street-Perrott, 1983). The hydrologic responses of most importance are fluctuations in both depth and water surface area, which are evident from abandoned shorelines and sometimes abrupt vertical and lateral facies changes. Changes in mineralogy, chemistry and/or biota, as revealed in the sediment accumulation, also reflect lake fluctuations.

Further information is gained by examining the hydrologic characteristics and changes of a closed-basin lake over time. The water surface area fluctuates in direct response to the balance between runoff and evaporation (Street-Perrott and Harrison, 1985). The association of lake size to inflow and outflow is a fundamental concept referred to as the lake's "water balance". The water balance, although sometimes difficult to relate to more commonly reported climatic parameters such as mean annual temperature or precipitation, is a quantitative hydroclimatic parameter of great practical significance in its own right.

The other main cause of lake fluctuations, besides climate, is a change in basin configuration. Tectonic events (for example, faulting, warping, erosion, landslides or lava flows) could possibly cause a change in configuration. Smith and Street-Perrott (1983) noted that the hydrologic responses in closed basins to these processes do not tend to exhibit fluctuations, but, instead, exhibit gradual changes that are long lasting.

OBJECTIVES AND APPROACH

The mid-latitude continental environment I have chosen to study is the paleo-Owens River closed-basin lake system located in southeast California (Fig. 1). Evidence from some of the basins, such as elevated shorelines and subsurface records of alternating muds and salines, show that the lake system fluctuated dramatically in the past. Lake waters deposited evaporites during arid periods, and carbonates and clastics during humid periods. Thus, the record left behind is climatically very sensitive. Independent dating of the sediments in the various basins would permit correlation between them and thus reconstruction of the lacustrine history. The evaporites are dated by a recently-developed method that uses the radioisotope ^{36}Cl.

Searles Lake is of particular interest; primary focus was on the abundant subsurface evidence from this basin. A 930-m surface-to-bedrock core (core KM-3) reveals one of the longest, nearly-continuous, climatically-sensitive accumulations of Quaternary lacustrine sediments in the United States.

A discussion of the specific objectives and approaches of this study follows.

OBJECTIVE I

To test and refine the use of the radioisotope ^{36}Cl as a geochronometer for continental evaporites.

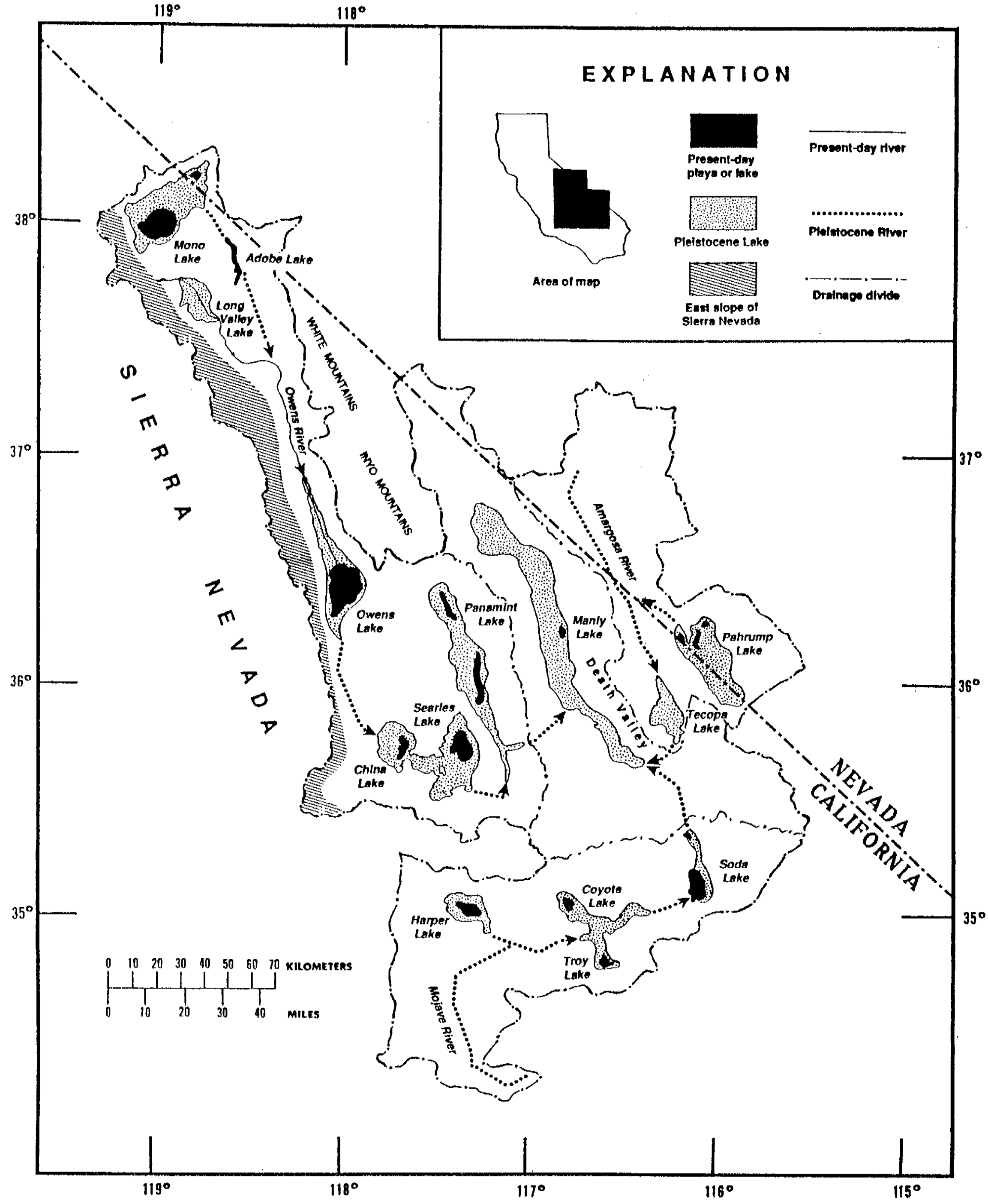

Figure 1. Map showing location of study area and configuration and drainage pattern of the paleo-Owens, -Amargosa and -Mojave River systems. Modified from Smith (1979).

The dating method used for evaporites is based on radioactive decay of ^{36}Cl. This method was previously tested on evaporites from intervals in the KM-3 core (Searles Lake) that were independently dated; the preliminary results were reported by Phillips and others (1983). In this study, the ^{36}Cl method is further tested and refined for use on continental evaporites from beneath the surface of Searles and Panamint Lakes in the paleo-Owens system, and from several other closed basins in southwest U.S.

OBJECTIVE II

To test the use of ^{36}Cl for dating exposure time of glacial erratics.

The radioisotope ^{36}Cl is tested for possible use as a geochronometer for dating exposure time of glacial erratics. In this method, age determination is based on the build-up of ^{36}Cl in the rocks. Erratics were collected from moraines on the east slope of the Sierra Nevada (Sierra Nevada bounds Owens Valley on the west).

OBJECTIVE III

To formulate a detailed chronology of the KM-3 core, Searles Lake, CA. The chronology is based on the new ^{36}Cl ages presented in this study, previously published absolute dates, and interpolated ages determined by using chemical data from the core.

Investigations at Searles Lake have reported ^{14}C dates to about 45 ka (Stuiver and Smith, 1979), U/Th dates to 230 ka (Bischoff and others, 1985) and paleomagnetic reversals beginning at 730 ka and extending to 3.15 Ma (Liddicoat and others, 1980). An altered ash has been tentatively correlated with the Lava Creek B ash (610 ka) based on its stratigraphic position (Hay and Guldman, 1987). However, the radiometric chronology of most of the mid-Pleistocene stratigraphic sequence (230 to 730 ka) has not yet been established. Chlorine-36 dates covering this interval for Searles Lake are presented in this study. Ages are determined by interpolation for intervals between the sediments dated by radiometric and magnetostratigraphic methods. The interpolation procedure is based on the data pertaining to the accumulation of the acid-insoluble residue available for the KM-3 core. The absolute and interpolated ages are used to construct a chronology for the past 2.0 Myr.

OBJECTIVE IV

To reconstruct the history of lake-level fluctuations of the ancestral Owens River system for the past 2.0 Myr. The lake-level chronology along with other criteria is used to determine the response of the paleo-Owens hydrologic system to climatic fluctuations. The lake-level and climatic response records will provide the basis for a climatic and hydrologic history for this part of the southwestern United States during the entire Quaternary Period.

In order to determine the lake-level history for the paleo-Owens system, many criteria are considered: (1) the $^{36}Cl/Cl$ ratios of modern waters and surficial evaporites are measured so the possible spatial distribution and evolution of ^{36}Cl and stable chloride in the paleo-Owens system can be determined, (2) the chemical, mineralogical and stratigraphical data available for the cores from Searles Lake are examined for evidence of changing lake environment, (3) the geochemical data from KM-3 core in Searles Lake are used to construct cumulative plots of solutes through time; again, to reveal intervals when lake environment changed, (4) the chloride budget for Searles Lake, which is determined from the chloride cumulative plot, is calculated so intervals of evaporite deposition and possible overflows can be determined, (5) the stratigraphy of the cores taken from the other closed basins in the ancestral Owens system are examined to aid in the reconstruction of the lake fluctuation curve, and, (6) the dated sediments from Searles Lake are correlated with the dated sediments from Panamint Lake (hydrologically connected in past) presented in this study, in order to infer the timing and extent of overflows. Evaporite minerals suitable for ^{36}Cl dating are lacking from Owens and China Lakes.

OBJECTIVE V

To compare the hydrologic responses to climatic change as inferred in the history of lake-level fluctuations of the paleo-Owens system with the Sierra Nevada glacial chronology and the marine ^{18}O record.

The lake-level chronology is compared with other chronologies that record responses to climatic change. First, the chronology is compared to glacial deposits from the east slope of the Sierra Nevada in order to correlate Sierra Nevada glacial events with lake size. Runoff from the east side of the Sierra Nevada is the major component of surface flow in the Owens River system. The amount of runoff varied from glacial to interglacial times. It is this fluctuation that is recorded in the lake-level curve. Next, the lake-level chronology is compared to the marine ^{18}O record in order to reveal possible correlations with high-latitude ice volumes or temperature changes.

PREVIOUS WORK

Closed-Basin Lakes

Water Balance. Street-Perrott and Harrison (1985) summarized the factors that affect the sensitivity of lakes to climatic fluctuations. They suggested that one of the important factors is the existence of an outlet. They further indicated that for closed-basin lakes, which lack an outlet, the equilibrium water surface area of closed lakes under natural conditions (assuming negligible ground-water transfers) is strictly dependent on the relationship of precipitation and evapotranspiration over its entire watershed. Any changes in this relationship (water balance) result in a change in lake depth, which directly influences lake area, thus, closed-basin lakes are sensitive to changes in climate.

An attempt has been made to classify the response of lakes to changes in climate according to their hydrological characteristics by Szestay (1974), Street (1980), and Street-Perrott and Harrison (1985). Of most interest here are amplifier lakes. Amplifier lakes are those in which precipitation directly on the lake surface is a negligible contribution to the lake water budget. Runoff from the drainage basin is the largest portion (>70%) of input into the lake. Amplifier lakes in closed basins exhibit large fluctuations in lake level; they also are the most sensitive group of lakes with respect to climatic variations. Thus, closed amplifier lakes have provided the most detailed records of lake-level fluctuations (Street-Perrott and Harrison, 1985). Street-Perrott and Harrison (1985) showed that for amplifier lakes there exists a simple relationship between basin runoff, lake evaporation, and lake area:

$$RA_B = EA_L \qquad (1)$$

where R is the annual volume of runoff per unit area of the watershed ($L^3L^{-2}T^{-1}$; L is length, and T is time), E is the annual volume of evaporation per unit area of the lake surface ($L^3L^{-2}T^{-1}$), and A_B and A_L are the areas (L^2) of the basin (watershed) and lake, respectively. Equation 1 may be rearranged as follows:

$$\frac{A_L}{A_B} = \frac{R}{E} = Z \qquad (2)$$

The "Z" factor is a means of quantifying the hydrologic balance of a basin (Snyder and Langbein, 1962), and is thus a fundamental hydrologic and paleohydrologic parameter. Mifflin and Wheat (1979) demonstrated the utility of the Z factor as a hydrologic index in the Great Basin.

Correlation to Glacial Events. During the Pleistocene, many of the closed basins of the western U.S. contained what are termed "pluvial" lakes (literally, pluvial means increased rainfall). It has long been believed that the pluvial lakes fluctuated in size according to glacial conditions (see Smith and Street-Perrott, 1983, for a summary of studies of pluvial lakes in the western U.S.). Several recent studies dealing with Pleistocene glaciation in the Great Basin have suggested that high lake stages correspond to glacial maxima (Atwater and others, 1986; Smith, 1984). A historic survey (1940 to 1960) of the fluctuation history of closed-basin lakes from the western U.S. and Canada showed the simultaneous growth of glaciers and lakes (Lawrence and Lawrence, 1961).

High lake levels correspond to a glacial environment referred to as a glacial stage, or a period of glacial growth (volume) or advance (position). Likewise, the climatic conditions which correspond to periods of high lake levels, are referred to as pluvial conditions, pluvial climate, or wet periods. Many investigators simply use the phrase "pluvial lakes form during pluvial times". Smith and Street-Perrott (1983) cautioned that this use should not imply that increased rainfall is the climatic parameter that changed the most or is the most important. Pluvial is commonly "understood" to mean increased moisture storage (Mifflin and Wheat, 1979) or runoff (Street-Perrott and Harrison, 1985) in the basin.

Paleo-Owens River System

Descriptive History. The interconnection of the lakes of the paleo-Owens River system was first proposed by Bailey (1902). Hamman (1912), Free (1914) and Gale (1914) suggested that salines in Searles Lake were derived from desiccation of runoff from Owens Lake overflow. Gale's discussion was the most insightful and thorough. He based his interpretations on faults scarps, lake terraces, spillway elevations, channel erosion features and shallow cores. He described a former chain of large lakes that once occupied the closed basins of southeastern California. Not only did Gale (1914) determine the flow path of these ancient waters -- from Owens River to Death Valley -- but he also suggested that this chain of lakes may have formed more than once in the past.

Subsequent investigations of the paleo-Owens system primarily focused on the mineralogy and stratigraphy as revealed by core samples from beneath the surface of the basins (Smith and Pratt, 1957; Flint and Gale, 1958; Haines, 1959; Smith, 1962). Alternating salt and mud units were apparent in the basins' cores, supporting Gales's (1914) suggestion that the chain of lakes may have overflowed repeatedly in the past. Droste (1961) concluded from his study of the clay mineral composition of the basin sediments in Owens, China, Searles, and Panamint Lakes that Owens Basin sediment had spilled over into Indian Wells Valley, and that China Basin sediment had overflowed into Searles Valley. However, according to Droste (1961), the clay data did not indicate that sediment from Searles Basin had been transported into Panamint Valley.

Other studies have suggested times when overflows possibly occurred. One of the earliest, by Blackwelder (1931, 1954), presented evidence for overflow of Searles Lake into Panamint Valley only during Tahoe time. However, Smith (1968) subsequently suggested that exposed lake deposits at the level of the spillway indicate that the lake also overflowed during Tioga time. Recent investigations have focused on interrelating core data, surface deposits and landforms, and lake level histories in Searles and Panamint Valleys. Panamint Basin was investigated by Smith, R.S.U. (1976). Smith and others (1983) have recently expanded and refined a curve of fluctuations in Searles Lake for the past 150 kyr (Smith, 1968, 1979) to cover the past 3.2 Myr.

Glacial Deposits. It was recognized almost 125 years ago that the Sierra Nevada were modified by glacial action (Whitney, 1865). Knopf (1918) was the first to describe the moraines in Owens Valley, separating them into old and young moraines. Early studies on the glaciation of the east slope of the Sierra Nevada were performed by Russell (1889) and Matthes (1924, 1929). Blackwelder (1931) was the first to thoroughly describe the evidence of extensive Pleistocene glaciation in the eastern Sierra Nevada. An early controversy among geologists was whether the topography was sculpted mainly by ice action or by fluvial processes. Blackwelder (1931) stated that the latter view had prevailed. Later studies that concentrated on the deposits and erosional features located on the east slope of the Sierra Nevada included those by Putnam (1950), Sharp and Birman (1963), Birman (1964), Wahrhaftig and Birman (1965), Bateman and Wahrhaftig (1966), Lajoie (1968), and Sharp (1969). Correlation and dating of glacial events and paleoclimatic reconstruction have been the focus of more recent studies (Dalrymple, 1964; Curry, 1966, 1968, 1969, 1971; Smith, 1968; Birkeland and Janda, 1971; Burke and Birkeland, 1979; Dalrymple and others, 1982; Smith and Street-Perrott, 1983; Gillespie and others, 1984).

Lake Histories and Paleoclimatic Reconstruction. A study by Broecker and Walton (1959) was one of the first attempts to determine the history and age of four Great Basin lakes by examining the accumulation of salt. One of their important assumptions was that the input of meteoric chloride to a lake was constant. However, Broecker and Walton (1959) assumed incorrectly that sources of chloride other than meteoric were negligible. The constancy of chloride input to a closed-basin lake has been borne out and is supported by Smith (1976, 1979) and this study. Feth (1959), Smith (1976), Friedman and others (1982), and Phillips and others (1983) have shown the importance of chloride input from surface weathering and solution of rocks at depth.

In recent years, attempts have been made to reconstruct lake histories and climatic conditions in the paleo-Owens River system. Most of these studies have concentrated on Searles Lake with extensions to Owens, China, and Panamint Lakes (Smith, 1976, 1979; Smith and others, 1983; Smith and Street-Perrott, 1983; Street-Perrott and Harrison, 1985; Horita and Matsuo, unpublished).

Searles Lake

Mineralogy and Stratigraphy. In 1873, borax was discovered in the playa deposits at Searles Lake. Since then, industry has exploited a variety of evaporite minerals (see Smith, 1979, for a detailed discussion of the historic development of the mineral and chemical resources).

Hanks (1889) published the first description of the surficial deposits of Searles Lake. Subsequent geologic investigations of the subsurface sediments have been intimately tied to the commercial development of the saline layers. The stratigraphy of subsurface deposits noted by Gale (1914) were based on numerous shallow core holes (<25 m). For the next 40 years, continued core drilling, mostly by chemical companies, revealed deeper lacustrine mud and saline layers and new minerals. In the early 1950's, the U.S. Geological Survey sponsored an investigation of saline deposits in the Mojave Desert and adjacent areas. Searles Lake was included in the study, and one hole reached a depth of 267 m. The mineralogy and stratigraphy of Searles Lake's alternating salts and muds have been described from these numerous cores (Smith and Pratt, 1957; Haines, 1957, 1959; Smith, 1962, 1964, 1968, 1979; Smith and Haines, 1964). In 1968, a surface-to-bedrock core (930 m) was drilled by the Kerr-McGee Chemical Corp. The U.S. Geological Survey was granted permission in 1976 to study the company's core description and accompanying detailed analyses (Smith and others, 1983), and make further studies.

Dating. Numerous methods have been utilized to date the sediments from Searles Lake. Carbon-14 dating was the first to be used (Flint and Gale, 1958; Rubin and Berthold, 1961; Ives and others, 1964; Stuiver, 1964; Smith, 1968; Stuiver and Smith, 1979). Uranium-series dating (Peng and others, 1978; Bischoff and others, 1985), and paleomagnetism (Liddicoat and others, 1980) have also been used. Most recently, ^{36}Cl dating has been attempted (Phillips and others, 1983).

CHAPTER II

STUDY AREA

GEOLOGIC, GEOMORPHIC, AND HYDROLOGIC ENVIRONMENT

The study area is located in Inyo, southern Mono, northeastern Kern, and northwestern San Bernardino Counties, east-central California (Fig. 1). The area is bounded on the west by the Sierra Nevada, on the east by Death Valley and on the south by Garlock Fault. It includes four valleys, Owens, Indian Wells, Searles, and Panamint, separated by numerous mountain ranges within the Great Basin section of the Basin and Range province of the western United States (Fig. 2). Each valley represents a hydrologically closed basin into which surface waters drain.

Owens Valley is bounded on the west by the Sierra Nevada (Fig. 3), on the east by the White and Inyo Mountains, and to the south by the Coso Range. The valley is a graben that formed during late Cenozoic time, concurrent with the uplift of the Sierra Nevada and White Mountains. In addition to the faults and warps along the valley's boundaries, faults and warps can be found within the valley block. Quaternary volcanics associated with the graben development include tuff, pumice, rhyolite, basalt flows and cinder cones. There are also Quaternary silts, sands, and gravels.

The Sierra Nevada mountain range is dominated by the Sierra Nevada batholith in the central and eastern part of the range. In the area adjacent to Owens Valley, the batholith is composed primarily of felsic quartz-bearing granitic rocks

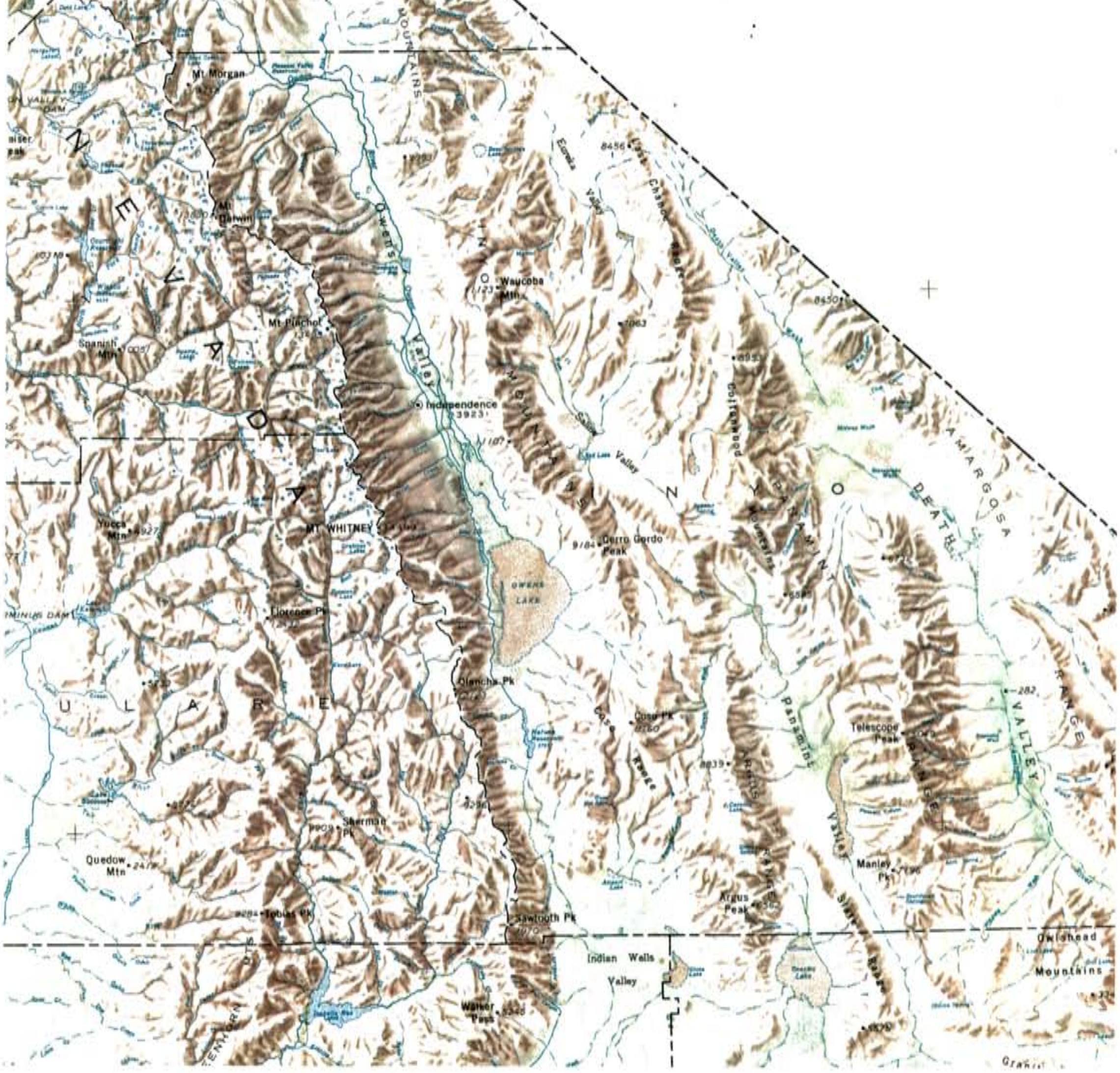

Figure 2. Map showing characteristic valley and range structure in the study area. The valleys contain hydrologically closed basins.

Figure 3. Aerial photo of the east slope of the Sierra Nevada which bounds Owens Valley on the west. View is to the northwest. Photo from John Shelton collection.

(Bateman, 1965). The White Mountains parallel the Sierra Nevada on the east side of Owens Valley. They are composed of strongly folded and faulted sedimentary rocks of late Precambrian and early Cambrian age (Strand, 1967). The Inyo Mountains follow the trend of the White Mountains southward. They are composed of highly folded and faulted sedimentary and metasedimentary rocks of Paleozoic and Mesozoic age and granitic rocks of Mesozoic age (Strand, 1967; Matthews and Burnett, 1965; Jennings, 1958). The Coso Range at the southern extent of the Owens Valley is composed of Mesozoic granitic rocks and Pleistocene volcanics (Jennings and others, 1962).

Owens River is a perennial stream that flows southward through Owens Valley and terminates in Owens Lake. The river derives most of its waters from the Sierra Nevada (because the White and Inyo Mountains are in the Sierra Nevada rainshadow) and is the principal source of water to Owens Lake. For the past 75 years, most of the flow from the Owens River has been diverted from Owens Lake to the Los Angeles Aqueduct.

Indian Wells Valley lies south of Owens Valley and is separated from it by the Coso Range. The Sierra Nevada bounds the valley to the west. The Argus Range bounds it to the east, and the El Paso Mountains to the south. The Argus Range is comprised primarily of Mesozoic granitic rocks adjacent to Indian Wells Valley (Jennings and others, 1962). The El Paso Mountains consist of Paleozoic and Cenozoic sedimentary rocks and Mesozoic granitic rocks (Jennings and others, 1962). A few ephemeral stream channels are found in the valley. The surface water sink is China Lake.

Searles Basin is separated from Indian Wells Valley, to its west, by the Argus Range and the Spangler Hills. The basin is bounded on the north and east by the Slate Range which is comprised of Cenozoic volcanics, Mesozoic granite and metavolcanics, Paleozoic limestone, and Precambrian metamorphic rocks (Jennings and others, 1962). The basin is bounded on the south by the Lava Mountains and other low hills that are comprised of late Tertiary sandstone, pyroclastic rocks, and andesite (Smith, 1968). A few ephemeral stream channels drain toward Searles Lake.

Panamint Valley lies northeast of Searles Basin. It is bounded on the west by the Argus and Slate Ranges and on the east by Panamint Range. Pre-Cenozoic sedimentary, metasedimentary and granitic rocks and Cenozoic sedimentary and volcanic rocks are represented in the Panamint Range (Jennings, 1958; Jennings and others, 1962). East of Panamint Range lies Death Valley. A few ephemeral stream channels are found in the Panamint Valley.

Indian Wells, Searles, Panamint, and Death Valleys are closed tectonic depressions which probably began forming in late Cenozoic time (Smith and others, 1968). All four valleys contain Late Quaternary fluvial, aeolian, playa and lacustrine deposits.

During wet periods of the past 3.0 Myr, these five closed basins were hydrologically connected due to the interaction of climatic, hydrologic and geomorphic conditions. A chain of lakes formed, linked by rivers carrying overflow from one basin to the next. The order of overflow was as follows: Owens Lake, China Lake, Searles Lake, Panamint Lake, Death Valley (Fig. 1). Figure 4 is a

Figure 4. Lake size, drainage order and core logs from each of the basins in the paleo-Owens system. (A) Diagrammatic cross section of the five lakes in the paleo-Owens River system. Letters correspond to sill elevations as shown in C. (B) Generalized cores from each of the closed basins. Unit A+B in the KM-3 core is reconstructed from a nearby core (289M). Abbreviations of units in the KM-3 core: OM - Overburden Mud, US - Upper Salt, PM - Parting Mud, LS - Lower Salt, BM - Bottom Mud. Units A+B, C, D+E, F and G are from the MIxed Layer. (C) Plot of lake area versus the Z factor or ratio of lake area to basin area. Cumulative elevation refers to the cumulative depth as runoff filled each successive basin. Capital letters mark locations of sill to a corresponding lake area when overflow to the next basin began. Sill elevations in parenthesis.

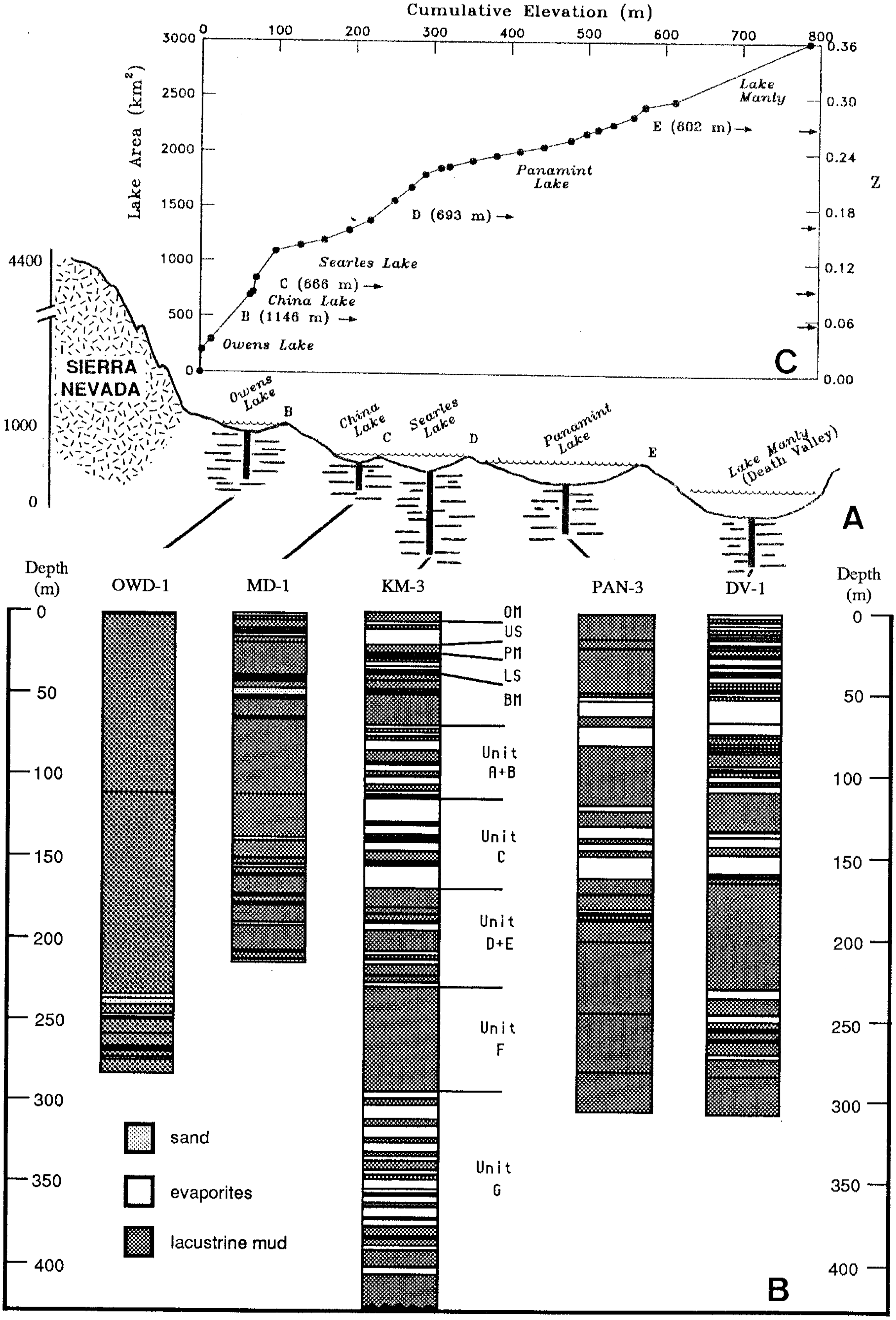
Cumulative Elevation (m)
Lake Area (km²)
Z
Owens Lake
B (1146 m)
China Lake
C (666 m)
Searles Lake
D (693 m)
Panamint Lake
E (602 m)
Lake Manly
C
SIERRA NEVADA
Owens Lake
China Lake
Searles Lake
Panamint Lake
Lake Manly (Death Valley)
A
Depth (m)
OWD-1
MD-1
KM-3
PAN-3
DV-1
OM
US
PM
LS
BM
Unit A+B
Unit C
Unit D+E
Unit F
Unit G
sand
evaporites
lacustrine mud
B

diagrammatic cross section of the five lakes that comprised this system. Each basin sequentially served as the terminus of the drainage system until it overflowed into the next basin. Extent of overflow during each wet period depended on the volume of runoff. As each successive basin overflowed and the depth of water in the terminal basin increased, the total lake area of the paleo-Owens River system also increased. During the most extreme wet periods, Lake Manly in Death Valley served as the common ultimate sink for the paleo-Owens, Amargosa, and Mojave Rivers (Fig. 1).

The present-day Owens River drains an area of about 8,500 km^2, yet most of the runoff is derived from about 16 percent of the catchment area that lies on the eastern slope of the Sierra Nevada (Fig. 1; Lee, 1912). The impressive Sierra Nevada massif creates such a strong rainshadow effect (Fig. 3) that even during the most extreme wet periods of the past, when individual drainage basins coalesced into one system, most of the runoff apparently still originated in a small, high-altitude portion of the combined drainage area.

The presence of hot, or thermal, springs (greater than 15°C) in Owens Valley is due to Late Cenozoic volcanism for which major activity was initiated 3.2 Ma (Sorey and others, 1978). About 0.7 Ma the extrusion of rhyolitic ash flows resulted in the formation of the Long Valley caldera located in southern Mono County, California (Fig. 5). The hot springs that are found within the caldera probably contributed most of the uncommon components found in Searles Lake (Smith, 1979). Discharge from the hot springs is less than 10% of the total Owens River streamflow (Smith, 1976; Sorey and others, 1978).

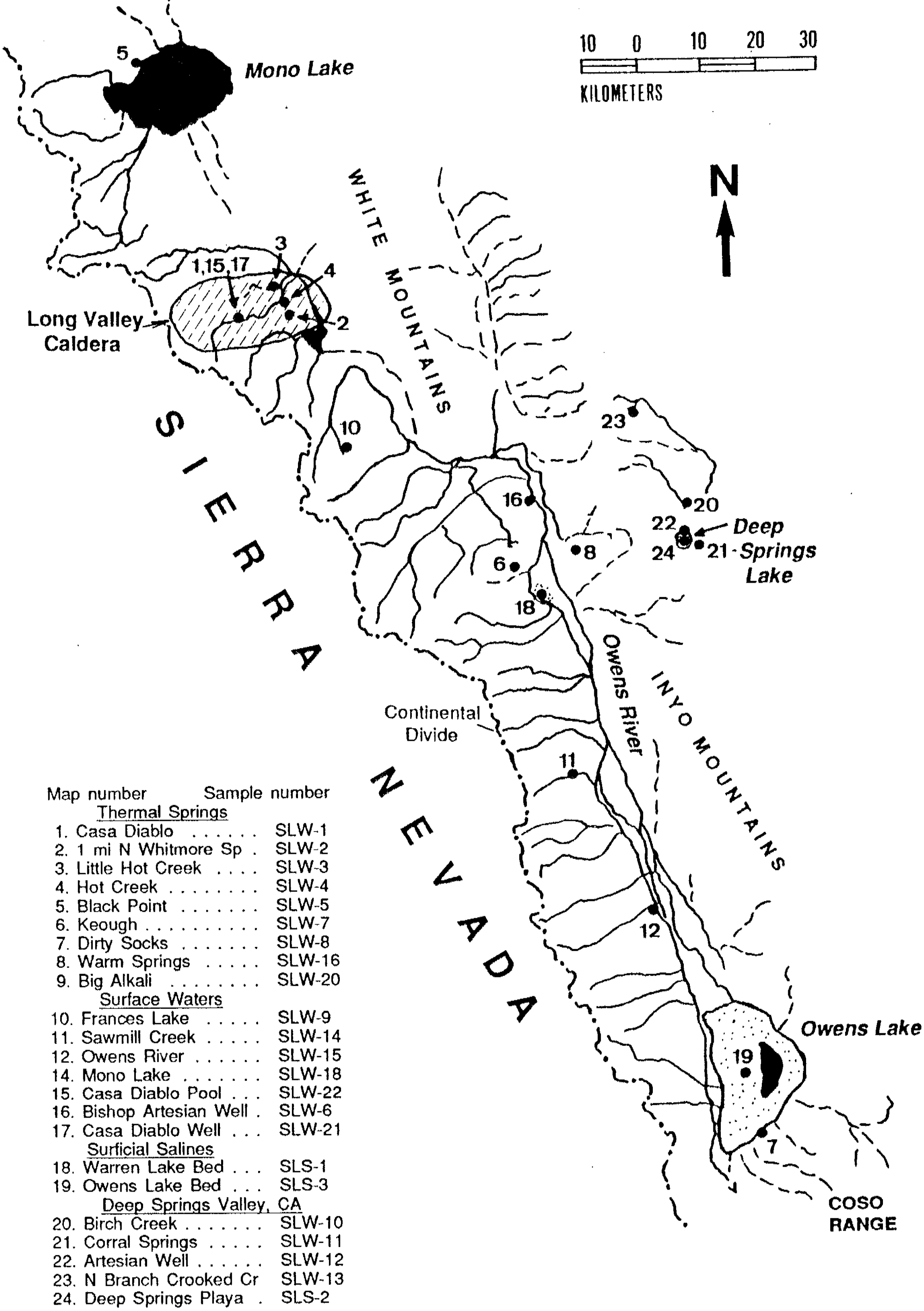

Figure 5. Sample location map for waters and surficial salines.

A two-component ground-water system has been formed in response to the geothermal environment (Sorey and others, 1978). The shallow subsystem is characterized by relatively short direct flow paths from areas of recharge to areas of discharge, water temperatures not much higher than ambient land-surface temperatures, and waters with relatively low dissolved solid concentrations. The deep subsystem is characterized by relatively long and circuitous flow paths, water temperatures higher than ambient land-surface temperatures, and waters with relatively high concentrations of dissolved solids -- of special interest here, alkali chlorides. The two subsystems are not sharply defined everywhere. Thus, thermal spring waters are a mixture of hot and cold components.

The chloride content of the thermal springs that are located within the caldera ranges from 150 to 280 mg/L (Sorey and others, 1978). The chloride content of the nonthermal springs is less than 10 mg/L. Smith (1979) indicated a chloride content of 14 mg/L for the Owens River downstream from the Long Valley caldera.

STRATIGRAPHIC RECORD

Subsurface sediments supply evidence that is invaluable in reconstructing the chemical and physical history of a lake in a closed basin. What follows is a brief description of the general nature of the sediments that underlie the floors of each of the successive basins in the paleo-Owens River system. Figure 4B shows a generalized stratigraphic column of the sediments underlying each basin.

A 280 m-core (described by Smith and Pratt, 1957) from beneath the surface of Owens Lake reveals sediments that are predominantly massive or laminated clay with interbedded silts. Evaporites are absent, except in the top meter where they are a result of the 20th century desiccation that resulted from diversion of the Owens River. Most of the clays are yellowish gray to olive-green gray in color and contain sparse to abundant diatoms and ostracodes. Coarser layers of fine- to medium-silty sand are found near the bottom of the core.

China Lake was a broad, shallow (<12 m), infrequently saline lake during wet periods. Subsurface sediments consist of silt- to sand-sized clastic sediments with some clay layers. Smith and Pratt (1957) noted the presence of diatoms, ostracodes and mollusks. Authigenic gaylussite (Na- Ca-carbonate) is found in the upper portion of the core, as is calcite. Both of these are found as crystals or disseminated in the clastic sediments. There are no layers of salines.

The lithologic log (described by Smith and Pratt, 1957) from a 300-m core recovered from near the center of the basin in Panamint Lake shows a sequence of clastic sediments ranging from clay to silt or sand, with two large interbedded zones of massive pure halite. Minor amounts of carbonates and gypsum are also present. A few ostracodes and several horizons rich in foraminifera were found in this core. Ostracodes and diatoms were present in a core from the northern basin, which contained no halite beds. A 300 m core drilled near the center of Death Valley, the ultimate sink of the paleo-Owens River system, revealed alternating thin beds of muds and salines (Hunt and Mabey, 1966).

SEARLES LAKE

A more detailed description of Searles Valley is warranted because most of the data used in this study are from the sediments revealed in Searles Lake cores. The preponderance of data gathered for the purpose of mineral exploration affords a detailed reconstruction of the subsurface stratigraphy. Searles Lake was the usual terminus of the paleo-Owens River system for the past 2.0 Myr and was thus the site of precipitation and accumulation of numerous minerals of commercial value.

The Searles Lake playa, located in Searles Valley, is dry most of the year (Fig. 6); however, several centimeters of water often stand for weeks or months during wet winters. The playa covers approximately 100 km^2 -- two-thirds of the area being mud and one-third hard salt (Smith, 1979). The surface of Searles Lake is barren and the surrounding area supports only sparse vegetation. Outward from the lake bed margin, the mud grades into the coarser alluvial deposits found on the adjacent slopes. Lacustrine sediments that indicate a near-shore depositional environment are exposed on the surrounding slopes. Well-preserved shorelines, beaches and bars are visible in prominent, but incomplete, step-like terraces (Fig. 7).

Stratigraphy

Most of the information derived from the core data that were used to reconstruct the lake fluctuation curve for the paleo-Owens River system is from Searles Lake (especially core KM-3). The discussion that follows is based mostly

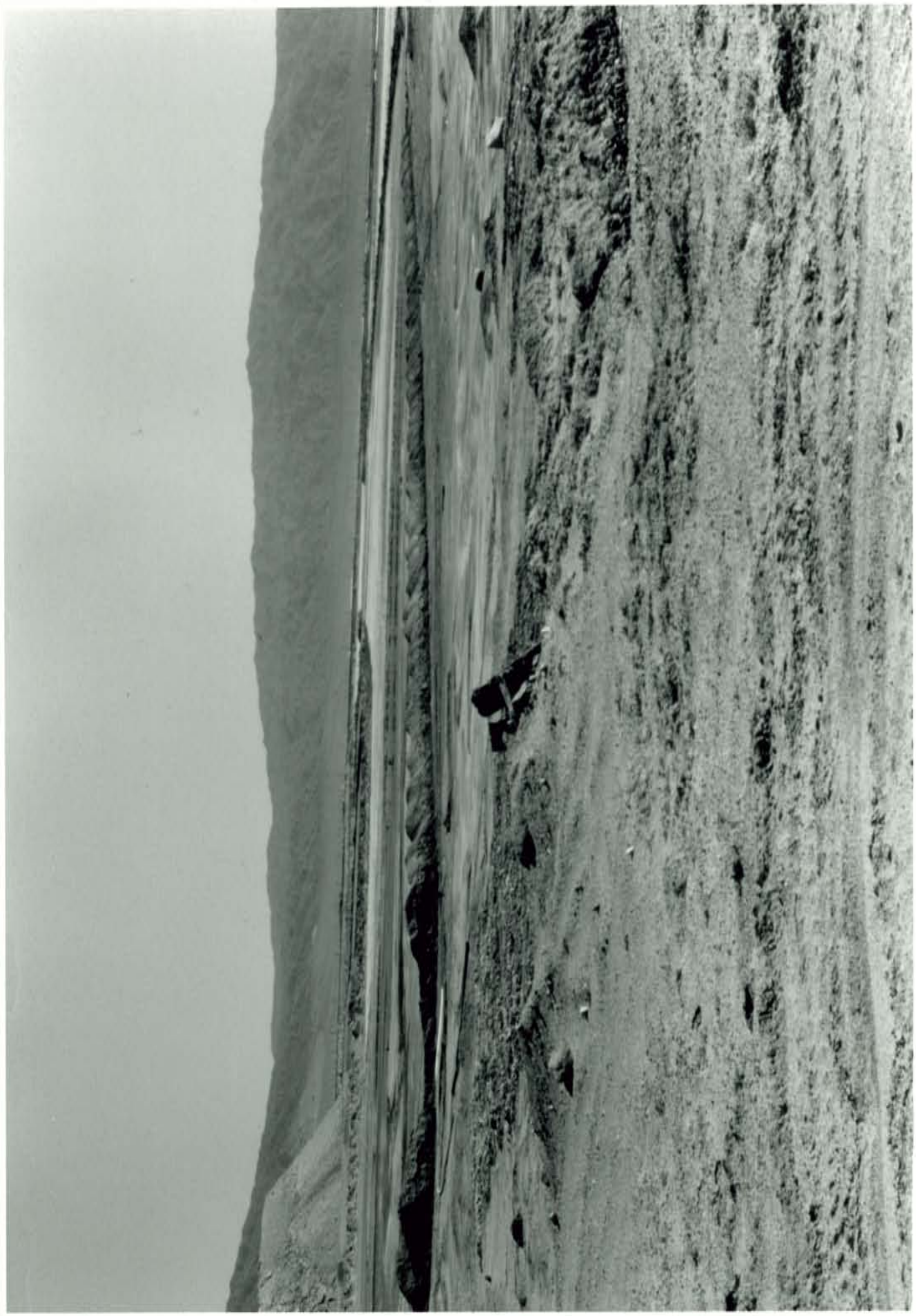

Figure 6. Searles lake playa. Brine evaporation ponds in center of photo. View to the southeast.

Figure 7. Aerial view of shorelines on the east side of Searles Valley about 7 miles east of Trona, CA, on the west flank of the Argus Range. View is to the east. These prominent shorelines which were engraved during high lake levels in Searles Valley are 150 to 200 meters above the valley floor. Photo from John Shelton collection.

on published data by Smith (1979) and Smith and others (1983). The first work was an extensive study on the stratigraphy and geochemistry of Searles Lake evaporites; the latter, a more specific detailed presentation of the stratigraphy, mineralogy and chemistry of the KM-3 core.

A generalized log of the KM-3 core from Smith and others (1983) is presented in Table 1. The KM-3 core is shown graphically in Figure 4B. The unit names used in the log are informal names first used by chemical company geologists. Continual use of the informal names by company geologists and the scientific community has perpetuated their use as sedimentary unit names. The unit names are used in this study.

The stratigraphy, as revealed in the cores from Searles Lake, consists of alternating marls and salines. The marls, traditionally termed "muds" (Smith, 1979), consist predominantly of alkaline earth carbonates (aragonite, calcite, and dolomite) with minor to major volumes of diagenetic minerals. The saline layers contain a variety of evaporite minerals ranging from thick beds of massive pure halite to thin layers of nahcolite, thenardite, hanksite, northupite, burkeite, and borax. Some of these minerals, along with authigenic minerals such as gaylussite, pirssonite, searlesite, and phillipsite, can also be found disseminated throughout some of the mud units.

Table 1. Generalized description of the KM-3 core, Searles Lake, CA (from Smith and others, 1983).

Depth to base of unit (m)	Thickness of unit (m)	Description
5.8	5.8	Not cored. Overburden Mud is included in this zone.
19.9	14.1	*Upper Salt.*—Salines, mostly trona and halite; abundant hanksite near top, borax at base; light- to medium-gray (N6-8) and yellowish-gray (5Y8/1), with some thin interbeds of olive-gray (5Y4/1) mud; mostly indistinctly bedded to massive, locally vuggy.
25.0	5.1	*Parting Mud.*—Megascopic crystals of gaylussite and pirssonite in soft mud composed of microscopic crystals of dolomite, halite, aragonite, other evaporite minerals, and clastic silicates; light- to moderate-olive-gray (5Y3-5/1-4); upper part finely laminated, lower part massive.
37.9	12.9	*Lower Salt.*—Seven saline layers interbedded with six mud layers; salines are mostly halite and trona in upper two layers, trona, halite, and burkeite in underlying two layers, and trona in lower three layers; interbedded mud layers contain megascopic crystals of gaylussite and pirssonite; salines range in color from white through dark gray to yellowish orange (N5-8, 10YR6/6), mud from dark olive gray to brown (5Y4-6/1-4); salts poorly bedded to massive; some mud layers have thin laminar bedding.
69.0	31.1	*Bottom Mud.*—Mud containing megascopic gaylussite crystals; mud is composed of microscopic crystals of dolomite, aragonite, calcite, and other carbonate minerals, and about 30 percent acid-insoluble silicates and organic residues; thin-bedded to massive, with some laminar bedding; medium- to dark-brown, brownish-gray, and olive (5YR4/4 to 5Y3-4/1-2). Discontinuous saline layers at 41.4 m (0.5 m thick), 48.5 m (0.4 m thick), and 54.4 m (0.8 m thick).
90.8	21.8	Interval of poor core recovery; recovered core (3.4 m) is composed of mud containing megascopic gaylussite crystals, massive, medium- to dark-brown and olive (5YR5/2 to 5Y3/2). Top of interval probably represents top of Mixed Layer. This and following three units probably represent Units A and B of Mixed Layer, of which most of the saline layers were lost during drilling (see text).
95.4	4.6	Salines, mostly trona, containing mud; faintly bedded to massive; moderate-brown to olive (5YR4/4 to 5Y5/1).
99.8	4.4	Mud, mostly acid-insoluble material, some dolomite; light-olive-gray (5Y5-6/1-2), thin-bedded.
114.0	14.2	Salines, mostly trona, with small amounts of other minerals and extensive mud impurities; light- to dark-green and brown (5GY5/1, 5Y4-6/1, 5YR3/4); faint bedding in lighter colored salines, with interbeds of mud common near base. Contact between Units B and C of Mixed Layer is at base of this interval.
124.0	10.0	Salines, with some interbedded mud; saline minerals are mostly halite, with smaller amounts of trona and other evaporite minerals; indistinct bedding, beds mostly 1 to 2 cm thick; salines light- to dark-olive-gray (5Y4-7/1-2) and moderate-brown (10YR4-6/2-4).
130.4	6.4	Salines and some mud; salines are about two-thirds halite and one-third trona, with some thenardite; yellowish-gray (5Y5-7/2); upper part of unit contains largest percentage of mud impurities.
135.6	5.2	Salines, mostly halite, with minor trona and thenardite; dark- to medium-gray (N3-5); upper part of unit contains mud impurities.
151.2	15.6	Interbedded mud and salines; salines are mostly halite, with some trona; salines olive-gray (5Y4/1 to 5Y6/1), mud brownish-black (5YR2/1); saline layers, 0.3 to 0.6 m thick, constitute about one-third of zone.
166.4	15.2	Salines, mostly halite, with smaller amounts of trona and thenardite, nearly pure in lower part; mostly gray to yellowish-gray (N4-7 to 5Y4-6/1); bedding 1 to 2 cm thick, some zones porous but most nonporous. Contact between Units C and D+E of Mixed Layer is at base of this interval.
178.6	12.2	Mud containing megascopic crystals of gaylussite and pirssonite, microscopic crystals of

Depth to base of unit (m)	Thickness of unit (m)	Description
		dolomite, halite, and probably other acid-soluble minerals; brownish-black (5YR2/1) in upper and lower part, moderate-brown (5YR3/4) in middle.
186.5	7.9	Mud, with interbedded salts at 179 and 184 m; salts, in beds 0.1 and 0.6 m thick, are mostly halite and trona, with some thenardite and northupite; mud is composed largely of microscopic crystals of dolomite and other carbonates; olive to brownish-black (5Y2/1 to 5YR2/1).
192.0	5.5	Salines interbedded with mud containing scattered saline crystals; salines are mostly halite, with subordinate trona, thenardite, and other minerals; salines olive-gray and medium- to dark-gray (5Y6/1 to N4-6), mud dark-olive-black (5Y1-2/1).
196.1	4.1	Mud, dark-olive-black (5Y1-2/1).
196.6	0.5	Salines, mostly halite; olive-gray (5Y4/1).
204.5	7.9	Mostly mud, with some disseminated saline crystals; brown (5YR3/4) in upper part, olive-gray (5Y4/1) in lower.
207.4	2.9	Salines, with interbedded mud; salines are mostly halite, distinctly bedded, averaging 1 cm in thickness; salines yellowish-gray (5Y7/2), mud olive-gray (5Y4/1).
210.9	3.5	Mud, moderate-brown (5YR4/4) in upper half, olive-black (5Y2/1) in lower part.
213.6	2.7	Salines, mostly halite, with mud impurities; olive-black (5Y2/1) to light-olive-gray (5Y6/1); upper part faintly bedded, lower part massive to mottled.
218.4	4.7	Mud, massive, olive-black (5Y3/1).
218.5	0.1	Salines, trona and halite.
227.4	8.9	Mud, massive, olive-black (5Y2/1).
227.7	0.3	Salines, trona and halite. Contact between Units D+E and F of Mixed Layer is at base of this interval.
248.1	20.4	Mud, mostly grayish-olive (5GY4/1), with a grayish-brown (5YR3/2) zone at 236-238 m and a greenish-gray (5GY6/2) zone at 244-245 m.
249.5	1.4	Mud, dark-greenish-gray (5GY4/1), mottled to faintly bedded; lower half extremely hard (limestone).
271.4	21.9	Mud, with irregular concentrations of a few mottled areas caused by light-colored dolomite or salts; mostly pale- to grayish-green (10G4-6/2), upper 3 m grayish-olive-green (5GY3/2); massive except near 260 and 268 m, where thin to laminar bedding is defined by pale-orange (10YR6-8/2-4) layers (dolomite?).
276.9	5.5	Mud, similar to interval above but containing searlesite.
291.1	14.2	Mud, similar to that at 249.5 m. Contact between Units F and G (new) of Mixed Layer is at base of this interval.
294.4	3.3	Impure salines with mud impurities similar to interval above; salines, mostly halite and thenardite, are mottled aggregates surrounded by mud.
299.3	4.9	Mud, dusky-yellow-green (5GY5/2); upper part mottled, lower part has buff laminae and thin beds.
306.3	7.0	Salines and some mud; salines are chiefly halite and thenardite, white to light-gray (N5-8); mud pale-green (10G6/2); upper part faintly bedded, lower part mottled.
324.3	18.0	Two saltbeds separated by mudbeds (see pl. 1); salts, largely halite, massive, light-greenish-gray (5GY6-8/1); muds massive, greenish-gray (5G6/1).
333.1	8.8	Three mud and two impure salt layers (pl. 1); mud pale-green (10G6/2), massive, with dispersed salts; saline layers, consisting of mottled zones of lighter colored secondary crystals oriented randomly in mud matrix, are halite, with some thenardite, glauberite, and anhydrite.
334.7	1.6	Impure salts, halite; dark-greenish-gray (5GY4/1).
337.3	2.6	Mud containing some halite; brownish-gray (5YR4/1).
341.1	3.8	Muddy salt grading downward into impure mud; salts largely halite and anhydrite; mud dark-greenish-gray (5GY4/1).
345.3	4.2	Mud with some dispersed salts; massive, faint mottled coloring; olive-gray (5Y4/1).
405.7	60.4	Nine alternating salt and mud layers in nearly equal volumes, with individual layers generally 4 to 6 m thick (see pl. 1); salts are halite and other saline minerals, mostly light- through medium-gray (N5-7) to light-olive-gray (5Y6/1) and grayish-orange-pink (5YR7/2); mud greenish-gray (5G4-6/1) to dark-greenish-gray (5GY4/1); mud is massive except in 0.5-m-thick zone below saltbeds, where it is thin bedded; salts are faintly bedded to massive.
413.3	7.6	Mud; inadvertently not photographed, but reported by field log as green to brown.
422.5	19.3	Core not recovered.
425.5	22.3	Mud, soft and plastic, olive-black (5Y2/1). Contact between Units G and H (new) of Mixed Layer is at base of this interval.
437.7	12.2	Mud, with small crystals of thenardite dispersed randomly; more coherent than interval above; average moderate-brown (5YR3/4).
444.6	6.9	Mud, soft and plastic, olive-black (5Y2/1).

Depth to base of unit (m)	Thickness of unit (m)	Description
449.6	5.0	Mud, more coherent than interval above; moderate-brown (5YR3/4).
451.4	1.8	Salts and mud; salts in thin beds and mottled areas, yellowish-gray (5Y8/1), chiefly glauberite and anhydrite, with some halite; mud massive, olive-gray (5Y4/1).
482.5	31.1	Mud, moderate-brown (5YR3/4), with some zones of light-olive-gray (5Y5-6/1-2); salts largely halite and anhydrite, both dispersed and concentrated in mottled zones.
483.4	0.9	Mud and some salts; mud olive-gray (5Y4/1), thin bedded; salts are chiefly anhydrite and halite.
494.4	11.0	Mud, moderate-yellowish- to pale-brown (10YR5/2-4), massive.
507.5	13.1	Mud, light-olive-gray (5Y5/2) to pale-yellowish-brown(10YR/2), 2-m-thick zone at 502 m is pale brown (5YR5/2).
507.8	0.3	Mud and salt; mud light-olive-gray (5Y5/2); salts are mostly glauberite.
516.6	8.8	Mud and disseminated salts; light-olive-gray (5Y6/1) to pale-yellowish-brown (10YR6/2).
524.0	7.4	Mud; moderate-brown (5YR4/4) in upper part, yellowish-brown (10YR6/2) to pale-brown (5YR5/2) in lower part.
530.1	6.1	Mud; upper part greenish-gray (5GY6/1), mottled, thin-bedded to massive; lower part yellowish-brown (10YR6/2), thin-bedded.
541.6	11.5	Mud, mottled, pale-brown (5YR5/2) to pale-yellowish-brown (10YR6/2). Contact between Units II and I (new) of Mixed Layer is at base of this interval.
582.2	40.6	Mud, olive-gray (5Y4/1) down to 558 m, light-olive-gray (5Y6/1) below that depth, with 2-m-thick pale-brown (5YR5/2) zone at base.
634.0	51.8	Mud, light-olive-gray (5Y5-6/1-2).
640.1	6.1	Mud, brownish- black (5YR2/1) to olive-black (5Y2/1).
649.2	9.1	Mud, light-olive-gray (5Y5-6/1-2) and pale-olive (10Y6/2).
658.7	9.5	Mud; grayish-olive (10Y4/2) in upper part, yellowish-gray (5Y6/2) in lower part.
681.5	22.8	Mud, mostly pale-olive (10Y6/2) to yellowish-gray (5Y7/2), with zones near-olive-gray (5Y4/1) at 662, 665, and 669 m.
684.0	2.4	Tuff mixed with mud, grading down into pure tuff; impure tuff is olive-gray (5Y4/1), pure tuff yellowish-gray (5Y7/2); well indurated in basal 40 cm.
690.4	6.4	Mud, silt- to sand-size; mottled, ranging in color from olive gray (5Y4/1) to dark yellowish brown (10YR4/2)
690.9	0.5	Tuff, yellowish-gray (5Y6-8/1), well-indurated, crossbedded.
693.4	2.5	Mud and sand; faint to conspicuous thin beds, light-olive-gray (5Y5/2), with streaks of pale-brown (5YR5/2). Contact between Unit I of Mixed Layer and alluvial sand and gravel is at base of this interval.
915.3	211.9	Pebbly arkosic sand and gravel, most commonly moderate brown (5YR3-4/4), with zones that average light brown (5YR6/4) in color between 726-740 and 748-798 m; mostly coarse to very coarse sand, poorly sorted, containing quartz monzonite and volcanic-rock fragments, as large as 15 cm in diameter; faintly bedded to massive; not cored between 748.3-793.4, 804.7-826.3, and 839.1-903.1 m.
929.6	14.3	Quartz monzonite, light- to medium-gray (N5-7), with pale-brown (5YR5/2) stains along fractures extending through cored interval; rock bit was used from 915.3 to 926.3 m, and so no core was recovered.

Chemistry

The Kerr-McGee Chemical Corporation had the KM-3 core divided into 254 intervals based on lithology. Detailed chemical analyses were performed on these intervals by the company's laboratory in Whittier, CA. Each analysis involved determining the percentages of acid-insoluble residue fraction and ten elements in the acid-soluble fraction. The results of the analyses were reduced to 144 units and presented by Smith and others (1983).

The acid-insoluble residue (AIR) fraction of the sediments includes clastics of fluvial (predominantly from local runoff) and aeolian origin, and authigenic silicates. The acid-soluble components include Na-, Ca-, and Mg-carbonates, as well as Na-, Ca-, and K-sulfates and chlorides. In this study, accumulation curves for AIR, chloride, sodium, sulfate, carbonate and calcium were constructed from the above analyses.

Mineralogy

The names and chemical compositions of the nonclastic minerals found in core KM-3 by Smith and others (1983) are presented in Table 2. The saline layers are composed of these minerals occurring in various assemblages and crystal habits. Nonclastic minerals were also found disseminated in the muds. The present mineralogy of the saline layers reflects a complex history. Many of the minerals are primary (for example, halite, trona) and have undergone virtually no change.

Table 2. Names and composition of the nonclastic minerals found in the KM-3 core (from Smith and others, 1983).

Mineral	*Composition*
Analcime	$NaAlSi_2O_6 \cdot H_2O$
Anhydrite	$CaSO_4$
Aragonite	$CaCO_3$
Borax	$Na_2B_4O_7 \cdot 10H_2O$
Burkeite	$2Na_2SO_4 \cdot Na_2CO_3$
Calcite	$CaCO_3$
Celestite	$(Sr, Ba) SO_4$
Dolomite	$CaMg (CO_3)_2$
Gaylussite	$CaCO_3 \cdot Na_2CO_3 \cdot 5H_2O$
Glauberite	$Na_2SO_4 \cdot CaSO_4$
Gypsum	$CaSO_4 \cdot 2H_2O$
Halite	$NaCl$
Hanksite	$9Na_2SO_4 \cdot 2Na_2CO_3 \cdot KCl$
Heulandite	$CaO \cdot Al_2O_3 \cdot 6SiO_2 \cdot 5H_2O$
Magnesite	$MgCO_3$
Nahcolite	$NaHCO_3$
Northupite	$Na_2CO_3 \cdot MgCO_3 \cdot NaCl$
Pirssonite	$CaCO_3 \cdot Na_2CO_3 \cdot 2H_2O$
Searlesite	$NaBSi_2O_6 \cdot H_2O$
Thenardite	Na_2SO_4
Tincalconite	$Na_2B_4O_7 \cdot 5H_2O$
Trona	$Na_2CO_3 \cdot NaHCO_3 \cdot 2H_2O$

Other saline layers contain large euhedral crystals reflecting recrystallization of the same primary mineral. Finally, diagenesis of the nonclastic minerals has occurred in both saline and mud layers. Within some layers complete replacement has taken place. Aragonite, calcite, dolomite, and northupite are the only nonclastic minerals, of those found in the muds, that are considered primary (Smith and others, 1983).

Although the present mineralogy reflects varying degrees of diagenesis, data on nonclastic mineral type and habit, and stratigraphy provide invaluable information on the chemical nature of the lake water, and its change through time. The chemical evolution of closed-basin lake waters is controlled by the chemistry of the inflow. During the past 2.0 Myr, when inflow to Searles Lake decreased or completely stopped, concentrated brines often formed. Hardie and Eugster (1970) suggested that saline lake brines are dominated by a relatively few major solutes (SiO_2, Ca, Mg, Na, K, HCO_3, CO_3, SO_4 and Cl), and most are dominated by the cation Na, and the anions Cl and SO_4. Therefore, only a few major brine types exist.

The brine in Searles Lake has been classified as a Na-Cl-(CO_3)-(SO_4)-type by Eugster and Hardie (1978). These authors constructed a flow diagram for brine evolution based on the chemical composition of the inflow, and subsequent concentration and precipitation due to evaporation (Fig. 8). Searles Lake and Deep Springs playa are proposed as examples of the Na-Cl-(CO_3)-(SO_4)-type brine. The undersaturated inflow for Searles Lake was, as previously discussed, predominantly from Sierra Nevada runoff, which contains solutes derived from weathering of the rocks (mostly sodium, calcium and bicarbonate). The initial solute component of

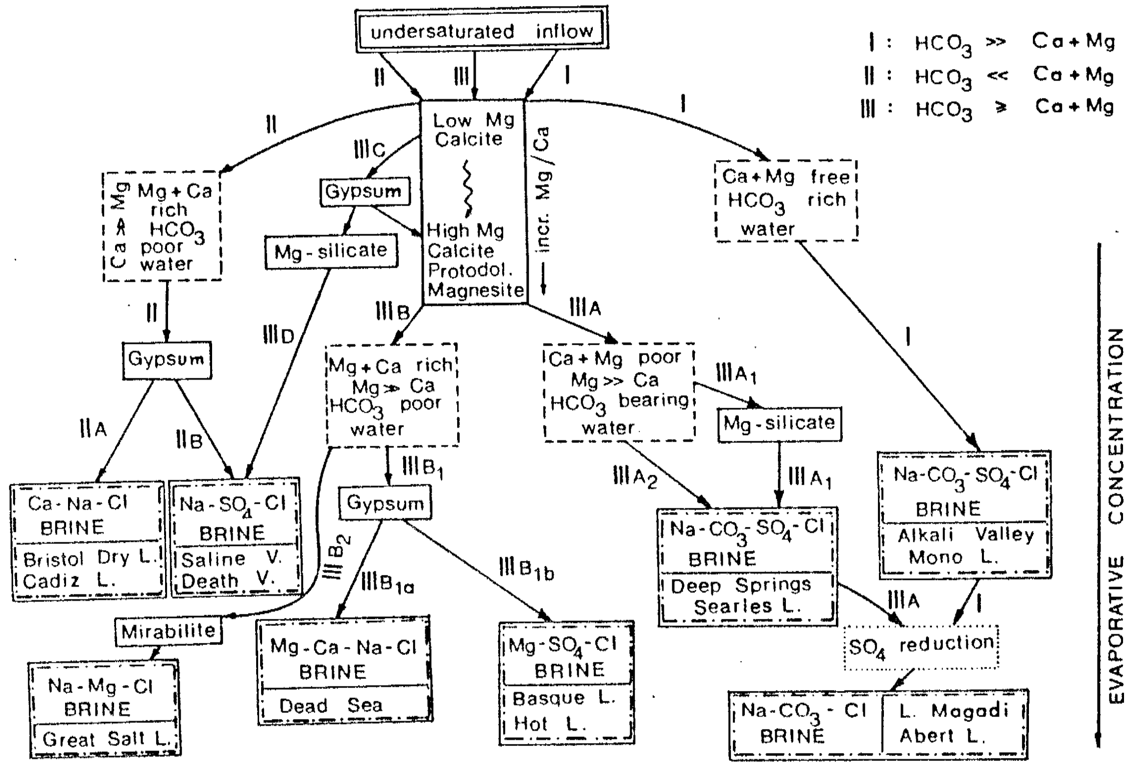

Figure 8. Diagram showing pathways of the geochemical evolution of closed-basin brines. Searles Lake and Deep Springs Lake are examples of a $Na\text{-}CO_3\text{-}SO_4\text{-}Cl$-type brine (after Eugster and Hardie, 1978).

the runoff was significantly altered by discharge from springs in the Owens Valley which contributed predominantly sodium, chloride and sulfate.

CHAPTER III

CHLORINE-36 AS A GEOLOGIC TOOL

CHLORINE-36

Natural Production

Chlorine-36 ($t_{1/2}$ = 301 ka) is the only long-lived unstable isotope of chlorine. It occurs naturally in the atmosphere (meteoric), at or slightly below the earth's surface (epigene), and in the subsurface (hypogene). Four reactions are significant in producing ^{36}Cl in these zones: cosmic-ray spallation of heavier nuclei, principally ^{40}Ar, K, and Ca; thermal neutron absorbsion by ^{36}Ar, ^{35}Cl and ^{39}K; and muon capture by ^{40}Ca.

The cosmic-ray-induced interactions are important mainly in the atmosphere, at the earth's surface, and in the upper 30 m of the lithosphere and hydrosphere (due to cosmic-ray attenuation as a function of the cumulative mass along the ray path, below the top of the atmosphere). Due to the relative abundances of the different target elements in the different terrestrial environments, spallation of ^{40}Ar is the most important meteoric reaction, and spallation of Ca and K (in low-chloride rocks), or neutron activation of ^{35}Cl (in high-chloride rocks) in near-surface rocks is the most important epigene reaction. Neutrons involved in the hypogene activation reactions are derived from the decay of U- and Th-series elements. The reaction involving muon capture by ^{40}Ca is important only at depth in Ca-rich rocks. For a more complete discussion of ^{36}Cl production, see Bentley and others (1986).

Bomb Production

Chlorine-36 was produced and entered the hydrosphere during the years 1955 to 1970 due to nuclear-weapons testing (Bentley and others, 1986). The reaction that produced most of this "bomb-^{36}Cl" was neutron activation of ^{35}Cl. Bentley and others (1986) suggested that only explosions which were set off near large amounts of chloride, and whose radioactive clouds entered the stratosphere, were the source for the subsequent fallout of bomb-36. The fallout of bomb ^{36}Cl is only important to this study in the $^{36}Cl/Cl$ measurement of modern waters, especially runoff samples derived mostly from precipitation. These samples may exhibit larger $^{36}Cl/Cl$ ratios than would be expected without the influence of bomb ^{36}Cl.

Analysis of ^{36}Cl

Chlorine-36 analyses can be performed by accelerator mass spectrometry (AMS) according to techniques developed by Elmore and others (1979, 1982). Accelerator mass spectrometry is an ultrasensitive form of high-energy mass spectrometry, consisting of two mass spectrometers separated by an MP tandem accelerator. The two mass spectrometers (MS) are connected by a tandem electrostatic accelerator that contains inert gas or a metal foil "stripper". The target material (AgCl) is ionized (for chlorine, Cl^-, a total of 18 electrons) and the first MS selects ions of the desired mass. These negative ions are accelerated, and attracted to, the positive terminal of the accelerator. Electrons are stripped off (for chlorine, 8 removed) by collision with inert Ar gas or metal foil. The ions, now positive, are repelled from the positive terminal (for chlorine, charge state 7+) The nuclei are further accelerated to high velocities before passing on to the second MS which separates out isotopes of the element of interest. Acceleration as negative ions eliminates interference from elements which do not form negative ions (for chlorine, ions such as ^{36}Ar). The high energy breaks up molecular species that might interfere; in addition, the high charge state ensures molecules will not stay bound. Accelerating the nuclei also enables the use of a highly sensitive multi-plate gas ionization detector. Separation of the remaining isobars (^{36}S in the case of ^{36}Cl) is accomplished by detection of differential energy loss as the different nuclei pass through the multi-plate detector. The signals are sent to a computer, where digital windows have been set. If a signal (event) passes all the windows, it is counted as an event of the radioisotope of interest (^{36}Cl).

Utilization of the multi-plate detector has dramatically increased the range of application of AMS due to the method by which nuclei of interest are measured. The method counts the actual number of nuclei in a sample, whereas previous methods counted decays. This allows for shorter counting times and smaller sample sizes (5-10 mg chloride). Accelerator mass spectrometry provides an analytical sensitivity of measuring ^{36}Cl in concentrations sufficiently low enough to yield an isotopic ratio of ^{36}Cl to stable chloride of 5×10^{-15}. Background levels typically yield $^{36}Cl/Cl$ ratios of 0 to 2 x 10^{-15}. Many of the limitations in using ^{36}Cl for geologic studies involving low-level samples, such as natural salines, have therefore been overcome.

CHLORINE-36 AS A GEOCHRONOMETER

Age Determination of Continental Evaporites

Chlorine (including its isotope species ^{36}Cl) is strongly hydrophilic and travels conservatively through hydrologic systems with minimal chemical interaction. Meteoric ^{36}Cl is washed out or falls out of the atmosphere with stable chloride (derived predominantly from sea spray). Epigene ^{36}Cl, derived from the weathering of rocks, can also move in either surface or ground water, whereas hypogene ^{36}Cl, derived from subsurface neutron-activation reactions, predominantly enters the deep ground-water system. In the paleo-Owens closed-basin drainage system, all chloride isotopic species were carried to the terminal sink, where ^{36}Cl was incorporated along with stable chloride in evaporites. Once ^{36}Cl is locked into evaporitic chloride minerals in the terminal sink, decay commences and the radioactive clock is started.

Characteristics unique to a closed-basin environment provide an excellent opportunity for the successful use of ^{36}Cl to date continental evaporites. However, three conditions must be fulfilled: (1) the $^{36}Cl/Cl$ ratio of the inflow to the terminal sink must be nearly constant, (2) any post-depositional production of ^{36}Cl must be negligible or calculable, and (3) chloride in analyzed samples should have remained immobile within halite crystals since the time of primary deposition.

Determining Exposure Time

When a rock is suddenly exposed at the earth's surface, production of ^{36}Cl by cosmic-ray interactions commences. For a period of time the amount of ^{36}Cl "builds up" in the rock at a rate greater than the concurrent decay. Since buildup is a function of time, exposure time can be determined by measuring the $^{36}Cl/Cl$ ratio. As previously discussed, reactions that produce ^{36}Cl within rocks include thermal neutron activation of ^{35}Cl (important in rocks with high chlorine content), spallation of potassium and calcium (important in rocks with low chlorine content) and the negative muon capture by ^{40}Ca (minor reaction important only in Ca-rich rocks at depth).

Phillips and others (1986a) have summarized the useful characteristics of buildup dating by ^{36}Cl as follows:

1. It builds up to measurable levels relatively quickly because the product element (chlorine) generally is present only in trace quantities.

2. Chlorine-36 activities produced by nuclear processes within the rock (due to uranium and thorium) are low enough that they should be much less than the cosmogenic activity after 5000 years of exposure or less.

3. The mobile and hydrophilic nature of chlorine should aid in the separation of the ^{36}Cl produced within the rock from meteoric (atmospheric) ^{36}Cl.

Early attempts to use the ^{36}Cl build-up method (Davis and Schaeffer, 1955; Bonner and others, 1961; Bagge and Willkom, 1966) were not successful because ^{36}Cl production was not fully understood and adequate analytical sensitivity was not available. The recent successful measurement (by AMS) of ^{36}Cl buildup in young volcanic rocks (Phillips and others, 1986a; Leavy and others, 1987) shows the potential of this method. Volcanic rocks were chosen for the preliminary testing of the method because they met the crucial criteria of being shielded from cosmic rays, then suddenly exposed to them on the surface. In this study, the ^{36}Cl build-up method will be tested for surface-exposure dating on glacial erratics found on moraines located on the east slope of the Sierra Nevada. Glacial erratics have the potential to also successfully meet the criteria of sudden exposure to cosmic rays.

Erratics are blocks of rock plucked by glacial ice from valley headwalls, transported by ice down slope, and deposited on or within morainal debris. The assumption that the erratic was shielded from cosmic rays when part of the headwall at first seems problematic. However, cosmic rays are attenuated in the first few meters of the lithosphere. In fact, 75% of the cosmic rays are attenuated by the first 80 cm of rock, and almost 90% by the first 120 cm. Thus, only a thin "skin" of rock is exposed to cosmic rays at the surface. With the onset of glaciation this thin "skin" would be quickly removed. Subsequent quarrying by the ice would remove blocks of rock that had been shielded from cosmic rays. If exposure time of an erratic can be determined, it can be inferred as the exposure time for the morainal deposit. This, in turn, provides an age control for the glacial event during which the moraine was deposited.

CHLORINE-36 AS A HYDROLOGIC TRACER

The geochemical nature of chloride (hydrophilic, conservative) makes it an excellent hydrologic tracer. Chloride was introduced into the paleo-Owens watershed from various sources (precipitation, runoff, springs, artesian wells, dissolution of surficial salines). Chlorine-36, also introduced from each of these sources, traveled with stable chloride in runoff to the distal sink. Measurement of the ^{36}Cl and stable chloride in modern waters and surficial salines will be used to determine the contribution from each source and spatial distribution within the watershed. Measurements in modern waters are assumed to reflect past conditions once the present $^{36}Cl/Cl$ ratio is corrected for possible bomb ^{36}Cl contamination. Therefore, a hypothesis of the evolution of the $^{36}Cl/Cl$ ratio and the chloride budget from the headwaters to the terminal sink can be presented.

CHAPTER IV

CHLORINE-36 DATA ACQUISITION AND PRESENTATION

SAMPLE COLLECTION AND PREPARATION

The following is a description of the different methods used to collect samples for ^{36}Cl analysis. Sample locations are described in Appendix 1. The ultimate target material needed for analysis is the solid AgCl, which readily precipitates out of chloride solutions with the addition of excess $AgNO_3$.

Saline Sediments

Saline samples were collected from cores from Searles and Panamint Lakes of the paleo-Owens River system. Other Basin and Range lake sediments were sampled from Bonneville Lake (in Utah), Clayton Valley and Walker Lake (both in Nevada), and Bristol, Danby, and Cadiz Lakes (in California). Crystal descriptions for the nonhalite core samples are presented in Appendix 1.

Surficial saline samples were collected from the Warren Lake and Owens Lake playas (both in Owens Valley), and from Deep Springs playa in Deep Springs Valley (east of Owens Valley, between the White and Inyo Mountains). Sample location for these surficial salines are shown in Figure 5. Additional surficial samples from within the Basin and Range Province were collected from the 8-Mile

Flat playa (in Nevada), and two geosols which have developed on Lake Lahonton sediments (in Nevada).

Pure halite crystals (1 to 3 g) were collected when possible. The exterior portion of the crystal (or crystals) was dissolved with deionized water to remove any secondary halite and reduce the risk of possible contamination. The remaining portion of the halite crystal was dissolved in deionized water, and the chloride was precipitated out as AgCl by the addition of excess $AgNO_3$.

Larger quantities (15-20 g) of non-halite evaporites were collected to ensure a sufficient quantity of chloride for analysis. These samples were crushed to speed dissolution. The grains were then washed and the remaining sample dissolved in deionized water. If necessary, particulates were filtered out, and excess $AgNO_3$ was added to precipitate AgCl.

Water Samples

Aqueous samples were collected from lakes, streams, thermal springs, and one naturally flowing well all within the Owens River drainage basin. Water samples from the Deep Springs Playa watershed were also collected. Sample locations are shown on Figure 5. Sufficient quantity was collected for chloride, ^{36}Cl and tritium analyses. Additional water samples from within the Basin and Range Province were collected from Truckee River, Pyramid Lake, Walker River and Walker Lake (all in Nevada).

Waters with high chloride concentrations (thermal springs, Bishop well, Mono Lake) were collected directly into a pre-treated one gallon plastic jug (Fig. 9). The pH was lowered with nitric acid to facilitate the precipitation of AgCl when excess $AgNO_3$ was added. For sites with low chloride concentration (Sawmill Creek, Frances Lake, Owens River and all waters in the Deep Springs Playa watershed), the water was run through an ion exchange column in the field. Chloride collected on the ion exchange resin in the column and was then eluted in the laboratory. This procedure is outlined in Appendix 2.

Rock Samples

Glacial erratics were collected from moraines (type localities when possible) deposited on the east flank of the Sierra Nevada. Rocks were sampled based on megascopic observation in the field of the following criteria: (1) composition and texture -- the rocks of the Sierra Nevada are predominantly in the granite-granodiorite family; erratics were chosen that showed similar composition and texture, reflecting this rock type; (2) degree of weathering -- rocks were sampled that exhibited only a small degree of chemical weathering, and (3) location and position -- erratics were collected from the crests of the moraines where erosion and reworking were determined to be of minor influence. Field reconnaissance was conducted to choose sites removed from areas of tectonic (for example, faulting) or igneous activity (for example, lava flow). The rocks were split, any surface rind removed, then ground to a fine powder (<100 mesh size) in preparation for chloride

Figure 9. Sampling of geothermal spring. Water was collected for chloride, tritium and ^{36}Cl analyses. Photo taken at Casa Diablo hot spring, October, 1983.

extraction by fusion. The chloride extraction and fusion procedures are presented in Appendix 3.

A carrier that would yield only a small quantity of AgCl (< 5 mg) when $AgNO_3$ was added was needed for samples with low chloride content. A carrier, which is added to the sample in the minimum amount necessary, is a source of chloride that does not contain ^{36}Cl. The extra chloride provides sufficient AgCl precipitate (with addition of $AgNO_3$) for AMS analysis. Table salt was determined to contain "dead" chloride (no ^{36}Cl) and was used as a carrier. Once $^{36}Cl/Cl$ measurements were completed, the measured ratio (R_m) was adjusted in accordance with the amount of carrier added such that:

$$R_f = R_m \left(\frac{Cl_s + Cl_c}{Cl_s} \right) \qquad (3)$$

where R_f is the final ratio, Cl_s is the chloride content (mg/L) of the sample, and Cl_c is the amount of chloride (mg/L) in the carrier.

The final step in sample preparation is purification of the AgCl precipitate. This is necessary in order to remove sulfur which is an interfering isobar (^{36}S) during AMS analysis. Sulfur was removed by repeated dissolution in ammonia and then reprecipitation by one of two means (dependent on sample size): (1) the addition of nitric acid, or (2) evaporation by heating. These two procedures are outlined in Appendix 4. For each set of samples purified at the same time, a lab blank (made with table salt) went through the same procedure and was analyzed by AMS. This was to check for background ^{36}Cl and ^{36}S levels which might be due to systematic contamination during laboratory procedures.

DETERMINATION OF $^{36}Cl/Cl$ RATIO

Measuring the Sample

Measurements of $^{36}Cl/Cl$ ratios were performed (Aug. 84, Oct. 84, Jan. 85, Apr. 85, Nov. 85, Dec. 85-Jan. 86) by accelerator mass spectrometry (AMS) at the Nuclear Structure Research Laboratory (NSRL), University of Rochester, New York, under the direction of David Elmore. The apparatus at NSRL, referred to as TAMS (tandem AMS), consists of a nominal 12 MV model MP tandem Van de Graaff accelerator (recently upgraded to 16 MV, Fig. 10)

Samples were loaded into a titanium sample wheel (23 mm diameter). Small samples (< 5 mg) were mixed with about 3 to 4 g of extremely pure (99.9999%) gold powder (-22 mesh). The addition of gold resulted in sample durability and enhanced stability of the beam current during initial ionization.

Chlorine-36 and stable ^{35}Cl and ^{37}Cl (not equally abundant), a known standard, and the appropriate lab blank were measured for each sample. For each wheel run, data were collected during a minimum of two non-successive sequences. Within each sequence isotopes were measured during a cycle; there were a minimum of two cycles in a sequence. The measured ratio (^{36}Cl atoms to stable chloride atoms) was then normalized to the standard and adjusted for background interference. Uncertainty statistics were then calculated.

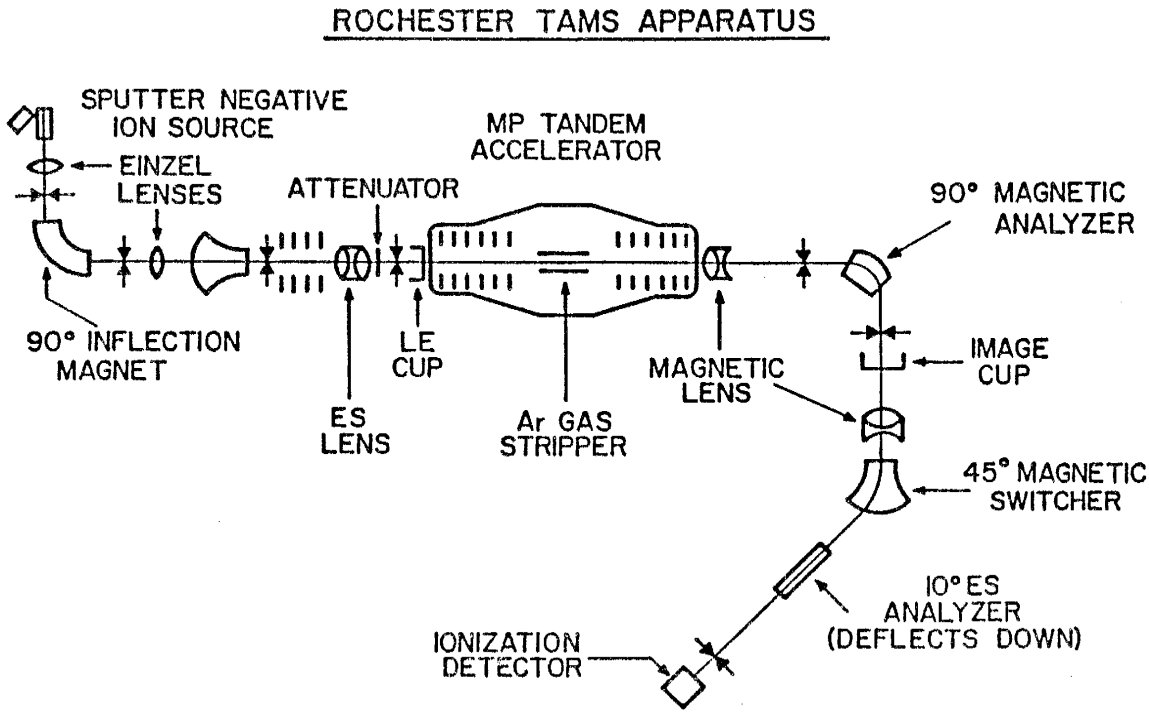

Figure 10. Schematic of the accelerator mass spectrometry (AMS) apparatus at the University of Rochester, Nuclear Structure Research Laboratory (from Elmore and others, 1979).

Statistical Analyses

Elmore and others (1984) presented a method for calculating final ratios and uncertainties (reported as one standard deviation) assuming a Poisson distribution for the counting rate. The final uncertainty was taken as the largest of either the external error (standard deviation of the mean of the ratios) or the internal error (sequence error derived from combining statistical or counting errors of each cycle).

Statistical analyses of data are particularly critical because of the need to obtain estimates of analytical uncertainty in cases where the uncertainty is a significant proportion of the measured value. These uncertainties translate into uncertainties in ages for the subsurface evaporite samples. In this study, an alternative for determining the uncertainties was examined.

A standard statistical method referred to as the nested or hierarchical model was used to calculate ratios and uncertainties. The main differences between the methods are as follows. For the method used in Elmore and others (1984), the final ratio (or mean) for a sequence is a weighted average calculated by using the estimated variances based on the assumption of a Poisson distribution. If there is more than one sequence, the final ratio for the run is determined by combining the ratios from the sequences, and again, calculating a weighted average. The final ratio determined in the nested method is not a weighted average. As stated above, the method used in Elmore and others (1984) calculates uncertainties based on a Poisson distribution for the counting rate. Two uncertainties are calculated for each sequence, the internal and external. Both are determined by combining errors calculated for the cycles. The internal error of a sequence is the combination of the statisitical errors of each cycle, and would reflect fluctuating experimental conditions. The external error of a sequence is the standard deviation of the mean of the ratios of the cycles for constant experimental conditions. The nested design allows isolation of the causes of variability or components of variance, whether between cycles, sequences, or runs, and then uses those to find uncertainties. Knowing the causes of variability would be invaluable information to the experimenter. The method attempts to analyze the variation of a response and to assign portions of the variation to each of a set of independent variables. The hierarchical method, along with the results from the hierarchical method and the method proposed by Elmore and others (1984), are presented in Appendix 5. In most cases, there were only small differences between final measured values and uncertainties determined by each method. I have chosen to use the hierarchical method in this study on the advice of A. Gutjar, Director of Applied Statistics Research Center, New Mexico Institute of Mining and Technology, Socorro, New Mexico.

DATA PRESENTATION

Chlorine-36/Cl ratios, with uncertainties, are presented as follows: Table 3 -- core samples, Table 4 -- waters and surficial salines, and Table 5 -- rocks. Chloride and tritium concentrations of water samples are also presented in Table 4. Tritium analyses were performed at the Los Alamos National Laboratory, New

Table 3. Chlorine-36 measurements and ages for core samples.

Location	Sample	Depth (m)	Unit* Searles Lake only	^{36}Cl/Cl (x 10^{-15})	Uncorrected ^{36}Cl age (Ma)	Residence time (Δt) (Ma)	Corrected ^{36}Cl age (Ma)†
Searles Lake, CA KM-3 core	SLC-1	3.0	OM	48 ± 10	0.067 ± 0.0100	..	..
	SLC-4	6.4	US	80 ± 6§	.. ..	..	
	PRE-1**	14.2	US	55 ± 3	0.010 ± 0.022	..	..
	SLC-3	19.2	US	75 ± 15§	.. ..	..	
	PRE-2**	32.5	LS	55 ± 3	.. ..	..	
	SLC-11	114.0	ML(C)	29 ± 3	0.286 ± 0.047	..	..
	SLC-5	126.5	ML(C)	24 ± 3	0.368 ± 0.058	0.059	0.339 ± 0.058
	SLC-14	140.8	ML(C)	23 ± 2	0.386 ± 0.040	..	..
	SLC-5.3	153.0	ML(C)	21 ± 3	0.426 ± 0.067	..	..
	SLC-15	161.8	ML(C)	14 ± 5	0.602 ± 0.192	..	..
	SLC-12	179.0	ML(D+E)	12 ± 1	0.669 ± 0.038	0.001	0.668 ± 0.038
	SLC-6	187.0	ML(D+E)	14 ± 3	0.602 ± 0.105	..	..
	PRE-3**	190.7	ML(D+E)	8.9 ± 1	0.799 ± 0.051	0.015	0.792 ± 0.051
	PRE-4**	206.5	ML(D+E)	7.7 ± 1	0.862 ± 0.060	..	..
	SLC-7	227.5	ML(D+E)	130 ± 33§	.. ..	..	
	SLC-8	293.0	ML(G)	3 ± 1	1.27 ± 0.176	0.006	1.27 ± 0.176
	PRE-5**	304.3	ML(G)	6.6 ± 2	0.929 ± 0.156	..	..
	SLC-10	399.3	ML(G)	2 ± 1	∞(>1.50) ± 0.298	0.003	∞(1.50) ± 0.298
	SLC-9	401.3	ML(G)	2 ± 1	∞(>1.50) ± 0.298	0.003	∞(1.50) ± 0.298
	PRE-6**	401.3	ML(G)	42 ± 8	.. ..	..	
Panamint Valley, CA DH-3 core	PVC-1	18.2		80 ± 3§	.. ..	..	
	PVC-5	40.9		33 ± 4	0.230 ± 0.05	..	0.175 ± 0.075
	PVC-10	68.3		33 ± 3	0.230 ± 0.041	..	0.175 ± 0.075
	PVC-15	136.0		92 ± 7§	.. ..		
	PVC-18	160.5		19 ± 2	0.470 ± 0.043		0.392 ± 0.090
Lake Bonneville, UT	LDS60-72	"surface"		34 ± 8			
	BYU-658	"surface"		30 ± 3			
	BONN C-4	67.0		25 ± 2	0.107 ± 0.036		
	BONN C-3	76.6		25 ± 1	0.107 ± 0.018		
Clayton Valley, NV	CVC-1	33.3-33.9		77 ± 9			
	CVC-2	88.4-88.7		51 ± 2	0.179 ± 0.018		
Bristol Lake, CA BLC-2	BLC-1	3.03		30 ± 5			
	BLC-2	48.4		30 ± 3			
	BLC-3	92.1		3 ± 1	1.00 ± 0.175		
	BLC-5	171.4		4 ± 2	0.875 ± 0.300		
Cadiz Lake, CA CLC-1	CLC-1	2.7		67 ± 3			
	CLC-2	27.1		45 ± 5	0.173 ± 0.051		
	CLC-3	43.9		1,163 ± 12§			
Walker Lake, NV WLC-4	WLC-1	24.0		219 ± 5			
	WLC-6	72.0		199 ± 12	0.042 ± 0.026		
	WLC-4	112.0		178 ± 9	0.090 ± 0.021		

*Units for Searles Lake cores plotted on Figure 4B.
†Adjusted ^{36}Cl ages for only Searles and Panamint Lakes as discussed in text.
§^{36}Cl/Cl greater than initial ratio (R_i) - ages cannot be determined.
**PRE samples from Phillips et al. (1983).
††Samples provided by D. R. Currey.
§§Samples provided by I. Kunasz.

Table 4. Chloride concentration, tritium concentration and $^{36}Cl/Cl$ ratios of modern waters and surficial salines.

Location	Sample	$^{36}Cl/Cl$ ($\times 10^{-15}$)	Cl^- (ppm)	Tritium (T.U.)*
Owens Valley, CA				
Thermal Springs				
Casa Diablo	SLW-1	35 ± 3	353	0.35 ± 0.09
1 mi N Whitmore Sp	SLW-2	47 ± 10	181	0.50 ± 1.0
Little Hot Creek	SLW-3	18 ± 5	214	0.16 ± 0.10
Hot Creek	SLW-4	10 ± 2	228	0.23 ± 0.10
Black Point	SLW-5	101 ± 13	361	0.12 ± 0.9
Keough	SLW-7	36 ± 5	185	0.44 ± 0.09
Dirty Socks	SLW-8	5 ± 3	1,470	1.30 ± 0.11
Warm Springs	SLW-16	270 ± 32	16	0.56 ± 0.12
Big Alkali†	SLW-20	14 ± 3	144	
Soda Flat†	SLW-23	23 ± 4	290	
Surface Waters				
Frances Lake	SLW-9	734 ± 20	0.83	
Sawmill Creek	SLW-14	507 ± 23	1.02	25.6 ± 0.8
Owens River	SLW-15	432 ± 35	9.88	15.8 ± 0.4
Snowmelt	SLW-17	1,117 ± 68		
Mono Lake	SLW-18	99 ± 11	18,000	
Casa Diablo Pool†	SLW-22	18 ± 4	241	
Bishop Artesian Well	SLW-6	86 ± 20	22.4	2.05 ± 0.13
Casa Diablo Well†	SLW-21	17 ± 4	275	
Surficial Salines				
Warren Lake Bed	SLS-1	240 ± 13		
Owens Lake Bed	SLS-3	82 ± 8		
Deep Springs Valley, CA				
Birch Creek	SLW-10	391 ± 1	6.22	6.95 ± 0.24
Corral Springs	SLW-11	775 ± 4	6.64	37
Artesian Well	SLW-12	1,050 ± 88	4.56	12
N Branch Crooked Cr	SLW-13	205 ± 2	1.52	44
Deep Springs Playa	SLS-2	770 ± 44		
Great Basin Samples, NV				
Eightmile Flat	BRS-1	181 ± 12		
Lake Lahontan geosol	GEO-1	376 ± 36		
	GEO-2	1,929 ± 176		
Walker Lake	GBL-1	84 ± 14		
Walker River	GBL-2	880 ± 36		
Truckee River	GBL-3	708 ± 71		13.1 ± 0.4
Pyramid Lake	GBL-4	169 ± 17		

*Tritium reported in Tritium Units (T.U.).
†Samples provided by F. Goff.

Table 5. Chlorine-36 measurements and preliminary ages for glacial erratics from the east slope of the Sierra Nevada, and for two basalt samples.

Location	Sample	$^{36}Cl/Cl$ (x 10^{-15})	Chloride (ppm)	^{36}Cl age (Ma)
Bloody Canyon				
Tioga moraine				
	BCM-1A	884 ± 41	208	0.037 ± 0.002
	BCM-3A	585 ± 25	123	0.023 ± 0.001
	BCM-4A	761 ± 68	62	0.023 ± 0.002
Tenaya moraine				
	BCM-2B	745 ± 33	154*	0.022 ± 0.001
	BCM-5B	860 ± 103	202	0.045 ± 0.005
	BCM-1B	905 ± 35	..	..
Tahoe moraine				
	BCM-2C	2606 ± 203	214	0.139 ± 0.011
	BCM-5C	1352 ± 74	..	..
Mono Basin				
	BCM-1D	5061 ± 309	123	0.220 ± 0.013
	BCM-2D	1519 ± 68	..	..
	BCM-5D	1857 ± 131	..	..
Rocky Creek Canyon				
Sherwin moraine				
	RCM-5	1323 ± 252	..	..
	RCM-4	228 ± 26	..	..
McGee Mountain				
McGee moraine				
	MMT-3	3714 ± 319	..	..
	MMT-2	986 ± 107	..	..
Ash Hill Channel basalt†				
	A479	1648 ± 88	..	..
	A477	318 ± 40	..	..

* Chloride concentration in xenoliths, concentration of matrix was 55 ppm.
† Samples provided by R. Hale.

Mexico. Chloride concentrations were determined by the standard titration method (American Public Health Association, 1975). Elemental and compositional analyses of the glacial erratics are given in Appendix 6.

Agreement of ^{36}Cl dates from this study, and those presented by Phillips and others (1983), with independent dates substantiates the conditions of a nearly constant $^{36}Cl/Cl$ influx and negligible post-depositional ^{36}Cl production by cosmic-ray reactions for Searles Lake. The lake waters would serve to attenuate the cosmic rays. Phillips and others (1983) suggest that hypogene production is insignificant in these sediments (except for some samples older than 1.0 Ma). Subsurface chloride translocation is more difficult to determine and quantify; therefore, an effort was made to sample primary crystals after visual inspection of the sample interval. The cores were sampled with the aid of G.I. Smith of the Mineral Resource section of the U.S. Geological Survey, Menlo Park, CA, who has worked extensively in the area.

CHAPTER V

DATA MANIPULATION AND CHRONOLOGY DEVELOPMENT

CHRONOLOGY OF KM-3 CORE, SEARLES LAKE, CA

Determination of ^{36}Cl Ages of Evaporites

Chlorine-36 ages (uncorrected) for lake sediments from Searles, Panamint, Bonneville, Clayton, Bristol, Cadiz and Walker Basins were determined by using the standard radiometric decay equation

$$t = \frac{-1}{\lambda_{36}} \ln \left(\frac{R_m}{R_i} \right) \tag{4}$$

where R_m is the measured ratio (by TAMS) for the sample, R_i is the initial ratio and λ_{36} ($\ln 2/t_{1/2}$) is the decay constant of ^{36}Cl. These ages are presented in Table 3.

An initial ratio (R_i) of 56 x 10^{-15} $^{36}Cl/Cl$ was used for all samples from Searles and Panamint Basins. This initial value was the $^{36}Cl/Cl$ ratio of the Upper Salt (the youngest Searles Lake evaporite unit derived from Owens River runoff) measured by Phillips and others (1983) and adjusted for the 10-kyr ^{14}C age of the unit. This value reflects mixing of large amounts of low $^{36}Cl/Cl$ hypogene chloride from hot springs with smaller amounts of high $^{36}Cl/Cl$ chloride from meteoric and epigene sources, as discussed previously. For each of the other basins (Bonneville, Clayton, Bristol, Cadiz), the observed ratio from the shallowest depth was used as R_i.

Most of the samples from Searles Lake were from saline units (with interstitial muds) that precipitated slowly but continuously, allowing equation 4 to be used directly. However, six samples from Searles Lake (126.5 m, 179.0 m, 190.7 m, 293.0 m, 399.3 m, 401.3 m) were from saline units that were determined to be the result of rapid precipitation during a desiccation event. Thus, soluble chloride resided in the lake waters for long intervals before incorporation into the evaporites. To account for ^{36}Cl decay during this residence time, a corrected ^{36}Cl age must be determined.

The ratio at the time of halite deposition (R_d) can be expressed as

$$R_d = \frac{M_{36}}{M_{Cl}} \qquad (5)$$

where M_{36} and M_{Cl} are the number of moles of ^{36}Cl and chloride, respectively. In the absence of halite precipitation, a constant influx of stable chloride (i_{Cl}) results in an accumulation of stable chloride with time:

$$i_{Cl} = \frac{dM_{Cl}}{dt} \qquad (6)$$

and, in the case of constant ^{36}Cl influx (i_{36}):

$$i_{36} - \lambda_{36}M_{36} = \frac{dM_{36}}{dt} \qquad (7)$$

Rearranging and integrating equation 6 over time yields

$$M_{Cl} = i_{Cl}(t_o - t_d) \qquad (8)$$

and doing the same for equation 7:

$$M_{36} = \frac{i_{36}}{\lambda_{36}}(1 - e^{-\lambda_{36}(t_o - t_d)}) \qquad (9)$$

with the assumption that M_{Cl} and $M_{36} = 0$ at t_o (t_o = time infilling began), and t_d = time of halite deposition. Substituting 8 and 9 into 5:

$$R_d = \frac{M_{36}}{M_{Cl}} = \frac{i_{36}(1 - e^{-\lambda_{36}(t_o - t_d)})}{i_{Cl}\lambda_{36}(t_o - t_d)} \qquad (10)$$

then:

$$R_d = R_i \frac{1 - e^{-\lambda(t_o - t_d)}}{\lambda_{36}(t_o - t_d)} = \frac{R_i}{\lambda_{36}\Delta t}(1 - e^{-\lambda_{36}\Delta t}) \qquad (11)$$

where $\Delta t = t_o - t_d$, and $R_i = i_{36}/i_{Cl}$.

The present ratio (R_p) reflects this ratio at time of deposition (R_d) with subsequent decay after burial. Therefore:

$$R_p = R_d e^{-\lambda_{36} t_d} = \frac{R_i}{\lambda_{36}\Delta t}(1 - e^{-\lambda_{36}\Delta t})e^{-\lambda_{36} t_d} \tag{12}$$

Rearranging and solving for time of deposition (t_d):

$$t_d = \frac{-1}{\lambda_{36}} \ln\left(\frac{R_p}{R_i} \frac{\lambda_{36}\Delta t}{e^{-\lambda_{36}\Delta t}} \right) \tag{13}$$

Equation 13 was used to calculate corrected ^{36}Cl ages for the Searles Lake samples listed above. These ages are shown in Table 3 and are plotted in Figure 11 along with other absolute dates. The length of residence (Δt) was estimated for each sample based on chloride budget methods (described below). The magnitude of the residence time corrections is, in general, small.

Chloride residence time for ^{36}Cl in Panamint Lake cannot be directly determined because a chloride budget is not applicable there. However, equation 12 can be used iteratively to solve for the time of deposition of the upper and lower salt layers. A computer program was written to calculate t_d, given the measured R_p, at an estimated t_o inferred from the Searles chronology. The ages (corrected) for the upper salt and lower salt are shown in Table 3. Ages for the Bonneville, Clayton, Bristol and Cadiz samples were not corrected because the initiation of chloride storage (t_o) could not be reliably inferred.

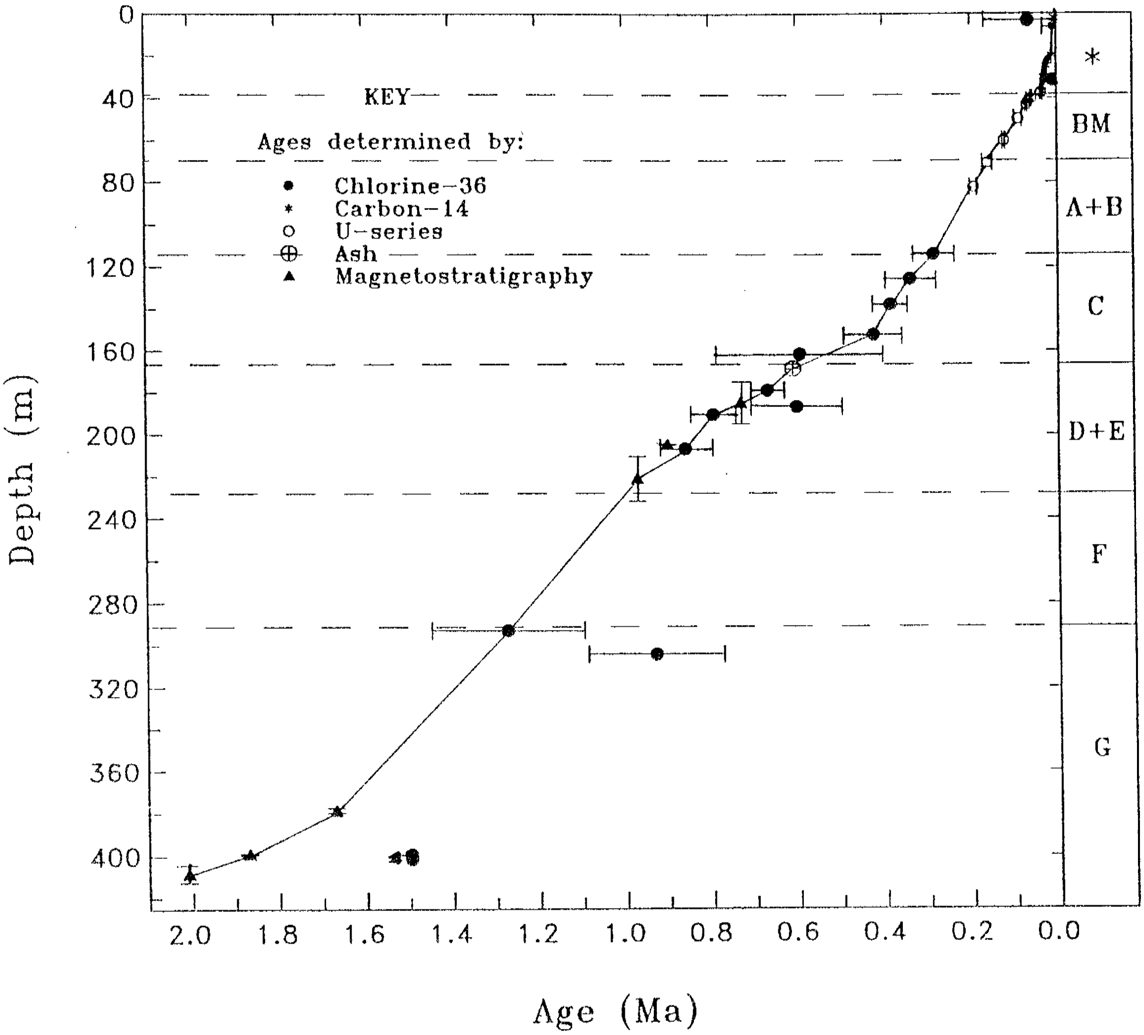

Figure 11. Plot of ages determined by radiometric and paleomagnetic methods versus depth for the KM-3 core, Searles Lake. Chlorine-36 ages as determined by this study and Phillips and others (1983). Carbon-14 ages from Smith (1979), U-Th ages from Bischoff (1985), and paleomagnetic ages from Liddicoat and others (1980). Core description is given in Table 1. Letters G, F, D+E, C, A+B represent units in the Mixed Layer, BM refers to the Bottom Mud, and (*) represents the units which overlie the Bottom Mud - Lower Salt, Parting Mud, Upper Salt, and the Overburden Mud (bottom to surface).

Discussion of ^{36}Cl Ages for Searles Lake

Ages determined by ^{36}Cl are concordant with those determined by other methods for the intervals where more than one method can be employed. However, for interpretations made during this study, ages determined by ^{14}C and U-Th series for samples from less than 100 m and by magnetostratigraphy for those greater than 300 m were used because those methods are more precise within the age ranges represented at these depths (Fig. 11).

Three samples, collected at 6.4 m, 19.2 m, and 227.5 m, were observed to have anomalously high $^{36}Cl/Cl$ ratios. The high value at 227.5 m was checked by processing a fresh crystal of halite from the original sample. The second measurement was also high. Since the high ratio was replicated, it was inferred that contamination during sample preparation was not the cause. Therefore, the high $^{36}Cl/Cl$ ratios are attributed to unknown causes at this time, and these values are not used in the chronology. A high $^{36}Cl/Cl$ ratio of a sample from 401.3 m was first reported by Phillips and others (1983). This depth interval was resampled and the remeasured ratio was very low, supporting the suggestion by Phillips and others (1983) that the first sample may have been contaminated during laboratory preparation. The corresponding ^{36}Cl age for the new ratio is consistent with the age values of adjacent samples (Table 3), and is used in the chronology presented in Figure 11.

Ratios measured at 161.8 m and 187.0 m have large analytical errors. In fact, the value at 187.0 m represents a reversal. In order to present a final data set that is internally consistent, neither of these samples were included in the chronology. Ages determined by ^{14}C, U-Th, ^{36}Cl, and paleomagnetic methods that are used in this study to produce the chronology of Searles Lake sediment are connected by a line in Figure 11. This data set includes the ash layer at 168.6 m which is correlated with the Lava Creek B ash.

The few anomalously high $^{36}Cl/Cl$ ratios in Table 3 are believed to be due to field or laboratory contamination. Overall, the data are internally consistent and in good agreement with independent dates.

AIR-Interpolated Ages

Examination of cumulative AIR as a function of depth through the entire core (Fig. 12) reveals a change in slope at about 400 m. This is due to a change of environment in Searles Basin from playa lakes to perennial lakes that underwent periodic desiccations and evaporite deposition (Smith and others, 1983). The constancy of accumulation (especially below 400 m) suggests that cumulative AIR is approximately a linear function of depth, totally independent of sedimentation rate. This relationship would apply as long as sediment density is approximately constant.

The slope changes in Figure 11 indicate that there were major fluctuations in the deposition rate (LT^{-1}) during the past 2.0 Myr in Searles Lake. At least part of the reason for these fluctuations is clear. Large amounts of certain solutes (principally sodium, chloride and carbonate) accumulated in the lake waters over long periods of time. Then, when environmental change caused a large decrease in lake

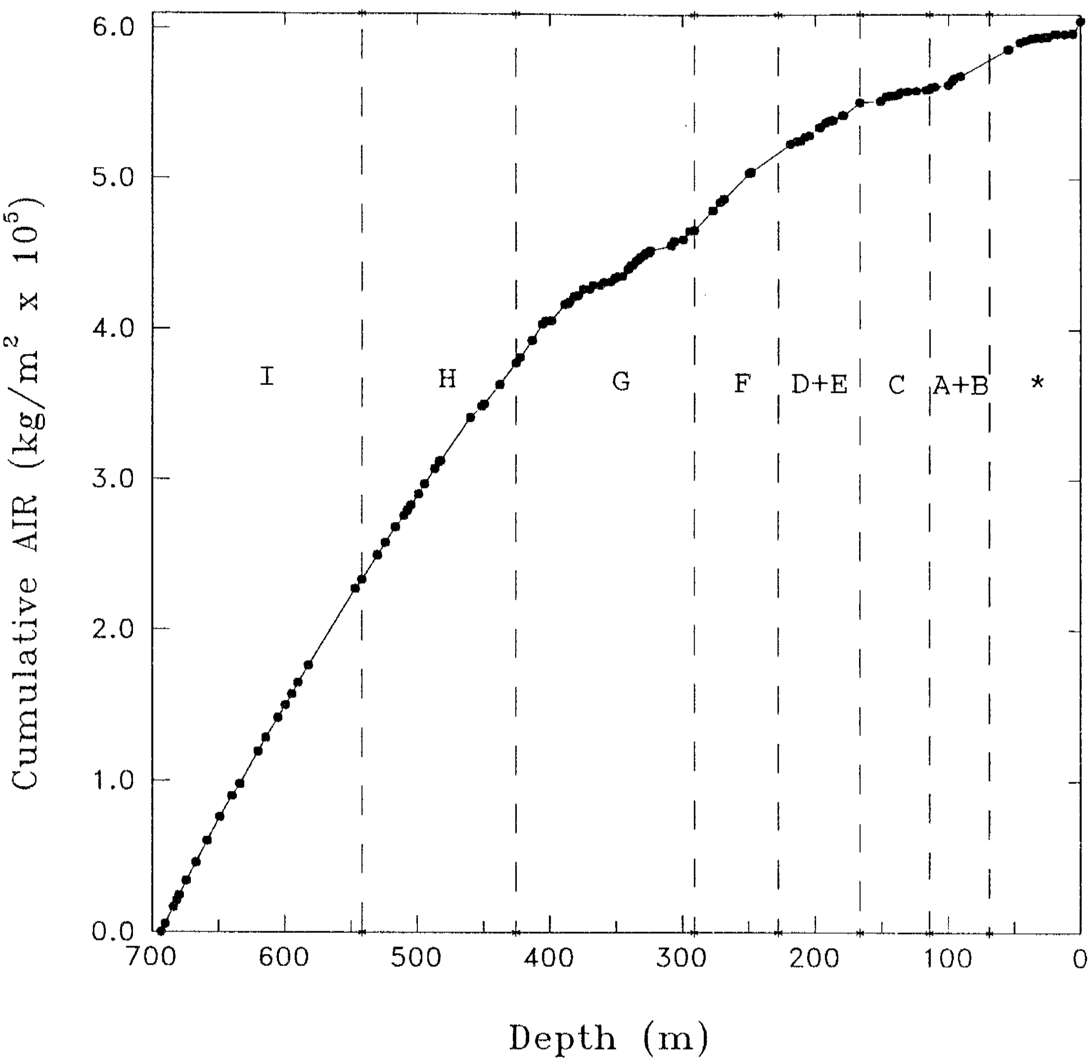

Figure 12. Plot of the mass accumulation of acid-insoluble residue (AIR) versus depth for the top 700 m of the KM-3 core, Searles Lake. Letters correspond to the names of units as described in Table 1. (*) refers to the Upper Units which overlie the Mixed Layer (from bottom to top, Bottom Mud, Lower Salt, Parting Mud, Upper Salt, and Overburden Mud). These units are also described in Table 1.

volume, these solutes precipitated out rapidly as beds of nearly pure evaporite minerals. Intervals showing clear examples of this phenomenon are Unit C and the Upper Salt. Sedimentary components such as AIR which have a short residence time in the lake waters should not be as subject to this type of fluctuation in deposition rate. An interpolation method was developed in response to the unique environment reflected in the alternation of slowly deposited mud with rapidly deposited salines. In an effort to more accurately interpolate sediment ages between absolutely dated points, I first determined the cumulative AIR for the dated depth intervals. For each AIR value, ages were linearly interpolated between the dated points. I then plotted cumulative AIR as a function of time (Fig. 13). Although the AIR-accumulation rate does show variations, it is relatively constant for long periods and is significantly more constant than the rate of depth change with age. Finally, the AIR ages (Fig. 13) were correlated with AIR depth intervals (Fig. 12). The resultant "AIR-interpolation age" versus depth is shown in Figure 14 (data in Appendix 7), with absolutely dated points included. This plot is more realistic than a simple linear depth interpolation in that many evaporitic intervals do show higher deposition rates.

Sedimentary Chronology -- Acid-Soluble Components

With ages interpolated as described above, the accumulation of chemical species of interest can be plotted over time. The accumulation curves for calcium and carbonate are shown in Figure 15, for sodium and sulfate in Figure 16, and for chloride in Figure 17 (data given in Appendix 7). The curves for chloride, sodium

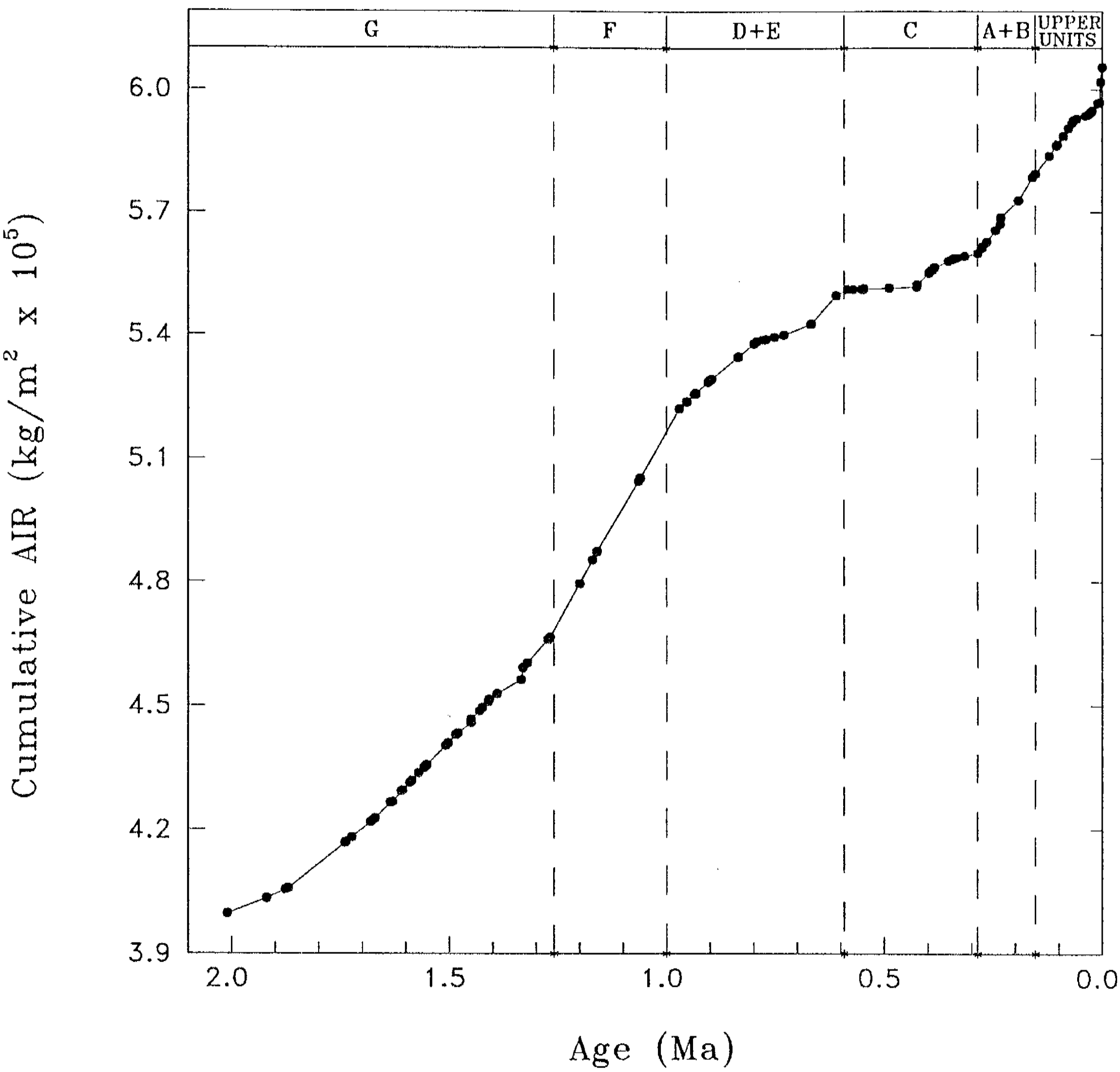

Figure 13. Mass accumulation of acid-insoluble residue (AIR) in the KM-3 core for the past 2.0 Myr. Units described in Table 1, abbreviations on Figure 12.

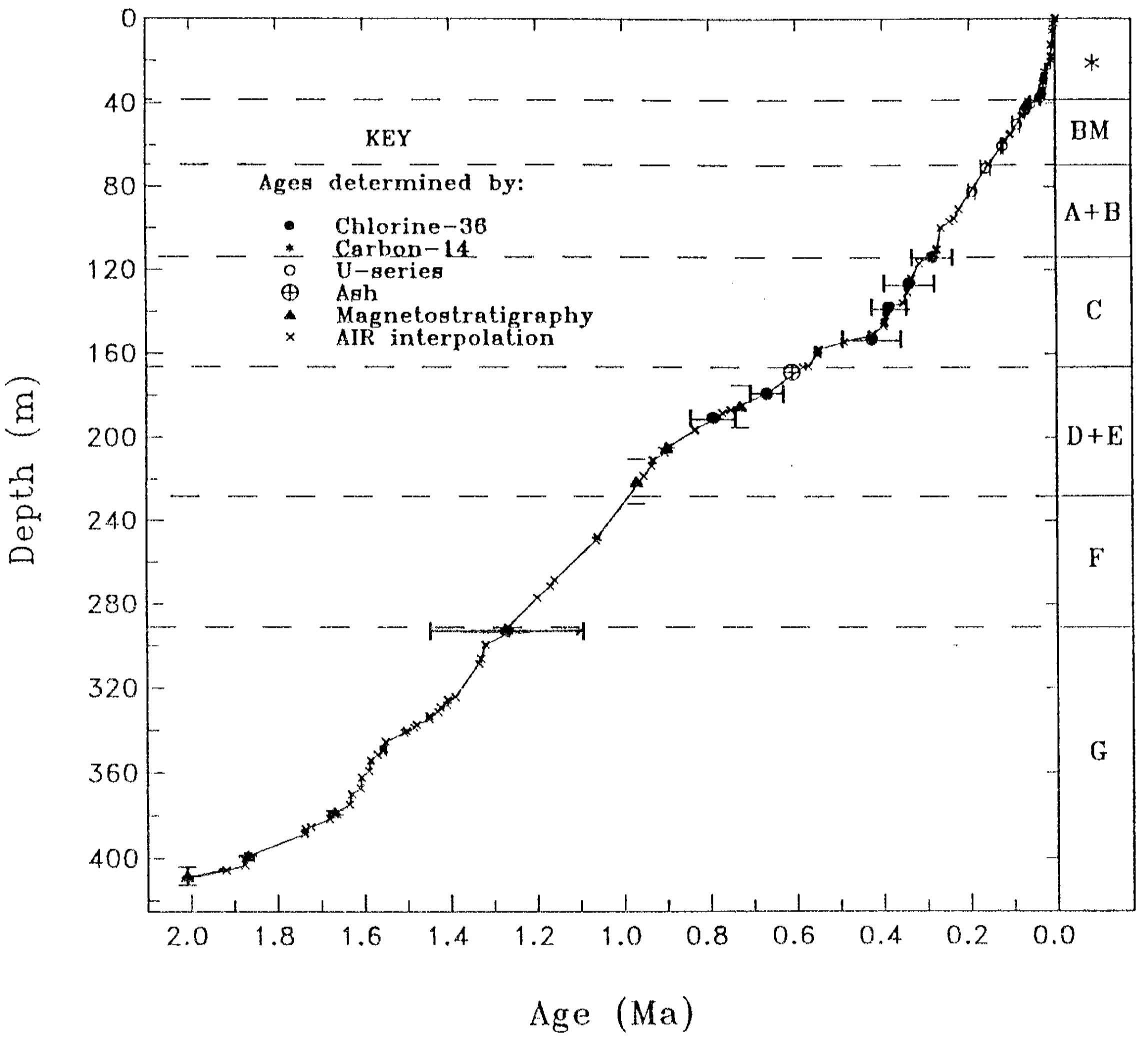

Figure 14. Chronology for the KM-3 core, Searles Lake. Ages determined by radiometric and paleomagnetic methods, and by an interpolation method using the mass accumulation of acid-insoluble residue (AIR). Ages determined by radiometric methods as shown in Figure 11. Units described in Table 1, abbreviations on Figure 12.

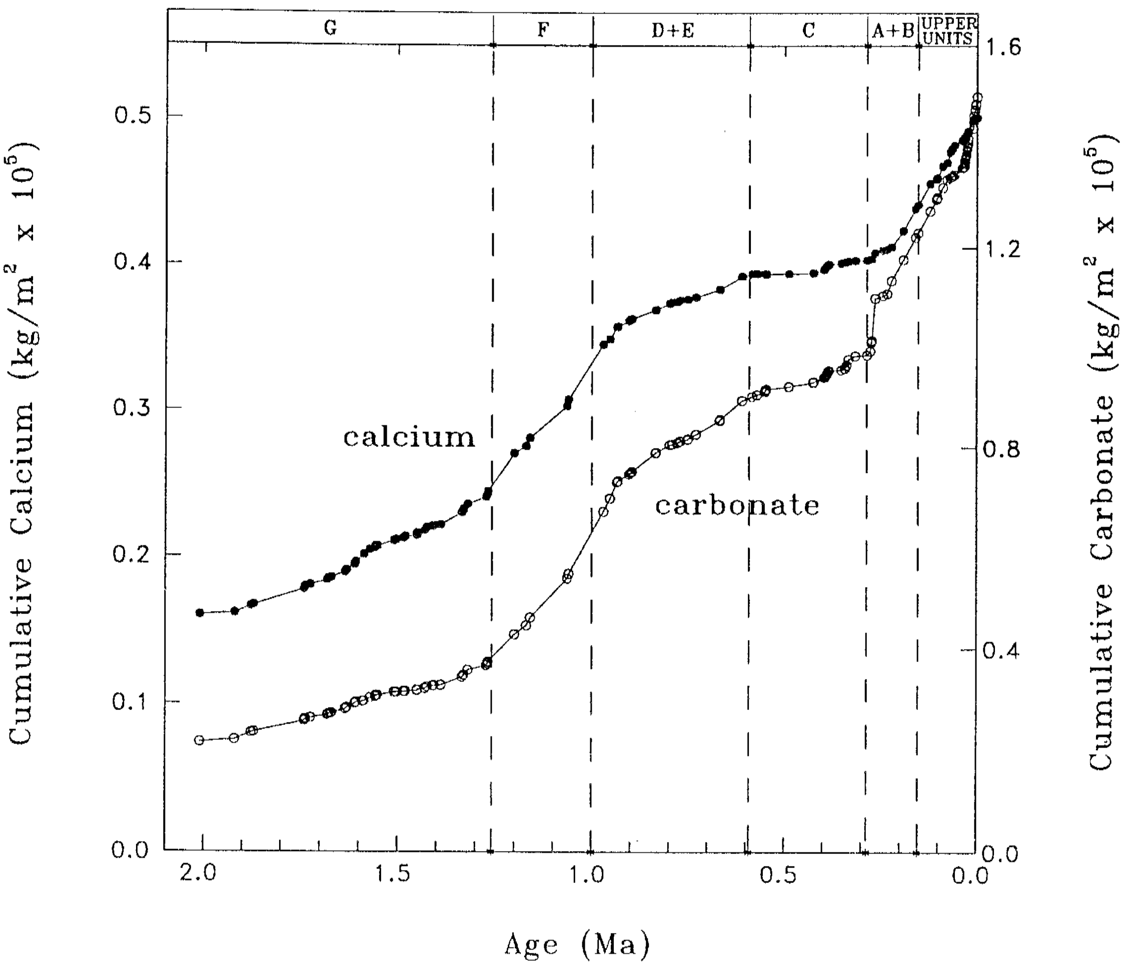

Figure 15. Mass accumulation of calcium and carbonate in the KM-3 core for the past 2.0 Myr. Units described in Table 1, abbreviations on Figure 12.

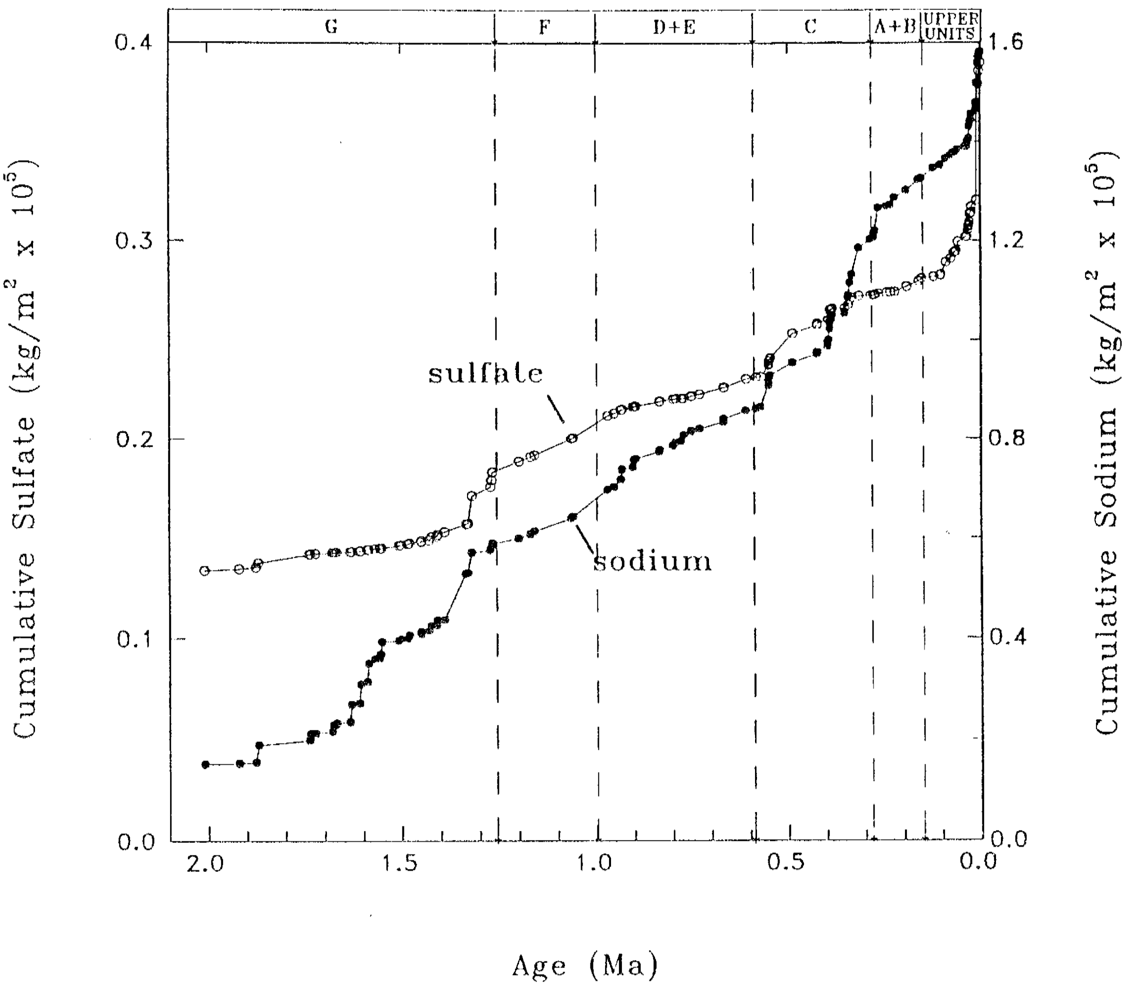

Figure 16. Mass accumulation of sodium and sulfate in the KM-3 core for the past 2.0 Myr. Units described in Table 1, abbreviations shown on Figure 12.

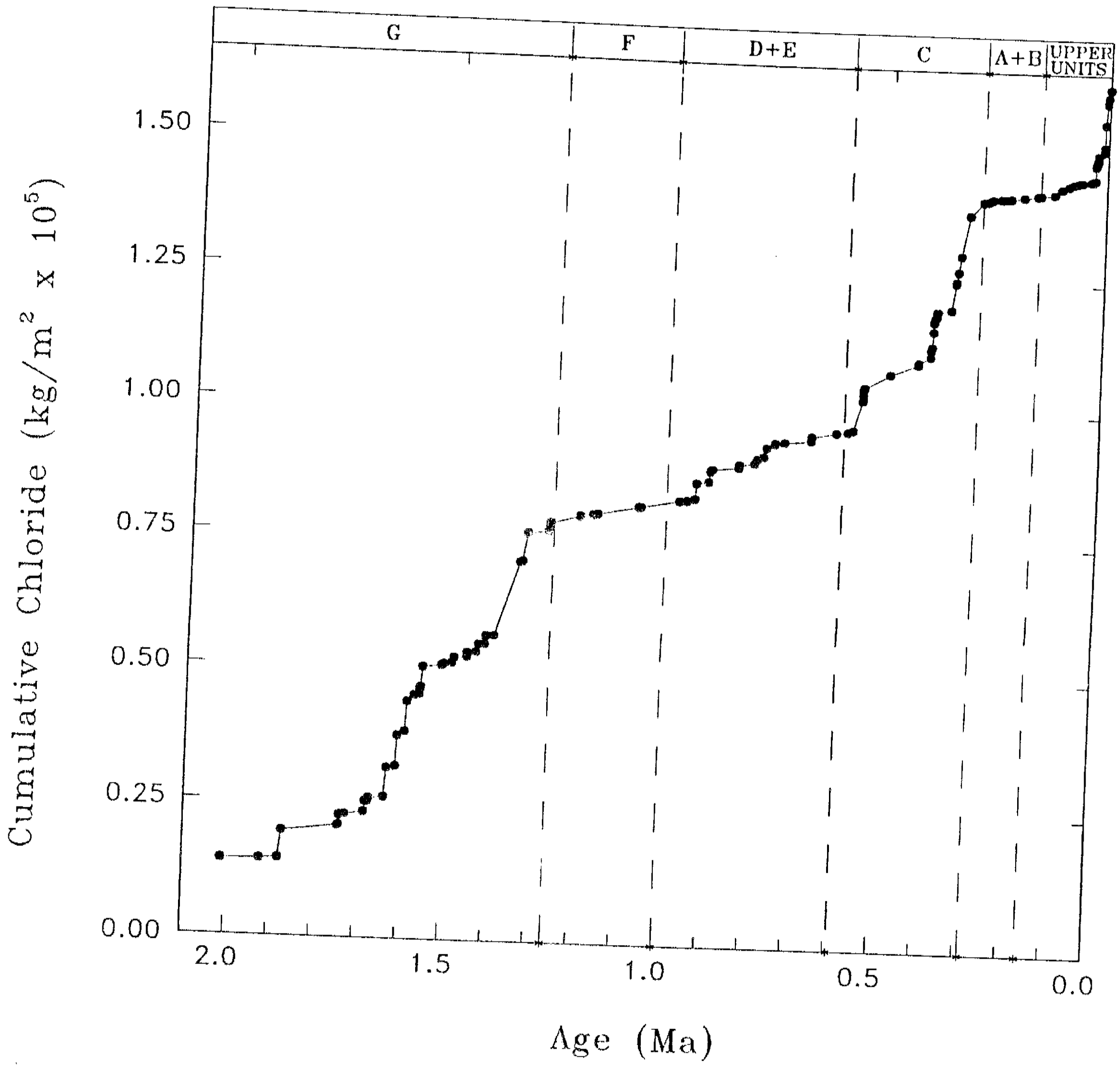

Figure 17. Mass accumulation of chloride in the KM-3 core for the past 2.0 Myr. Units described in Table 1, abbreviations shown on Figure 12.

and sulfate are quite different from the calcium and carbonate curves. The contrast is due to the solubilities of the elements.

Calcium carbonate minerals are relatively insoluble; therefore, calcium has a short residence time in the lake waters and a relatively constant rate of deposition in the sediments. Thus, it is no coincidence that the calcium accumulation curve resembles that for AIR. The similarity between the two tends to validate the AIR-interpolation procedure.

On the other hand, chloride, sodium, sulfate, and some of the carbonate form relatively soluble minerals and thus tend to be stored in the lake waters until they are precipitated during episodes of low lake level or desiccation. Their accumulation rates, therefore, show a characteristic stair-step pattern (Figs. 15, 16, 17).

Chloride is of particular interest because it stays in solution until the lake is close to desiccation due to its high solubility. If the chloride input rate has remained constant, then a mass balance on the chloride can yield information on the lake overflow history. Evidence for relative constancy in the input of dissolved solids, especially chloride, can be found in the relative constancy of the AIR, calcium and carbonate accumulations (Figs. 13, 15). Further support comes from examining the rate of chloride accumulation during periods when Searles Lake was apparently the terminus of the river system. For example, during the period from 1.7 to 1.55 Ma (Unit G of the Mixed Layer, Fig. 17), the lake level fluctuated rhythmically about a fairly low baseline producing a very regular stair-step pattern. Another example is the period from 0.04 to 0.01 Ma (Lower Salt to Parting Mud), for which independent evidence indicates that Searles Lake was the river terminus, except for relatively brief overflows to Panamint Valley (which does not contain halite of these ages). For the first period, the chloride accumulation rate was 0.20 kg m^{-2} yr^{-1}, and for the second, 0.18 kg m^{-2} yr^{-1}. The similarity of these rates, separated in time by 1.5 Myr, is further evidence for the relative constancy of the chloride input. I conclude that it is highly unlikely that the stair-step-like deposition pattern of sulfate, sodium, and chloride is a result of input variations. Smith (1976) also concluded that the chloride load of the Owens River over the past 20 kyr was constant (approximately 5.9×10^6 kg yr^{-1}).

The modern rate of 5.9×10^6 kg yr^{-1} can be compared to a reconstructed rate of input. The reconstructed rate is calculated based on the chloride accumulation rate determined above. First, the fraction of the Upper Salt chlorine contributed in one year is calculated

$$\frac{Cl_{ac}}{Cl_T/\text{unit}} = \text{fraction of Upper Salt Cl yr}^{-1} \qquad (14)$$

where Cl_{ac} is the average chloride accumulation rate (at KM-3, 0.19 kg m^{-2} yr^{-1};), and Cl_T/unit is the total chloride per unit area in the Upper Salt (at KM-3, 0.12×10^5 kg m^{-2}; Fig. 17). The fraction of Upper Salt chloride contributed in one year would be equal to 1.5×10^{-5} yr^{-1}. This portion of the Upper Salt chloride attributed to one year is then multiplied by the total chloride in the Upper Salt:

$$(\text{fraction of Upper Salt Cl yr}^{-1}) \times (Cl_T) = Cl_T \text{ yr}^{-1} \qquad (15)$$

where Cl_T, the total chloride in the Upper Salt, is 448×10^9 kg (Smith, 1979). Thus, the reconstructed annual input would equal 6.7×10^6 kg yr^{-1}. This value is quite similar to the value (5.9×10^6 kg yr^{-1}) presented by Smith (1976). The agreement of the measured value and the reconstructed value is support for the constancy of chloride input.

If Searles Lake had always been the terminus of the river system, and given an average chloride input of 0.19 kg m^{-2} yr^{-1} (at the location of KM-3), the total chloride accumulation over the past 2.0 Myr (425 m depth) should have totaled 3.85×10^5 kg m^{-2}. Instead, the total accumulation is only 1.63×10^5 kg m^{-2} (Fig. 17). The intervals of "missing" chloride can be identified by drawing lines representing a constant 0.19 kg m^{-2} yr^{-1} input rate on the stair-step pattern sections of the accumulation curve (when Searles Lake was the terminus) in Figure 18. Two episodes of inferred chloride loss, indicated by long, subhorizontal slopes, can be seen in the intervals 1.3 to 0.95 Ma and 0.30 to 0.03 Ma. The most plausible mechanism of loss is overflow from Searles Lake into downstream basins. The chloride deficit is not attributed to deposition in upstream basins as cores in these basins reveal no layers of salt in the upper several hundred meters, except for the top 1 m of Owens Lake. (Fig. 4C).

Sedimentation Rates

The chronology of the KM-3 core presented in this study (Fig. 14) is based on ages determined by ^{36}Cl, ^{14}C, U-series, magnetostratigraphy, correlation with the Lava Creek B ash, and interpolation methods.

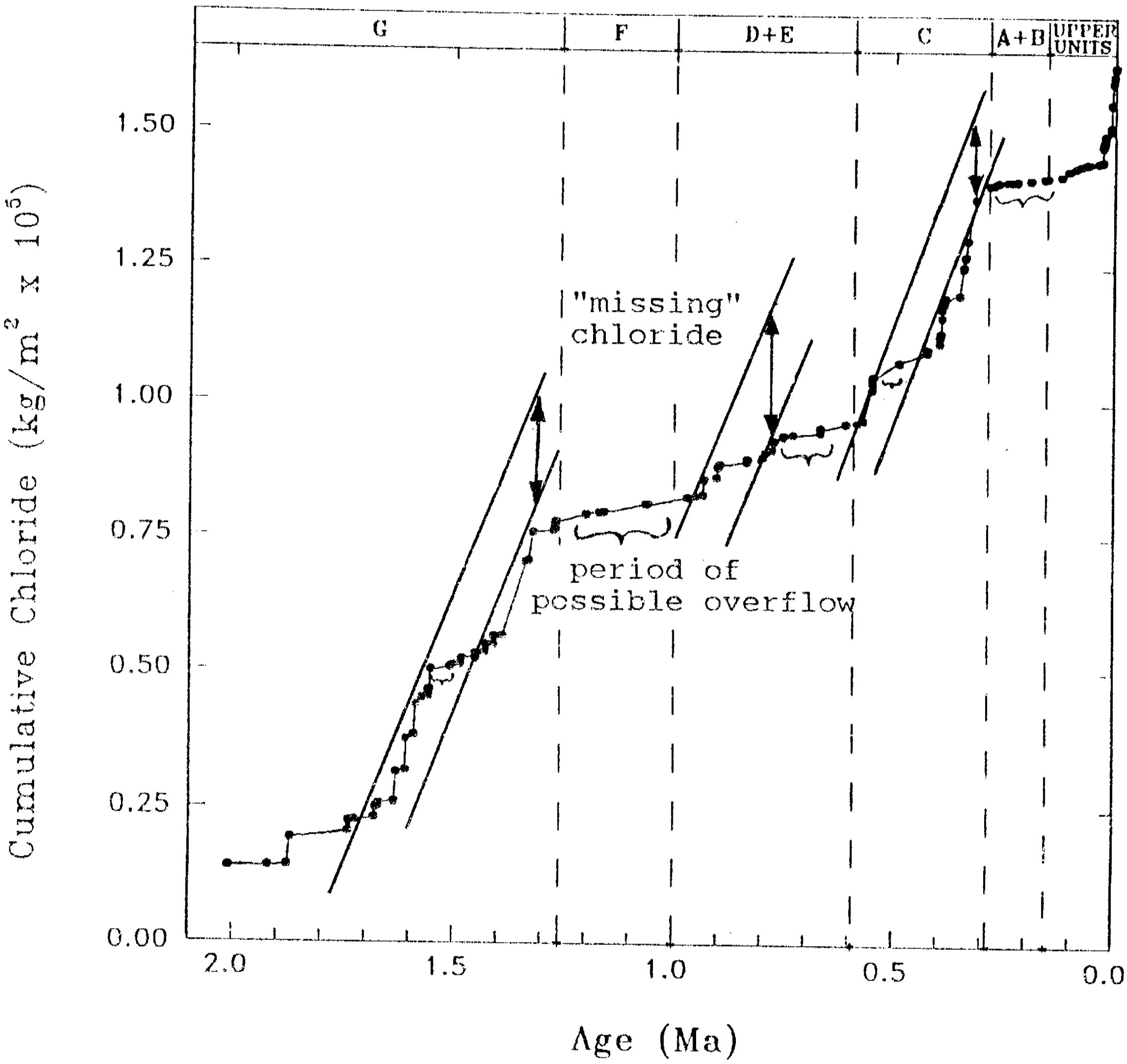

Figure 18. Chloride accumulation curve for the KM-3 core showing intervals in which possible overflow to downstream basins occurred (brackets), with subsequent loss of chloride from the accumulation curve (arrows). An average accumulation rate of 0.19 kg m^{-2} yr^{-1} is inferred. Units described in Table 1, abbreviations shown on Figure 12.

Ages for the unit boundaries and sedimentation rates are presented in Table 6 along with those from Smith and others (1983) for comparison. The largest relative differences are seen in the ages reported for the boundaries between the Bottom Mud and Unit A+B, and between Units A+B and C. In this study, the age for the A+B/C boundary is based on a ^{36}Cl date. The age for the Bottom Mud/A+B boundary is determined by AIR interpolation between U-series dates. Interpolation of ages between dated horizons is based on the AIR-accumulation rate, which fluctuated through time but was fairly constant for long periods (Fig. 13). Thus, a change in slope is inferred to reflect a change in the nature of the sediments.

The chronology for the KM-3 core is presented as a curve in Figure 19. The stair-step pattern characteristic of Units C and G indicates abrupt changes in relatively short time intervals, whereas the more linear patterns of Unit F and the Bottom Mud show a fairly consistent trend for long periods. The apparent rate of deposition is estimated by linear regression. An average apparent rate of sedimentation for the past 2.0 Myr is 20 cm/1000 yr (Fig. 20). A more detailed discussion of the sedimentation rates for each unit follows.

Unit G. Several segments of the age curve in Unit G show a distinct stair-step pattern (Fig. 21). This pattern reflects the nature of the unit -- 134 m of alternating beds of mud and salines which range in thickness from 2 to 10 m. Most of the muds are green, some are distinctly bedded. The salines are dominated by halite which is coarse grained. The apparent sedimentation rate (average) of the salines is about 100 cm/1000 yr, and for the muds, about 15 cm/1000 yr. The

Table 6. Comparison of unit boundary ages and sedimentation rates in core KM-3.

Stratigraphic unit	Depth to base (m)	Age of base (Ma) (Smith and others, 1983)		Age of base (Ma) (this study)	Sedimentation rate (cm/1000 yr) (Smith and others, 1983)	Sedimentation rate (cm/1000 yr) (this study)
Overburden Mud	5.8	0.006		0.006	..	100
Upper Salt	19.9	0.010		0.010	>26	350
Parting Mud	25.0	0.024		0.024	26-42	36
Lower Salt	37.9	0.032		0.0388	>26	130
Bottom Mud	69.0*	0.13		0.1538	22	32
Mixed Layer						
Unit A+B	114.0	0.31		0.286	..	33
Unit C	166.4	0.57		0.584	..	28
Unit D+E	227.7	1.00		0.992	}	14
Unit F	291.1	1.28		1.270	}	21
Unit G	425.5	2.04		..	} 21	18 (to 2.0 Ma)
Unit H	541.6	2.56		..	}	..
Unit I	693.4	3.18		..	}	..
Alluvial sand and gravel	915.5	?	..	..		
Bedrock	929.6	..	..	..		
Overall					22	20

* Depth in core 289M, 150 m north of KM-3 (Smith and others, 1983).

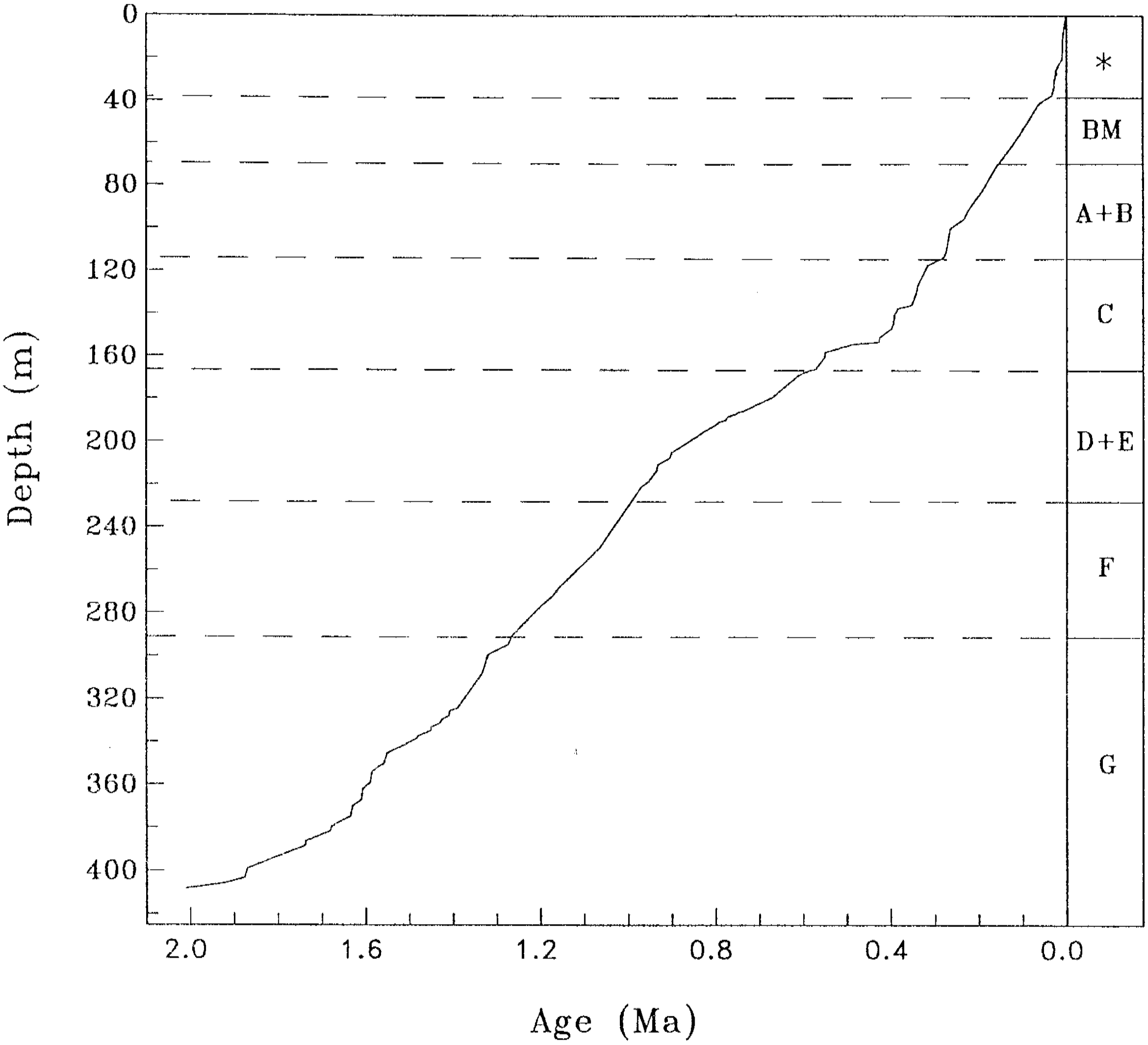

Figure 19. Chronology curve for the KM-3 core, Searles Lake. Data points not visible in order to show configuration of curve. Units described in Table 1, abbreviations shown on Figure 12.

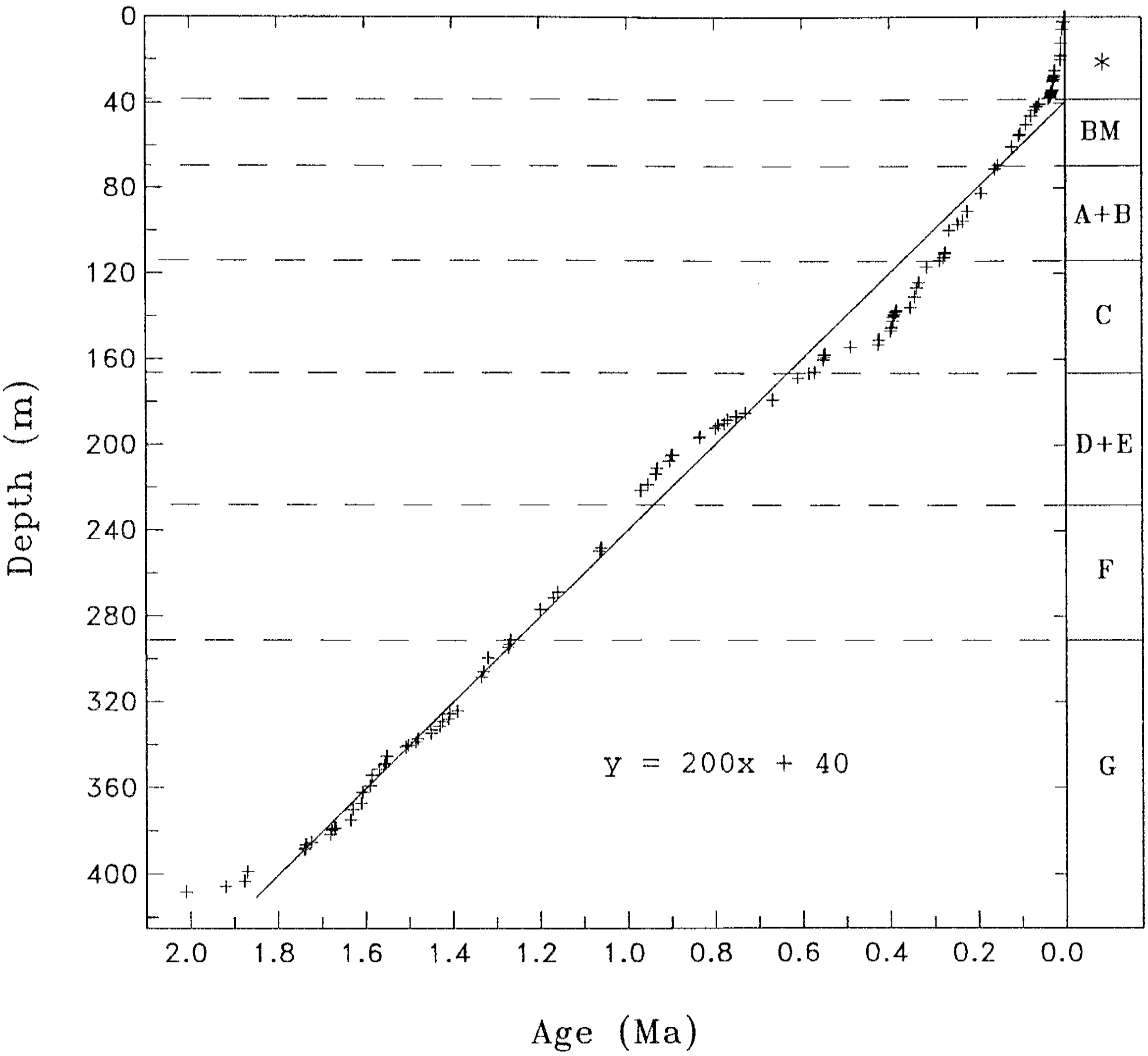

Figure 20. Linear regression of age versus depth data shows an average apparent sedimentation rate of 20 cm/1000 yr for the past 2.0 Myr. Units described in Table 1, abbreviations shown on Figure 12.

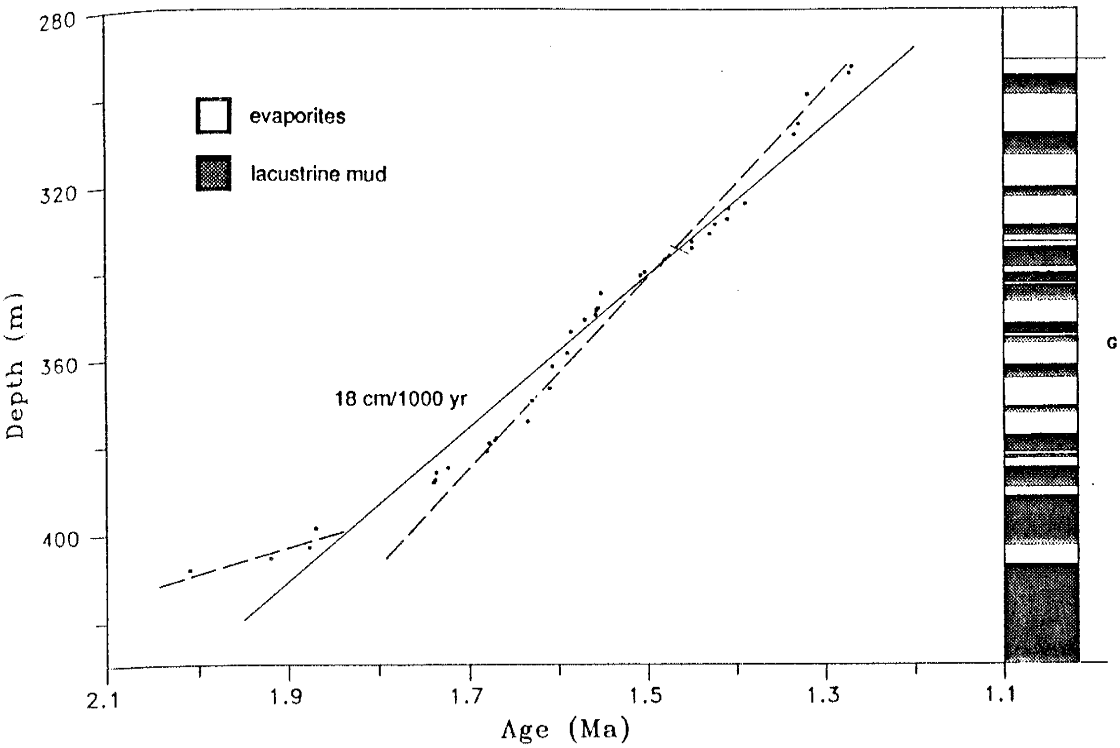

Figure 21. Plot of age versus depth for Unit G of the Mixed Layer (in the KM-3 core). The average apparent sedimentation rate is 18 cm/1000 yr (solid line). Slopes depicted by dashed lines are discussed in text.

average sedimentation rate for Unit G, from 2.0 to 1.27 Ma, is 18 cm/1000 yr. However, there is a distinct change in slope at about 1.75 Ma, which marks the beginning of the stair-step pattern. Before the slope change (2.0 to 1.75 Ma), the apparent sedimentation rate is 6 cm/1000 yr; after the change (1.75 to 1.27 Ma), the rate is 20 cm/1000 yr (Fig. 21, dashed lines).

Unit F. The linear regression for data in Unit F results in a correlation coefficient of 0.99. It is inferred that the sediment accumulated fairly consistently at an apparent rate of 21 cm/1000 yr (Fig. 22). The constant slope indicates there is very little change in the depositional environment. The nature of the F Unit supports this -- over 63 m of massive mud which contains significant amounts of dolomite and pirssonite. The dolomite averages 15% of the total composition and the pirssonite averages 20% (Smith and others, 1983).

Unit D+E. Unit D+E is mostly comprised of muds with some interbedded saline layers. Most of the muds are brown and massive. The saline layers are mostly halite with mud impurities. The thickness of Unit D+E is 61 m. The apparent sedimentation rate is 14 cm/1000 yr (Fig. 23). A subdued stair-step pattern is evident from 970 to 900 ka, indicating the interbedded nature of this section of the unit. There appears to be a slope break at 900 ka. The sedimentation rate for 970 to 900 ka is 25 cm/1000 yr, and for 900 to 600 ka the rate is 12 cm/1000 yr (Fig. 23, dashed lines). The Lava Creek B ash (610 ka) is found neat the top of this unit.

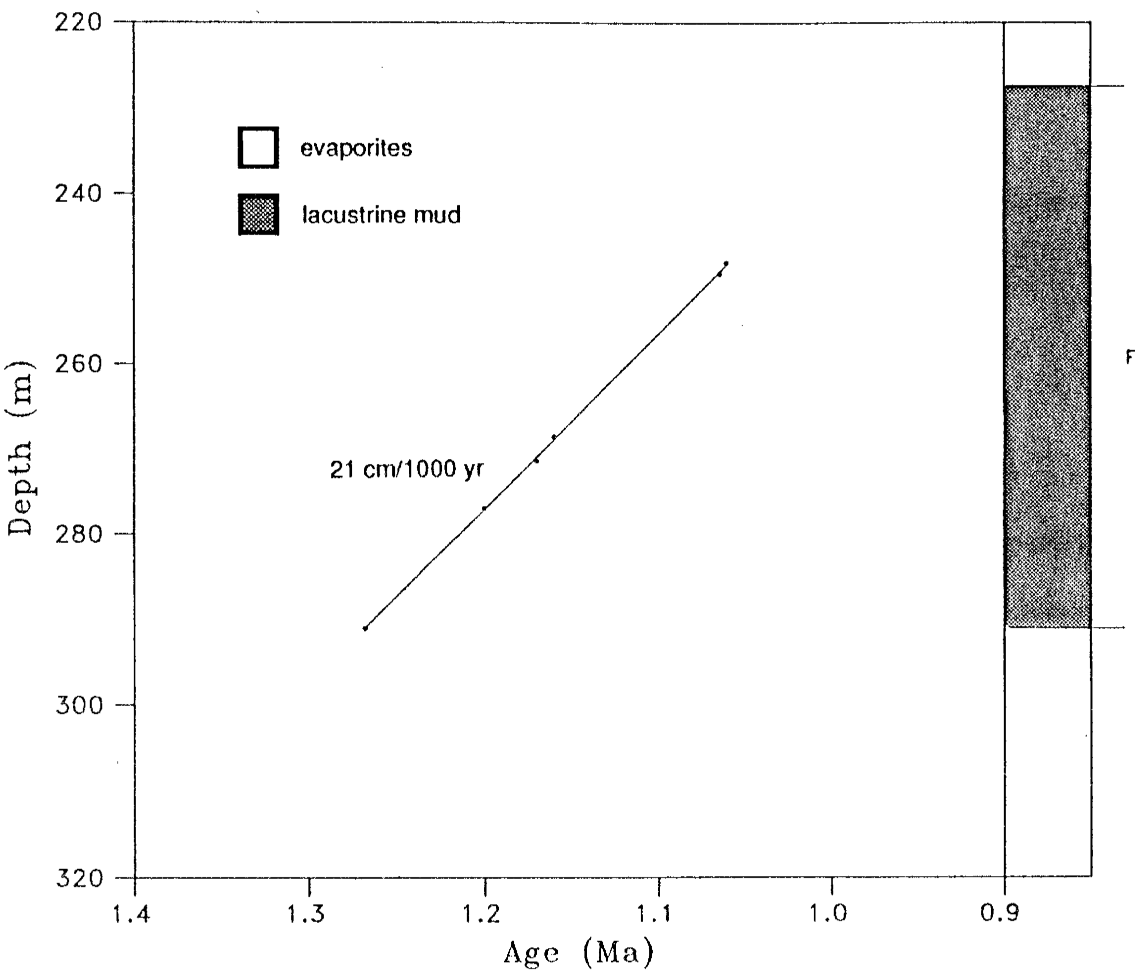

Figure 22. Plot of age versus depth for Unit F of the Mixed Layer (in the KM-3 core). The average apparent sedimentation rate is 21 cm/1000 yr.

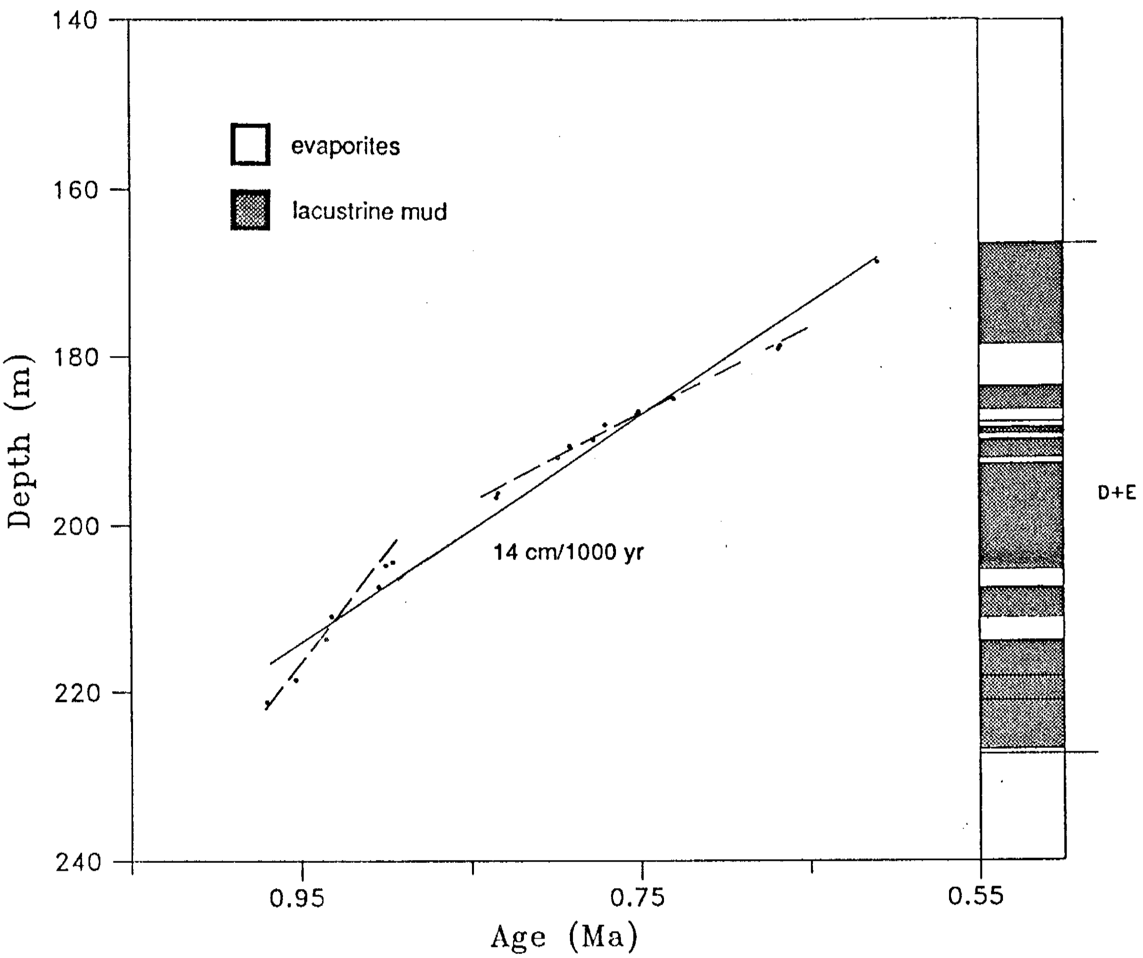

Figure 23. Plot of age versus depth for Unit D+E of the Mixed Layer (in the KM-3 core). The average apparent sedimentation rate is 14 cm/1000 yr (solid line). Slopes depicted by dashed lines are discussed in the text.

Unit C. Unit C is a 52-m interval comprised of salines with interbedded thin mud layers. Halite dominates the saline units; most of the muds are dark brown. The apparent rate of deposition is 15 cm/1000 yr (Fig. 24). However, the age curve for Unit C has two segments which exhibit a distinct stair-step pattern, similar to that observed in Unit G (Fig. 21). The apparent sedimentation rate for these segments is 28 cm/1000 yr. They are separated by an interval (550 to 420 ka) exhibiting a subhorizontal slope with a sedimentation rate of 4 cm/1000 yr (Fig. 24, dashed lines).

Interval 550 to 420 ka. Low sedimentation rates observed in core KM-3 are usually associated with intervals of mud deposition suggesting deep perennial lakes. The lowest sedimentation rate calculated from the Searles Lake chronology is for the interval 550 to 420 ka, which is not associated with a thick massive mud sequence. Two possible factors may have contributed to this anomalously low rate. First, the subhorizontal slope may be due to lack of absolute age control for the overlap point of the slopes in Units C and D+E. The largest change in slope of the age curve is near the boundary of Units C and D+E. This is predominantly due to the nature of the sediments comprising each unit. Degree of compaction may also influence the slope change. It seems most likely that the slope change should occur at the boundary of Units C and D+E (166.4 m). However, the actual position of the slope change is problematic. The age of the boundary reported in this study (584 ka) is controlled by the correlation of a volcanic ash layer found near the top of Unit D+E (168.6 m) with the Lava Creek B tephra (610 ka), and by a ^{36}Cl age of a saline layer from the lower portion of Unit C (153 m, 426 ka). The age of the C/D+E boundary

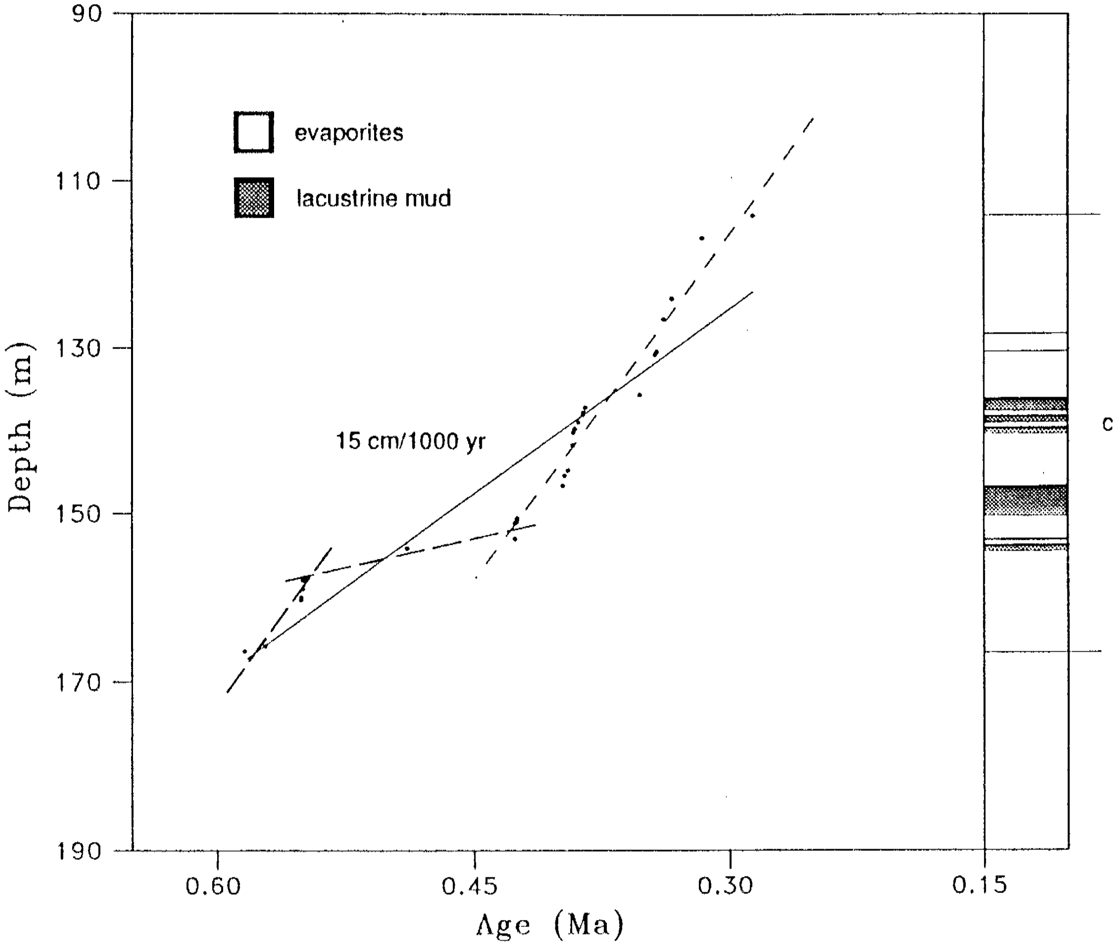

Figure 24. Plot of age versus depth for Unit C of the Mixed Layer (in the KM-3 core). The average apparent sedimentation rate is 15 cm/1000 yr (solid line). Slopes depicted by dashed lines are discussed in the text.

is determined by extrapolating the slope calculated by linear regression of the ages in Unit D+E. Ages for the sediments between 166.4 to 153 m in basal C are then interpolated based on the AIR-accumulation rate, as discussed previously. The slope for the lowest section of Unit C (166.4 to 157.5 m) is fairly steep, reflecting the basal unit of massive, nearly pure halite (Fig. 24). The next section (between 157.5 and 153 m) exhibits the subhorizontal slope in question. This interval corresponds to a section of Unit C which is composed of salines with thin interbedded mud layers. However, the muds comprise only 0.34 m of the section. The low estimated sedimentation rate is possibly a consequence of the lack of age control on the C/D+E boundary. Thus, the length of the interval may, in a sense, be the result of graphically depicting a slope change based on interpolated ages.

On the other hand, the anomalously low sedimentation rate may truly reflect the depositional environment. Since the muds comprise less than 1% of the sediment accumulation, perhaps the low apparent rate is, in fact, related to the periods of evaporite deposition. Examination of the core log reveals that the evaporites consist mostly of halite, thenardite and trona. Smith (1979) suggested that the occurrence of this mineral suite can possibly reflect deposition in a shallow to dry lake (playa) environment. Jones (1965) suggested that thenardite is a major constituent of the saline crusts in the Deep Springs Lake playa. Thus, the low value may possibly reflect a sedimentation rate characteristic of playa conditions. However, under present playa conditions (represented by the Overburden Mud), the average sedimentation rate is about 100 cm/1000 yr (Smith and others, 1983). In the KM-3 core, a rate of this magnitude would usually reflect saline deposition. Yet, the calculated mean composition of the Overburden Mud shows that clastics and other fine-grained minerals account for 83% of the total volume (Smith, 1979). This anomalously high sedimentation rate for a unit with high clastic content is possibly due to floods which can carry large amounts of sediment into the center of the playa. On the other hand, the exceptionally low deposition rate of interval 550 to 420 ka could be attributed to an extensive but shallow lake in a semiarid climate where relatively little sediment was carried into the lake. Sediment that did enter the lake was trapped near the lake shoreline.

Finally, the long interval with the low sedimentation rate may be due to a combination of the factors discussed above.

Unit A+B. Unit A+B, which is 45 m thick, exhibits an apparent sedimentation rate of 33 cm/1000 yr (Fig. 25). The AIR-interpolated ages provide detail on the configuration of the curve for the lower half of the unit. However, due to core loss, much of the upper section of A+B is not represented in KM-3. Therefore, chemical analyses are not available, and the age curve is constructed based on two U-series dates from Bischoff and others (1985). In a nearby core (289M), layers assigned to Unit A+B are composed of numerous layers of interbedded salines and muds. The muds are typically massive except for the mud at the base of Unit A which is laminated. Saline units are mostly monomineralic, composed of either halite or trona (Smith and others, 1983).

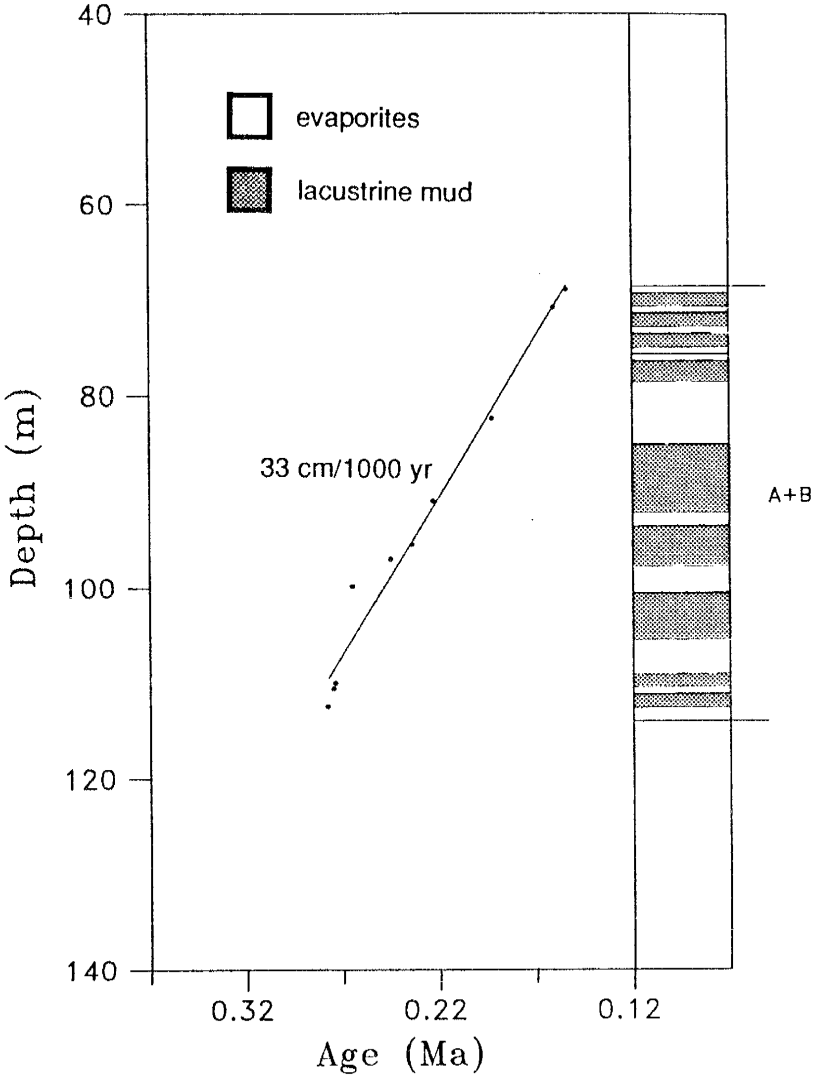

Figure 25. Plot of age versus depth for Unit A+B of the Mixed Layer (in the KM-3 core, as reconstructed from a nearby core, 289M). The average apparent sedimentation rate is 33 cm/1000 yr.

Upper Units. The less compacted upper units (total thickness, 69 m) that overlie the Mixed Layer exhibit higher apparent rates of sedimentation. The Bottom Mud, which is massive to thin-bedded, was deposited at a fairly consistent rate of 32 cm/1000 yr (Fig. 26). The steady accumulation is similar to that exhibited in Unit F. The average rate from the base of the Lower Salt to the surface is about 100 cm/1000 yr. Rates for the individual units are as follows: Lower Salt (salines interbedded with mud), 130 cm/1000 yr; Parting Mud (olive gray mud, finely laminated to massive), 36 cm/1000 yr; Upper Salt (mostly salines that are dominated by halite and trona), 350 cm/1000 yr; and Overburden Mud (discontinuous beds of salines and muds, oxidized near the surface), 100 cm/1000 yr (Fig. 27).

The average rates of deposition for each of the units in the KM-3 core are summarized in Figure 28.

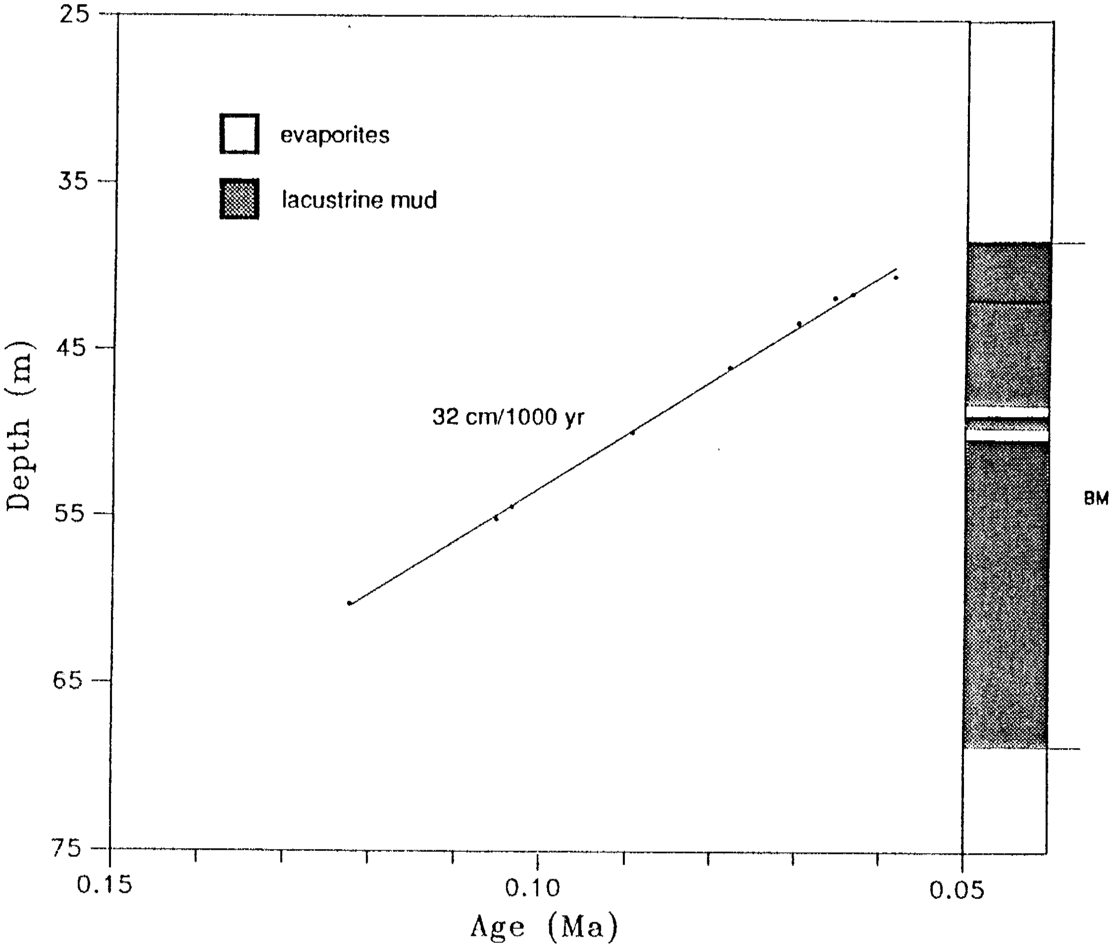

Figure 26. Plot of age versus depth for the Bottom Mud (BM) in the KM-3 core. The average apparent sedimentation rate is 32 cm/1000 yr.

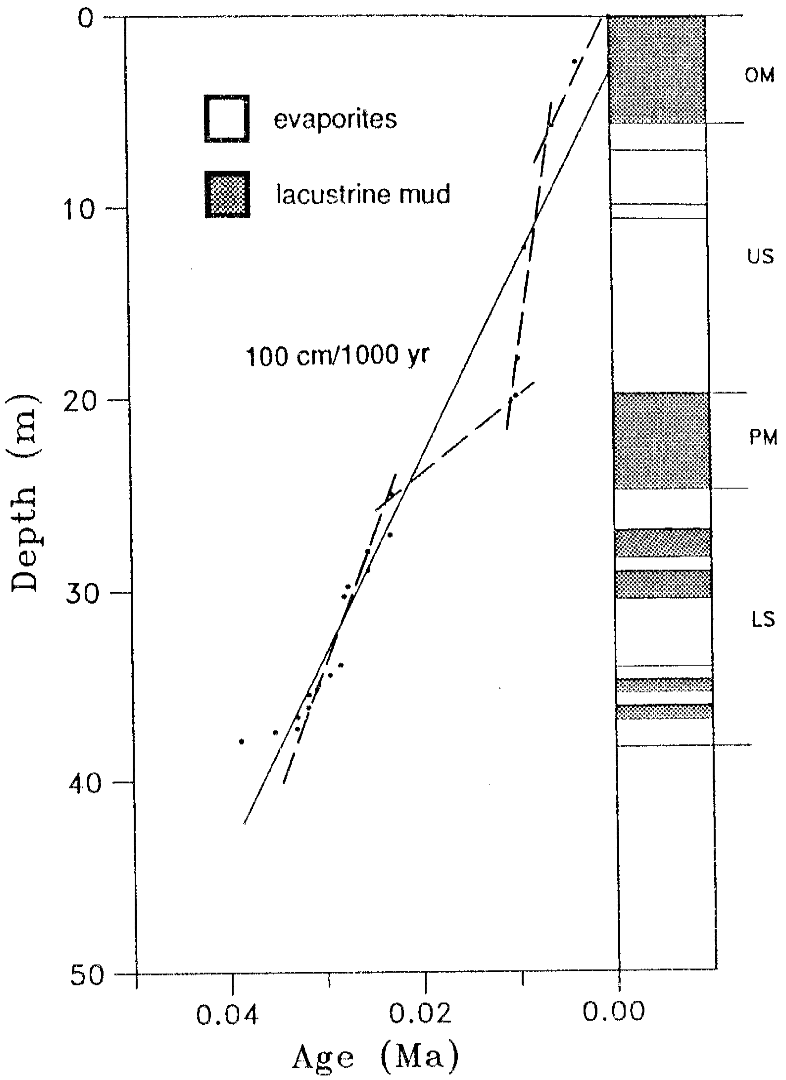

Figure 27. Plot of age versus depth for the units that overlie the Bottom Mud in the KM-3 core: LS - Lower Salt, PM - Parting Mud, US - Upper Salt, OM - Overburden Mud. The average apparent sedimentation rate from the base of the Lower Salt to the surface is 100 cm/1000 yr (solid line). Dashed lines are for slopes of the individual units as discussed in the text.

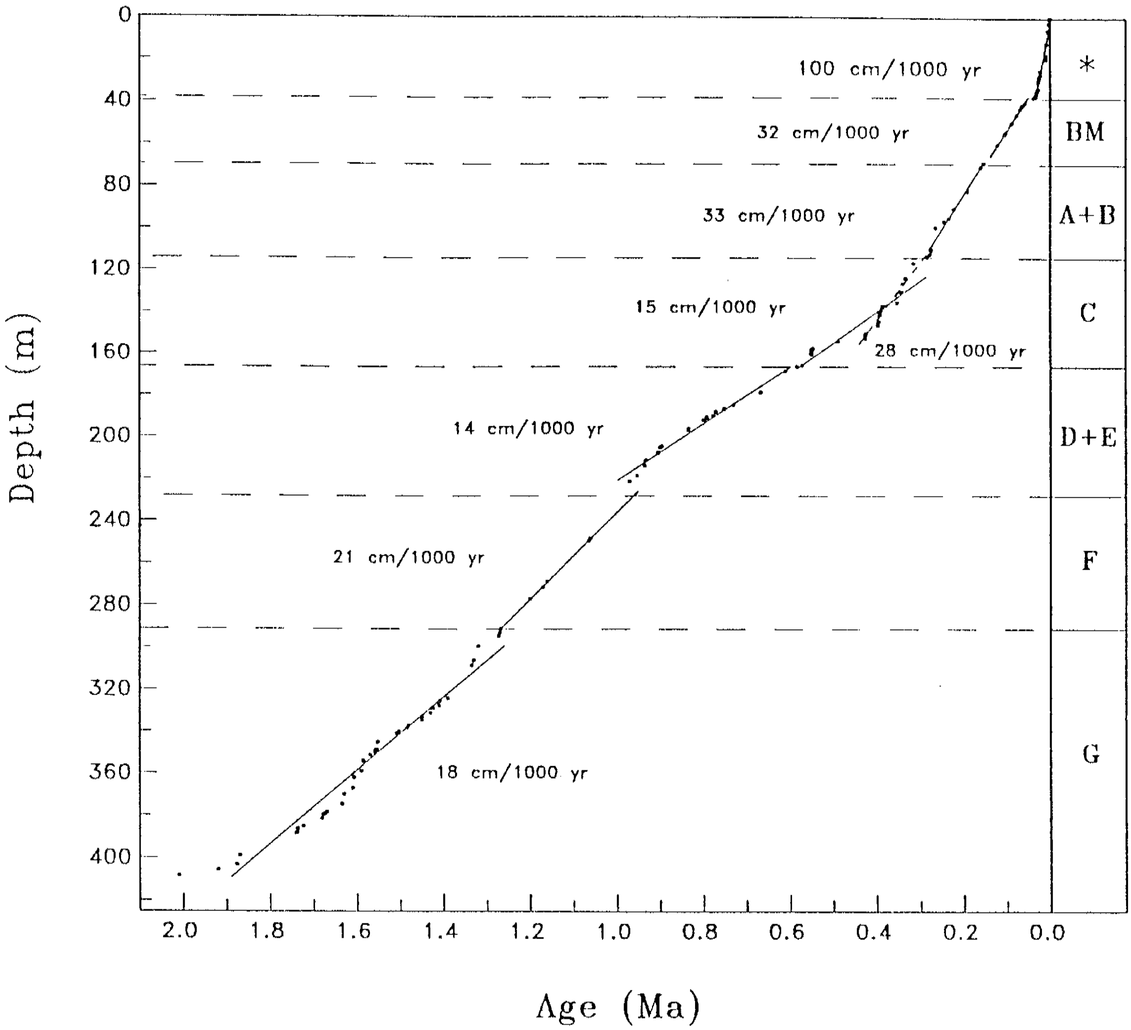

Figure 28. Plot of age versus depth for the past 2.0 Myr (in the KM-3 core) showing the average sedimentation rates for each of the units. Units G, F, D+E, C, and A+B are from the Mixed Layer. BM refers to the Bottom Mud. (*) refers to the units that overlie the Bottom Mud: Lower Salt, Parting Mud, Upper Salt and Overburden Mud (bottom to surface).

MODERN WATERS AND SURFICIAL EVAPORITES

Owens Valley

Waters. The measured $^{36}Cl/Cl$ ratios for thermal springs, runoff and an artesian well in the Owens watershed are plotted versus distance from the headwaters of the Owens River (Fig. 29). The $^{36}Cl/Cl$ value for precipitation (meteoric input) at the headwaters is shown as a range, derived from the estimates determined by Bentley and Davis (1982). The $^{36}Cl/Cl$ ratios of surficial salines from Warren and Owens Lake beds, and the Upper Salt beneath Searles Lake are included. The measured ratios were presented in Table 4, and the sample locations were shown in Figure 5. As discussed previously, the $^{36}Cl/Cl$ ratio measured for the Upper Salt from beneath Searles Lake is 56×10^{-15}.

In the paleo-Owens closed-basin drainage system, precipitation falling on the high altitude sections of the Sierra Nevada can be considered the initial input into the basin's hydrologic budget. Precipitation that becomes runoff is influenced by subsequent inputs, such as ground-water discharge, as it flows to the terminal sink. Water loss by evaporation was the major output in the ancestral Owens drainage system.

Precipitation falling on the Sierra Nevada thus contains what can be considered an initial $^{36}Cl/Cl$ ratio. The relative abundance of ^{36}Cl to stable chloride in the terminal sink will be different than the initial ratio. Figure 29 shows the evolution of the $^{36}Cl/Cl$ ratio in the Owens watershed from headwaters to Searles

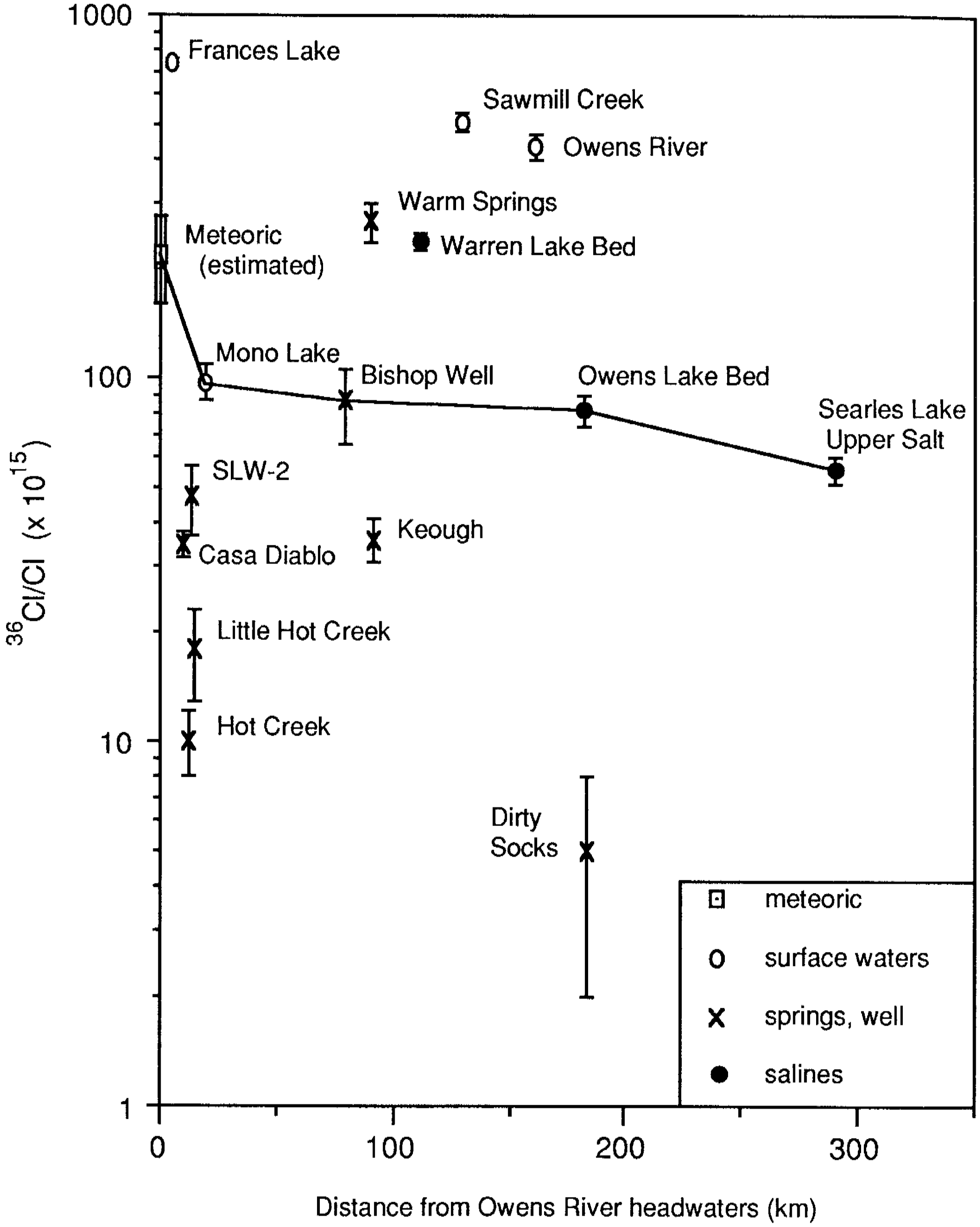

Figure 29. Plot of chlorine-36/chloride ratios of modern waters and surficial salines versus distance of the samples from the headwaters of the Owens River.

Lake, the usual terminal sink. Starting with an estimated range of values for meteoric input from 160 to about 280 x 10^{-15} $^{36}Cl/Cl$ (Bentley and Davis, 1982), the ratio is progressively lowered as the runoff travels to the terminal basin. This is due to numerous thermal springs in Owens Valley whose discharge is high in stable chloride but low in ^{36}Cl. This is illustrated in Figure 30 which shows the relationship between chloride concentration and the $^{36}Cl/Cl$ ratio for the thermal springs and surface-water samples. Most of the thermal springs have similar chloride concentrations (100 to 400 ppm) and $^{36}Cl/Cl$ ratios (10 to 50 x 10^{-15}). Dirty Socks hot spring, which is located on the southern edge of the Owens Lake playa, shows the lowest $^{36}Cl/Cl$ and highest chloride concentration of all the water samples except for high chloride concentration of Mono Lake. The position of Mono Lake to the right of the trend line is due to evaporation.

The samples inferred to reflect the evolution of the $^{36}Cl/Cl$ ratio are joined by a line in Figure 29. The low ^{36}Cl, high stable chloride, discharge of the thermal springs mixes with runoff, diluting the $^{36}Cl/Cl$ ratio. The effect of mixing is most clearly shown in Figure 31 which is a plot of $^{36}Cl/Cl$ ratio versus inverse chloride of Owens Valley waters downstream from Mono Lake. A mixing line (dashed) between the springs, the well, and the runoff upstream from the Owens River sample is shown. Evaporation and addition of epigene ^{36}Cl results in the value shown for Owens River. Runoff samples (Frances Lake, Sawmill Creek, Owens River) are inferred to contain at least some bomb-^{36}Cl. This inference is supported by the high tritium (TU) concentrations for the Sawmill Creek and Owens River samples (Fig. 32). Tritium concentrations over 10 TU indicate contamination by bomb-tritium. All

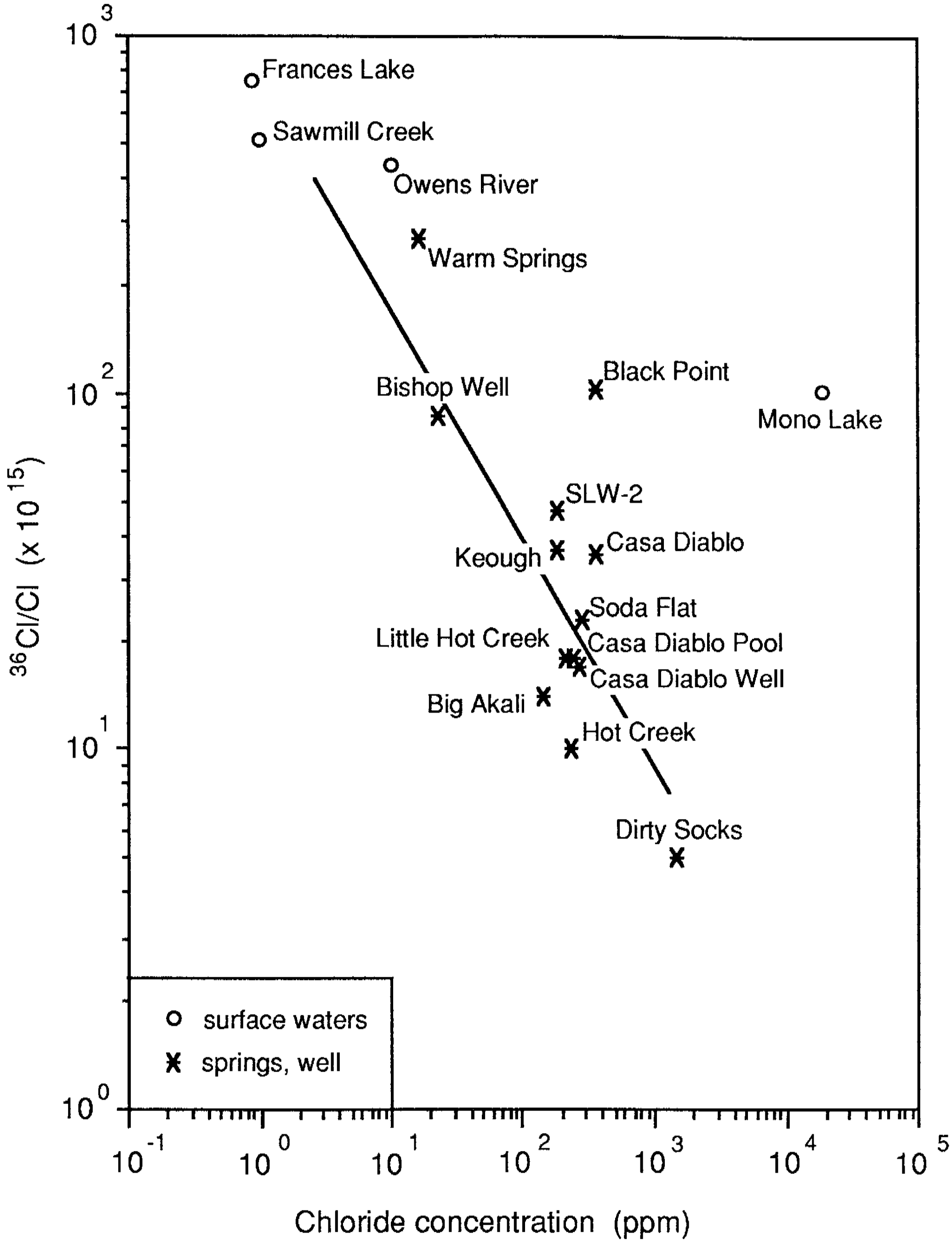

Figure 30. Plot of chlorine-36/chloride ratios of modern waters from the Owens Valley versus chloride concentration of the samples.

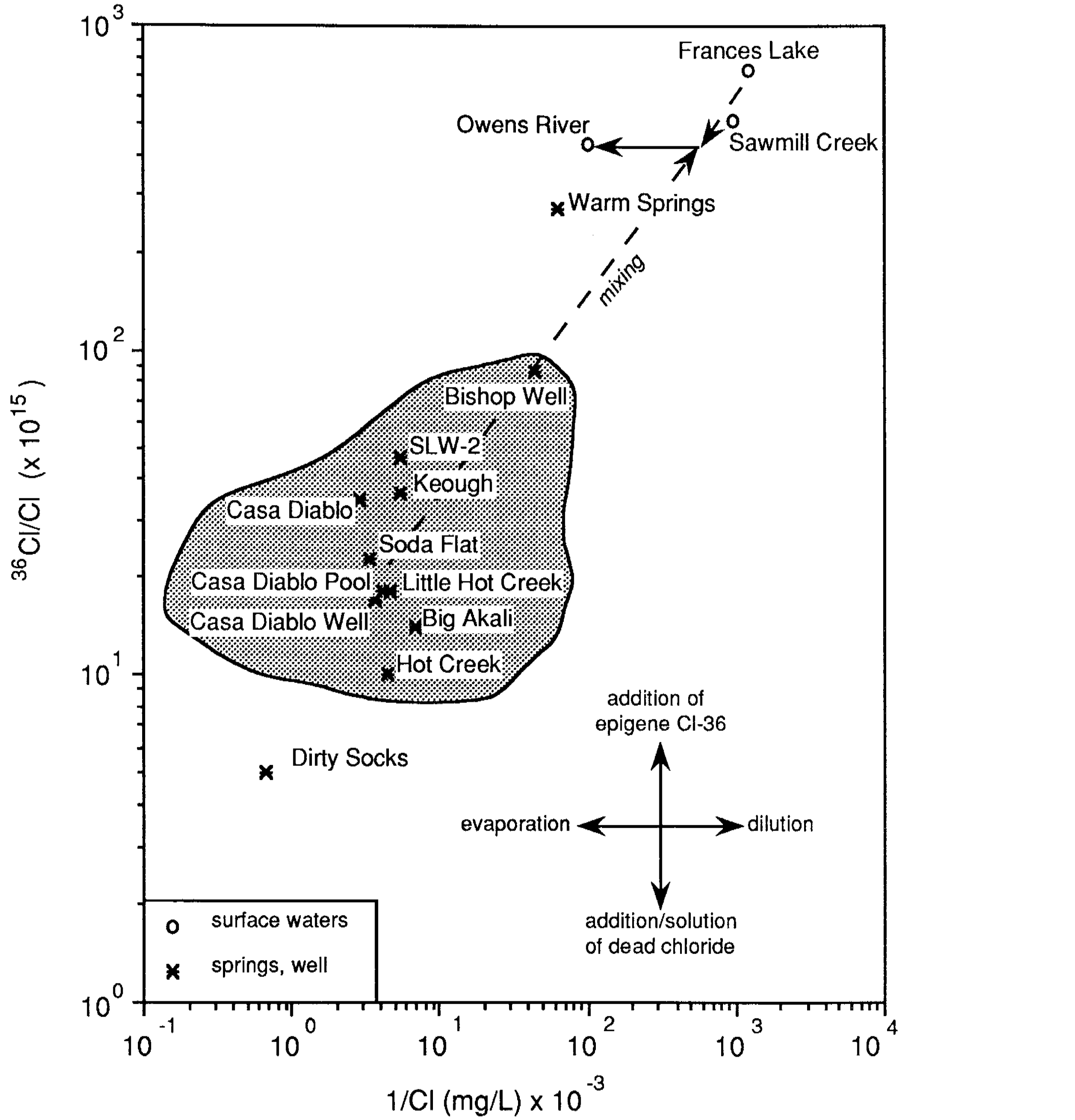

Figure 31. Plot of chlorine-36 ratios for modern waters from Owens Valley versus inverse chloride concentration for the samples

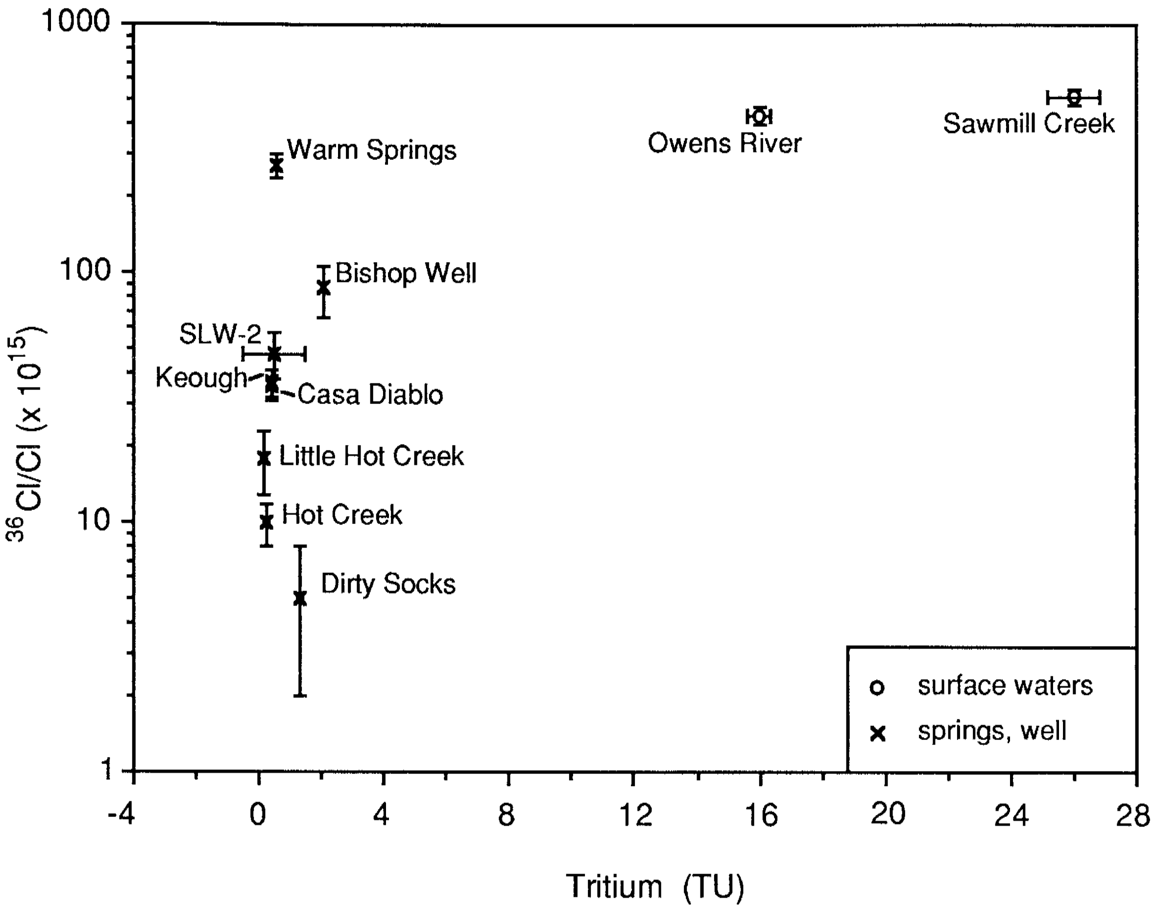

Figure 32. Plot of chlorine-36/chloride ratio of modern waters from Owens Valley versus tritium concentrations of the samples.

thermal spring samples, along with the Bishop well sample, show low tritium concentrations and low $^{36}Cl/Cl$ ratios suggesting that their discharges are not affected by bomb-produced ^{36}Cl or tritium at this time. The high $^{36}Cl/Cl$ ratios of Frances Lake, Sawmill Creek, Owens River, Warm Springs and Warren Lake probably reflect addition of small amounts of very high $^{36}Cl/Cl$ chloride produced by cosmic-ray reactions in rocks at high altitude and released by weathering. During the Pleistocene, Frances Lake waters (high altitude runoff near headwaters) probably reflected the initial input $^{36}Cl/Cl$ value.

The Warm Springs sample is the only thermal spring located on the east side of Owens Valley (Fig. 5). Its chloride concentration and $^{36}Cl/Cl$ ratio are distinctly different from the other thermal springs (Fig. 30). Warm Springs discharge is derived mostly from recharge in the White Mountains, whereas the discharge for the other thermal springs is derived from a more complex ground-water system (recharge from Sierra Nevada) as discussed previously.

In order to delineate the impact of spring discharge on the ^{36}Cl budget the ^{36}Cl concentration was calculated. Figure 33 is a diagram of the $^{36}Cl/Cl$ ratios of Owens Valley water samples plotted against their ^{36}Cl concentration. Usually, on a diagram such as this, evolution pathways can easily be detected. However, with higher ^{36}Cl concentrations in runoff samples due to epigene and bomb-^{36}Cl, interpretation is problematic. A pathway (vertical dotted line) from the $^{36}Cl/Cl$ estimate of modern precipitation (meteoric input) to the value for Frances Lake (high-altitude runoff) reflects the addition of ^{36}Cl relative to stable chloride. As noted previously, the low $^{36}Cl/Cl$ ratios characteristic of the thermal springs suggest the addition of large

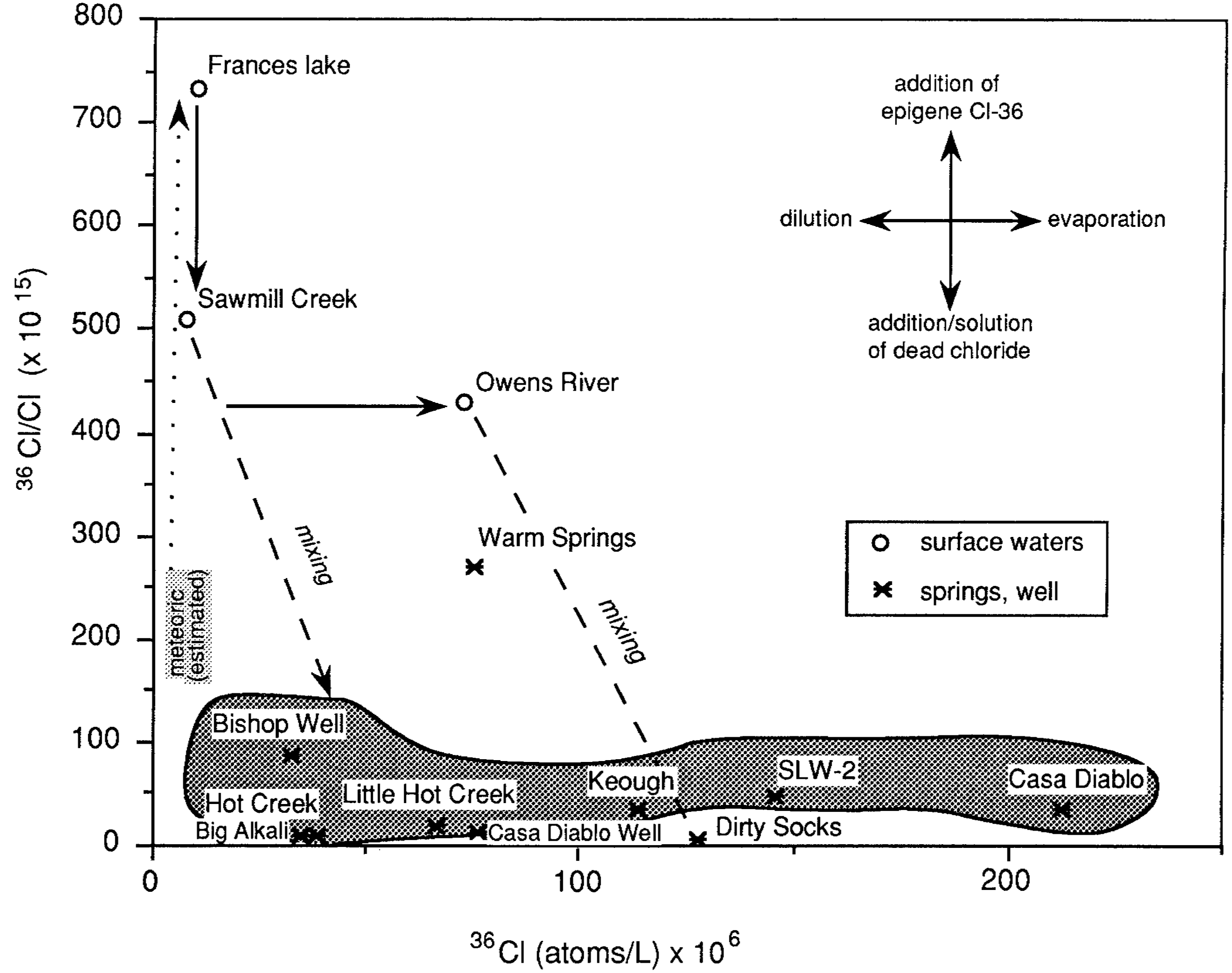

Figure 33. Plot of chlorine-36/chloride ratios of modern waters from the Owens Valley versus chlorine-36 concentration of the samples. Possible pathways of mixing are shown.

amounts of dead chloride, relative to ^{36}Cl. The Bishop well sample is included in this group. With progressive lowering of an initial concentration, samples would fall on a vertical line ($^{36}Cl/Cl$ would decrease, but ^{36}Cl concentration would remain the same). However, this trend is not directly observable on the diagram because runoff samples contain epigene and bomb-^{36}Cl. However, the overall effect of the springs is apparent. Mixing (shown by a dashed line on Figure 33) of spring waters (located upstream from the Owens River sample) with high-altitude runoff (Frances Lake and Sawmill Creek) ultimately lowers the $^{36}Cl/Cl$ ratio of the runoff. A horizontal pathway from the mixing line to the Owens River value indicates the effect of evaporation. Further mixing with spring waters downstream (predominantly Dirty Socks) would further lower the $^{36}Cl/Cl$ ratio in the Owens River (dashed line from Owens River to Dirty Socks hot spring). The thermal springs do appear to fall on a horizontal line which would usually indicate a pathway of dilution (decrease ^{36}Cl concentration) or evaporation (increase ^{36}Cl concentration), where $^{36}Cl/Cl$ remains the same. However, discharge from the springs did not evolve from a common initial concentration, therefore pathways between them cannot be deduced.

Finally, probable pathways of ^{36}Cl from headwaters to deposition in evaporites in Searles Lake during the Pleistocene can be inferred. Figure 34 is a log-log plot of the $^{36}Cl/Cl$ ratio versus ^{36}Cl concentration for the Owens Valley waters that also includes the data for Mono Lake and Black Point hot spring (located just north of Mono Lake). Values for Owens Lake and Searles Lake include estimated ^{36}Cl concentrations based on reconstructed salinity values determined by Smith (1979). During the Pleistocene, the $^{36}Cl/Cl$ ratio for Frances Lake (high-altitude runoff)

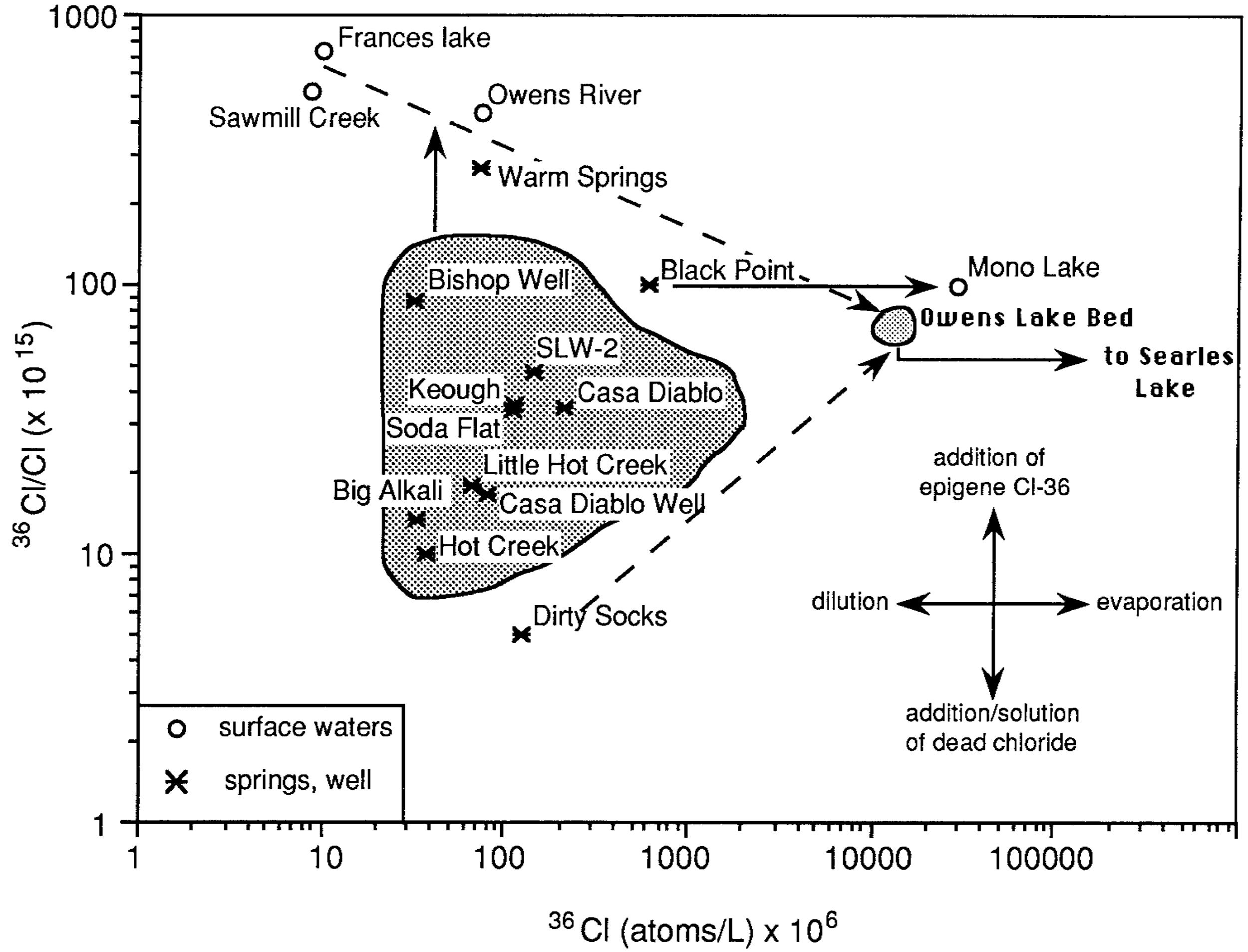

Figure 34. Plot of chlorine-36/chloride ratios versus chlorine-36 concentration. Possible mixing pathways for runoff in the paleo-Owens River system from high-altitude locations to Searles Lake, the usual terminus.

probably reflected the initial input ratio. As previously shown in Figure 33, discharge from the thermal springs and the artesian well mixed with high-altitude runoff, lowering the $^{36}Cl/Cl$ ratio. This runoff filled Owens Basin and ^{36}Cl concentration increased due to evaporation. The $^{36}Cl/Cl$ ratio was furthered lowered by discharge from springs downstream of Owens Lake. Runoff then filled Searles Lake, the usual terminal sink, and again, the ^{36}Cl concentration increased due to evaporation (horizontal line, increased ^{36}Cl concentration) but the $^{36}Cl/Cl$ ratio remained fairly constant. A similar relationship is noted between the Black Point hot spring and Mono Lake. Black Point hot spring, located just north of Mono Lake, discharges into Mono Lake. Mono Lake is upstream from the other thermal springs, so its $^{36}Cl/Cl$ ratio would not be affected by their discharge.

Surficial Salines. The measured $^{36}Cl/Cl$ ratios for saline crusts from the Warren Lake and Owens Lake playas were included on the plot of $^{36}Cl/Cl$ versus distance from the headwaters of the Owens River (Fig. 29). The value for the Owens Lake bed (82×10^{-15}) was included on the line that was drawn to show the evolution of the $^{36}Cl/Cl$ ratio in the ancestral Owens system. The Owens value reflects the dilution of the meteoric input by the numerous thermal springs located upstream from Owens Lake (Fig. 5). On the other hand, the Warren Lake saline crust exhibits a $^{36}Cl/Cl$ ratio (240×10^{-15}) similar in value to the meteoric input. Warren Lake, which is closer to the source of high-altitude runoff (Fig. 5), would not be affected by discharge from the low ^{36}Cl thermal springs. This suggests that the Warren Lake bed ratio should be most similar to the meteoric input, which indeed is the case.

Great Basin Samples

Runoff and lake waters were sampled from the Walker Lake and Pyramid Lake basins located in western Nevada. A surficial saline was collected from the Eightmile Flat playa which is located about 25 miles northeast of Walker Lake. Two soils (geosols) that are developing on Lake Lahontan sediments were also sampled (Table 3, descriptions in Appendix 1). All of the above samples were collected in order to note any $^{36}Cl/Cl$ evolution trends, and any similarities with the Owens Valley samples. The Eightmile Flat and geosol GEO-1 saline samples are similar to the value of the Warren Lake saline sample. These samples possibly represent the $^{36}Cl/Cl$ ratio of recent meteoric input. The other geosol (GEO-2) sample has a very high $^{36}Cl/Cl$ ratio which is possibly due to high ^{36}Cl runoff from sources that cannot be delineated at this time. The runoff samples taken from the Truckee River and Walker River both exhibit higher ratios than the lakes they empty into. As in the Owens system, the runoff samples are probably influenced by epigene and some bomb-^{36}Cl. The Truckee River sample showed a tritium level of 13 TU, indicating the influence of bomb tritium. Dilution by other runoff must lower the ratio to what is ultimately exhibited in the lake waters

Deep Springs Valley

Samples were collected from the small closed-basin system in Deep Springs Valley (Fig. 5) in order to note any similarities with the Owens Valley system.

Unfortunately, two, and possibly all, of the four water samples showed high tritium concentration (Fig. 35) suggesting high $^{36}Cl/Cl$ ratios might be due to bomb-^{36}Cl.

The runoff samples from Deep Springs Valley have lower $^{36}Cl/Cl$ ratios than the spring and well sample -- just opposite as that observed in Owens Valley (Fig. 33). The lake bed sample (saline crust) also shows a high $^{36}Cl/Cl$ ratio, which indicates the influence of the nearby spring and well discharge. The Birch Creek and well samples show tritium levels near pre-bomb levels, suggesting these samples may contain bomb-^{36}Cl. But, the well sample has a very high $^{36}Cl/Cl$ ratio which possibly indicates input from a source with very high ^{36}Cl concentration. Crooked Creek is also an interesting sample. The tritium concentration is the highest of all samples measured (Fig. 35), yet the $^{36}Cl/Cl$ ratio is very close to the value estimated for meteoric input. Enrichment of $^{36}Cl/Cl$ in Deep Springs is probably due to progressive addition of epigene ^{36}Cl from weathering in an environment with low sedimentary chloride.

LAKE HISTORY RECONSTRUCTION

The KM-3 core recovered from Searles Valley is one of the most complete records of Pleistocene lacustrine sedimentation in the world. Reconstruction of the lake history for the paleo-Owens River system is based primarily on the information revealed in the sediments recovered from the KM-3 core and, to a lesser extent, the cores from the other basins. Although detailed studies examining other criteria such as shorelines and exposed lacustrine sediments can also serve as a basis for lake

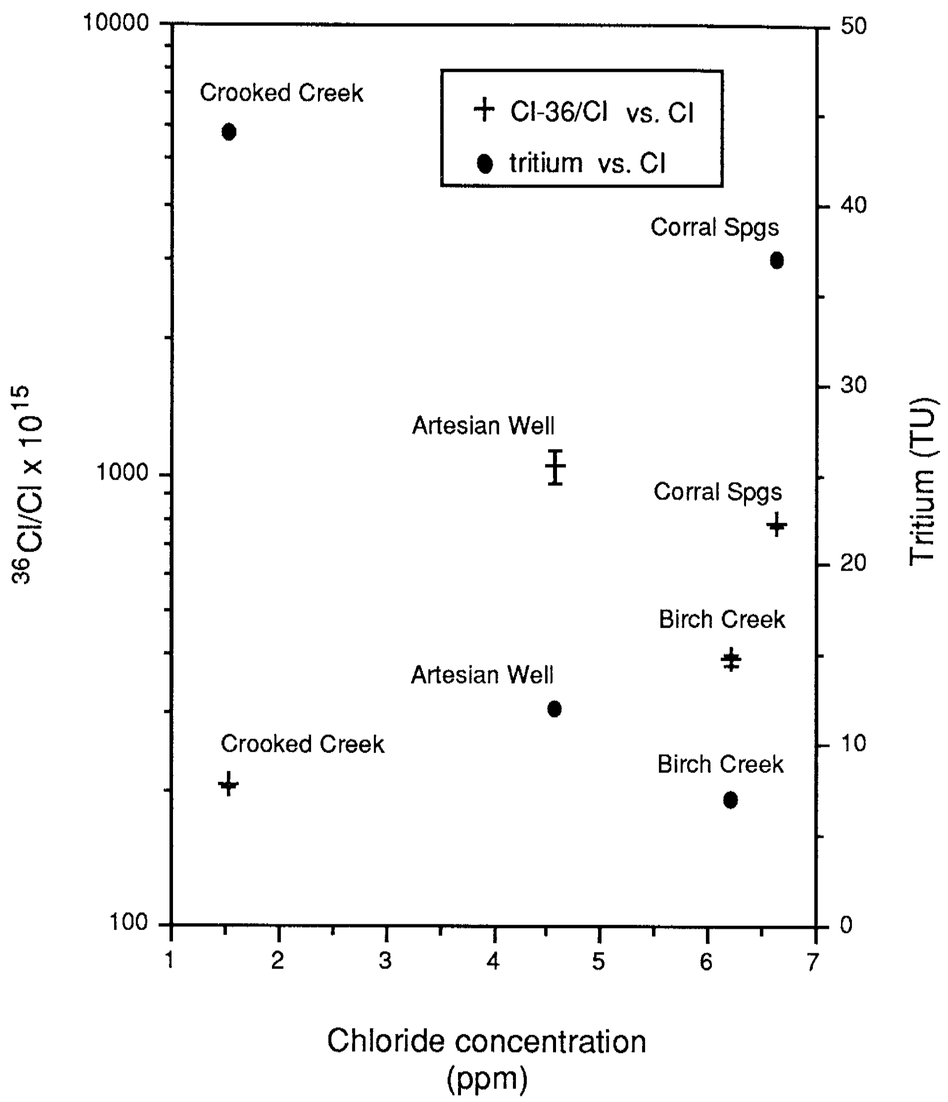

Figure 35. Plot of Chlorine-36/Cl ratio, tritium concentration, and chloride concentration for waters from Deep Springs Valley, CA. Error bars not shown are within size of symbol.

history reconstruction, this study concentrates on the excellent record revealed in the subsurface cores. The following is a brief discussion of the criteria used.

Sedimentological Criteria

The two predominant types of interbedded sediments -- muds and evaporite minerals -- are apparent from macroscopic observation of the KM-3 core. Muds deposited during the past 2.0 Myr represent times of medium-to-high lake levels, and lithologic and mineralogic variations within the muds signify changes in the chemical nature of the lake waters (Smith, 1979). The mud color itself also suggests lake depths and environments of deposition. For example, black or dark green muds usually are a product of deep, possibly stratified, perennial lakes with a reducing environment; more yellowish or orange muds indicate an oxygenated, and presumably shallow or unstratified lake environment. The yellowish muds may also indicate ash layers (yellow color due to oxidized biotite).

Saline layers represent times when the lake was at medium-to-shallow levels. The mineralogy of the salts depended upon temperature, ion concentration, and the type of solutes available. Salt mineralogy is also an indicator of lake salinity at the time of precipitation (Smith, 1979). Beds of monomineralic salts are interpreted as products of winter cooling and salinities between about 3 and 15%; beds of moderately soluble monomineralic or bimineralic salts, that probably crystallized throughout the year, indicate lakes with low-to-medium salinity (15-30% salinity);

and beds of multimineralic salts of the more soluble species indicate a highly saline lake (greater than 30% salinity).

Other criteria useful in analyzing lacustrine sediments include structures such as laminations, mineral habits, grain sizes, and abrupt or gradational sedimentological boundaries.

Correlation with Panamint Valley

As noted previously, two subsurface zones that are dominated by halite underlie Panamint Valley. The chloride in the Panamint Valley upper salt is hypothesized to have begun residence in Searles Lake at about 286 ka (after deposition of Unit C, see Fig. 18). Figure 18 indicates that the lake desiccated and deposited its entire chloride burden by that time (286 ka). This was followed by a new cycle of chloride accumulation. There are no major halite beds in Searles above this horizon and below the Lower Salt, dated at 39 ka. Accumulation of chloride in the lake water can thus be inferred to have been continuous. An overflow event at some point after 286 ka carried chloride into Panamint Lake where it stayed in solution until deposition as salt.

My correlation between the Searles and Panamint Basins is shown in Figure 36. One of the assumptions necessary for correlation of Searles Lake overflow events with Panamint Valley saline deposition is that most of the chloride originated in the paleo-Owens River system and not from local sources. There is a strong case for a paleo-Owens River source. First, local runoff in the Panamint basin is not of sufficient quantity to sustain a lake of any significant size (Smith, 1976); second,

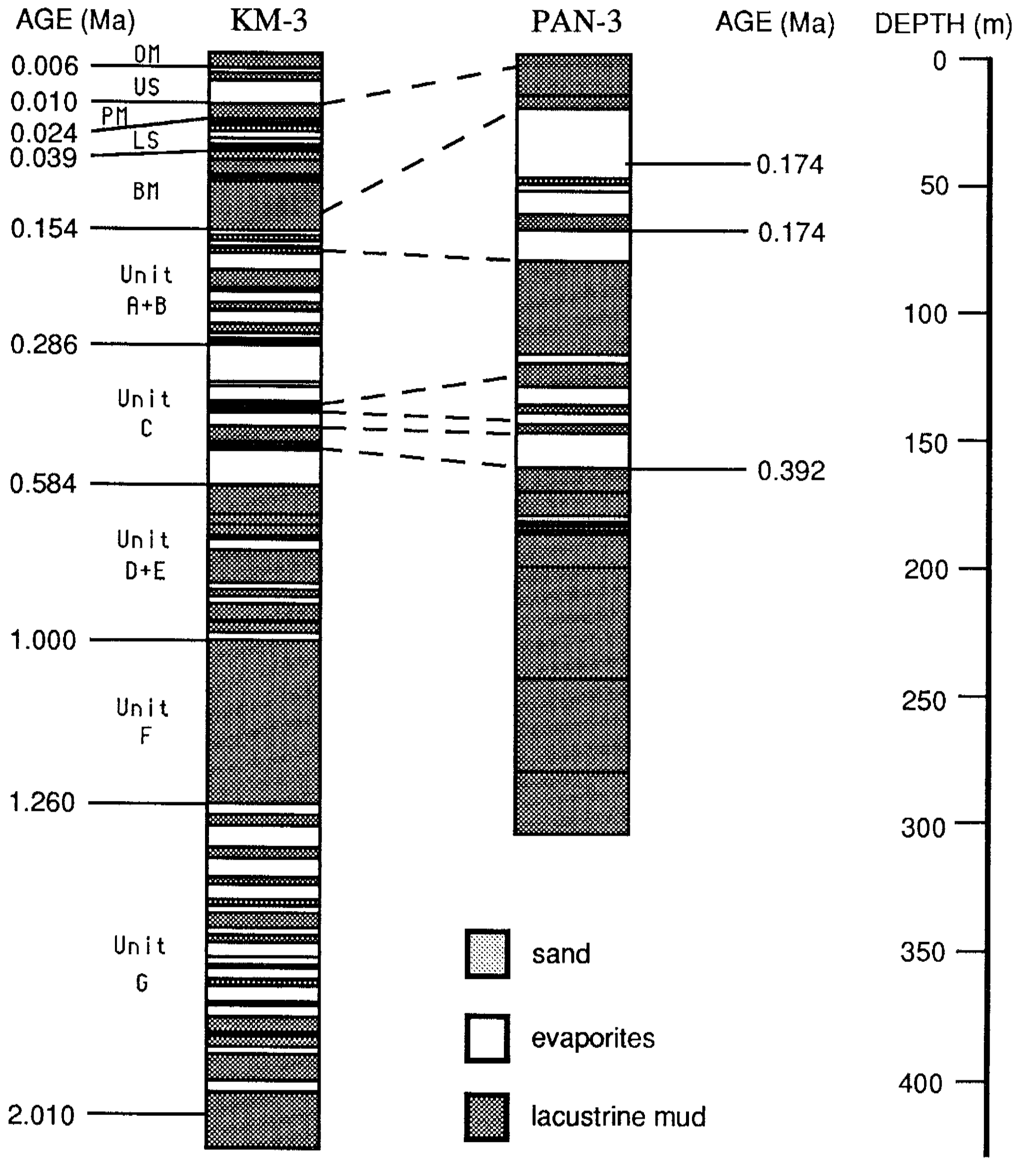

Figure 36. Correlation between Searles Lake and Panamint Lake based on the chronology for the KM-3 core, the reconstructed lake curve for the paleo-Owens River system, and ages determined for evaporites from Panamint Lake.

examination of the geology of the Panamint drainage basin does not reveal any rock units that could supply a sufficient quantity of chloride.

The history of overflows into Panamint Valley can be refined by considering the chloride budget in Searles Lake.

Chloride Budget

As noted above, large amounts of chloride are "missing" from Searles Lake compared to the amount that is expected when I assume a constant influx rate from the paleo-Owens River. Overflows from Searles Lake may be inferred from the intervals with subhorizontal slopes on the plot of chloride accumulation as a function of time (Fig. 18). Three of the overflows since 1.0 Ma may be inferred to have occurred in the intervals between 750 to 600 ka, 500 to 400 ka, and 200 to 100 ka. These last two intervals match reasonably well with the ^{36}Cl dates of 392 and 175 ka (both corrected), for the lower and upper halite intervals respectively, in Panamint Valley, suggesting that these two desiccations correspond with the terminations of the two overflow events. The inference that the Panamint Valley halite beds are the result of Searles Lake overflows may be further tested by "adding" the chloride in the Panamint halite into the Searles Lake mass-accumulation plot (Fig. 37). The calculation of the Panamint chloride mass in Figure 37 takes into account the difference in valley geometries by multiplying the Panamint chloride kg m^{-2} values by the ratio of the area of the Searles playa to the area of the Panamint playa. The combined chloride accumulation in the two valleys approximates a constant

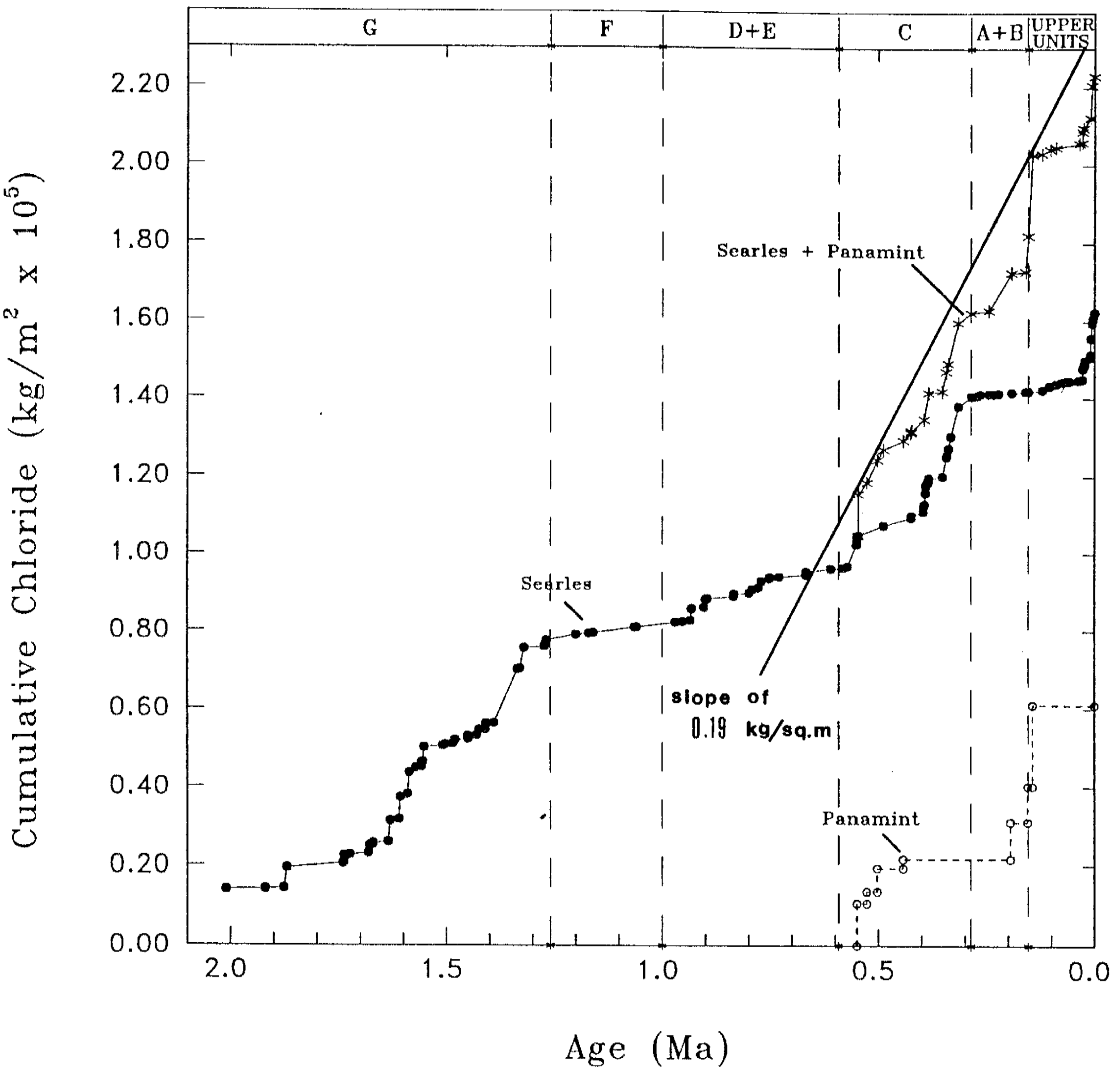

Figure 37. Chloride mass accumulation over time for Searles Lake. An estimated mass accumulation of chloride in Panamint Lake for the past 550 kyr has been added in.

influx over the past 650 ka and accounts for nearly all of the "missing" chloride during this period, supporting the overflow hypothesis.

Nevertheless, the chloride missing from the period prior to 650 ka is not accounted for. There are no significant halite beds in Panamint Valley between 160.0 m and the bottom of the core (303.5 m; extrapolated age: ~1.5 Ma). The lost chloride may have been transported to Death Valley during an overflow of the lake in Panamint Valley.

Determination of Lake Size

The water surface area and volume of Searles Lake when it was at maximum size can be easily determined based on outlet elevation and basin configuration. Elevated shorelines can also be used to infer water surface areas when Searles was a deep perennial lake for long periods of time. These times of high lake level can be associated with mostly clastic deposition. Lake sizes associated with evaporite deposition are more difficult to determine, due to lack of surficial evidence. Complete desiccation of the lake was not necessary for evaporite precipitation. An estimate of lake levels during evaporite deposition was determined by using data on sodium chloride from the Upper Salt. First, lake volume was calculated based on the cumulative concentration of sodium chloride. From the plot of the mass accumulation of chloride, the rate of chloride influx and the length of time of chloride influx for the Upper Salt can be determined (Fig. 17). A corresponding lake volume can be calculated based on the soublity of sodium chloride. That is, there exists a relationship between the length of chloride influx, the time when chloride saturation would occur, and lake volume. This procedure is outlined in Appendix 8. Next, lake volume can be related to lake depth. Finally, water surface area can be estimated based on calcualtions by Smith (1979, p. 78).

Presentation of Lake History Chronology

Figure 38 is the reconstructed history of the lakes in the paleo-Owens River system for the past 2.0 Myr. The cumulative-lake-area reconstruction is based primarily on sediment characteristics from the KM-3 core beneath the surface of Searles Lake, the reconstructed chloride budget for Searles and Panamint basins, and the new ^{36}Cl ages for salts in Searles and Panamint Valleys. The reconstruction represents all five lakes in the paleo-Owens system.

From about 2.0 to 1.2 Ma (Unit G in the KM-3 core), Searles Lake was the usual terminus for the paleo-Owens system. The stratigraphic record is characterized by a cyclic pattern of mostly green muds intercalated with beds of nearly pure halite. Green muds are indicative of a medium to deep perennial lake, and the halite beds indicate the lake was shallow and highly saline. The inference of one period of desiccation at about 1.5 to 1.45 Ma, interrupted by a brief period of shallow lake levels (1.46 Ma), is supported by the presence of brown mud containing anhydrite, probably indicating that playa conditions briefly prevailed in Searles Lake. The chloride accumulation curve (Fig. 17) shows that Unit G exhibits the typical stair-step pattern of a soluble solute, as discussed above. The lack of chloride accumulation in

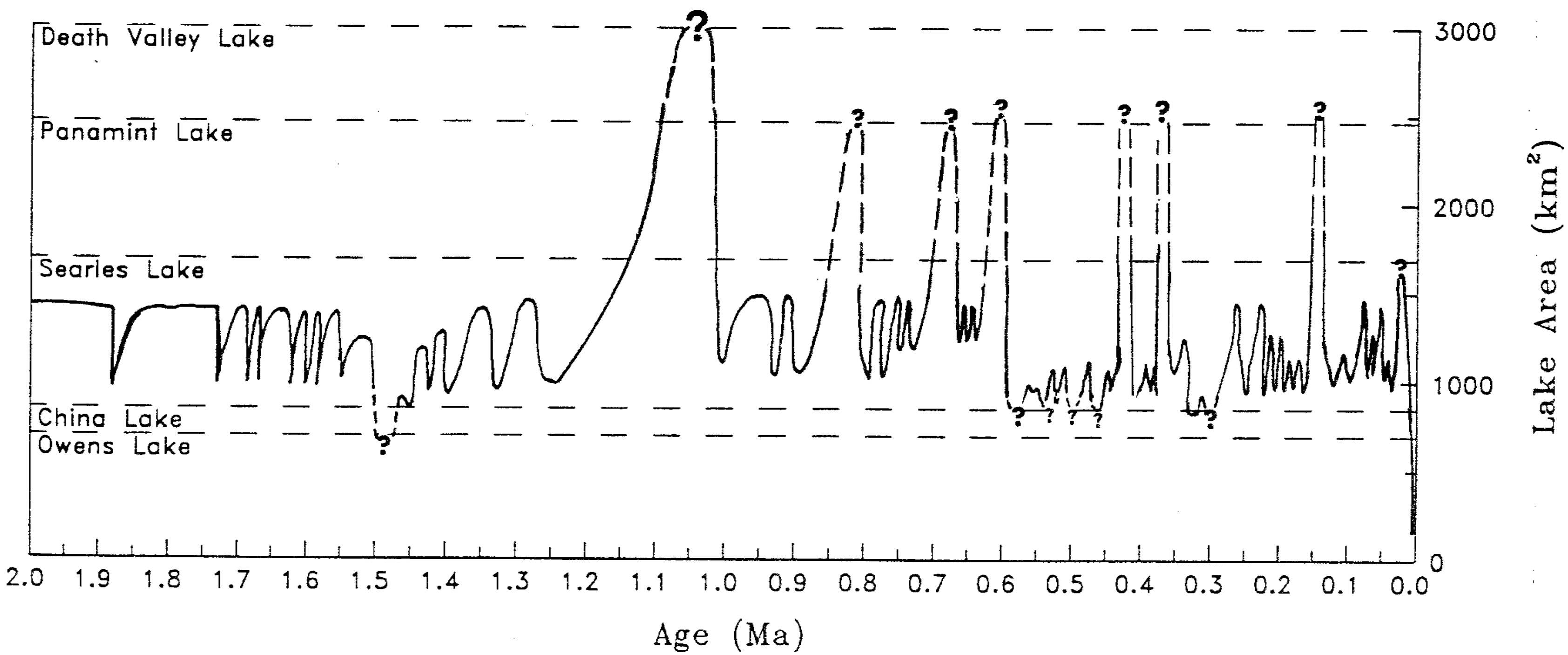

Figure 38. Lake history curve for the paleo-Owens River system for the past 2.0 Myr. The reconstructed curve is for all five lakes in the system. Lake names appear below their overflow level. This curve is a diagrammatic representation of lake size, and reflects relative, not absolute fluctuations. Most of the minor perturbations have yet to be discerned.

KM-3 between 1.5 to 1.45 Ma concurs with the proposed period of desiccation since the chloride would be in residence in China or Owens Lakes. The estimated ages of the bottoms of cores from Owens and China Lakes are younger than this age, and thus interpretations based on these cores do not confirm or deny this hypothesis.

The interval from 1.2 to 1.0 Ma (Unit F in the KM-3 core) was a period of major overflow for the entire paleo-Owens system. All lakes are inferred to have been at overflow levels (except possibly Lake Manly), and, as is apparent from the long subhorizontal slope in the chloride accumulation curve (Fig. 18), chloride was lost from the Searles waters to downstream lakes. The deep, perennial, overflowing lake in the Searles basin is recorded by massive black and dark green muds.

Searles Lake was again the terminus for the system for the interval from 1.0 Ma to 600 ka (Unit D+E in the KM-3 core). The chloride accumulation curve (Fig. 17) shows a subdued stair-step pattern, which suggests that high lake levels fluctuated periodically to depths shallow enough to deposit evaporites. An overflow event could be inferred for the period from 900 to 800 ka, but the lakes could have been consistently deep with only minor overflow(s). During the interval from 750 to 600 ka I propose at least two probable overflows of Searles Lake into Panamint Lake, and possibly overflow from Panamint Lake into Death Valley during each event. The chloride accumulation curve shows a major loss of chloride during this time (Fig. 18), and the small number of salt beds in core KM-3 indicate that Searles Lake was rarely very shallow at this time.

For most of the past 600 kyr Searles Lake was once again the terminal sink. The abundant and sometimes-thick salt beds indicate that the lake in Searles Basin was frequently intermediate to small in size. Evidence from the KM-3 core and from the chloride accumulation curve indicates that there probably were overflow events between 440 and 400 ka and 380 and 350 ka (Unit C in KM-3 core) and between 150 and 80 ka (Bottom Mud), but there is no evidence that Searles was a deep, perennial lake for long periods of time during Unit C. The upper salt in Panamint Valley is correlated with the overflow event starting at about 150 ka, which I propose was the last major overflow event from Searles in the paleo-Owens system. Playa sediments (characterized by coarse grain size and halite) indicate two possible periods of complete desiccation in Searles Lake during the interval from 325 to 285 ka (Unit C), although the small thickness of playa sediments suggests only a brief interval of subaerial conditions. From 285 to 150 ka (Unit A+B in the KM-3 core) the interbedded muds and monomineralic salines (stratigraphy from Searles Lake cores other than KM-3, Smith and others, 1983) appear to record deposition in fluctuating shallow lakes. The long subhorizontal slope on the chloride accumulation plot (Fig. 17) for this interval is partially due to lack of data because of KM-3 core loss.

During much of the past 10 kyr (Upper Salt and Overburden Mud in the KM-3 core) there has been only enough runoff from the Sierra Nevada to create a small- to moderate-sized saline lake in the Owens basin, except for one brief pluvial period. Smith (1976) proposed that Sierra Nevada runoff created a small lake in the Panamint basin at about 10 to 12 ka. This inference is based on ^{14}C dates on tufa.

DETERMINATION OF EXPOSURE TIME

Accumulation of ^{36}Cl in glacial erratics is proportional to the length of time (t) the erratic has been exposed on the surface of a moraine. Buildup of ^{36}Cl depends on the production rates (ψ) of the reactions that produce ^{36}Cl, rock composition, rock location, background ^{36}Cl content, and the ^{36}Cl decay rate.

Chlorine-36 buildup over time can be expressed as follows (Bentley and others, 1986):

$$R_m = \frac{ELD(\psi_K + \psi_{Ca} + \psi_n)}{\lambda_{36} N_{Cl}} (1 - e^{-\lambda_{36} t}) + R_o \qquad (16)$$

where R_m is the measured $^{36}Cl/Cl$ ratio, E is the elevation correction factor (Yokoyama and others, 1977), L is the latitude correction factor (Yokoyama and others, 1977), D is the depth correction factor (Lal and Peters, 1967), ψ_K is the production rate for potassium (2670 atoms ^{36}Cl kg^{-1} yr^{-1} (% $K_2O)^{-1}$ at sea level as calculated by Yokoyama and others, 1977), ψ_{Ca} is the production rate for calcium (710 atoms ^{36}Cl kg^{-1} yr^{-1} (% CaO$)^{-1}$ at sea level as calculated by Yokoyama and others, 1977), ψ_n is the production rate for thermal neutron activation of ^{35}Cl (atoms ^{36}Cl kg^{-1} yr^{-1}), λ_{36} is the decay constant for ^{36}Cl, N_{Cl} is the chloride concentration in the rock (atoms kg^{-1}), and R_o is the background $^{36}Cl/Cl$ ratio due to nuclear reactions caused by uranium and thorium within the rock. In order for equation 16 to be used in a direct manner for determining surface exposure time, the erratic should have been totally shielded from cosmic rays, then suddenly exposed to them on the surface.

The production rate of thermal neutron activation reactions (ψ_n) is given by:

$$\psi_n = \varnothing_n \frac{\sigma_{35}N_{35}}{\sum_i \sigma_i N_i} \tag{17}$$

where $\varnothing_n$ is the thermal neutron flux at sea level (about 10^6 n kg^{-1} yr^{-1}, with uncertainty), σ_{35} is the thermal neutron capture activation cross section of ^{35}Cl (43 barns), N_{35} is the concentration of ^{35}Cl (atoms kg^{-1}), σ_i is the thermal neutron absorption cross section for each element i, and N_i is the concentration of each element. Elemental and compositional analyses of the rocks by XRF were performed at New Mexico Institute of Mining and Technology (Appendix 7).

The ^{36}Cl build-up ages for Sierra Nevada glacial erratics presented in this study are tentative (Table 5). The attempt to extract chloride from glacial erratics to determine a ^{36}Cl build-up age of moraines has been problematic. Much has been learned from this initial effort. For example, the published production constants for ^{36}Cl have proven to be inadequate. In particular, the determination of a build-up age is quite sensitive to the chloride concentration. Recent efforts at New Mexico Institute of Mining and Technology has been directed to more accurately determining the chloride concentration (especially in low-chloride rocks). However, even with the complications associated with chloride extraction and measurement, the implications of this and other related studies (Phillips and others, 1986a; Leavy and others, 1987) are encouraging.

The ages presented in Table 5 are preliminary values for those samples in which the determination of chloride concentration was attempted. The data for each moraine are scattered, which probably indicates the exposure history of the erratics did vary. For example, a boulder could initially been buried in till, removed from interaction with cosmic rays. During the next ice advance, reworking could subsequently expose the boulder at or near the surface of the moraine. Subsequently, the ^{36}Cl build-up age for the boulder and the moraine it was originally buried in would appear too young. Thus, it is assumed the oldest ages are most likely correct.

Two basalt samples were collected from the Ash Hill Channel for ^{36}Cl analyses. The samples were from a channel that had cut through a basalt flow. It is hypothesized that the channel was cut by overflow waters from Death Valley. Unfortunately, at this time, chloride concentrations of the samples have not been performed.

CHAPTER VI

DISCUSSION OF THE LAKE-FLUCTUATION CHRONOLOGY FOR THE PALEO-OWENS RIVER SYSTEM, 0-2.0 Ma

LAKE-FLUCTUATION CURVE

Hydrologic Response of the Paleo-Owens System

During Pleistocene pluvial periods, the cumulative lake area in the Owens River system fluctuated in response to changes in climate. One of the stimuli that affected the closed-basin system was the fluctuation of runoff amount.
As discussed previously, the runoff originated predominantly from the east flank of the Sierra Nevada; it was derived from direct precipitation, or with lag time, from shallow ground-water discharge and glacier meltwater. The most direct hydrologic response to this stimulus was the change in lake size. Thus, the reconstructed radiometric and paleomagnetic lake-level chronology discussed in this paper (Fig. 38) is a record through time of the hydrologic response.

The lake-level chronology indicates that for the past 2.0 Myr Searles Lake was the terminus for 75 to 80% of the time. The nature of the lacustrine sediments revealed in cores from beneath the surface of Searles Lake was an important criterion for the lake history reconstruction. Occurrence of numerous evaporite beds, with large mineralogical and chemical diversity (which mostly reflects the chemical nature of runoff), is strong evidence for inferring Searles Lake was the usual sink. Smith and Street-Perrott (1983) calculated (based on present climatic conditions) that in order to maintain a lake in Searles Valley, Owens River discharge had to increase between 2.6 and 6.0 times. They also suggested that in order for a lake to be maintained in Panamint Valley, Owens River discharge had to increase between 6.0 and 8.8 times; and for the lake in Death Valley, an increase in flow of between 8.8 and 11.4 times. The maximum pluvial condition inferred between 1.1 to 1.0 Ma (Fig. 38) was not totally dependent on Owens discharge. The Mojave and Amargosa River systems also contributed runoff to the lake in Death Valley (Fig. 1).

During interpluvial times of the past 2.0 Myr, runoff contribution was only enough to maintain a shallow to nearly dry lake in Searles Valley (Fig. 38). Complete desiccation of the lake in Searles Valley possibly occurred during some intervals of the time represented by sediments in Units G and C. Maximum interpluvial conditions of the 2.0-Myr chronology are inferred for the period 10 ka to present.

Discharge and the **Z** Factor

Smith and Street-Perrott (1983, Table 10-2) calculated the relative discharge needed to fill each successive lake in the paleo-Owens River system based on the historic flow (prior to 1872) of the Owens River. This was done not only for present climatic conditions (discussed above) but for conditions with lake water temperatures reduced by 5° and 10°C. They found that with a lake temperature decrease (correlated to an air temperature decrease) of 5°C the discharge was reduced by 28%; for a 10°C decrease, discharge was reduced by 50%. Table 10-2 from Smith and Street-Perrott is presented in Table 7 for comparison with the relative Z factor of each lake. The relative Z factor remains constant for each lake, obviously not dependent on temperature changes. There is a high degree of correlation between the relative discharge calculated with present climatic conditions and the relative Z factor. This correlation is interesting since the Z factor is dependent on basin configuration. Examination of the cumulative lake area vs. cumulative lake elevation plot (Fig. 4C) shows that rate of lake growth was fairly constant, especially when infilling began in Searles Valley. This reflects the gross similarity in size and shape of the Searles and Panamint basins.

Periodicity

I infer from the lake history chronology (Fig. 38) that prior to about 800 ka, the frequency of the lake level fluctuation was roughly 45 to 50 kyr. Very few fluctuations with smaller frequencies are observed. Subsequent to 800 ka, the major fluctuations had a frequency of about 100 kyr and the frequency of minor fluctuations increased. Smith (1984) perceived a 400-kyr cyclicity in the water levels at Searles Lake. My inference from the lake history chronology tends to confirm this periodicity. Especially high lake phases occur in the intervals between 1.0 to 1.1 Ma, 600 to 700 ka and 130 to 150 ka.

Table 7

Comparison of relative inflow volumes and relative Z-factor

Table 10.2 *

Relative Inflow Volumes Required to Balance Evaporation at Varying Temperatures and for Various Lengths of the Owens River System of Pluvial Lakes

Size of Last Lake in Chain	Elevation of Water Surface[a] (m)	Added (and Cumulative) Area (km^2)	Evaporation[b] (m/year)			Cumulative Volume[c] ($10^9 m^3$)			Relative Discharge of Owens River and Its Tributaries[d]			Relative Z factor
			T = 0°	T = 5°	T = 10°	T = 0°	T = 5°	T = 10°	T = 0°	T = 5°	T = 10°	
Owens Lake, historic	1095	290	1.27[e]	—	—	0.41[f]	—	—	1.0	—	—	1
Owens Lake, abnormal[g]	1085	—	—	—	—	0.74[h]	—	—	1.8	—	—	
Lake Owens, full	1145	694 (694)	1.23	0.89	0.62	0.85	0.62	0.43	2.1	1.5	1.1	2.4
China Lake, full	665	155 (849)	1.41	1.02	0.70	1.07	0.78	0.54	2.6	1.9	1.3	2.9
Searles Lake, full	690	839 (1688)	1.65	1.19	0.82	2.45	1.78	1.23	6.0	4.3	3.0	5.8
Lake Panamint, small[i]	355[i]	175 (1863)	1.80	1.30	0.90	2.76	2.01	1.39	6.7	4.9	3.4	
Lake Panamint, full	602	707 (2570)	1.65	1.19	0.82	3.62	2.62	1.81	8.8	6.4	4.4	8.5
Lake Manly, full[j]	87	533 (3103)	1.97	1.42	0.98	4.67	3.38	2.33	11.4	8.2	5.7	10.3

[a] Surface of last lake in chain

[b] Net evaporation rate for last lake in chain, except for Owens Lake, rates for present evaporation (T = 0°) adapted from Meyers' data on present gross annual rates (1962: Plate 3), which indicate approximately 1.52 m for China, 1.78 m for Searles, 1.93 m for Panamint, and 2.13 m for Death Valley, reduced to net rates by assuming 10 cm annual precipitation on the lakes in China, Searles, and Panamint Valleys, 5 cm on lake in Death Valley, effects of reducing lakes' water temperatures by 5° and 10° (T = 5° and T = 10°) calculated by use of factors 0.72 and 0.50, the approximate reduction in vapor pressure of water with 5° and 10° reductions in the range of 0° to 30°C; corrected for changes in pluvial lake surface elevations above present valley floors using lapse rate of 6.5°C/1000 m (0.61 m/year/1000 m).

[c] Except as noted, figures are sums of losses from each lake in chain, the product of (evaporation rate for that lake) × (area of that lake), and values represent volumes of both total evaporation loss and offsetting total Owens River inflow.

[d] Relative to calculated volume of present Owens River, 0.41 × 10^9 m^3/year

[e] Average of net rates observed in May 1939 through April 1940 (Dub, 1947: Table 3) and September 1969 through August 1970 (Friedman et al., 1976: Figure 1), both corrected for salinity effect by assuming coefficient = 0.9.

[f] Calculated conditions in 1872, prior to irrigation, from data of Gale (1914: 254, 255, 261), calculated by using ratio of lake size to river flow in 1909-1912 and determining flow necessary to balance lake size in 1872.

[g] 1968-1969, record wet season (Friedman et al. 1976, Figure 1)

[h] Flow in Owens River observed in 1969 (Friedman et al., 1976: 503) plus volume diverted into Owens Valley Aqueduct during same period

[i] Latest Pleistocene lake, 61 m deep (Smith 1978a)

[j] This "maximum pluvial" condition apparently did not occur during the period 25,000 to 10,000 yr B.P. Calculation uses Death Valley evaporation rate for highest shoreline level but assumes that the volume of water required from the Owens River system was only one third of total because the Mojave River and Amargosa River systems also contributed their flow to the lake in the valley.

*from Smith and Street-Perrott (1983)

PALEOCLIMATIC IMPLICATIONS

The lake fluctuation history presented in this study (Fig. 38) documents the hydrologic response in a closed-basin system to changes in climatic conditions. Understanding of past climatic changes may aid in predicting the effects of future shifts (Roederer, 1986). Climate is a complex expression of several interdependent factors: precipitation, temperature, evaporation, humidity, wind and cloud type and cover. One can be easily drawn into the controversy dealing with Pleistocene climate reconstruction, especially in the proposing of changes of paleotemperatures and amounts of precipitation. Even with a complex model it would be very difficult to delineate which climatic factor changed, when it changed, and by how much. Most of the parameters would have to be estimated based on present conditions. This assumes present values can be measured accurately and then directly applied to periods in the past. Thus, it is very difficult to delineate and quantify the changes that were responsible for the fluctuation in lake levels. The one factor that lake fluctuations most directly reflect is change in absolute precipitation. During Pleistocene pluvial times increased precipitation produced increased runoff. As noted by Smith and Street-Perrott (1983), the estimates of the volume of pluvial runoff may be of more interest than the paleotemperatures and precipitation that caused them. Estimates of pluvial runoff may be more directly applied to quantifying concurrent pluvial processes such as sedimentation and erosion. However, estimates of pluvial runoff are somewhat tied to estimates of temperature values during the pluvial period. In order to estimate net volumes of runoff, losses from evaporation must be accounted for. The amount of the evaporation loss is dependent on vapor pressure, which is predominantly controlled by temperature.

Several studies in the southwestern U.S., dealing with temperature-sensitive parameters such as isotopes and biota, have resulted in proposed temperature decreases in the range of 5°C to 10°C for the late Wisconsinan (Brackenridge, 1978; Van Devender and Spaulding, 1979; Adam and West, 1983; Galloway, 1983; Spaulding and others, 1983; Phillips and others, 1986b). Assuming the same temperature decrease occurred during previous pluvial periods, the relative volume of discharge can be determined. Runoff estimates are based on the lake level reconstruction for the past 2.0 Myr presented in this study (Fig. 38), and the discharge estimates by Smith and Street-Perrott (1983). For maximum pluvial conditions, such as between 1.0 to 1.1 Ma, Owens River runoff increased 5.7 to 8.2 times. As a result, the cumulative lake area and Z factor increased by an order of magnitude (Table 7). The lower relative discharge value (5.7), based on a 50% reduction in evaporation, is preferred in this study. The full 10° temperature decrease is not necessarily preferred, but the lower evaporation rate is. Benson (1981) suggests that cloud cover should be considered the "master variable" since all other climatic factors are functions of the amount and type of cloud cover. In Benson's (1981) model for Lake Lahontan, Nevada (N of Owens Valley) maximum evaporation rates were found to be an order of magnitude less for a 10% increase in cloud cover and a temperature decrease of 10° K (10° C). For the 75% to 80% of the past 2.0 Myr that Searles Lake was the terminus of the system, relative discharge increased by 3.0 to 4.3 times. Again, the lower value is preferred. Consequently, the cumulative lake area and Z factor increased by 5.8 times. To correlate these relative discharge amounts to precipitation amounts is beyond the scope of this study.

Another climatic implication that can be inferred from the lake level curve is the anomalous aridity of the Holocene. The mixture of halite and coarse-grained clastic sediments in the Overburden Mud is diagnostic of playa and shallow saline-lake conditions. It is also virtually unique in the Searles sediment column. The absence of similar sediments during nearly all earlier interglacial periods may possibly result from tectonic as well as climatic factors. The entire lake-level curve for the past 1.2 Myr seems to show a gradual trend toward increasing aridity. This is similar to the trend toward lighter deuterium content of ground waters (preserved in fluid inclusions) over the past 2.0 Myr in the Death Valley area (Winograd and others, 1985). Together with Winograd and others (1985), I hypothesize that the trend may be attributed to the gradual uplift of the Sierra Nevada over this time. The indications of a fundamental difference between Holocene climate and that of at least the previous interglaciation are supported by other studies in geographically distant sites (for example, Gascoyne and others, 1981; King and Saunders, 1986).

For the past 2.0 Myr, a maximum of 3 intervals possibly experienced similar arid conditions (1.5 to 1.47 Ma, 580 to 420 ka, and 350 to 300 ka). However, sedimentological evidence indicates these intervals were never as arid as the present conditions. The lack of evaporite beds in the top several hundred meters of sediments revealed from cores beneath Owens and China Lakes supports the conclusion that these basins were rarely the terminus of the system. However, evaporites could have been deposited in Owens and China Lakes and subsequently dissolved during the next pluvial period, thereby destroying any record of a shallow saline-lake or playa environment.

CORRELATION OF THE LAKE FLUCTUATION CHRONOLOGY WITH OTHER RECORDS

Marine ^{18}O Record

The KM-3 core, the lake fluctuation chronology for the paleo-Owens system, and an oxygen isotope chronology for the past 1.88 Myr are shown in Figure 39. The $\delta^{18}O$ chronology is a composite record proposed by Williams and others (1988). Heavy values (increase in positive direction) of $\delta^{18}O$ reflect a decrease in temperature and are indicative of increasing global ice volumes.

Previous investigations have shown that the paleoclimatic history from the paleo-Owens River lake system exhibits both marked similarities to and strong differences from the marine ^{18}O record (Smith, 1984). The frequency of the ocean water ^{18}O fluctuations prior to 850 ka is characterized by fairly constant cycles of approximately 40 kyr (Watts and Hayden, 1984) to 50 kyr duration (Williams and others, 1988). After 850 ka the cycles become more variable, increasing in amplitude and decreasing in frequency. Hays and others (1976) inferred a 100 kyr periodicity for this period. This shift in frequency has not been satisfactorily

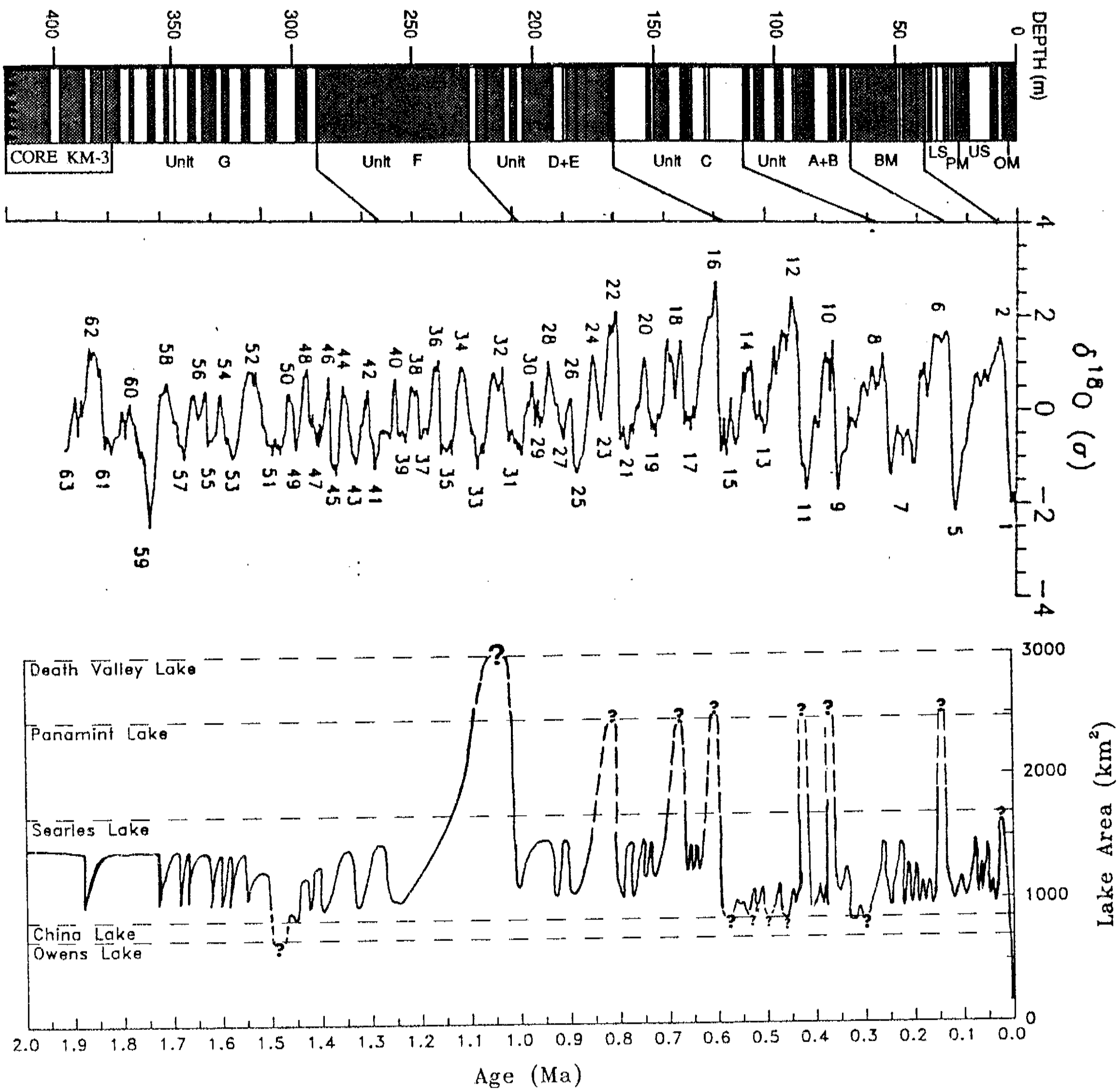

Figure 39. Lake fluctuation curve for the paleo-Owens systen for the past 2.0 Myr shown with the composite oxygen isotope curve presented by Williams and others (1988).

explained (Ruddiman and Wright, 1987). Cycle duration in the ^{18}O record has a fairly strong correspondence to the lake history record. One of the most striking similarities is in the periodicity of the interval between 1.2 and 1.88 Ma (Unit G of KM-3). The sediments exhibit a regular alternation of evaporites and muds that is obvious to even casual examination.

However, there are also marked differences, most notably in the amplitude of individual cycles. The marine ^{18}O curve is characterized by an almost monotonous similarity in the amplitude of the individual cycles. The lake-level curve, on the other hand, exhibits much greater variability in the cycle amplitude. As Smith (1984) noted, the 100 kyr or less cycles exhibited by the marine ^{18}O record are not recorded in the Searles Lake sediment record during the wettest or driest hydrologic regimes (for example, Unit F and Unit C, respectively).

The intervals separating the maxima also appear to show characteristic differences from each other (for example, the interval prior to 1.2 Ma has generally low lake levels, that between 1.0 and 600 ka high levels). Evidence for a similar cyclicity at various locations around the globe has been noted by Jensen and others (1986).

Other Great Basin Sediments

Chlorine-36 ages were determined for salines from four separate basins in an attempt to correlate past lake levels within the western Basin and Range Province. Age determination of trends in lake response would provide a valuable means of correlating the stratigraphic records found in these disconnected basins, and thus provide a broader areal extent for paleoclimatic reconstruction.

The $^{36}Cl/Cl$ ratios for two deep samples from Lake Bonneville (67.0 and 76.6 m) are similar and the approximate age is 107 ka. According to the lake history of the Bonneville Lake presented by Currey and others (1984), this interval corresponds to a time in which a relatively small lake was oscillating in size, with possibly complete desiccation about 130 to 110 kyr ago. For the paleo-Owens system, this interval corresponds to a time (Bottom Mud in the KM-3 core) of medium to deep perennial lakes in Searles Lake.

The ^{36}Cl age determined for the salines (88.4 to 88.7 m) in Clayton Valley is about 179 ka. In Searles Lake, this period corresponds to a time (Unit A+B in the KM-3 core) of fluctuating levels in small- to medium-sized lakes in which the dominant evaporite mineral being deposited was trona. A similar age was calculated for the salines recovered from 27 m in Cadiz Lake in southeast California. The ^{36}Cl ratios for the nearby Bristol Lake evaporites (92.1 and 171.4 m) were very low and were beyond the detection limit of the ^{36}Cl method.

The Walker Lake core sample from 72 m was dated at about 42 ka. This correlates with a low lake level in the Walker Basin and the Searles Basin. The $^{36}Cl/Cl$ age for the deeper sample from Walker also correlates to a low lake level in Searles. Determining the evolution of ^{36}Cl in the Walker and Pyramid Basins was problematical due to high ratios which are probably influenced by bomb^{36}Cl.

Correlation between these lakes, Searles Lake and other Great Basin lakes is difficult because detailed stratigraphic and mineralogic data are unavailable, and the paleo-hydrologic settings of the basins vary considerably.

Sierra Nevada Glacial Chronology

As most of the runoff in the paleo-Owens River system came from the east side of the Sierra Nevada, lake-area fluctuations in this study are correlated with Sierra Nevada glacial events. Glacial events are correlated with even-numbered ^{18}O cycles, which reflect increasing global ice volume. Major overflow periods occurred in Searles Lake between 1.3 to 1.0 Ma, 750 to 600 ka, and 150 to 120 ka. The oldest overflow is here tentatively correlated with the Sherwin glaciation (oxygen-isotope stage 32) and the youngest with the Tahoe glaciation (oxygen-isotope stage 6) (Fig. 39).

I infer that the ~150 ka highstand produced the largest overflow event since the 700 to 600 ka events. As noted by Blackwelder (1931), the most conspicuous moraines in the Sierra Nevada are of Tahoe age. Dorn and others (1987) have obtained cation-ratio dates of 180 to 145 ka for the Tahoe moraines at Pine Creek. They suggest that the Tahoe glaciation should be correlated with oxygen-isotope stage 6 instead of stage 4. My results concur with this correlation.

The date of 150 to 120 ka for the Tahoe does not agree with Gillespie and others' (1984) conclusion that the moraine below a dated basalt (119 ± 7 ka) in Sawmill Canyon could not be from the Tahoe. However, if the interpretation of the overflow at 150 to 120 ka does correspond to the Tahoe advance, it would be consistent with the age determined for the basalt.

The data indicate no major overflows of Searles Lake after 120 ka. In Panamint Valley there are no halite beds above the salt dated at 175 ka (correlated to Searles overflow between 150 to 120 ka), indicating that very little chloride was introduced subsequent to that time by Searles overflow. Also, there is no clear indication of lacustrine conditions in the sediment texture or color (Smith and Pratt, 1957). However, the main lines of evidence that we are using (chemical and textural composition of sediments, chloride budgets, etc.) tend to reflect only long-term, major trends in lake level. In particular, strongly stratified lake conditions could mask the chloride budget effects of short-term overflow.

CHAPTER VII

SUMMARY AND SIGNIFICANCE OF RESULTS

1) The successful use of ^{36}Cl as geochronometer for dating Pleistocene continental evaporite deposits has been demonstrated. A revised chronology for the past 2.0 Myr has been determined for Searles Lake lacustrine sediments that are revealed in the KM-3 core. Thus a chronology is presented for one of the longest, continuous, climatically-sensitive records of continental deposition.

2) One of the primary goals of this study was to obtain an independent climatic record for the Quaternary from a mid-latitude continental setting in order to evaluate the correlation between climatic changes in this location and the high-latitude ice volume fluctuation revealed in the $\delta^{18}O$ of marine foraminifera. While comparison of the lake levels in the paleo-Owens River system with the deep-sea ^{18}O curve shows some similarities, it also shows strong and systematic differences. I believe that these differences reflect climatic processes important at the mid-latitudes. More detailed investigations in the paleo-Owens system, and additional studies in other closed basins, have the potential to greatly advance our understanding of Quaternary climatic change in the mid-latitudes.

3) If the possibility of a fundamental difference between Holocene climate and that of at least the previous interglaciation is borne out by further investigations, it will imply that the Holocene is not a good model for reconstruction of paleoecological patterns during previous interglaciations, or for prediction of future hydrologic conditions. Such differences in climate might possibly help to explain the massive faunal extinctions at the end of the Pleistocene.

APPENDIX 1

SAMPLE LOCATIONS AND DESCRIPTIONS

Core Samples

The core samples listed in Table 3 were collected with the aid of G.I. Smith of the Sedimentary Processes Branch of the US Geological Survey, Menlo Park, CA, who has worked extensively in the area. All of the samples were pure halite crystals except the following:

SLC-1	Loose aggregate of sand, clay and halite granules. This is the only core sample that was collected from core KM-6 because this interval (Overburden Mud) was not recovered in the KM-3 core.
SLC-4	Halite crystal with mud impurities.
SLC-3	Loose aggregate of sand, clay and halite granules.
CLC-2	Predominantly gypsum with minor halit.
WLC-1	Lacustrine mud. Chlorine extracted from pore fluid.
WLC-6	Lacustrine mud. Chlorine extracted from pore fluid.
WLC-4	Lacustrine mud. Chlorine extracted from pore fluid.
LDS60-72	Sample from surface of Bonneville Salt Flats, UT, collected during or prior to 1943. Saline crust of predominantly halite with mud impurities.
BYU-658	Sample from surface of Bonneville Salt Flat, UT, collected during or prior to 1891. Saline crust of predominantly halite with mud impurities.
BONN C-3	Collected from core at a location on the Southern Pacific railway causeway, near what is now the deepest part of Great Salt Lake, UT. Halite crystal with mud impurities.
BONN C-4	same description as BONN C-3.
CVC-1	Tufa deposit
CVC-2	Tufa deposit

Waters

SLW-1	Casa Diablo hot springs. Mt. Morrison, CA Quad. T.3S., R.28E., sec. 32, SW1/4 of NW1/4. T° - boiling. 10/22/83
SLW-22	Casa Diablo Pool. Location same as sample SLW-1.
SLW-21	Casa Diablo Well. Location same as sample SLW-1
SLW-20	Big Akali hot springs. Mt. Morrison, CA Quad. T.3S., R.29E., sec. 21, SE1/4 OF SW1/4.
SLW-2	HS SLW-2. Hot springs 1 mile north of Whitmore hot springs. Mt. Morrison, CA Quad. T.3S., R.29E., sec. 31, NE1/4. 58°C. 10/22/83
SLW-3	Little Hot Creek hot springs. Mt. Morrison, CA Quad. T.3S., R.28E., sec. 13, NW1/4. 84°C. 10/22/83
SLW-4	Hot Creek hot springs. Mt. Morrison, CA Quad. T.3S., R.28E., sec. 25, NE1/4. 86°C. 10/22/83
SLW-5	Black Point Hot Well. North shore of Mono Lake. 1.3 km E. of Deschambean Ranch (sec. 10). Bodie, CA Quad. T.2N., R.26E., sec. 11, SW1/4, of NW1/4. 60°C. 10/23/83
SLW-6	Bishop flowing well. Bishop, CA Quad. T.7S., R.33E., sec. 10, NW1/4 of NE1/4. 26°C. 10/24/83
SLW-7	Keough hot spring. Bishop, CA Quad. T.8S., R.33E., sec. 17, SE1/4 of NW1/4. 52°C. 10/24/83
SLW-8	Dirty Socks hot spring. South shore of Owens Lake. Keeler, CA Quad. T.18S., R.37E., sec. 34, NE1/4 of NE1/4. 29°C. 10/24/83
SLW-9	Stream N. of Francis Lake. Mt. Tom, CA Quad. 3.2 km NE of Mt. Tom. Used anion-exchange resin. 7/13/84
SLW-10	Birch Creek, Deep Springs Valley. Blanco Mtn.,CA Quad. T.7S., R.36E., sec. 20, NE1/4 of NE1/4. Used anion-exchange resin. 7/14/84
SLW-11	Corral Springs, Deep Springs Valley, Blanco Mtn., CA Quad. T.8S., R.36E., sec. 3, SW1/4 of SW1/4. 7/14/84
SLW-12	Artesian well on north side of Deep Springs Lake Playa. Blanco Mtn., CA Quad. T.8S., R.36E., sec. 4, NE1/4 of NW1/4. 14°C. 7/14/84

SLW-13 North Fork Crooked Creek. Mt. Barcroft, CA Quad. Spring at head of stream. White Mtn. Research Station, Crooked Creek Laboratory, Univ. of CA. Used anion-exchange resin. 7/14/84

SLW-14 Sawmill Creek. Mt. Pinchot, CA Quad. T.12S., R.34E., sec 8, SW1/4 of SW1/4. Used anion-exchange resin. 7/15/84

SLW-15 Owens River at Alabama Gates. Lone Pine, CA Quad. T.14S., R.35E., sec. 24, NW1/4. Used anion-exchange resin. 7/15/84

SLW-16 Warm Springs. Bishop, CA Quad. T.8S., R.34E., sec. 8, NW1/4 of SW1/4. 28°C. 7/17/84

GBL-1 Walker Lake at "Sportman's Beach". Walker Lake, NV, 250,000 series map. T.9N., R.29E., NW1/4. 7/9/84

GBL-2 Walker River at 6 miles south of Schurz, NV. Walker Lake, NV, 250,000 series map. T.12N., R.29E., Nw1/4 of SW1/4. 7/9/84

GBL-3 Truckee River at the Nixon Bridge on Highway 34. Reno, NV, 250,000 series map. T.23N., R.23E., SE1/4 OF SE1/4. 7/9/84

GBL-4 Pyramid Lake at 5 miles north of Nixon, NV on Nevada #446. Reno, NV, 250,000 series map. T.23N., R.23E., W1/2 OF NW1/4. 7/9/84

Surficial Salines

SLS-1 Warren Lake bed. Big Pine, CA Quad. T.9S., R.33E., sec 2, E1/2. 10/24/83

SLS-2 Deep Springs Lake bed. Blanco Mtn., CA Quad. T.8S., R.36E., sec. 4, SW1/4 of NW1/4. 7/14/84

SLS-3 Owens Lake bed. Keeler, CA Quad. T.18S., R.37E., sec. 24, N1/2. 7/14/84

BRS-1 Eightmile Flat playa at approximately 16 miles southeast of Fallon, NV. Reno, NV, 250,000 map series. T.17N., R.31E., SW1/4. 7/9/84

Glacial erratics

Rock Creek Moraine. Casa Diablo Mtn., CA Quad. T.4S., R.30E., sec. 33, NW1/4. 7/20/84 no's. RCM 1-5.

Bloody Canyon Moraine. Mono Craters, CA Quad. T.1S., R.26E., sec's 5, 6, 8. 7/12/84 no's. BCM A1-S, BCM B1-5, BCM C1-5, BCM D1-5.

McGee Mtn. Till. Mt. Morrison, CA Quad. T.4S., R.29E., sec. 30, N1/2. 7/19/84 no's. MMT 1-3.

APPENDIX 2

CHLORIDE EXTRACTION FROM FRESH WATER USING ANION-EXCHANGE RESIN

Note: DD refers to distilled deionized (18 Mohm) water

A. Resin preparation.

1. When resin is purchased, it is initially in chloride form. Elute with 2 M $NaNO_3$ (AR grade) or 2 M HNO_3 until no chloride is detected in the eluant when tested with a solution of $AgNO_3$. The flow rate should be about 0.4 mL/min/cm^2 bed per recommendation in BioRad™ catalog. Takes about 5 or more bed volumes of NO_3 solution.
2. Rinse with DD water until the pH returns to normal (pH 5-6).
3. Elute resin with 2 M NaAc. Check for chloride in eluant by $AgNO_3$ test. Check for NO_3 in eluant, for example by Hach™ kit Cd reduction method. Residual NO_3 on resin will reduce efficiency of chloride capture but otherwise is not of concern.
4. Rinse with DD water. Pack columns or store resin in bottles for packing of columns in the field.

B. Column preparation.

1. With one end capped and plugged, fill PVC column partially with distilled water. Add saturated glass wool plug, tamp into place. Minimize presence of entrapped air as much as possible (affects flow rate in field).
2. Slurry into column about 30 cm^3 of resin. At 1.4 meq/cm^3, this amount should be adequate to collect the desired quantity of chloride.
3. Add saturated glass wool plug to top of resin, fill column with DD water and screw on top endcap.

C. Field operation.

1. Collect sufficient sample to yield at least 200 mg chloride by collecting the sample in a large carboy with a stop-cock outlet, or by placing apparatus directly in flow (for example, flowing stream) and using a funnel to direct the flow into the column.
2. If using the carboy method, connect flexible tubing to stop-cock outlet, fill tubing with sample water by opening stop-cock, then connect resin column to end of tubing.
3. If possible set up column so that flow travels up through column to maximize exchange efficiency. Flow rate should be on the order of 3 $mL/min/cm^2$ bed cross-section. For a column of 3 cm diameter, this rate is about 1.2 L/hr.

4. The flow may slow considerably if the sample degasses in the tubing or in the column. In that case, let the air bubbles out and re-start the flow.

D. Extraction of chloride.

1. Slurry resin from column into buret containing small glass wool plug on bottom.
2. Elute resin with 2 M $NaNO_3$ until chloride content of eluant is negligible. This takes about four bed volumes. Resin volume will decrease by about 20%.
3. If a separate sample was not taken for the determination of chloride concentration, remove an aliquot at this time for this purpose.
4. Add sufficient $AgNO_3$ solution to eluant to precipitate AgCl. Let sit overnight to allow precipitate to form and settle.
5. Purify by normal procedure.

APPENDIX 3

CHLORIDE EXTRACTION FROM SILICATE ROCK SAMPLES

Note: DD refers to distilled deionized (18 Mohm) water

A. Leach out meteoric chloride.

1. Wash 100 g of 100 mesh rock powder in 1000 mL DD water by thoroughly mixing in blender.
2. Pour into 1000 mL beaker, cover, and allow to settle (at least 48 hours).
3. When supernatant is clear (or nearly so), decant. If chloride analysis of leachate is desired, place supernatant in 1000 mL plastic bottles; otherwise discard.
4. Dry rock powder at 110°C overnight.
5. Remove dry rock powder and grind gently to homogenize.

B. Determine minimum sample size.

1. Estimate $^{36}Cl/Cl$ for sample by using the age equation and an approximate age.
2. Estimate chloride concentration of rock samples from published analyses of silicate rocks in the Sierra Nevada.
3. Grams of sample required = $0.4/[(\text{ppm Cl} \times 10^{-2})(^{36}\text{Cl/Cl} \times 10^{15})]$.

4. Since recovery is typically 50-60%, double the result in 3 above to get minimum sample size (typically 30-40 g).

C. NaOH fusion.

1. Prepare 100 mL nickel crucible by washing, rinsing with DD water, leaching for 1 hour in 10% HNO_3, rinsing in DD water and drying.
2. Weigh out ultrapure NaOH, 6x sample weight, and place into crucible(s).
3. Place crucible on clay dish and fuse NaOH at 565°C for 15 min to drive off water.
4. Remove crucible from furnace and allow to cool until NaOH is solid.
5. Weigh rock powder and pour carefully on top of NaOH cake in crucible.
6. Replace crucible on clay dish and fuse at 565^0 C for 30 min. Swirl crucible to ensure mixture of rock powder and flux. Fuse an additional 30 min.
7. Remove crucible, cover, and allow to cool.
8. Remove cake from crucible and store in sealable container.
9. Repeat until necessary amount of rock powder is fused.

D. Chloride extraction.

1. Dissolve fusion cake(s) in 1000 mL hot DD water and 10 mL ethanol, stirring.
2. Decant supernatant and discard particulate material. If solution is cloudy, filter or centrifuge to remove suspended particles before proceeding.

3. Acidify supernatant to pH 2-3 with HNO_3, stirring. The addition of strong acid causes a violent reaction and should be done drop by drop. The supernatant begins as an extremely basic solution (pH ~12) and will require a large volume, typically 80-100 mL, of HNO_3 to lower the pH to 2-3. The general reaction occurs as follows:
   i. no change to pH 9
   ii. at pH 9, colloidal precipitate forms and persists
   iii. pH decreases slowly to ~7 (with evolution of CO_2 in carbonate)
   iv. CO_2 evolves rapidly in carbonate solution at pH 7
   v. solution may or may not clear as pH lowers to 1-2 (CO_2 production subsides)
4. Centrifuge to remove colloidal material or precipitate before proceeding. If a large amount of rock powder is needed (> 100 g), there will be more than 3 fusion cakes (from one sample) to dissolve (Step 1, this section). This results in a large quantity of liquid and colloidal material to centrifuge and from which to precipitate out often a small amount of AgCl. I used a large centrifuge with the largest possible plastic bottles. I did not have distillation apparatus, but it would be very helpful to reduce the quantity of liquid (250 mL) before the addition of $AgNO_3$.
5. If chloride concentration is not known, remove an aliquot of water for this purpose.
6. Add an excess of $AgNO_3$ to precipitate AgCl.

7. Cover and allow to sit in a dark place overnight to allow precipitate to form and settle.
8. If storage is necessary, centrifuge AgCl, decant all but enough supernatant to cover AgCl, and place in dark bottle.
9. Filter out precipitate and purify by normal procedure.

APPENDIX 4

AgCl PURIFICATION PROCEDURE

Note: DD refers to distilled deionized (18 Mohm) water.

There are two procedures for AgCl purification - the choice basically depends on sample size. I also found the evaporative method (A) more successful in removing sulfur. The reprecipitation method (B) was used for samples that yielded very small amounts of AgCl (< 10 mg). The small sample size was handled easier in small test tubes, and fewer transfers of sample (where sample can be lost) were needed.

Great care must be taken during the purification process to avoid contamination of the samples. The entire purification process is performed in a laboratory fume hood. Only reagent-grade chemicals should be used. Clean plastic or rubber gloves should be worn at all times, and all equipment should be washed and treated each time it is used. Samples should be covered whenever possible.

Plastic and glassware should be washed with laboratory soap and rinsed with distilled water. They should then be rinsed with dilute HNO_3, followed by DD water, and rinsed again with dilute NH_4OH, followed by several rinses with DD water. Metal bases of filter funnels, holding the plastic support screens, should not be rinsed with HNO_3 (plastic filter funnels are preferred). The metal should be rinsed with DD water, followed by dilute NH_4OH, and then rinsed again in DD water. Laboratory squeeze bottles containing DD water, dilute reagent-grade HNO_3 and dilute reagent-grade NH_4OH are useful for treating the equipment.

A. Evaporative method

If AgCl was previously precipitated in the field or laboratory, proceed with step 2.

1. Remove an aliquot of water for determination of chloride concentration (if not previously done), set aside.
2. Add $AgNO_3$ in an amount sufficient to precipitate at least 200 mg AgCl. Let stand for 24 hours in the dark.
3. Decant and discard the supernatant. Filter the AgCl precipitate to near dryness in a filter funnel, with 0.45 micron filter paper, using a vacuum pump. Wash the precipitate thoroughly in the filter funnel with DD water and discard solution.
4. Transfer the filter funnel to a filter flask with a 25x200-mm test tube inside (lower and raise test tube into and out of the flask with treated plastic forceps). Dissolve the precipitate by adding 25-50 mL NH_4OH to the filter funnel. Allow sufficient time for the precipitate to dissolve and gravity filter. Only if necessary, gently draw the solution into the test tube with the vacuum pump. Use NH_4OH to rinse and dissolve any precipitate that may stick to the sides of the funnel. Remove filter funnel and discard used filter paper with any remaining precipitate.

5. Transfer solution from test tube to a treated 200 mL beaker. Carefully add 1 mL $Ba(NO_3)_2$ to solution in beaker as sputtering may occur. Cover beaker with parafilm and let it stand overnight. The addition of barium nitrate ($Ba(NO_3)_2$) results in precipitation of barium sulfate. Sulfate is a very abundant form of sulfur in the environment. If high sulfur or sulfate content is known or suspected, additional barium precipitations are suggested. (To make the $Ba(NO_3)_2$ solution, place a good amount of solid $Ba(CO_3)_2$ in a flask. Add sufficient HNO_3 to dissolve some of the $Ba(CO_3)_2$, but leave some in solid form in the bottom of the flask. When using the $Ba(NO_3)_2$ solution, draw off the liquid from the top.)
6. Filter solution into a test tube and transfer to a treated 400 mL beaker (more efficient during evaporation process). Discard used filter paper.
7. Lay a glass stirring rod across the top of the beaker and cover with a chemical watch glass (concave side up). Evaporate the NH_4OH and reprecipitate the AgCl by heating the beaker at 50°-60°C for 1 to 3 hours. Do not let samples "boil or sputter" as cross-contamination might occur. Add small amounts of DD water during the heating process to buoy up the precipitate and prevent it from sticking to the bottom and sides of the beaker.
8. Using DD water, rinse the precipitate from the beaker into the filter apparatus. Wash the precipitate thoroughly with DD water and filter it to near dryness.
9. Transfer filter funnel to a filter flask with a test tube set up. Redissolve the AgCl precipitate by adding 25-50 mL NH_4OH to the filter funnel. Again allow sufficient time for the precipitate to dissolve and gravity filter. Only if

necessary, draw solution into test tube with the vacuum pump. Use NH_4OH to rinse and dissolve any precipitate that may stick to the sides of the funnel. Remove the filter funnel and discard used filter paper.

10. Transfer solution to a 400 mL beaker and repeat steps 6 and 7. If sulfur contamination is a concern (that is, solution has color) or a known problem, repeat steps 8 and 9. During final filtering process, try to "gather" precipitate from filter funnel sides onto the micropore filter paper using DD water.

11. Crumple and then flatten a blue filter-cover paper (found between the individual 0.45 micron filters), and lay it on a treated watch glass (concave up). Using treated forceps, place the filter paper with the AgCl precipitate on top of the blue filter-cover paper. Place the watch glass in an oven allowing the precipitate to dry overnight at 45°C (if time is of the essence, a drying time of 1-2 hours at 65°C should be sufficient).

12. Weigh a treated and dried sample bottle. Transfer the dry powder sample to the dark-glass sample bottle, reweigh to obtain sample weight. Wrap parafilm around the bottle cap. Label, date, and store in a dark location.

B. Reprecipitation method

If AgCl has been previously precipitated in sufficient quantity, proceed to step 3.

1. Remove an aliquot of water for determination of chloride concentration (if not previously done), set aside.

2. If needed, concentrate the remaining solution to about 250 mL by distillation.
3. Add excess $AgNO_3$ to precipitate AgCl. If needed, add carrier and sufficient $AgNO_3$ to produce a total of about 10 mg of sample (AgCl). Let sit overnight to allow precipitate to form and settle.
4. Decant or pipette the solution and discard.
5. Suspend the precipitate in DD water (~10 mL) and transfer to a clean pretreated centrifuge tube. Spin precipitate down to a pellet or film at the bottom of the tube. Decant or pipette the solution and discard.
6. Dissolve the precipitate with 2 mL of NH_4OH and 10 mL of DD water. A vortex mixer can be used to speed up the dissolution.
7. Add 1 mL of $Ba(NO_3)_2$ to solution still in centrifuge tube. Let sit overnight in order for $BaSO_4$ to form.
8. Centrifuge the solution. Pipette into another pre-treated centrifuge tube leaving the $BaSO_4$ behind.
9. Acidify the solution with nitric acid (5-10 mL) to precipitate AgCl. Let sit in dark for several hours (5-6).
10. Repeat steps 4, 5, 6, and 9 one or more times in same tube.
11. Wash precipitate with DD water, spin and pipette or decant solution. Repeat.
12. Cover tubes (aluminum foil works fine) and dry in oven (75°-100°) several hours or overnight. Store in dark.

APPENDIX 5

PART A. DESCRIPTION OF THE HIERARCHICAL OR NESTED METHOD

The following is a reproduction of a section from a statistical text (Li, 1964) which explains the hierarchical method. The description presents the concepts and the equations used in the procedure, along with an example.

Hierarchical classification is a continued or repeated one-way classification into minor groups within each major group.

1. A three-rank hierarchy

Notations and a numerical example are given in Table 9.1, in which the subscript h specifies the *major* group, the subscript i indicates a *minor* group within a major group, and α, as usual, indicates the individual member in a minor group. A clear distinction should be made between the number of observations and the number of groups. The letters n and N are employed to denote the former and K and H to denote the latter. Thus, n_{hi} is the number of observations in the ith minor group of the hth major group, so that $n_{hi}\bar{y}_{hi} = Y_{hi}$ is the total of that minor group. The "size" of a major group is $N_h = \sum_i n_{hi}$. The summation covers all the minor groups of the hth major group, so that $N_h\bar{y}_h = Y_h$ is the total of that major group. The grand total number of observations is

$$N = \sum_h N_h = \sum_h \sum_i n_{hi}$$

Let H be the number of major groups. Then

$$N = N_1 + N_2 + \cdots + N_H$$

Also, let k_1 be the number of minor groups in the first major group, etc., so that $K = k_1 + k_2 + \cdots$ is the *total* number of minor groups in the entire set of data. An examination of Table 9.1 will make the meaning of the symbols clear.

The sizes (n and N) appear explicitly in calculating the various sums of squares, and the number of groups (K and H) appear in calculating the various degrees of freedom. The arithmetical procedure and the statistical model are such obvious extensions of the preceding chapters that some of the details are omitted (but understood) in the following paragraphs.

Table 9.1 Hierarchical classification with three ranks

Single values $y_{hi\alpha}$	Minor groups			Major groups			Entire group		
	Size n_{hi}	Total Y_{hi}	Mean $\bar{y}_{hi}$	Size N_h	Total Y_h	Mean $\bar{y}_h$	Size N	Total Y	Mean $\bar{y}$
6 2 9 3	4	20	5	6	36	6	12	84	7
12 4	2	16	8						
4 8	2	12	6	6	48	8			
9	1	9	9						
10 6 11	3	27	9						
	K = 5 minor groups			H = 2 major groups			One whole group		

2. Basic quantities and *ssq*

We may construct four rows of squares (Fig. 9.1) based on the data of Table 9.1 and similar to our Fig. 5.1 for simple classifications. The areas of the four series of squares are

$$A = \sum_h \sum_i \sum_\alpha y_{hi\alpha}^2 = 6^2 + 2^2 + 9^2 + \cdots + 6^2 + 11^2 = 708$$

$$B_1 = \sum_h \sum_i \left(\frac{Y_{hi}^2}{n_{hi}}\right) = \frac{20^2}{4} + \frac{16^2}{2} + \frac{12^2}{2} + \frac{9^2}{1} + \frac{27^2}{3} = 624$$

$$B_2 = \sum_h \left(\frac{Y_h^2}{N_h}\right) = \frac{36^2}{6} + \frac{48^2}{6} = 600$$

$$C = \frac{Y^2}{N} = \frac{84^2}{12} = 588$$

These are the four basic quantities from which the various sums of squares are obtained. Thus,

Within minor groups: $ssq_W = A - B_1 = 84$
Between minor, within major: $ssq_B = B_1 - B_2 = 24$
Between major groups: $ssq_H = B_2 - C = 12$

Total: $ssq_T = ssq_W + ssq_B + ssq_H = A - C = 120$

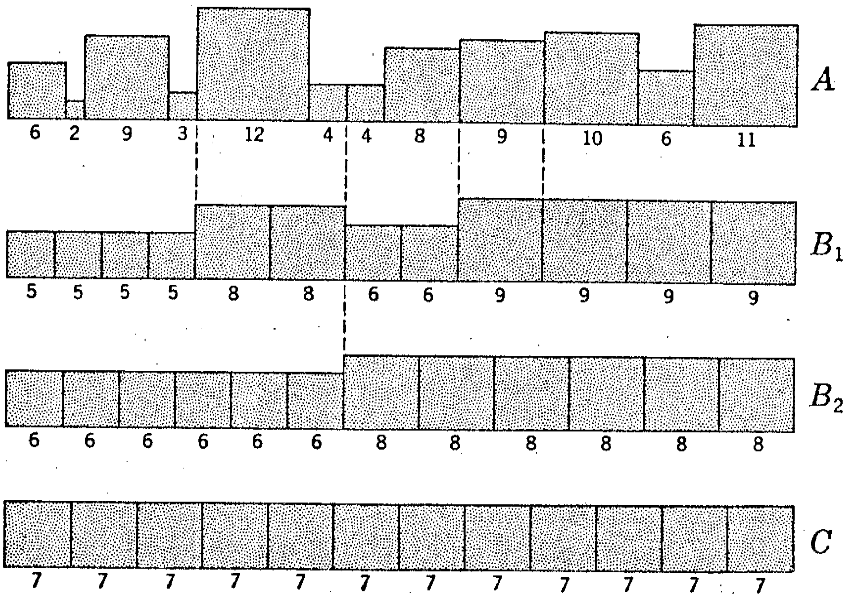

Fig. 9.1 The four areas A, B_1, B_2, C corresponding to the groupings of Table 9.1.

Table 9.2 The linear model of a three-rank classification

$\bar{y}$	m_h	$\bar{y}_h$	t_{hi}	$\bar{y}_{hi}$	$e_{hi\alpha}$	$y_{hi\alpha}$	$d_{hi\alpha} = y_{hi\alpha} - \bar{y}$
7	−1	6	−1	5	+1	6	−1
7	−1	6	−1	5	−3	2	−5
7	−1	6	−1	5	+4	9	+2
7	−1	6	−1	5	−2	3	−4
7	−1	6	+2	8	+4	12	+5
7	−1	6	+2	8	−4	4	−3
7	+1	8	−2	6	−2	4	−3
7	+1	8	−2	6	+2	8	+1
7	+1	8	+1	9	0	9	+2
7	+1	8	+1	9	+1	10	+3
7	+1	8	+1	9	−3	6	−1
7	+1	8	+1	9	+2	11	+4
84	0	84	0, 0	84	0, 0 0, 0, 0	84	0
ssq	12		24		84		120

The various *ssq*, if written out in terms of deviations, will take the following forms:

$$ssq_W = \sum_h \sum_i \sum_\alpha (y_{hi\alpha} - \bar{y}_{hi})^2 = \sum_h \sum_i \sum_\alpha e_{hi\alpha}^2$$

$$ssq_B = \sum_h \sum_i n_{hi}(\bar{y}_{hi} - \bar{y}_h)^2 = \sum_h \sum_i n_{hi}t_{hi}^2$$

$$ssq_H = \sum_h N_h(\bar{y}_h - \bar{y})^2 = \sum_h N_h m_h^2$$

Adding
$$ssq_T = \sum_h \sum_i \sum_\alpha (y_{hi\alpha} - \bar{y})^2 = ssq_H + ssq_B + ssq_W$$

3. The linear model

The meaning of the above expressions is at once clear if the data of Table 9.1 are rewritten in the form of Table 9.2, which is analogous to our Table 6.1 for a simple one-way classification. Thus, we see that each observed number may be regarded as consisting of four component parts; for instance, the fifth number in the column $y_{hi\alpha}$ of Table 9.2 is

$$12 = 7 - 1 + 2 + 4$$

Generally,

$$y_{hi\alpha} = u + m_h + t_{hi} + e_{hi\alpha}$$

where $u = \bar{y}$ is the sample estimate of the general population mean, $m_h = \bar{y}_h - \bar{y}$ is the sample estimate of the major group effect, $t_{hi} = \bar{y}_{hi} - \bar{y}_h$ is the minor group effect, and $e_{hi\alpha} = y_{hi\alpha} - \bar{y}_{hi}$. Following the reasoning of Chap. 6, we see that these are the least-square estimates which minimize the quantity

$$Q = \Sigma\Sigma\Sigma(y_{hi\alpha} - u - m_h - t_{hi})^2 = \Sigma\Sigma\Sigma e_{hi\alpha}^2$$

In other words, the ssq_W is a minimum when the estimates take on such values.

4. Expected value of mean square

This section may be omitted by those who do not care for the details of the expectations of the various mean squares. The numerical values of *ssq*'s given in Sec. 2, when divided by their corresponding degrees of freedom, may be subjected to the F test in the usual manner. The four basic expectations to be found are those of $E\{A\}$, $E\{B_1\}$, $E\{B_2\}$, and $E\{C\}$, each single term of which is as follows:

(A single value)^2:

$$y_{hi\alpha}^2 = (u + m_h + t_{hi} + e_{hi\alpha})^2$$

(Minor group total)^2:

$$Y_{hi}^2 = \left(n_{hi}u + n_{hi}m_h + n_{hi}t_{hi} + \sum_\alpha e_{hi\alpha}\right)^2$$

(Major group total)^2:

$$Y_h^2 = \left(N_h u + N_h m_h + \sum_i n_{hi}t_{hi} + \sum_i \sum_\alpha e_{hi\alpha}\right)^2$$

(Grand total)^2:

$$Y^2 = \left(Nu + \sum_h N_h m_h + \sum_h \sum_i n_{hi}t_{hi} + \sum_h \sum_i \sum_\alpha e_{hi\alpha}\right)^2$$

Some simplifying assumptions have to be made here as before, when a common variance was assumed for all the groups. By analogy, we assume that the variance of the groups of the same rank in the hierarchy is the same, so that $E\{e^2\} = \sigma_e^2$, no matter to which individual it belongs; $E\{t^2\} = \sigma_t^2$, no matter to which minor group it belongs; and $E\{m^2\} = \sigma_m^2$, no matter to which major group it belongs. These can be accepted as definitions of the expectations (or as a matter of notation). We shall not discuss the difference between the so-called models I and II, although the notation employed here is more consistent with the concept of model II. Another assumption is that the components u, m, t, e, are all statistically independent so that the expected value of any product

Table 9.3 The analysis of variance for hierarchical classifications (data taken from Table 9.1)

Source of variation	df	ssq	msq	Expectation
Between major groups	$H - 1 = 1$	$ssq_H = 12$	$s_H^2 = 12$	$\sigma_e^2 + c_1\sigma_t^2 + c_2\sigma_m^2$
Between minor (within major) groups	$K - H = 3$	$ssq_B = 24$	$s_B^2 = 8$	$\sigma_e^2 + c_3\sigma_t^2$
Within minor groups (error)	$N - K = 7$	$ssq_W = 84$	$s_W^2 = 12$	σ_e^2
Total	$N - 1 = 11$	$ssq_T = 120$		

term is zero. Now, squaring each term, taking the expectations, and summing, we obtain the following results:

$$E\{A\} = E\left\{\sum\sum\sum y_{hi\alpha}^2\right\} = N\mu^2 + N\sigma_m^2 + N\sigma_t^2 + N\sigma_e^2$$

$$E\{B_1\} = E\left\{\sum\sum \frac{Y_{hi}^2}{n_{hi}}\right\} = N\mu^2 + N\sigma_m^2 + N\sigma_t^2 + K\sigma_e^2$$

$$E\{B_2\} = E\left\{\sum \frac{Y_h^2}{N_h}\right\} = N\mu^2 + N\sigma_m^2 + \sum \frac{n_{hi}^2}{N_h}\sigma_t^2 + H\sigma_e^2$$

$$E\{C\} = E\left\{\frac{Y^2}{N}\right\} = N\mu^2 + \sum \frac{N_h^2}{N}\sigma_m^2 + \sum \frac{n_{hi}^2}{N}\sigma_t^2 + \sigma_e^2$$

The expected values of the various sums of squares may then be obtained by taking the appropriate differences of the above expectations. For example,

$$E\{ssq_W\} = E\{A\} - E\{B_1\} = (N - K)\sigma_e^2$$

The complete analysis of variance is given in Table 9.3. For brevity, the quantities like $(N - \Sigma N_h^2/N)$, obtained by taking differences, will simply be denoted by a constant symbol c. The value of $F = s_B^2/s_W^2$ is used to test if $\sigma_t^2 = 0$, that is, if there are minor group effects. The value of $F = s_H^2/s_W^2$ may be used to test if both σ_t^2 and σ_m^2 are zero. However, the use of $F = s_H^2/s_B^2$ for unequal groups is very doubtful, because in general $c_1 \neq c_3$.

PART B. Example of statistical analyses of $^{36}Cl/Cl$ measurements using the hierarchical method. The format from the example above will be used.

Terminology:

Run - represents the measuring of samples on one sample wheel.
Sequence - the number of times one sample is measured during a wheel run.
Cycle - the number of times a sample is measured within a sequence, during a wheel run.

Sample SLC-12:

This sample was measured once during one run, and three times during another run - the two runs were months apart. The numbers have already been normalized to the standard and adjusted to a blank.

Summary:

Cycles - total of 13 $^{36}Cl/Cl$ ratios were measured.
Sequences - total of 4. The first run had only 1 sequence of 2 cycles. The second run had 3 sequences, 2 had 4 cycles each, the third had 3 cycles.
Runs - total of 2

Diagram of "hierarchy" for $^{36}Cl/Cl$ measurements:

Cycle measurements $^{36}Cl/Cl$ ratios	Minor Groups Sequences Size	Total	Mean	Major Groups Runs Size	Total	Mean	Entire Group Final Ratio Size	Total	Mean
8.67									
16.49	3	35.57	11.86						
10.41									
14.05									
10.64									
11.85	4	43.87	10.97	11	121.60	11.01			
7.33									
12.08							13	157.24	12*
6.48									
7.79	4	42.16	10.54						
15.81									
18.11									
17.53	2	35.64	17.82	2	35.64	17.82			

* The final mean (μ), or ratio, is 12. Next, the uncertainty (σ) will be calculated.

The uncertainty (σ) is determined by performing an analysis of variance (Table 9.3 above).

Analyses of variance (ANOVA) for determination of error (σ) in hierarchical classification:

Source of error		df	SS	μS	Expectation
Between runs			ssq_H =	$ssq_H/H\text{-}1$ =	$\sigma_B^2+C_1\sigma_t^2+C_2\sigma_H^2$
Between sequences	K-1	3	ssq_B = 80.54	$ssq_B/K\text{-}1$ = 26.84	$\sigma_B^2+C_3\sigma_t^2$
Between cycles	N-K	9	ssq_W = 111.65	$ssq_W/N\text{-}K$ = 12.41	σ_B^2
	N-1	12			

where

df = degrees of freedom
SS = sum of squares
μS = means of squares

and

$$ssq_H = \Sigma\left(\frac{(\text{run total})^2}{\text{number of cycles in run}}\right) - \left(\frac{(\text{final total sum})^2}{\text{total number of cycles}}\right)$$

-For this particular example, ssq_H is not determined since there was only one run

$$ssq_B = \Sigma\left(\frac{(\text{seq. total})^2}{\text{number of cycles in seq}}\right) - \Sigma\left(\frac{(\text{run total})^2}{\text{number of cycles in run}}\right)$$

$$= \left(\frac{(35.57)^2}{3} + \frac{(43.87)^2}{4} + \frac{(42.16)^2}{4} + \frac{(35.64)^2}{2}\right) - \left(\frac{(157.24)^2}{13}\right) = 80.54$$

$$ssq_W = \Sigma\left(\begin{matrix}\text{value of}\\ \text{each cycle}\end{matrix}\right)^2 - \Sigma\left(\frac{(\text{seq. total})^2}{\text{number of cycles in seq}}\right)$$

$$= [(8.67)^2 + (16.49)^2 + (10.41)^2 + (14.05)^2 + (10.64)^2 + (11.85)^2 + (9.33)^2 +$$
$$(12.08)^2 + (6.48)^2 + (7.79)^2 + (15.81)^2 + (18.11)^2 + (17.53)^2] -$$
$$\left(\frac{(35.57)^2}{3} + \frac{(43.87)^2}{4} + \frac{(42.16)^2}{4} + \frac{(35.64)^2}{2}\right)$$

$$= 2094.10 - 1982.35 = 111.65$$

For a sample with one run the total error is as follows:

The variation between sequences: $\mu sq_B = \sigma_B^2 + C_3\sigma_t^2$

rearranging $\sigma_t^2 = \dfrac{\mu sq_B - \sigma_B^2}{C_3}$

where

$\mu sq_B = ssq_B/K\text{-}1$

and

$$C_3 = \frac{(\text{total number of cycles}) - \dfrac{\Sigma(\text{number of cycles in sequence})^2}{(\text{total number of cycles})}}{K\text{-}H}$$

$= 13 - (3.46/4) = 2.38$

and

$\sigma_t^2 = (26.84 - 12.41)/2.38$
$= 6.05$

The variation between cycles: $\mu sq_W = \sigma_B^2$

where

$\mu sq_W = ssq_W/N\text{-}K$

The final variation (σ^2) is $\dfrac{\sigma_B^2}{N} + \dfrac{\sigma_t^2}{K}$

$= 12.41/13 + 6.05/4$
$\sigma^2 = 2.18$
$\sigma = 1$

The final ratio and uncertainty is 12 ± 1

The uncertainty (σ) is determined by performing an analysis of variance (Table 9.3 above).

Analyses of variance (ANOVA) for determination of error (σ) in hierarchical classification:

Source of error		df	SS	μS	Expectation
Between runs			ssq_H =	$ssq_H/H\text{-}1$ =	$\sigma_E^2+C_1\sigma_t^2+C_2\sigma_M^2$
Between sequences	K-1	3	ssq_B = 80.54	$ssq_B/K\text{-}1$ = 26.84	$\sigma_B^2+C_3\sigma_t^2$
Between cycles	N-K	9	ssq_W = 111.65	$ssq_W/N\text{-}K$ = 12.41	σ_E^2
	N-1	12			

where

df = degrees of freedom
SS = sum of squares
μS = means of squares

and

$$ssq_H = \Sigma\left(\frac{(\text{run total})^2}{\text{number of cycles in run}}\right) - \left(\frac{(\text{final total sum})^2}{\text{total number of cycles}}\right)$$

-For this particular example, ssq_H is not determined since there was only one run

$$ssq_B = \Sigma\left(\frac{(\text{seq. total})^2}{\text{number of cycles in seq}}\right) - \Sigma\left(\frac{(\text{run total})^2}{\text{number of cycles in run}}\right)$$

$$= \left(\frac{(35.57)^2}{3} + \frac{(43.87)^2}{4} + \frac{(42.16)^2}{4} + \frac{(35.64)^2}{2}\right) - \left(\frac{(157.24)^2}{13}\right) = 80.54$$

$$ssq_W = \Sigma\left(\begin{matrix}\text{value of}\\ \text{each cycle}\end{matrix}\right)^2 - \Sigma\left(\frac{(\text{seq. total})^2}{\text{number of cycles in seq}}\right)$$

$$= [(8.67)^2 + (16.49)^2 + (10.41)^2 + (14.05)^2 + (10.64)^2 + (11.85)^2 + (9.33)^2 + (12.08)^2 + (6.48)^2 + (7.79)^2 + (15.81)^2 + (18.11)^2 + (17.53)^2] - \left(\frac{(35.57)^2}{3} + \frac{(43.87)^2}{4} + \frac{(42.16)^2}{4} + \frac{(35.64)^2}{2}\right)$$

$$= 2094.10 - 1982.35 = 111.65$$

For a sample with one run the total error is as follows:

The variation between sequences: $\mu sq_B = \sigma_B^2+C_3\sigma_t^2$

rearranging $\sigma_t^2 = \dfrac{\mu sq_B - \sigma_B^2}{C_3}$

where

$\mu sq_B = ssq_B/K\text{-}1$

and

$$C_3 = \frac{(\text{total number of cycles}) - \dfrac{\Sigma(\text{number of cycles in sequence})^2}{(\text{total number of cycles})}}{K\text{-}H}$$

$= 13 - (3.46/4) = 2.38$

and

$\sigma_t^2 = (26.84 - 12.41)/2.38$
$= 6.05$

The variation between cycles: $\mu sq_W = \sigma_E^2$

where

$\mu sq_W = ssq_W/N\text{-}K$

The final variation (σ^2) is $\dfrac{\sigma_E^2}{N} + \dfrac{\sigma_t^2}{K}$

$= 12.41/13 + 6.05/4$
$\sigma^2 = 2.18$
$\sigma = 1$

The final ratio and uncertainty is 12 ± 1

PART C. COMPARISON OF FINAL RATIOS AND UNCERTAINTIES

H = hierarchical method
R = method proposed by Elmore and others (1984)

CORE SAMPLES

SAMPLE	H	R
SLC-1	48 ± 10	43 ± 13
SLC-4	80 ± 6	76 ± 8
SLC-3	75 ± 15	69 ± 14
SLC-11	29 ± 3	27 ± 4
SLC-5	24 ± 3	24 ± 5
SLC-14	23 ± 2	24 ± 3
SLC-5.3	21 ± 3	19 ± 3
SLC-15	14 ± 5	13 ± 3
SLC-12	12 ± 1	11 ± 2
SLC-6	14 ± 3	13 ± 3
SLC-7	130 ± 33	125 ± 32
SLC-8	3 ± 1	3 ± 1
SLC-10	2 ± 1	2 ± 1
SLC-9	2 ± 1	2 ± 1
PVC-1	80 ± 3	80 ± 7
PVC-5	33 ± 4	31 ± 4
PVC-10	33 ± 3	31 ± 3
PVC-15	92 ± 7	91 ± 8
PVC-18	19 ± 2	19 ± 4
LDS60-72	34 ± 8	31 ± 6
BYU-658	30 ± 3	29 ± 6
BONN C-4	25 ± 2	23 ± 5
BONN C-3	25 ± 1	24 ± 6
CVC-1	77 ± 9	72 ± 12
CVC-2	51 ± 2	48 ± 9
BLC-1	30 ± 5	30 ± 3
BLC-2	30 ± 3	29 ± 5
BLC-3	3 ± 1	3 ± 2
BLC-5	4 ± 2	3 ± 3
CLC-1	67 ± 3	68 ± 5
CLC-2	45 ± 5	45 ± 4
CLC-3	1,163 ± 12	1,164 ± 78
WLC-1	219 ± 5	218 ± 11
WLC-6	199 ± 12	195 ± 13
WLC-4	178 ± 9	184 ± 12

WATER AND SURFICIAL SALINES

SAMPLES	H	R
SLW-1	35 ± 3	35 ± 7
SLW-2	47 ± 10	42 ± 11
SLW-3	18 ± 5	16 ± 4
SLW-4	10 ± 2	9 ± 3
SLW-5	101 ± 13	99 ± 19
SLW-7	36 ± 5	35 ± 7
SLW-8	5 ± 3	5 ± 6
SLW-16	270 ± 32	262 ± 46
SLW-9	734 ± 20	732 ± 48
SLW-14	507 ± 23	508 ± 35
SLW-15	432 ± 35	426 ± 43
SLW-17	1,117 ± 68	1,098 ± 91
SLS-1	240 ± 13	238 ± 29
SLS-3	82 ± 8	79 ± 9
SLW-10	391 ± 1	391 ± 76
SLW-11	775 ± 4	774 ± 63
SLW-12	1,050 ± 88	1,095 ± 108
SLW-13	205 ± 2	204 ± 61
SLS-2	770 ± 44	749 ± 142
GEO-1	376 ± 36	349 ± 51
GEO-2	1,929 ± 176	1,898 ± 222
GBL-1	84 ± 14	88 ± 20
GBL-2	880 ± 36	1,120 ± 55
GBL-3	708 ± 71	694 ± 92
GBL-4	169 ± 17	162 ± 18

APPENDIX 6

ANALYSES OF ROCKS

Constituents

Sample	SiO_2	TiO_2	Al_2O_3	Fe_2O_3	MnO	MgO	CaO	Na_2O	K_2O	P_2O_5
A479	48.94	2.12	13.90	12.70	0.18	9.44	8.80	3.00	0.77	0.28
BCMB2	71.24	0.26	14.94	3.11	0.16	0.51	2.40	4.12	2.86	0.10
BCMC2	76.41	0.10	13.14	1.28	0.03	0.43	0.89	5.80	1.31	0.03
BCMD2	74.43	0.15	13.86	1.64	0.06	0.58	1.91	3.35	3.60	0.05
MMT1	68.95	0.39	15.17	2.36	0.08	1.52	2.92	3.35	3.84	0.13
RCM4	64.73	0.54	14.96	5.09	0.09	2.00	4.96	2.90	3.72	0.16

Elemental

Sample	Sc	Cr	Co	Zn	As	Rb	Sb	Cs	Ba	La
A479	23.98	398	53.6	130	1.5	13	0.12	0.21	260	13.4
BCM1A	2.51	<2	35.6	29	..	138	0.10	1.83	1000	16.2
BCMB2	5.16	<2	28.9	50	..	146	<0.02	4.37	940	21.7
BCMC2	2.16	<1.5	36.4	25	..	58	0.06	1.39	480	19.0
BCMD2	2.53	<1.5	19.2	14	..	101	0.22	0.96	1210	32.9
MMT1	6.33	58	6.4	40	..	162	0.41	3.50	910	28.5
RCM4	10.91	20	31.8	37	..	153	0.62	1.91	815	42.2

Sample	Ce	Nd	Sm	Eu	Gd	Tb	Yb	Lu	Hf	Ta
A479	30.6	..	4.78	1.52	~4.0	0.65	1.84	0.268	3.94	1.06
BCM1A	30.3	8.6	1.82	0.36	~2.1	0.40	2.39	0.379	2.40	1.52
BCMB2	42.6	14.0	3.26	0.47	~3.4	0.46	2.73	0.429	2.98	1.70
BCMC2	34.1	11	2.02	0.33	~1.7	0.32	1.42	0.234	2.32	1.96
BCMD2	56.3	15.6	2.90	0.42	~1.7	0.32	1.42	0.235	2.90	1.00
MMT1	52.7	17.7	3.04	0.79	~2.2	0.39	1.52	0.259	7.90	1.41
RCM4	70.8	26.4	5.02	1.03	~4.2	0.71	2.53	0.382	5.10	1.59

Sample	Th	U	Na_2O %	FeO* %
A479	1.4	0.6	2.89	11.77
BCM1A	15.6	6.2	3.30	1.47
BCMB2	19.1	4.4	3.97	2.86
BCMC2	18.0	2.7	5.60	1.16
BCMD2	29.0	3.2	3.50	1.52
MMT1	23.9	7.2	3.10	2.31
RCM4	18.8	4.8	2.76	4.75

APPENDIX 7

DATA SETS FOR THE KM-3 CORE, SEARLES LAKE, CA

CUMULATIVE ACID-INSOLUBLE RESIDUE (AIR) versus DEPTH

ΣAIR	Depth
605381	0.0
596810	5.79
596657	12.16
596613	18.01
596603	19.93
594768	24.99
594744	27.13
594501	27.98
594501	28.96
594280	29.78
594238	30.3
594199	33.89
594098	34.41
593979	34.99
593961	35.2
593888	35.48
593876	36.15
593769	36.67
593760	37.23
592596	41.36
592581	41.54
591106	46.02
586578	54.41
586302	55.17
568618	90.83
567054	95.4
565510	96.93
562754	99.82
561590	110.03
561386	110.64
561082	112.47
559908	114
559222	116.74
558797	124.05
558513	130.45
558454	130.76
558005	135.64
556469	137.16
556371	138.07
555990	138.99
555855	139.75
555758	140.21
555732	141.72
555457	144.78
555219	145.39
555081	146.61
552235	150.57
552194	150.97
552099	151.12

ΣAIR	Depth
551199	166.42
542742	178.64
542670	179.41
539465	186.54
539450	186.9
538980	188.15
538799	189.95
537828	192.02
534735	196.14
534641	196.66
529307	204.52
528557	207.45
525820	210.92
525527	213.66
523735	218.54
505233	248.11
504508	249.48
487306	268.53
485246	271.42
479548	276.91
466498	291.08
465927	294.44
460297	299.31
459157	306.02
456279	308.46
452856	324.31
451451	325.53
450978	327.96
449449	329.18
448668	331.32
446664	333.15
445835	334.67
443270	337.26
442872	338.63
440884	340.31
440293	341.07
435573	345.34
435238	348.69
435025	349.15
434863	350.22
433680	351.43
431826	354.18
431377	359.05
429481	362.1
429300	367.13
426700	370.03
426596	374.75
422740	378.56
422548	379.17

ΣAIR	Depth
422074	379.63
421805	381.61
418125	385.27
417067	386.33
416976	388.01
416760	388.62
405749	398.98
405448	403.25
403394	405.69
392497	413.31
380829	422.45
377376	425.5
362867	437.69
349910	449.58
348725	451.41
341061	459.94
312393	482.5
311826	483.41
307200	486.77
297078	494.39
290219	499.26
283088	504.75
279680	507.19
279050	507.8
275811	510.08
268412	516.58
257956	523.95
249571	530.05
233177	541.63
227160	546.81
176380	582.17
164804	590.09
157471	594.66
150047	599.54
141858	605.24
128489	614.48
119368	620.27
97672	633.98
89772	640.08
75829	649.22
60160	658.67
45732	667.21
33626	674.34
24083	679.7
20769	681.53
16363	683.97
5172	690.37
0.0	693.42

CUM AIR	DEPTH	KG/SQ.M	AIR%	Density
596917.3	0	0	0	0
596810.2	5.7912	107.1372	1	1.85
596657	12.16152	153.2062	1.3	1.85
596613.7	18.01368	43.30598	.4	1.85
596603	19.93392	10.65734	.3	1.85
594768.4	24.9936	1834.64	19.6	1.85
594744.7	27.1272	23.68296	.6	1.85
594501.6	27.98064	243.1453	15.4	1.85
594501.6	28.956	0	0	1.85
594280.8	29.77896	220.7588	14.5	1.85
594238.6	30.29712	42.17834	4.4	1.85
594198.7	33.89376	39.92269	.6	1.85
594098.1	34.41192	100.6529	10.5	1.85
593979.1	34.99104	118.9224	11.1	1.85
593961.3	35.2044	17.88056	4.53	1.85
593888.2	35.47872	73.07898	14.4	1.85
593875.8	36.14928	12.40534	1	1.85
593768.5	36.66744	107.3631	11.2	1.85
593759.5	37.27704	9.022081	.8	1.85
592595.8	41.36136	1163.622	15.4	1.85
592581.3	41.54424	14.54825	4.3	1.85
591105.8	46.0248	1475.448	17.8	1.85
586577.9	54.4068	4527.957	29.2	1.85
586302.8	55.1688	275.082	19	1.9
568618.3	90.8304	17684.59	26.1	1.9
567054.6	95.40241	1563.624	19	1.8
565510.2	96.9264	1544.422	56.3	1.8
562753.9	99.822	2756.322	50.1	1.9
561589.9	110.0328	1164.031	6	1.9
561386.3	110.6424	203.6064	16.7	2
561082.7	112.4712	303.5808	8.3	2
559908.1	113.9952	1174.547	36.7	2.1
559222.3	116.7384	685.8001	12.5	2
558796.6	124.0536	425.7447	2.91	2
558513.6	130.4544	282.9154	2.21	2
558453.9	130.7592	59.7408	9.8	2
558005.2	135.636	448.6656	4.6	2
556469	137.16	1536.192	48	2.1
556371.1	138.0744	97.93224	5.1	2.1
555990.9	138.9888	380.2075	19.8	2.1
555854.9	139.7508	136.017	8.5	2.1
555757.9	140.208	96.97212	10.1	2.1
555732.3	141.732	25.6032	.8	2.1
555457	144.78	275.2344	4.3	2.1
555218.9	145.3896	238.1098	18.6	2.1
555080.6	146.6088	138.2573	5.4	2.1
552234.8	150.5712	2845.796	34.2	2.1
552194.1	150.9674	40.77271	4.9	2.1
552098.7	151.1198	95.37192	29.8	2.1
551199	166.4208	899.6966	2.8	2.1
542742.3	178.6433	8456.729	37.4	1.85
542670.2	179.4053	72.08521	4.4	2.15
539465	186.5376	3205.268	21.4	2.1
539449.6	186.9034	15.36208	2	2.1
538979.8	188.1531	469.7519	17.9	2.1
538798.6	189.9514	181.2714	4.8	2.1
537828	192.024	970.6155	22.3	2.1
534734.5	196.1388	3093.506	35.8	2.1
534640.9	196.657	93.58037	8.600001	2.1
529306.8	204.5208	5334.04	32.3	2.1
528557.1	207.4469	749.6598	12.2	2.1
525820.8	210.9216	2736.348	37.5	2.1
525527	213.6648	293.7967	5.1	2.1
523734.7	218.5416	1792.224	17.5	2.1
505232.6	248.1072	18502.15	29.8	2.1
504508.4	249.4788	724.2048	24	2.2
487306.2	268.5288	17202.15	42	2.15
485245.6	271.4244	2060.654	33.1	2.15
479548.2	276.9108	5697.352	48.3	2.15
466597.5	291.084	12950.76	42.5	2.15
465927.1	294.4368	670.3925	9.3	2.15
460296.6	299.3136	5630.51	53.7	2.15

CUM AIR	DEPTH	KG/SQ.M	AIR%	Density
459156.6	306.0192	1139.952	8.5	2
456279.3	308.4576	2877.312	59	2
452855.8	324.3072	3423.514	10.8	2
451451.3	325.5264	1404.518	57.6	2
450978.2	327.9648	473.0496	9.7	2
449449.3	329.184	1528.877	62.7	2
448668.4	331.3176	780.8975	18.3	2
446664.1	333.1464	2004.365	54.8	2
445835	334.6704	829.056	27.2	2
443270.1	337.2612	2564.892	49.5	2
442872.3	338.6328	397.764	14.5	2
440884.1	340.3092	1988.211	59.3	2
440292.8	341.0712	591.312	38.8	2
435573.3	345.3384	4719.523	55.3	2
435238	348.6912	335.28	5	2
435024.9	349.1484	213.0552	23.3	2
434862.8	350.2152	162.1536	7.6	2
433680.2	351.4344	1182.624	48.5	2
431825.7	354.1776	1854.403	33.8	2
431377.1	359.0544	448.6656	4.6	2
429481.2	362.1024	1895.856	31.1	2
429300.2	367.1316	181.0512	1.8	2
426699.9	370.0272	2600.249	44.9	2
426596	374.7516	103.9368	1.1	2
422740.3	378.5616	3855.72	50.6	2
422547.7	379.1712	192.6336	15.8	2
422074	379.6284	473.6592	51.8	2
421804.6	381.6096	269.4432	6.8	2
418125	385.2672	3679.546	50.3	2
417066.8	386.334	1058.266	49.6	2
416976.2	388.0104	90.52561	2.7	2
416760.4	388.62	215.7984	17.7	2
405748.5	398.9832	11011.94	48.3	2.2
405448.1	403.2504	300.4109	3.2	2.2
403393.5	405.6888	2054.596	38.3	2.2
392496.9	413.3088	10896.6	65	2.2
380829.1	422.4528	11667.74	58	2.2
377375.8	425.5008	3453.384	51.5	2.2
362867.3	437.6928	14508.48	59.5	2
349910.2	449.58	12957.05	54.5	2
348725.2	451.4088	1185.062	32.4	2
341061.3	459.9432	7663.892	44.9	2
312393.6	482.4984	28667.66	62	2.05
311825.6	483.4128	567.9795	30.3	2.05
307200	486.7656	4625.691	67.3	2.05
297077.5	494.3856	10122.41	64.8	2.05
290219.3	499.2624	6858.243	68.6	2.05
283088.6	504.7488	7130.674	63.4	2.05
279679.5	507.1872	3409.127	68.2	2.05
279049.6	507.7968	629.8388	50.4	2.05
275811.4	510.0828	3238.234	69.1	2.05
268411.5	516.5751	7399.872	55.6	2.05
257955.9	523.9512	10455.68	67.5	2.1
249570.8	530.0472	8385.048	65.5	2.1
233177.1	541.6296	16393.73	67.4	2.1
227159.7	546.8112	6017.392	55.3	2.1
176380.2	582.168	50779.45	66.8	2.15
164803.7	590.0928	11576.55	66.4	2.2
157471.1	594.6648	7332.574	72.9	2.2
150046.7	599.5416	7424.441	69.2	2.2
141858.4	605.2413	8188.254	65.3	2.2
128489.2	614.4768	13369.24	65.8	2.2
119368	620.268	9121.141	70	2.25
97672.76	633.984	21695.28	70.3	2.25
89772.34	640.08	7900.416	57.6	2.25
75828.66	649.224	13943.69	66.3	2.3
60159.72	658.6728	15668.95	72.1	2.3
45732.32	667.2072	14427.4	73.5	2.3
33625.96	674.3395	12106.35	73.8	2.3
24082.77	679.704	9543.193	75.7	2.35
20769.25	681.5328	3313.511	77.1	2.35
16362.7	683.9712	4406.555	76.9	2.35
5171.541	690.372	11191.16	74.4	2.35
0	693.42	5171.541	72.2	2.35

CUMULATIVE AIR versus AGE

AGE	ΣAIR
0.000000E+000	605381
3.520000E-003	601828
6.000000E-003	596810
9.000000E-003	596657
9.800000E-003	596613
1.000000E-002	596603
2.300000E-002	594768
2.320000E-002	594744
2.550000E-002	594501
2.550000E-002	594501
2.760000E-002	594280
2.800000E-002	594238
2.840000E-002	594199
2.950000E-002	594098
3.070000E-002	593979
3.090000E-002	593961
3.170000E-002	593888
3.180000E-002	593876
3.290000E-002	593769
3.300000E-002	593760
3.530000E-002	593712
3.880000E-002	593583
5.840000E-002	592856
6.340000E-002	592581
6.550000E-002	592469
6.980000E-002	591741
7.780000E-002	590491
8.930000E-002	588658
1.034000E-001	586578
1.052000E-001	586302
1.223000E-001	583773
1.538000E-001	579444
1.605000E-001	578522
1.925000E-001	572838
2.330000E-001	568618
2.340000E-001	567054
2.450000E-001	565510
2.650000E-001	562754
2.740000E-001	561590
2.750000E-001	561386
2.780000E-001	561082
2.860000E-001	559908
3.160000E-001	559222
3.340000E-001	558797
3.390000E-001	558690
3.430000E-001	558513
3.440000E-001	558454
3.530000E-001	558005
3.850000E-001	556469
3.860000E-001	556402

AGE	ΣAIR
3.863000E-001	556371
3.890000E-001	555990
3.910000E-001	555855
3.920000E-001	555758
3.922000E-001	555732
3.950000E-001	555457
3.970000E-001	555219
3.980000E-001	555081
4.247000E-001	552235
4.250000E-001	552194
4.259000E-001	552099
4.260000E-001	551732
4.890000E-001	551518
5.470000E-001	551323
5.487000E-001	551318
5.499000E-001	551314
5.505000E-001	551312
5.510000E-001	551310
5.514000E-001	551309
5.720000E-001	551239
5.840000E-001	551199
6.100000E-001	549691
6.670000E-001	542742
6.680000E-001	542670
7.300000E-001	540000
7.510000E-001	539465
7.520000E-001	539450
7.710000E-001	538980
7.780000E-001	538799
7.920000E-001	538444
7.990000E-001	537828
8.340000E-001	534735
8.350000E-001	534641
8.960000E-001	529307
9.000000E-001	529000
9.040000E-001	528557
9.320000E-001	525820
9.350000E-001	525527
9.530000E-001	523735
9.700000E-001	522047
1.06	505233
1.064	504508
1.16	487306
1.17	485246
1.2	479548
1.268	466498
1.27	466210
1.273	465927
1.32	460297
1.33	459157

AGE	ΣAIR
1.335	456279
1.39	452856
1.408	451451
1.41	450978
1.424	449449
1.43	448668
1.45	446664
1.45	445835
1.48	443270
1.485	442872
1.503	440884
1.508	440293
1.552	435573
1.555	435238
1.557	435025
1.558	434863
1.57	433680
1.586	431826
1.59	431377
1.607	429481
1.61	429300
1.63	426700
1.635	426596
1.67	422740
1.672	422548
1.678	422074
1.681	421805
1.724	418125
1.737	417067
1.738	416976
1.74	416760
1.87	405749
1.877	405448
1.92	403394
2.01	399662

AGE versus DEPTH

AGE	Depth
0.000000E+000	0.0
3.520000E-003	2.4
6.000000E-003	5.791
9.000000E-003	12.16
9.800000E-003	18.01
1.000000E-002	19.93
2.300000E-002	24.99
2.320000E-002	27.13
2.550000E-002	27.98
2.550000E-002	28.96
2.760000E-002	29.78
2.800000E-002	30.3
2.840000E-002	33.89
2.950000E-002	34.41
3.070000E-002	34.99
3.090000E-002	35.2
3.170000E-002	35.48
3.180000E-002	36.15
3.290000E-002	36.67
3.300000E-002	37.28
3.530000E-002	37.45
3.880000E-002	37.9
5.840000E-002	40.45
6.340000E-002	41.54
6.550000E-002	41.78
6.980000E-002	43.3
7.780000E-002	46.02
8.930000E-002	49.95
1.034000E-001	54.41
1.052000E-001	55.17
1.223000E-001	60.27
1.538000E-001	69
1.605000E-001	70.86
1.925000E-001	82.32
2.230000E-001	90.83
2.340000E-001	95.4
2.450000E-001	96.93
2.650000E-001	99.82
2.740000E-001	110.03
2.750000E-001	110.64
2.780000E-001	112.47
2.860000E-001	114
3.160000E-001	116.74
3.340000E-001	124.05
3.390000E-001	126.5
3.430000E-001	130.45
3.440000E-001	130.76
3.530000E-001	135.64
3.850000E-001	137.16
3.860000E-001	137.78

AGE	Depth
3.863000E-001	138.07
3.890000E-001	138.99
3.910000E-001	139.75
3.920000E-001	140.21
3.922000E-001	141.72
3.950000E-001	144.78
3.970000E-001	145.39
3.980000E-001	146.61
4.247000E-001	150.57
4.250000E-001	150.97
4.259000E-001	151.12
4.260000E-001	153
4.890000E-001	154.1
5.470000E-001	157.7
5.487000E-001	157.88
5.499000E-001	158
5.505000E-001	159
5.510000E-001	160
5.514000E-001	160.3
5.720000E-001	165.8
5.840000E-001	166.42
6.100000E-001	168.6
6.670000E-001	178.64
6.680000E-001	179
7.300000E-001	185
7.510000E-001	186.54
7.520000E-001	186.9
7.710000E-001	188.15
7.780000E-001	189.95
7.920000E-001	190.7
7.990000E-001	192.02
8.340000E-001	196.14
8.350000E-001	196.66
8.960000E-001	204.52
9.000000E-001	204.9
9.040000E-001	207.45
9.320000E-001	210.92
9.350000E-001	213.66
9.530000E-001	218.54
9.700000E-001	221.2
1.06	248.11
1.064	249.48
1.16	268.53
1.17	271.42
1.2	276.91
1.268	291.08
1.27	293
1.273	294.44
1.32	299.31
1.33	306.02

AGE	Depth
1.335	308.46
1.39	324.31
1.408	325.53
1.41	327.96
1.424	329.18
1.43	331.32
1.45	333.15
1.45	334.67
1.48	337.26
1.485	338.63
1.503	340.31
1.508	341.07
1.552	345.34
1.555	348.69
1.557	349.15
1.558	350.22
1.57	351.43
1.586	354.18
1.59	359.05
1.607	362.1
1.61	367.13
1.63	370.03
1.635	374.75
1.67	378.56
1.672	379.17
1.678	379.63
1.681	381.61
1.724	385.27
1.737	386.33
1.738	388.01
1.74	388.62
1.87	398.98
1.877	403.25
1.92	405.69
2.01	408.3

CUMULATIVE CALCIUM versus AGE

AGE	ΣCa	AGE	ΣCa	AGE	ΣCa
0.000000E+000	50116	3.863000E-001	40097	1.408	22084
3.520000E-003	50105	3.890000E-001	39984	1.41	22037
6.000000E-003	50089	3.910000E-001	39946	1.424	21981
9.000000E-003	50007	3.920000E-001	39915	1.43	21764
9.800000E-003	50007	3.922000E-001	39915	1.45	21588
1.000000E-002	50007	3.950000E-001	39793	1.45	21439
2.300000E-002	49211	3.970000E-001	39788	1.48	21356
2.320000E-002	49154	3.980000E-001	39722	1.485	21235
2.550000E-002	49051	4.247000E-001	39497	1.503	21151
2.550000E-002	49051	4.250000E-001	39491	1.508	21076
2.760000E-002	48923	4.259000E-001	39479	1.552	20718
2.800000E-002	48923	4.260000E-001	39477	1.555	20718
2.840000E-002	48923	4.890000E-001	39423	1.557	20656
2.950000E-002	48923	5.470000E-001	39395	1.558	20585
3.070000E-002	48860	5.487000E-001	39395	1.57	20459
3.090000E-002	48860	5.510000E-001	39395	1.586	20140
3.170000E-002	48823	5.520000E-001	39395	1.607	19622
3.180000E-002	48812	5.720000E-001	39395	1.61	19461
3.290000E-002	48747	5.840000E-001	39395	1.63	19073
3.300000E-002	48747	6.100000E-001	39206	1.635	18941
3.530000E-002	48633	6.670000E-001	38310	1.67	18583
3.880000E-002	48575	6.680000E-001	38310	1.672	18538
5.840000E-002	48247	7.300000E-001	37746	1.678	18487
6.340000E-002	48044	7.510000E-001	37591	1.681	18384
6.550000E-002	47960	7.520000E-001	37591	1.724	18069
6.980000E-002	47789	7.710000E-001	37536	1.737	17950
7.780000E-002	47066	7.780000E-001	37430	1.738	17893
8.930000E-002	46834	7.920000E-001	37388	1.74	17774
1.034000E-001	46012	7.990000E-001	37313	1.87	16703
1.052000E-001	45968	8.340000E-001	36880	1.877	16637
1.223000E-001	45619	8.350000E-001	36859	1.92	16143
1.538000E-001	44155	8.960000E-001	36248	2.01	16017
1.605000E-001	43911	9.000000E-001	36230		
1.925000E-001	42409	9.040000E-001	36106		
2.230000E-001	41293	9.320000E-001	35712		
2.340000E-001	41120	9.350000E-001	35689		
2.450000E-001	41068	9.530000E-001	34850		
2.650000E-001	40892	9.700000E-001	34476		
2.740000E-001	40481	1.06	30690		
2.750000E-001	40458	1.064	30249		
2.780000E-001	40443	1.16	28078		
2.860000E-001	40392	1.17	27512		
3.160000E-001	40353	1.2	27016		
3.340000E-001	40296	1.268	24426		
3.390000E-001	40266	1.27	24196		
3.430000E-001	40218	1.273	24023		
3.440000E-001	40213	1.32	23551		
3.530000E-001	40165	1.33	23215		
3.850000E-001	40097	1.335	22972		
3.860000E-001	40097	1.39	22147		

CUM Ca	DEPTH	KG/SQ.M	Ca%	Density
50116.23	0	0	0	0
50089.44	5.7912	26.7843	.25	1.85
50006.95	12.16152	82.49565	.7	1.85
50006.95	18.01368	0	0	1.85
50006.95	19.93392	0	0	1.85
49211.32	24.9936	795.6346	8.5	1.85
49153.69	27.1272	57.62854	1.46	1.85
49051.06	27.98064	102.6263	6.5	1.85
49051.06	28.956	0	0	1.85
48923.17	29.77896	127.8878	8.399999	1.85
48923.17	30.29712	0	0	1.85
48923.17	33.89376	0	0	1.85
48923.17	34.41192	0	0	1.85
48859.96	34.99104	63.211	5.9	1.85
48859.96	35.2044	0	0	1.85
48823.42	35.47872	36.53949	7.2	1.85
48812.26	36.14928	11.16481	.9	1.85
48747.08	36.66744	65.18471	6.8	1.85
48747.08	37.27704	0	0	1.85
48044.37	41.36136	702.707	9.3	1.85
48044.37	41.54424	0	0	1.85
47066.26	46.0248	978.1061	11.8	1.85
46011.81	54.4068	1054.456	6.8	1.85
45968.37	55.1688	43.434	3	1.9
41293.14	90.8304	4675.236	6.9	1.9
41120.32	95.40241	172.8216	2.1	1.8
41068.2	96.9264	52.1208	1.9	1.8
40892.15	99.822	176.0525	3.2	1.9
40480.86	110.0328	411.291	2.12	1.9
40457.69	110.6424	23.1648	1.9	2
40443.06	112.4712	14.6304	.4	2
40391.86	113.9952	51.2064	1.6	2.1
40353.45	116.7384	38.4048	.7	2
40296.39	124.0536	57.05856	.39	2
40218.3	130.4544	78.08976	.61	2
40213.43	130.7592	4.8768	.8	2
40164.66	135.636	48.768	.5	2
40097.45	137.16	67.2084	2.1	2.1
40097.45	138.0744	0	0	2.1
39984.16	138.9888	113.2942	5.9	2.1
39945.75	139.7508	38.4048	2.4	2.1
39915.03	140.208	30.72384	3.2	2.1
39915.03	141.732	0	0	2.1
39793.42	144.78	121.6152	1.9	2.1
39788.29	145.3896	5.12064	.4	2.1
39721.73	146.6088	66.56831	2.6	2.1
39497.06	150.5712	224.6681	2.7	2.1
39491.24	150.9674	5.824673	.7	2.1
39478.76	151.1198	12.48156	3.9	2.1
39395.21	166.4208	83.54325	.26	2.1
38309.86	178.6433	1085.356	4.8	1.85
38309.86	179.4053	0	0	2.15
37590.92	186.5376	718.9386	4.8	2.1
37590.92	186.9034	0	0	2.1
37535.81	188.1531	55.11056	2.1	2.1
37430.07	189.9514	105.7417	2.8	2.1
37312.55	192.024	117.5185	2.7	2.1
36880.49	196.1388	432.054	5	2.1
36858.73	196.657	21.76288	2	2.1
36247.71	204.5208	611.02	3.7	2.1
36106.38	207.4469	141.3293	2.3	2.1
35712.35	210.9216	394.0341	5.4	2.1
35689.31	213.6648	23.04288	.4	2.1
34849.52	218.5416	839.7849	8.2	2.1
30689.64	248.1072	4159.88	6.7	2.1
30249.08	249.4788	440.5579	14.6	2.2
28078.33	268.5288	2170.748	5.3	2.15
27511.81	271.4244	566.5242	9.100001	2.15
27016.39	276.9108	495.4219	4.2	2.15
24426.24	291.084	2590.153	8.5	2.15
24022.56	294.4368	403.6771	5.6	2.15
23550.73	299.3136	471.8305	4.5	2.15

CUM Ca	DEPTH	KG/SQ.M	Ca%	Density
23215.45	306.0192	335.28	2.5	2
22971.61	308.4576	243.84	5	2
22147.43	324.3072	824.1791	2.6	2
22084.03	325.5264	63.3984	2.6	2
22037.21	327.9648	46.81728	.96	2
21981.13	329.184	56.0832	2.3	2
21763.5	331.3176	217.6272	5.1	2
21587.94	333.1464	175.5648	4.8	2
21438.59	334.6704	149.352	4.9	2
21355.68	337.2612	82.9056	1.6	2
21234.98	338.6328	120.7008	4.4	2
21151.16	340.3092	83.82	2.5	2
21076.48	341.0712	74.676	4.9	2
20718.04	345.3384	358.4448	4.2	2
20718.04	348.6912	0	0	2
20655.86	349.1484	62.1792	6.8	2
20585.45	350.2152	70.4088	3.3	2
20458.65	351.4344	126.7968	5.2	2
20140.44	354.1776	318.2112	5.8	2
20140.44	359.0544	0	0	2
19622.28	362.1024	518.1601	8.5	2
19461.35	367.1316	160.9344	1.6	2
19073.34	370.0272	388.0104	6.7	2
18941.06	374.7516	132.2832	1.4	2
18582.91	378.5616	358.14	4.7	2
18537.8	379.1712	45.1104	3.7	2
18486.6	379.6284	51.2064	5.6	2
18383.57	381.6096	103.0224	2.6	2
18069.02	385.2672	314.5536	4.3	2
17949.54	386.334	119.4816	5.6	2
17892.54	388.0104	56.99761	1.7	2
17774.28	388.62	118.2624	9.7	2
16702.73	398.9832	1071.555	4.7	2.2
16637.01	403.2504	65.71488	.7	2.2
16143.48	405.6888	493.5322	9.2	2.2
15774.67	413.3088	368.808	2.2	2.2
15251.63	422.4528	523.0368	2.6	2.2
15023.64	425.5008	227.9904	3.4	2.2
14933.42	437.6928	90.2208	.37	2
14457.93	449.58	475.488	2	2
14201.9	451.4088	256.032	7	2
13553.29	459.9432	648.6144	3.8	2
11750	482.4984	1803.288	3.9	2.05
11577.54	483.4128	172.4558	9.2	2.05
11460.7	486.7656	116.8451	1.7	2.05
11129.53	494.3856	331.1652	2.12	2.05
10859.6	499.2624	269.9309	2.7	2.05
10454.71	504.7488	404.8963	3.6	2.05
10379.73	507.1872	74.9808	1.5	2.05
10269.75	507.7968	109.9718	8.8	2.05
10199.46	510.0828	70.2945	1.5	2.05
9507.385	516.5751	692.0743	5.2	2.05
9151.118	523.9512	356.2678	2.3	2.1
8703.061	530.0472	448.056	3.5	2.1
8143.632	541.6296	559.4299	2.3	2.1
7403.699	546.8112	739.9325	6.8	2.1
5883.357	582.168	1520.342	2	2.15
5395.189	590.0928	488.1677	2.8	2.2
5204.08	594.6648	191.1096	1.9	2.2
4946.585	599.5416	257.4951	2.4	2.2
4545.323	605.2413	401.2621	3.2	2.2
3874.828	614.4768	670.494	3.3	2.2
3470.892	620.268	403.9362	3.1	2.25
2761.089	633.984	709.803	2.3	2.25
2198.733	640.08	562.356	4.1	2.25
1252.329	649.224	946.4039	4.5	2.3
991.5419	658.6728	260.7869	1.2	2.3
677.476	667.2072	314.0659	1.6	2.3
480.6248	674.3395	196.8512	1.2	2.3
304.1325	679.704	176.4923	1.4	2.35
295.5371	681.5328	8.59536	.2	2.35
294.3911	683.9712	1.146048	.02	2.35
128.9304	690.372	165.4607	1.1	2.35
0	693.42	128.9304	1.8	2.35

CUMULATIVE CARBONATE versus AGE

AGE	ΣCO_3	AGE	ΣCO_3	AGE	ΣCO_3
0.000000E+000	150000	3.863000E-001	95158	1.335	34351
3.520000E-003	148459	3.890000E-001	94732	1.39	32760
6.000000E-003	147373	3.910000E-001	94528	1.408	32685
9.000000E-003	146184	3.920000E-001	94369	1.41	32605
9.800000E-003	145011	3.922000E-001	94269	1.424	32482
1.000000E-002	143771	3.950000E-001	93979	1.43	32143
2.300000E-002	141644	3.970000E-001	93910	1.45	31844
2.320000E-002	140723	3.980000E-001	93849	1.45	31685
2.550000E-002	140246	4.247000E-001	92967	1.48	31547
2.550000E-002	139836	4.250000E-001	92938	1.485	31495
2.760000E-002	139403	4.259000E-001	92871	1.503	31398
2.800000E-002	139146	4.260000E-001	92863	1.508	31359
2.840000E-002	138455	4.890000E-001	91991	1.552	30751
2.950000E-002	138260	5.470000E-001	91408	1.555	30740
3.070000E-002	137946	5.487000E-001	91385	1.557	30618
3.090000E-002	137779	5.499000E-001	91321	1.558	30502
3.170000E-002	137621	5.505000E-001	91217	1.57	30263
3.180000E-002	137070	5.510000E-001	91067	1.586	29666
3.290000E-002	136742	5.514000E-001	90922	1.59	29576
3.300000E-002	136201	5.720000E-001	90311	1.607	29357
3.530000E-002	136056	5.840000E-001	90011	1.61	29138
3.880000E-002	135834	6.100000E-001	89208	1.63	28334
5.840000E-002	134596	6.670000E-001	85394	1.635	28050
6.340000E-002	134280	6.680000E-001	85201	1.67	27240
6.550000E-002	134183	7.300000E-001	82453	1.672	27158
6.980000E-002	133984	7.510000E-001	81523	1.678	27077
7.780000E-002	133614	7.520000E-001	81397	1.681	26883
8.930000E-002	132005	7.710000E-001	81079	1.724	26332
1.034000E-001	130033	7.780000E-001	80722	1.737	26136
1.052000E-001	129665	7.920000E-001	80437	1.738	26035
1.223000E-001	127311	7.990000E-001	80295	1.74	25703
1.538000E-001	122975	8.340000E-001	78781	1.87	23562
1.605000E-001	122053	8.350000E-001	78704	1.877	23396
1.925000E-001	117648	8.960000E-001	74998	1.92	22013
2.230000E-001	113450	9.000000E-001	74717	2.01	21546
2.340000E-001	110791	9.040000E-001	74436		
2.450000E-001	110391	9.320000E-001	73083		
2.650000E-001	109840	9.350000E-001	72842		
2.740000E-001	101374	9.530000E-001	69633		
2.750000E-001	101009	9.700000E-001	67021		
2.780000E-001	99261	1.06	54732		
2.860000E-001	98457	1.064	53776		
3.160000E-001	98269	1.16	46101		
3.340000E-001	97556	1.17	44545		
3.390000E-001	96389	1.2	42767		
3.430000E-001	95689	1.268	37403		
3.440000E-001	95659	1.27	37032		
3.530000E-001	95397	1.273	36661		
3.850000E-001	95227	1.32	35755		
3.860000E-001	95180	1.33	34791		

CUM CO3	DEPTH	KG/SQ.M	CO3%	Density
34790.82	306.0192	964.2652	7.19	2
34351.42	308.4576	439.3997	9.01	2
32760.12	324.3072	1591.3	5.02	2
32685.02	325.5264	75.10273	3.08	2
32605.53	327.9648	79.49184	1.63	2
32482.14	329.184	123.383	5.06	2
32143.33	331.3176	338.8157	7.94	2
31844.5	333.1464	298.8259	8.17	2
31684.79	334.6704	159.7152	5.24	2
31547.47	337.2612	137.3124	2.65	2
31495.08	338.6328	52.39512	1.91	2
31397.51	340.3092	97.56649	2.91	2
31359.57	341.0712	37.9476	2.49	2
30751.06	345.3384	608.5028	7.13	2
30739.66	348.6912	11.39952	.17	2
30618.05	349.1484	121.6152	13.3	2
30501.98	350.2152	116.0678	5.44	2
30263.26	351.4344	238.7194	9.79	2
29665.79	354.1776	597.469	10.89	2
29576.06	359.0544	89.73312	.92	2
29356.6	362.1024	219.456	3.6	2
29138.34	367.1316	218.2673	2.17	2
28333.94	370.0272	804.3977	13.89	2
28050.47	374.7516	283.464	3	2
27239.71	378.5616	810.768	10.64	2
27158.51	379.1712	81.19873	6.66	2
27077.22	379.6284	81.29016	8.890001	2
26882.66	381.6096	194.5538	4.91	2
26331.83	385.2672	550.8346	7.53	2
26135.96	386.334	195.8645	9.18	2
26035.04	388.0104	100.9193	3.01	2
25703.3	388.62	331.7443	27.21	2
23562.47	398.9832	2140.83	9.390001	2.2
23396.3	403.2504	166.1648	1.77	2.2
22013.88	405.6888	1382.427	25.77	2.2
20649.29	413.3088	1364.59	8.140001	2.2
19039.94	422.4528	1609.344	8	2.2
18534.34	425.5008	505.6023	7.54	2.2
18356.34	437.6928	178.0032	.73	2
17300.75	449.58	1055.583	4.44	2
17131.41	451.4088	169.3469	4.63	2
16387.21	459.9432	744.1997	4.36	2
15041.68	482.4984	1345.531	2.91	2.05
14928.27	483.4128	113.4085	6.05	2.05
14773.62	486.7656	154.6479	2.25	2.05
14389.35	494.3856	384.2766	2.46	2.05
14124.41	499.2624	264.9322	2.65	2.05
13781.38	504.7488	343.0372	3.05	2.05
13665.4	507.1872	115.9703	2.32	2.05
13608.79	507.7968	56.61051	4.53	2.05
13476.17	510.0828	132.6223	2.83	2.05
12657.66	516.5751	818.5111	6.15	2.05
11815.01	523.9512	842.6508	5.44	2.1
10861.29	530.0472	953.7192	7.45	2.1
9584.332	541.6296	1276.96	5.25	2.1
8549.514	546.8112	1034.817	9.51	2.1
7211.614	582.168	1337.901	1.76	2.15
6636.273	590.0928	575.3405	3.3	2.2
6431.082	594.6648	205.1914	2.04	2.2
6037.329	599.5416	393.7528	3.67	2.2
5524.466	605.2413	512.8631	4.09	2.2
4669.078	614.4768	855.3878	4.21	2.2
4245.596	620.268	423.4815	3.25	2.25
3418.522	633.984	827.0748	2.68	2.25
3015.271	640.08	403.2504	2.94	2.25
2485.285	649.224	529.9862	2.52	2.3
2044.12	658.6728	441.1645	2.03	2.3
1476.839	667.2072	567.2816	2.89	2.3
953.5424	674.3395	523.2962	3.19	2.3
614.425	679.704	339.1174	2.69	2.35
575.3161	681.5328	39.10889	.91	2.35
530.6203	683.9712	44.69587	.78	2.35
308.0004	690.372	222.6198	1.48	2.35
0	693.42	308.0004	4.3	2.35

CUM CO3	DEPTH	KG/SQ.M	CO3%	Density
150052	0	0	0	0
147373.6	5.7912	2678.43	25	1.85
146184.5	12.16152	1189.116	10.09	1.85
145011.9	18.01368	1172.509	10.83	1.85
143771.1	19.93392	1240.869	34.93	1.85
141644.4	24.9936	2126.685	22.72	1.85
140723.1	27.1272	921.2671	23.34	1.85
140246.1	27.98064	476.9754	30.21	1.85
139836.2	28.956	409.9629	22.72	1.85
139403.2	29.77896	432.9917	28.44	1.85
139146.5	30.29712	256.7127	26.78	1.85
138455.1	33.89376	691.3279	10.39	1.85
138260.1	34.41192	195.0748	20.35	1.85
137946.4	34.99104	313.698	29.28	1.85
137779.6	35.2044	166.7668	42.25	1.85
137621.6	35.47872	158.0333	31.14	1.85
137070.1	36.14928	551.4175	44.45	1.85
136742.4	36.66744	327.7449	34.19	1.85
136201.4	37.27704	540.9865	47.97	1.85
134316.9	41.36136	1884.464	24.94	1.85
134280.4	41.54424	36.57363	10.81	1.85
133613.9	46.0248	666.4384	8.04	1.85
130033.4	54.4068	3580.497	23.09	1.85
129664.7	55.1688	368.7547	25.47	1.9
113450.4	90.8304	16214.26	23.93	1.9
110791.4	95.40241	2658.984	32.31	1.8
110390.9	96.9264	400.5072	14.6	1.8
109840.2	99.822	550.7142	10.01	1.9
101373.8	110.0328	8466.387	43.64	1.9
101008.8	110.6424	365.0285	29.94	2
99261.18	112.4712	1747.601	47.78	2
98457.24	113.9952	803.9405	25.12	2.1
98269.06	116.7384	188.1835	3.43	2
97556.56	124.0536	712.5005	4.87	2
95688.81	130.4544	1867.754	14.59	2
95659	130.7592	29.80944	4.89	2
95396.62	135.636	262.3719	2.69	2
95227.32	137.16	169.3012	5.29	2.1
95157.62	138.0744	69.70471	3.63	2.1
94732.48	138.9888	425.1411	22.14	2.1
94528.13	139.7508	204.3456	12.77	2.1
94369.04	140.208	159.0919	16.57	2.1
94268.55	141.732	100.4926	3.14	2.1
93979.24	144.78	289.3162	4.52	2.1
93909.72	145.3896	69.51268	5.43	2.1
93849.56	146.6088	60.16752	2.35	2.1
92967.52	150.5712	882.0302	10.6	2.1
92937.9	150.9674	29.62262	3.56	2.1
92871.14	151.1198	66.76034	20.86	2.1
90011.39	166.4208	2859.75	8.899999	2.1
85394.11	178.6433	4617.284	20.42	1.85
85201.44	179.4053	192.6641	11.76	2.15
81522.88	186.5376	3678.569	24.56	2.1
81396.91	186.9034	125.969	16.4	2.1
81079.1	188.1531	317.8042	12.11	2.1
80721.85	189.9514	357.2557	9.46	2.1
80294.86	192.024	426.9838	9.810001	2.1
78780.95	196.1388	1513.917	17.52	2.1
78703.69	196.657	77.25821	7.1	2.1
74997.93	204.5208	3705.754	22.44	2.1
74436.3	207.4469	561.6304	9.140001	2.1
73082.72	210.9216	1353.58	18.55	2.1
72841.93	213.6648	240.7981	4.18	2.1
69633.33	218.5416	3208.593	31.33	2.1
54732.26	248.1072	14901.06	24	2.1
53776.62	249.4788	955.6486	31.67	2.2
46101.18	268.5288	7675.435	18.74	2.15
44545.42	271.4244	1555.763	24.99	2.15
42766.62	276.9108	1778.801	15.08	2.15
37403.48	291.084	5363.14	17.6	2.15
36661	294.4368	742.4776	10.3	2.15
35755.09	299.3136	905.9144	8.640001	2.15

CUMULATIVE SODIUM versus AGE

AGE	ΣNa
0.000000E+000	158187
3.520000E-003	157299
6.000000E-003	156044
9.000000E-003	151931
9.800000E-003	148023
1.000000E-002	146837
2.300000E-002	145723
2.320000E-002	144408
2.550000E-002	144198
2.550000E-002	143565
2.760000E-002	143440
2.800000E-002	143149
2.840000E-002	140733
2.950000E-002	140493
3.070000E-002	140304
3.090000E-002	140192
3.170000E-002	140114
3.180000E-002	139735
3.290000E-002	139577
3.300000E-002	139235
3.530000E-002	139074
3.880000E-002	138986
5.840000E-002	138495
6.340000E-002	138091
6.550000E-002	137864
6.980000E-002	137866
7.780000E-002	137229
8.930000E-002	136660
1.034000E-001	135399
1.052000E-001	135228
1.223000E-001	134748
1.538000E-001	132732
1.605000E-001	132396
1.925000E-001	130327
2.230000E-001	128791
2.340000E-001	127277
2.450000E-001	127046
2.650000E-001	126738
2.740000E-001	122043
2.750000E-001	121840
2.780000E-001	120800
2.860000E-001	120339
3.160000E-001	118600
3.340000E-001	113245
3.390000E-001	111613
3.430000E-001	108982
3.440000E-001	108781
3.530000E-001	105309
3.850000E-001	104951
3.860000E-001	104480

AGE	ΣNa
3.863000E-001	104258
3.890000E-001	104100
3.910000E-001	103713
3.920000E-001	103464
3.922000E-001	102229
3.950000E-001	99944
3.970000E-001	99599
3.980000E-001	98703
4.247000E-001	97480
4.250000E-001	97198
4.259000E-001	97152
4.260000E-001	97135
4.890000E-001	95319
5.470000E-001	92729
5.487000E-001	92623
5.499000E-001	92387
5.505000E-001	91657
5.510000E-001	90944
5.514000E-001	90724
5.720000E-001	86412
5.840000E-001	85970
6.100000E-001	85616
6.670000E-001	83935
6.680000E-001	83359
7.300000E-001	81938
7.510000E-001	81547
7.520000E-001	81276
7.710000E-001	80647
7.780000E-001	79446
7.920000E-001	79089
7.990000E-001	78462
8.340000E-001	77624
8.350000E-001	77290
8.960000E-001	75837
9.000000E-001	75616
9.040000E-001	74134
9.320000E-001	73682
9.350000E-001	71654
9.530000E-001	70128
9.700000E-001	69592
1.06	64168
1.064	63893
1.16	61272
1.17	60687
1.2	59838
1.268	58893
1.27	58102
1.273	57509
1.32	57027
1.33	53003

AGE	ΣNa
1.335	52857
1.39	43664
1.408	43540
1.41	42511
1.424	42440
1.43	41450
1.45	41296
1.45	40760
1.48	40584
1.485	39925
1.503	39754
1.508	39588
1.552	39281
1.555	36827
1.557	36666
1.558	36000
1.57	35829
1.586	35007
1.59	31398
1.607	30855
1.61	27184
1.63	26941
1.635	23482
1.67	23231
1.672	22910
1.678	22871
1.681	21607
1.724	21256
1.737	21143
1.738	19959
1.74	19860
1.87	18902
1.877	15533
1.92	15345
2.01	15207

CUM Cl	DEPTH	KG/SQ.M	Cl conc.	Density
162292.1	0	0	0	0
159613.7	5.7912	2678.43	25	1.85
155630.3	12.16152	3983.361	33.8	1.85
151321.4	18.01368	4308.945	39.8	1.85
150571.8	19.93392	749.5661	21.1	1.85
149701.3	24.9936	870.5179	9.3	1.85
148722.4	27.1272	978.8956	24.8	1.85
148619.8	27.98064	102.6263	6.5	1.85
148004.5	28.956	615.3053	34.1	1.85
147937.5	29.77896	66.98887	4.4	1.85
147737.1	30.29712	200.3471	20.9	1.85
144982.5	33.89376	2754.666	41.4	1.85
144933.6	34.41192	48.88853	5.1	1.85
144878.9	34.99104	54.64002	5.1	1.85
144869.5	35.2044	9.473142	2.4	1.85
144845.1	35.47872	24.35966	4.8	1.85
144806.7	36.14928	38.45656	3.1	1.85
144749.1	36.66744	57.51592	6	1.85
144730	37.27704	19.17192	1.7	1.85
144435.3	41.36136	294.6836	3.9	1.85
144427.5	41.54424	7.781623	2.3	1.85
144104.2	46.0248	323.2724	3.9	1.85
143204.9	54.4068	899.3886	5.8	1.85
143141.1	55.1688	63.7032	4.4	1.9
141108.4	90.8304	2032.711	3	1.9
141009.7	95.40241	98.75519	1.2	1.8
140971.3	96.9264	38.4048	1.4	1.8
140855.7	99.822	115.5344	2.1	1.9
140487.1	110.0328	368.6099	1.9	1.9
140450.6	110.6424	36.576	3	2
140388.4	112.4712	62.1792	1.7	2
140314.8	113.9952	73.6092	2.3	2.1
137780.1	116.7384	2534.717	46.2	2
130128.4	124.0536	7651.699	52.3	2
125225.3	130.4544	4903.013	38.3	2
124930.9	130.7592	294.4368	48.3	2
119868.8	135.636	5062.119	51.9	2
119414.3	137.16	454.4568	14.2	2.1
118412	138.0744	1002.365	52.2	2.1
118304.4	138.9888	107.5334	5.6	2.1
117806.8	139.7508	497.6622	31.1	2.1
117505.3	140.208	301.4776	31.4	2.1
115677.9	141.732	1827.428	57.1	2.1
112714.3	144.78	2963.57	46.3	2.1
112212.5	145.3896	501.8227	39.2	2.1
110868.3	146.6088	1344.168	52.5	2.1
109703.4	150.5712	1164.946	14	2.1
109354.7	150.9674	348.6483	41.9	2.1
109318.2	151.1198	36.48456	11.4	2.1
96144.09	166.4208	13174.13	41	2.1
95126.57	178.6433	1017.521	4.5	1.85
94364.76	179.4053	761.8096	46.5	2.15
93720.71	186.5376	644.0491	4.3	2.1
93428.83	186.9034	291.8794	38	2.1
92722.89	188.1531	705.94	26.9	2.1
91027.25	189.9514	1695.643	44.9	2.1
89743.25	192.024	1283.998	29.5	2.1
89337.12	196.1388	406.1307	4.7	2.1
88859.42	196.657	477.6952	43.9	2.1
88330.97	204.5208	528.4498	3.2	2.1
86008.25	207.4469	2322.716	37.8	2.1
85658	210.9216	350.2525	4.8	2.1
82720.03	213.6648	2937.967	51	2.1
82361.59	218.5416	358.4448	3.5	2.1
80995.66	248.1072	1365.931	2.2	2.1
80944.36	249.4788	51.29785	1.7	2.2
79502.66	268.5288	1441.704	3.52	2.15
79365.7	271.4244	136.9619	2.2	2.15
79047.21	276.9108	318.4855	2.7	2.15
77584.54	291.084	1462.675	4.8	2.15
76020.29	294.4368	1564.249	21.7	2.15
75621.85	299.3136	398.4346	3.8	2.15

CUM Cl	DEPTH	KG/SQ.M	Cl conc.	Density
70391.49	306.0192	5230.368	39	2
70191.54	308.4576	199.9488	4.1	2
56307.29	324.3072	13884.25	43.8	2
56212.19	325.5264	95.09759	3.9	2
54710.14	327.9648	1502.055	30.8	2
54615.04	329.184	95.09759	3.9	2
53198.33	331.3176	1416.71	33.2	2
52986.19	333.1464	212.1408	5.8	2
52208.95	334.6704	777.24	25.5	2
51991.32	337.2612	217.6272	4.2	2
51020.23	338.6328	971.0928	35.4	2
50782.18	340.3092	238.0488	7.1	2
50545.96	341.0712	236.22	15.5	2
50144.85	345.3384	401.1168	4.7	2
46383	348.6912	3761.842	56.1	2
46137.94	349.1484	245.0592	26.8	2
45120.22	350.2152	1017.727	47.7	2
44864.19	351.4344	256.032	10.5	2
43629.74	354.1776	1234.44	22.5	2
38099.45	359.0544	5530.291	56.7	2
37288.68	362.1024	810.7681	13.3	2
31655.98	367.1316	5632.704	56	2
31296.93	370.0272	359.0544	6.2	2
25986.7	374.7516	5310.226	56.2	2
25620.94	378.5616	365.76	4.8	2
25129.6	379.1712	491.3376	40.3	2
25072	379.6284	57.6072	6.3	2
23170.05	381.6096	1901.952	48	2
22665.3	385.2672	504.7488	6.9	2
22505.28	386.334	160.02	7.5	2
20694.77	388.0104	1810.512	54	2
20548.46	388.62	146.304	12	2
19362.91	398.9832	1185.55	5.2	2.2
14331.03	403.2504	5031.882	53.6	2.2
14143.27	405.6888	187.7568	3.5	2.2
13707.41	413.3088	435.864	2.6	2.2
12902.74	422.4528	804.672	4	2.2
12527.22	425.5008	375.5136	5.6	2.2
11771.32	437.6928	755.904	3.1	2
10844.12	449.58	927.2016	3.9	2
10770.96	451.4088	73.152	2	2
10019.94	459.9432	751.0273	4.4	2
8956.458	482.4984	1063.478	2.3	2.05
8922.717	483.4128	33.74136	1.8	2.05
8764.632	486.7656	158.0845	2.3	2.05
8374.106	494.3856	390.525	2.5	2.05
8124.171	499.2624	249.936	2.5	2.05
7899.228	504.7488	224.9424	2	2.05
7789.257	507.1872	109.9718	2.2	2.05
7769.261	507.7968	19.99488	1.6	2.05
7661.477	510.0828	107.7849	2.3	2.05
7368.676	516.5751	292.8007	2.2	2.05
7027.898	523.9512	340.7779	2.2	2.1
6823.073	530.0472	204.8256	1.6	2.1
6385.258	541.6296	437.8147	1.8	2.1
6211.157	546.8112	174.1018	1.6	2.1
4614.797	582.168	1596.36	2.1	2.15
4266.106	590.0928	348.6912	2	2.2
4085.055	594.6648	181.0512	1.8	2.2
3902.662	599.5416	182.3923	1.7	2.2
3702.031	605.2413	200.631	1.6	2.2
3356.625	614.4768	345.406	1.7	2.2
3135.112	620.268	221.5134	1.7	2.25
2579.614	633.984	555.498	1.8	2.25
2168.134	640.08	411.48	3	2.25
1831.634	649.224	336.4992	1.6	2.3
1483.919	658.6728	347.7158	1.6	2.3
1169.853	667.2072	314.0659	1.6	2.3
907.3843	674.3395	262.4683	1.6	2.3
743.4986	679.704	163.8857	1.3	2.35
580.1868	681.5328	163.3118	3.8	2.35
356.7075	683.9712	223.4794	3.9	2.35
85.9536	690.372	270.7539	1.8	2.35
0	693.42	85.9536	1.2	2.35

CUMULATIVE SULFATE versus AGE

AGE	ΣSO_4	AGE	ΣSO_4	AGE	ΣSO_4
0.000000E+000	39021	3.863000E-001	26556	1.335	15671
3.520000E-003	38577	3.890000E-001	26527	1.39	15291
6.000000E-003	37949	3.910000E-001	26511	1.408	15159
9.000000E-003	36217	3.920000E-001	26505	1.41	15047
9.800000E-003	32070	3.922000E-001	26498	1.424	15032
1.000000E-002	32037	3.950000E-001	26005	1.43	14883
2.300000E-002	31719	3.970000E-001	25995	1.45	14847
2.320000E-002	31442	3.980000E-001	25986	1.45	14778
2.550000E-002	31409	4.247000E-001	25811	1.48	14738
2.550000E-002	31395	4.250000E-001	25720	1.485	14674
2.760000E-002	31370	4.259000E-001	25716	1.503	14638
2.800000E-002	31361	4.260000E-001	25712	1.508	14606
2.840000E-002	30935	4.890000E-001	25300	1.552	14486
2.950000E-002	30796	5.470000E-001	24049	1.555	14473
3.070000E-002	30758	5.487000E-001	23917	1.557	14468
3.090000E-002	30743	5.499000E-001	23911	1.558	14462
3.170000E-002	30731	5.505000E-001	23906	1.57	14448
3.180000E-002	30578	5.510000E-001	23759	1.586	14421
3.290000E-002	30540	5.514000E-001	23704	1.59	14393
3.300000E-002	30530	5.720000E-001	23109	1.607	14352
3.530000E-002	30225	5.840000E-001	23081	1.61	14340
3.880000E-002	30183	6.100000E-001	22991	1.63	14315
5.840000E-002	29951	6.670000E-001	22561	1.635	14305
6.340000E-002	29495	6.680000E-001	22560	1.67	14276
6.550000E-002	29462	7.300000E-001	22229	1.672	14271
6.980000E-002	29395	7.510000E-001	22139	1.678	14267
7.780000E-002	29114	7.520000E-001	22117	1.681	14259
8.930000E-002	28936	7.710000E-001	22020	1.724	14213
1.034000E-001	28308	7.780000E-001	22011	1.737	14193
1.052000E-001	28259	7.920000E-001	22000	1.738	14170
1.223000E-001	28198	7.990000E-001	21980	1.74	14162
1.538000E-001	28114	8.340000E-001	21868	1.87	13752
1.605000E-001	27964	8.350000E-001	21862	1.877	13526
1.925000E-001	27703	8.960000E-001	21614	1.92	13451
2.230000E-001	27446	9.000000E-001	21609	2.01	13382
2.340000E-001	27412	9.040000E-001	21577		
2.450000E-001	27395	9.320000E-001	21453		
2.650000E-001	27349	9.350000E-001	21436		
2.740000E-001	27283	9.530000E-001	21262		
2.750000E-001	27276	9.700000E-001	21150		
2.780000E-001	27261	1.06	20020		
2.860000E-001	27242	1.064	19978		
3.160000E-001	27227	1.16	19158		
3.340000E-001	27153	1.17	19065		
3.390000E-001	27006	1.2	18840		
3.430000E-001	26769	1.268	18292		
3.440000E-001	26767	1.27	17864		
3.530000E-001	26591	1.273	17543		
3.850000E-001	26570	1.32	17102		
3.860000E-001	26560	1.33	15708		

CUM SO4	DEPTH	KG/SQ.M	SO4%	Density
39020.75	0	0	0	0
37949.38	5.7912	1071.372	10	1.85
36216.97	12.16152	1732.409	14.7	1.85
32070.42	18.01368	4146.547	38.3	1.85
32037.03	19.93392	33.39299	.94	1.85
31718.78	24.9936	318.2539	3.4	1.85
31442.48	27.1272	276.3012	7	1.85
31409.32	27.98064	33.15618	2.1	1.85
31395.43	28.956	13.89399	.77	1.85
31369.54	29.77896	25.88206	1.7	1.85
31360.92	30.29712	8.627387	.9	1.85
30935.07	33.89376	425.842	6.4	1.85
30796.08	34.41192	138.9968	14.5	1.85
30757.51	34.99104	38.56942	3.6	1.85
30743.3	35.2044	14.20971	3.6	1.85
30730.61	35.47872	12.68732	2.5	1.85
30578.02	36.14928	152.5857	12.3	1.85
30539.68	36.66744	38.34395	4	1.85
30529.87	37.27704	9.811512	.87	1.85
29660.93	41.36136	868.9387	11.5	1.85
29495.49	41.54424	165.4441	48.9	1.85
29114.19	46.0248	381.2956	4.6	1.85
28307.85	54.4068	806.3484	5.2	1.85
28258.62	55.1688	49.2252	3.4	1.9
27445.54	90.8304	813.0845	1.2	1.9
27411.79	95.40241	33.74136	.41	1.8
27395.34	96.9264	16.4592	.6	1.8
27349.12	99.822	46.21378	.84	1.9
27283.16	110.0328	65.96177	.34	1.9
27275.6	110.6424	7.55904	.62	2
27261.34	112.4712	14.26464	.39	2
27242.14	113.9952	19.2024	.6	2.1
27227.32	116.7384	14.81328	.27	2
27152.71	124.0536	74.61504	.51	2
26768.66	130.4544	384.048	3	2
26766.77	130.7592	1.88976	.31	2
26591.2	135.636	175.5648	1.8	2
26565.6	137.16	25.6032	.8	2.1
26555.62	138.0744	9.985248	.52	2.1
26526.81	138.9888	28.8036	1.5	2.1
26510.81	139.7508	16.002	1	2.1
26505.43	140.208	5.376672	.56	2.1
26498.07	141.732	7.36092	.23	2.1
26005.21	144.78	492.8616	7.7	2.1
25995.1	145.3896	10.11326	.79	2.1
25985.88	146.6088	9.217152	.36	2.1
25811.14	150.5712	174.7418	2.1	2.1
25720.44	150.9674	90.69847	10.9	2.1
25716.28	151.1198	4.16052	1.3	2.1
23081.45	166.4208	2634.826	8.2	2.1
22561.39	178.6433	520.0662	2.3	1.85
22557.95	179.4053	3.44043	.21	2.15
22138.57	186.5376	419.3808	2.8	2.1
22117.06	186.9034	21.50691	2.8	2.1
22019.96	188.1531	97.09955	3.7	2.1
22010.52	189.9514	9.441218	.25	2.1
21980.48	192.024	30.0325	.69	2.1
21868.15	196.1388	112.334	1.3	2.1
21862.17	196.657	5.984792	.55	2.1
21614.45	204.5208	247.7109	1.5	2.1
21576.97	207.4469	37.48299	.61	2.1
21452.93	210.9216	124.0478	1.7	2.1
21435.64	213.6648	17.28216	.3	2.1
21261.54	218.5416	174.1018	1.7	2.1
20019.79	248.1072	1241.755	2	2.1
19977.54	249.4788	42.24529	1.4	2.2
19158.39	268.5288	819.15	2	2.15
19065.01	271.4244	93.3831	1.5	2.15
18840.89	276.9108	224.1195	1.9	2.15
18292.39	291.084	548.5029	1.8	2.15
17542.7	294.4368	749.6861	10.4	2.15
17102.32	299.3136	440.3751	4.2	2.15

CUM SO4	DEPTH	KG/SQ.M	SO4%	Density
15707.56	306.0192	1394.765	10.4	2
15671.47	308.4576	36.08832	.74	2
15291.08	324.3072	380.3904	1.2	2
15159.41	325.5264	131.6736	5.4	2
15047.24	327.9648	112.1664	2.3	2
15031.88	329.184	15.36192	.63	2
14882.53	331.3176	149.352	3.5	2
14847.05	333.1464	35.47872	.97	2
14776.95	334.6704	70.104	2.3	2
14737.57	337.2612	39.38016	.76	2
14674.47	338.6328	63.0936	2.3	2
14637.59	340.3092	36.8808	1.1	2
14605.59	341.0712	32.004	2.1	2
14486.11	345.3384	119.4816	1.4	2
14473.37	348.6912	12.74064	.19	2
14468.25	349.1484	5.12064	.56	2
14462.06	350.2152	6.18744	.29	2
14448.16	351.4344	13.89888	.57	2
14421.28	354.1776	26.88336	.49	2
14392.99	359.0544	28.28544	.29	2
14352.15	362.1024	40.8432	.67	2
14340.08	367.1316	12.07008	.12	2
14315.18	370.0272	24.90216	.43	2
14304.78	374.7516	10.39368	.11	2
14275.06	378.5616	29.718	.39	2
14271.16	379.1712	3.90144	.32	2
14266.59	379.6284	4.572	.5	2
14258.67	381.6096	7.9248	.2	2
14212.58	385.2672	46.08576	.63	2
14192.52	386.334	20.05584	.94	2
14170.4	388.0104	22.12848	.66	2
14161.98	388.62	8.412481	.69	2
13751.6	398.9832	410.3827	1.8	2.2
13526.29	403.2504	225.3082	2.4	2.2
13451.19	405.6888	75.10273	1.4	2.2
13250.02	413.3088	201.168	1.2	2.2
12847.69	422.4528	402.336	2	2.2
12643.83	425.5008	203.8503	3.04	2.2
11302.71	437.6928	1341.12	5.5	2
10066.45	449.58	1236.269	5.2	2
9393.448	451.4088	672.9984	18.4	2
7823.118	459.9432	1570.33	9.2	2
6667.164	482.4984	1155.954	2.5	2.05
6612.803	483.4128	54.36108	2.9	2.05
6502.832	486.7656	109.9718	1.6	2.05
6252.896	494.3856	249.936	1.6	2.05
6132.927	499.2624	119.9693	1.2	2.05
5941.725	504.7488	191.201	1.7	2.05
5866.744	507.1872	74.9808	1.5	2.05
5831.753	507.7968	34.99104	2.8	2.05
5752.086	510.0828	79.6671	1.7	2.05
5113.248	516.5751	638.8379	4.8	2.05
4896.389	523.9512	216.8587	1.4	2.1
4802.938	530.0472	93.45168	.73	2.1
4635.109	541.6296	167.829	.69	2.1
4439.244	546.8112	195.8645	1.8	2.1
3222.97	582.168	1216.274	1.6	2.15
2961.452	590.0928	261.5184	1.5	2.2
2830.693	594.6648	130.7592	1.3	2.2
2701.945	599.5416	128.7475	1.2	2.2
2513.854	605.2413	188.0916	1.5	2.2
2188.766	614.4768	325.088	1.6	2.2
1954.222	620.268	234.5436	1.8	2.25
1429.585	633.984	524.637	1.7	2.25
1072.969	640.08	356.616	2.6	2.25
736.4696	649.224	336.4992	1.6	2.3
538.7063	658.6728	197.7634	.91	2.3
456.264	667.2072	82.44231	.42	2.3
370.9618	674.3395	85.30219	.52	2.3
307.9288	679.704	63.03299	.5	2.35
243.4636	681.5328	64.4652	1.5	2.35
151.7797	683.9712	91.68384	1.6	2.35
47.99076	690.372	103.789	.69	2.35
0	693.42	47.99076	.67	2.35

CUM Na	DEPTH	KG/SQ.M	Na%	Density
158187.2	0	0	0	0
156044.4	5.7912	2142.744	20	1.85
151931.4	12.16152	4112.998	34.9	1.85
148023.1	18.01368	3908.364	36.1	1.85
146836.5	19.93392	1186.517	33.4	1.85
145722.6	24.9936	1113.888	11.9	1.85
144408.2	27.1272	1314.404	33.3	1.85
144198.3	27.98064	209.9892	13.3	1.85
143564.9	28.956	633.3495	35.1	1.85
143440.1	29.77896	124.8429	8.2	1.85
143148.7	30.29712	291.414	30.4	1.85
140733.3	33.89376	2415.323	36.3	1.85
140492.7	34.41192	240.6083	25.1	1.85
140304.2	34.99104	188.5616	17.6	1.85
140192.1	35.2044	112.0989	28.4	1.85
140114.4	35.47872	77.64642	15.3	1.85
139734.8	36.14928	379.6035	30.6	1.85
139576.6	36.66744	158.1688	16.5	1.85
139234.9	37.27704	341.7113	30.3	1.85
138192.2	41.36136	1042.726	13.8	1.85
138090.7	41.54424	101.4994	30	1.85
137228.6	46.0248	862.0596	10.4	1.85
135398.9	54.4068	1829.791	11.8	1.85
135228	55.1688	170.8404	11.8	1.9
128791.1	90.8304	6436.919	9.5	1.9
127276.8	95.40241	1514.246	18.4	1.8
127046.4	96.9264	230.4288	8.399999	1.8
126738.3	99.822	308.0919	5.6	1.9
122043.4	110.0328	4694.927	24.2	1.9
121839.8	110.6424	203.6064	16.7	2
120815.7	112.4712	1024.128	28	2
120338.8	113.9952	476.8596	14.9	2.1
118599.6	116.7384	1739.189	31.7	2
113244.9	124.0536	5354.726	36.6	2
108982	130.4544	4262.933	33.3	2
108781.4	130.7592	200.5584	32.9	2
105309.1	135.636	3472.282	35.6	2
104950.7	137.16	358.4448	11.2	2.1
104257.5	138.0744	693.2066	36.1	2.1
104100	138.9888	157.4597	8.2	2.1
103712.8	139.7508	387.2484	24.2	2.1
103464.1	140.208	248.6711	25.9	2.1
102228.7	141.732	1235.354	38.6	2.1
99943.64	144.78	2285.086	35.7	2.1
99599.28	145.3896	344.363	26.9	2.1
98703.18	146.6088	896.112	35	2.1
97479.98	150.5712	1223.193	14.7	2.1
97197.9	150.9674	282.0806	33.9	2.1
97151.81	151.1198	46.08576	14.4	2.1
85969.87	166.4208	11181.94	34.8	2.1
83934.83	178.6433	2035.042	9	1.85
83359.13	179.4053	575.6986	35.14	2.15
81546.81	186.5376	1812.324	12.1	2.1
81276.43	186.9034	270.3726	35.2	2.1
80646.6	188.1531	629.835	24	2.1
79445.68	189.9514	1200.923	31.8	2.1
78462	192.024	983.6732	22.6	2.1
77623.81	196.1388	838.1847	9.7	2.1
77289.75	196.657	334.0601	30.7	2.1
75836.52	204.5208	1453.237	8.8	2.1
74134.43	207.4469	1702.096	27.7	2.1
73682.02	210.9216	452.4094	6.2	2.1
71654.25	213.6648	2027.774	35.2	2.1
70128.29	218.5416	1525.951	14.9	2.1
64167.87	248.1072	5960.425	9.600001	2.1
63893.27	249.4788	274.5944	9.100001	2.2
61271.99	268.5288	2621.28	6.4	2.15
60686.79	271.4244	585.2008	9.399999	2.15
59837.5	276.9108	849.2948	7.2	2.15
58892.85	291.084	944.6439	3.1	2.15
57508.82	294.4368	1384.036	19.2	2.15
57026.5	299.3136	482.3155	4.6	2.15

CUM Na	DEPTH	KG/SQ.M	Na%	Density
53003.14	306.0192	4023.36	30	2
52856.84	308.4576	146.304	3	2
43664.07	324.3072	9192.768	29	2
43539.71	325.5264	124.3584	5.1	2
42510.71	327.9648	1029.005	21.1	2
42439.99	329.184	70.7136	2.9	2
41450	331.3176	989.9904	23.2	2
41296.38	333.1464	153.6192	4.2	2
40759.93	334.6704	536.448	17.6	2
40583.76	337.2612	176.1744	3.4	2
39925.39	338.6328	658.368	24	2
39754.4	340.3092	170.9928	5.1	2
39588.28	341.0712	166.116	10.9	2
39281.04	345.3384	307.2384	3.6	2
36826.79	348.6912	2454.25	36.6	2
36665.86	349.1484	160.9344	17.6	2
36000.17	350.2152	665.6833	31.2	2
35829.49	351.4344	170.688	7	2
35006.52	354.1776	822.9601	15	2
31397.69	359.0544	3608.832	37	2
30855.15	362.1024	542.544	8.899999	2
27183.83	367.1316	3671.316	36.5	2
26940.6	370.0272	243.2304	4.2	2
23482.34	374.7516	3458.261	36.6	2
23230.88	378.5616	251.46	3.3	2
22910.23	379.1712	320.6496	26.3	2
22870.91	379.6284	39.3192	4.3	2
21606.9	381.6096	1264.006	31.9	2
21255.77	385.2672	351.1296	4.8	2
21142.69	386.334	113.0808	5.3	2
19959.15	388.0104	1183.539	35.3	2
19860.4	388.62	98.75521	8.100001	2
18902.84	398.9832	957.5597	4.2	2.2
15532.6	403.2504	3370.235	35.9	2.2
15344.85	405.6888	187.7568	3.5	2.2
14942.51	413.3088	402.336	2.4	2.2
14339.01	422.4528	603.504	3	2.2
14010.43	425.5008	328.5744	4.9	2.2
13254.53	437.6928	755.904	3.1	2
12042.03	449.58	1212.494	5.1	2
11672.62	451.4088	369.4176	10.1	2
10426.59	459.9432	1246.023	7.3	2
9178.163	482.4984	1248.43	2.7	2.05
9131.3	483.4128	46.863	2.5	2.05
8973.215	486.7656	158.0845	2.3	2.05
8582.689	494.3856	390.525	2.5	2.05
8362.746	499.2624	219.9437	2.2	2.05
8126.557	504.7488	236.1895	2.1	2.05
8016.586	507.1872	109.9718	2.2	2.05
7986.594	507.7968	29.99232	2.4	2.05
7874.122	510.0828	112.4712	2.4	2.05
7381.685	516.5751	492.4375	3.7	2.05
7040.907	523.9512	340.7779	2.2	2.1
6848.883	530.0472	192.024	1.5	2.1
6459.715	541.6296	389.1687	1.6	2.1
6252.969	546.8112	206.7458	1.9	2.1
4656.61	582.168	1596.36	2.1	2.15
4290.484	590.0928	366.1257	2.1	2.2
4109.432	594.6648	181.0512	1.8	2.2
3927.04	599.5416	182.3923	1.7	2.2
3701.33	605.2413	225.7099	1.8	2.2
3335.606	614.4768	365.724	1.8	2.2
3075.002	620.268	260.604	2	2.25
2457.782	633.984	617.22	2	2.25
2032.586	640.08	425.196	3.1	2.25
1654.024	649.224	378.5616	1.8	2.3
1328.041	658.6728	325.9836	1.5	2.3
1112.121	667.2072	215.9203	1.1	2.3
849.6522	674.3395	262.4683	1.6	2.3
698.3731	679.704	151.2792	1.2	2.35
547.9543	681.5328	150.4188	3.5	2.35
341.6656	683.9712	206.2886	3.6	2.35
85.9536	690.372	255.712	1.7	2.35
0	693.42	85.9536	1.2	2.35

CUMULATIVE CHLORIDE versus AGE

AGE	ΣCl
0.000000E+000	162292
3.520000E-003	160721
6.000000E-003	159614
9.000000E-003	155630
9.800000E-003	151321
1.000000E-002	150572
2.300000E-002	149701
2.320000E-002	148722
2.550000E-002	148620
2.550000E-002	148005
2.760000E-002	147938
2.800000E-002	147737
2.840000E-002	144983
2.950000E-002	144934
3.070000E-002	144879
3.090000E-002	144870
3.170000E-002	144845
3.180000E-002	144807
3.290000E-002	144749
3.300000E-002	144730
3.530000E-002	144707
3.880000E-002	144672
5.840000E-002	144478
6.340000E-002	144428
6.550000E-002	144381
6.980000E-002	144284
7.780000E-002	144104
8.930000E-002	143700
1.034000E-001	143205
1.052000E-001	143141
1.223000E-001	142093
1.538000E-001	141785
1.605000E-001	141719
1.925000E-001	141406
2.230000E-001	141108
2.340000E-001	141010
2.450000E-001	140971
2.650000E-001	140856
2.740000E-001	140487
2.750000E-001	140451
2.780000E-001	140388
2.860000E-001	140315
3.160000E-001	137780
3.340000E-001	130128
3.390000E-001	127064
3.430000E-001	125225
3.440000E-001	124931
3.530000E-001	119869
3.850000E-001	119414
3.860000E-001	118731

AGE	ΣCl
3.863000E-001	118412
3.890000E-001	118304
3.910000E-001	117807
3.920000E-001	117505
3.922000E-001	115678
3.950000E-001	112714
3.970000E-001	112213
3.980000E-001	110868
4.247000E-001	109703
4.250000E-001	109355
4.259000E-001	109318
4.260000E-001	109298
4.890000E-001	107294
5.470000E-001	104658
5.487000E-001	104615
5.499000E-001	104312
5.505000E-001	103282
5.510000E-001	102420
5.514000E-001	102248
5.720000E-001	96544
5.840000E-001	96144
6.100000E-001	95967
6.670000E-001	95127
6.680000E-001	94365
7.300000E-001	93860
7.510000E-001	93720
7.520000E-001	93429
7.710000E-001	92723
7.780000E-001	91027
7.920000E-001	90566
7.990000E-001	89743
8.340000E-001	89337
8.350000E-001	88859
8.960000E-001	88331
9.000000E-001	88030
9.040000E-001	86008
9.320000E-001	85658
9.350000E-001	82720
9.530000E-001	82362
9.700000E-001	82239
1.06	80996
1.064	80944
1.16	79503
1.17	79366
1.2	79047
1.268	77585
1.27	76691
1.273	76020
1.32	75622
1.33	70391

AGE	ΣCl
1.335	70192
1.39	56307
1.408	56212
1.41	54710
1.424	54615
1.43	53198
1.45	52986
1.45	52209
1.48	51991
1.485	51020
1.503	50782
1.508	50546
1.552	50145
1.555	46383
1.557	46138
1.558	45120
1.57	44864
1.586	43629
1.59	38099
1.607	37289
1.61	31656
1.63	31297
1.635	25987
1.67	25621
1.672	25130
1.678	25072
1.681	23170
1.724	22665
1.737	22505
1.738	20695
1.74	20548
1.87	19363
1.877	14331
1.92	14143
2.01	13994

APPENDIX 8

DETERMINATION OF LAKE VOLUME

Data from the Upper Salt from beneath Searles Lake is used to calculate the lake volume at which halite saturation would occur for a given period of chloride influx.

Known:

- chloride content of Upper Salt = 448 x 10^{12} grams
  (Smith, 1979, Table 17)

- average of chloride accumulation = 0.12 x 10^5 kg/m_2
  (from chloride accumulation plot, this study, Fig. 18)

- solubility of NaCl = 360,000 g/m^3 (solution)

- average annual rate of chloride accumulation = 0.19 $kg/m^2/yr$
  (from chloride accumulation plot, this study, Fig. 18)

- molecular weight of NaCl = 58.44 grams

- molecular weight of chloride = 35.45 grams

Solve for influx rate (i) of NaCl in (kg/yr)

First determine the total amount of chloride in the Upper Salt:

$$\frac{\text{total chloride (kg)}}{\text{kg/m}^2} = \frac{0.448 \times 10^{12}\ \text{kg}}{0.12 \times 10^5\ \text{kg/m}^2}$$

$$= 3.7 \times 10^7\ \text{m}^2$$

Next, determine the toatl amount of NaCl:

$$(3.7 \times 10^7\ \text{m}^2)\frac{(58.44)}{35.45} = 6.2 \times 10^7/\text{m}^2$$

the influx rate (i) is

$$i = (6.2 \times 10^7\ \text{m}^2) \times (0.19\ \text{kg/m}^2/\text{yr})$$

$$= 1.2 \times 10^7\ \text{kg/yr of NaCl}$$

Solve for lake volume when NaCl would occur after a time interval (t) where:

$$\text{Volume} = \frac{\text{influx (kg/yr)} \times (\text{t (yr)})}{\text{Solubility (kg/m}^3\text{)}}$$

$$\text{Volume} = \frac{(1.2 \times 10^7 \text{ kg/yr})(\text{t(yr)})}{360 \text{ kg/m}^3}$$

Equation for slope:

$$V = \underset{\text{slope}}{(3.2 \times 10^4 \text{ m}^3/\text{yr})}\text{t(yr)} + 0$$

Example

given - chloride influx of 100,000 years

lake volume for NaCl saturation given above:

$$\text{Volume} = \frac{\text{it}}{\text{solubility}}$$

Using the equation with the slope relationship:

$$V = (3.2 \times 10^4 \text{ m}^3/\text{yr})\ (100{,}000 \text{ yr})$$

$$= 3.2 \times 10^9 \text{ m}^3$$

The relationship between lake volume, period of influx, and solubility is shown on a plot of volume versus time (Figure A below) with depth also included. Depth was determined from calculations by Smith (1979, his Figure 32, shown below) where the relationship between lake volume, area, depth and salinity were graphically presented.

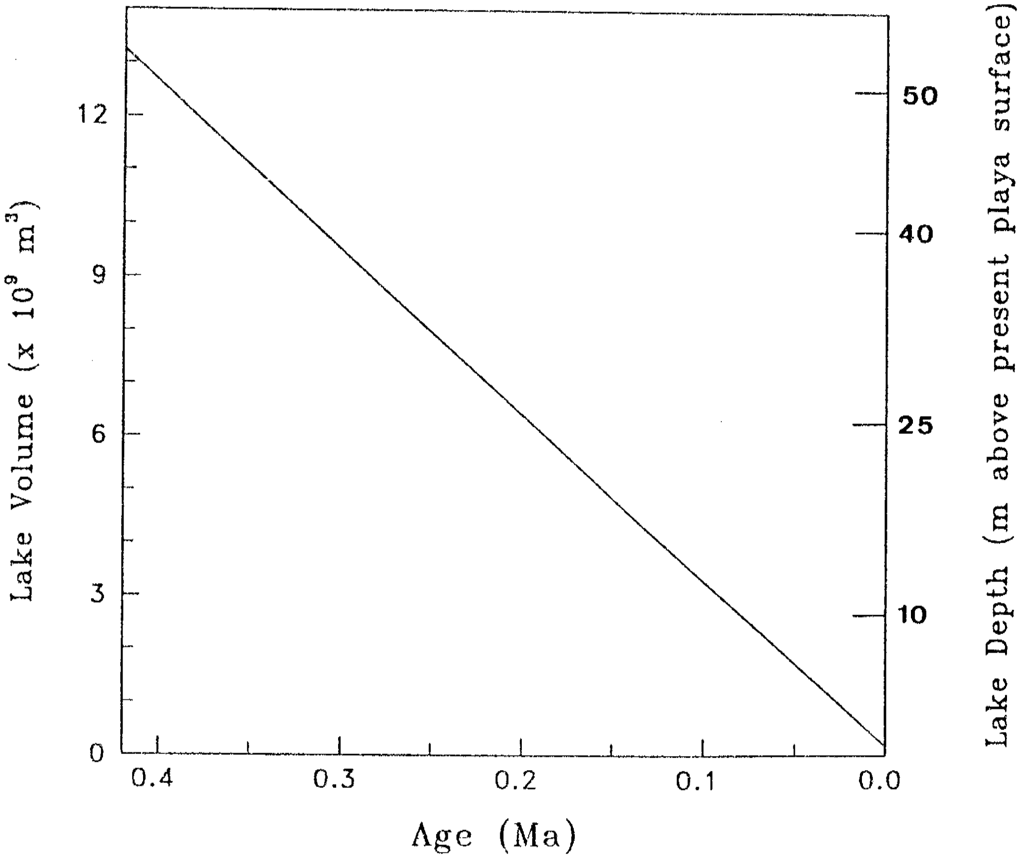

Figure A. PLot of lake volume and corresponding depth versus time.

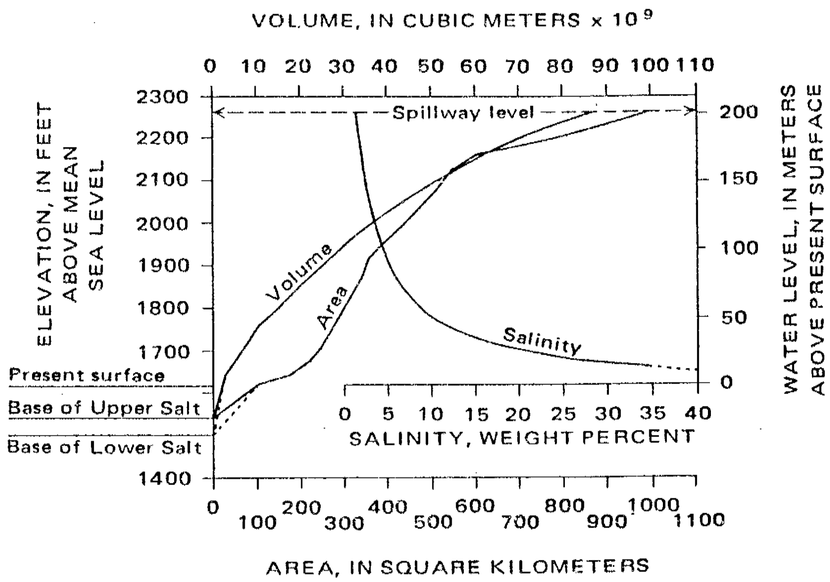

From Smith (1979)

REFERENCES CITED

Adam, D. P., and West, G. J., 1983, Temperature and precipitation estimates through the last glacial cycle from Clear Lake, California, pollen data: Science (Washington), v. 219, p. 168-170.

American Public Health Association, 1975, Standard methods for the the examination of water and wastewater, Thirteenth edition: American Public Health Association, Washington, D. C.

Atwater, B. F., Adam, D. P., Bradbury, J. P., Forester, R. M., Mark, R. K., Lettis, W. R., Fischer, G. R., Gobalet, K. W., and Robinson, S. W., 1986, A fan dam for Tulare Lake, California, and implications for the Wisconsin glacial history of the Sierra Nevada: Geological Society of America Bulletin, v. 97, p. 97-109.

Bagge, E., and Willkom, H., 1966, Geologic age determination with ^{36}Cl: Atomkernenergie, v. 11, p. 176-184. (German)

Bailey, G. E., 1902, The saline deposits of California: California State Mining Bureau Bulletin 24, 216 p.

Bateman, P. C., 1965, Geology and tungsten mineralization of the Bishop district, California: U.S. Geological Survey Professional Paper 470, 208 p.

Bateman, P. C., and Wahrhaftig, C., 1966, Geology of the Sierra Nevada: California Division of Mines and Geology Bulletin 190, p. 107-172.

Benson, L. V., 1981, Paleoclimatic significance of lake-level fluctuations in the Lahontan Basin: Quaternary Research, v. 16, p. 390-403.

Bentley, H. W., and Davis, S. N., 1982, Application of AMS to hydrology, in Kutchera, M., ed., Annual Symposium on Accelerator Mass Spectrometry: Argonne, Illinois, Argonne National Laboratories, 193 p.

Bentley, H. W., Phillips, F. M., and Davis, S. N., 1986, ^{36}Cl in the terrestrial environment, in Fritz, P., and Fontes, J. C., eds., Handbook of Environmental Isotope Geochemistry: Amsterdam, The Netherlands, Elsevier, v. 2B, p. 427-480.

Birkeland, P. W., and Janda, R. J., 1971, Clay mineralogy of soils developed from Quaternary deposits of the eastern Sierra Nevada, California: Geological Society of America Bulletin, v. 82, p. 2495-2514.

Birman, J. H., 1964, Glacial geology across the crest of the Sierra Nevada, California: Geological Society of America Special Paper 75, 80 p.

Bischoff, J. L., Rosenbauer, R. J., and Smith, G. I., 1985, Uranium-series dating of sediments from Searles Lake, California: Documentation of differences between land and sea climate records: Science, v. 227, p. 1222-1224.

Blackwelder, E., 1931, Pleistocene glaciation in the Sierra Nevada and Basin Ranges: Geological Society of America Bulletin, v. 42, p. 865-922.

-----1954, Pleistocene lakes and drainage in the Mojave region, southern California, in Jahns, R. H., ed., Geology of Southern California: California Division of Mines Bulletin, v. 170, p. 35-40.

Bonner, F. T., Roth, E., Schaffer, O. A., and Thompson, S. O., 1961, Chlorine-36 and deuterium study of Great Basin lake waters: Geochimica et Cosmochimica Acta, v. 25, p. 261-266.

Brakenridge, G. R., 1978, Evidence for a cold, dry full glacial climate in the American Southwest: Quaternary Research, v. 9, p. 22-40.

Broecker, W. S., and Walton, A. F., 1959, Re-evaluation of the salt chronology of several Great Basin lakes: Bulletin of the Geological Society of America, v. 70, p. 601-618.

Burke, R. M., and Birkeland, P. W., 1979, Reevaluation of multiparameter relative dating techniques and their application to the glacial sequence along the eastern escarpment of the Sierra Nevada, California: Quaternary Research, v. 11, p. 21-51.

Currey, D. R., Oviatt, C. G., and Czarnomski, J. E., 1984, Late Quaternary Geology of Lake Bonneville and Lake Waring: Geology of northwest Utah, southern Idaho, and northeast Nevada: Utah Geological Association Publication 13, p. 227-238.

Curry, R. R., 1966, Glaciation about 3,000,000 years ago in the Sierra Nevada: Science, v. 154, no. 3750, p. 770-771.

-----1968, Quaternary climatic and glacial history of the Sierra Nevada, California: Ann Arbor, Michigan, University Microfilms, Incorporated, no. 68-13896.

-----1969, Holocene climatic and glacial history of the central Sierra Nevada, California, in Schumm, S. A., and Bradley, W. C., eds., United States contributions to Quaternary research: Boulder, Colorado, Geological Society of America Special Paper 123, p. 1-47.

-----1971, Glacial and Pleistocene History of the Mammoth Lakes, Sierra Nevada, California (A Geologic Guidebook): Missoula, Montana, University of Montana, Department of Geology, Geological Series Publication no. 2, 49 p.

Dalrymple, G. B., 1964, Potassium-argon dates of three Pleistocene interglacial basalt flows from the Sierra Nevada, California: Geological Society of America Bulletin, v. 75, p. 753-758.

Dalrymple, G. B., Burke, R. M., and Birkeland, P. W., 1982, Concerning K-Ar dating of a basalt flow from the Tahoe-Tioga interglaciation, Saw Mill Canyon, southeastern Sierra Nevada, California: Quaternary Research, v. 17, p. 120-122.

Davis, R. Jr., and Schaffer, O. A., 1955, Chlorine-36 in nature: Annals of the New York Academy of Science, v. 62, art. 5, p. 105-122.

Dorn, R. I., Turrin, B. D., Jull, A. J. T., and Donahne, D. J., 1987, Radiocarbon and cation-ratio ages for rock varnish on Tioga and Tahoe morainal boulders of Pine Creek, eastern Sierra Nevada, California, and their paleoclimatic implications: Quaternary Research, v. 28, p. 38-49.

Droste, J. B., 1961, Clay minerals in sediments of Owens, China, Searles, Panamint, Bristol, Cadiz, and Danby lake basin, California: Geological Society of America Bulletin, v. 72, p. 1713-1722.

Elmore, D., Fultin, B. R., Clover, M. R., Marsden, J. R., Gove, H. E., Naylor, H., Purser, K. H., Kilius, L. R., Beukens, R. P., and Litherland, A. E., 1979, Analysis of ^{36}Cl in environmental water samples using an electrostatic accelerator: Nature, v. 277, p. 22-25.

Elmore, D., Tubbs, L. E., Neuman, X. Z. Ma, Finkel, R., Nishiizumi, K., Bear, J., Oeschgan, H., and Andree, M., 1982, ^{36}Cl bomb pulse measured in a shallow ice core from Dye 3, Greenland: Nature, v. 300, no. 5894, p. 735-737.

Elmore, D., Conrad, N., and Kubik, D. W., 1984, Computer controlled isotope ratio measurements and data analysis: Rochester, New York, The University of Rochester, Nuclear Structure Research Laboratory, v. 282, p. 1-14.

Eugster, H. P., and Hardie, L. A., 1978, Saline lakes, in Lerman, A., ed., Lakes: Chemistry, geology, and physics: New York, New York, Springer-Verlag, chap. 8, p. 237-293.

Feth, J. H., 1959, Re-evaluation of the salt chronology of several Great Basin lakes: A discussion: Bulletin of the Geological Society of America, v. 70, p. 637-640.

Flint, R. F., and Gale, W. A., 1958, Stratigraphy and radio-carbon dates at Searles Lake, California: American Journal of Science, v. 256, no. 10, p. 689-714.

Free, E. E., 1914, The topographic features of the Desert Basin of the U.S. with reference to the possible occurrence of potash: U.S. Department of Agriculture Bulletin 54, 68 p.

Friedman, I., Smith, G. I., and Matso, S., 1982, Economic implications of the deuterium anomaly in the brine and salts in Searles Lake, California: Economic Geology, v. 77, no. 3, p. 694-702.

Gale, H. S., 1914, Salines in the Owens, Searles, and Panamint Basins, southeastern California: U.S. Geological Survey Bulletin 580-L, p. 251-323.

Galloway, R. W., 1983, Full-glacial southwestern United States: Mild and wet or cold and dry?: Quaternary Research, v. 19, p. 236-248.

Gascoyne, M., Currant, A. R., and Lord, T., 1981, Ipswichian fauna of Victoria Cave and the marine paleoclimatic record: Nature, v. 294, p. 652-654.

Gillespie, A. R., Huneke, J. C., and Wasserburg, G. J., 1984, Eruption age of ~100,000-year-old basalt from ^{40}Ar-^{39}Ar analysis of partially degassed xenoliths: Journal of Geophysical Research, v. 89, p. 1033-1048.

Haines, D. V., 1957, Core logs from Searles Lake, San Bernardino County, California: U.S. Geological Survey Open-File Report.

-----1959, Core logs from Searles Lake, San Bernardino County, California: U.S. Geological Survey Bulletin 1045-E, p. 139-317.

Hamman, W. D., 1912, Potash solutions in the Searles Lake region: Mining Science, v. 65, p. 372-373.

Hanks, H. G., 1889, On the occurrence of hanksite in California: American Journal of Science, ser. 3, v. 37, p. 63-66.

Hardie, L. A., and Eugster, H. P., 1970, The evolution of closed-basin brines, in Morgan, B. A., ed., Fiftieth Anniversary Symposia on Mineralogy and Petrology of the Upper Mantle; Sulfides; Mineralogy and Geochemistry of Non-Marine Evaporites: Mineralogical Society of America Special Paper 3, p. 273-290.

Hay, R. L., and Guldman, S. G., 1987, Diagenetic alteration of silicic ash in Searles Lake, California: Clays and Clay Minerals, v. 35, no. 6, p. 449-457.

Hays, J. D., Imbrie, J., and Shackleton, N. J., 1976, Variations in the Earth's orbit: Pacemaker of the ice ages: Science, v. 194, p. 1121-1132.

Horita, J., and Matsuo, Sadao, The isotope paleoclimatology of brine inclusions in halite: a case study of Searles Lake, California, unpublished manuscript.

Hunt, C. B., and Mabey, D. R., 1966, Stratigraphy and structure of Death Valley, California: U.S. Geological Survey Professional Paper 494-A, 162 p.

Ives, P. C., Levin, B., Robinson, R. D. and Rubin, M., 1964, U.S. Geological Survey radiocarbon dates VII: Radiocarbon, v. 6, p. 37-76.

Jennings, C. W., compiler, 1958, Map of California, Olaf P. Jenkins edition, Death Valley Sheet: California Division of Mines and Geology, scale, 1:250,000.

Jennings, C. W., Burnett, J. L., and Troxel, B. W., compilers, 1962, Geologic map of California, Olaf P. Jenkins edition, Trona sheet: California Division of Mines and Geology, scale, 1:250,000.

Jones, B. F., 1965, The hydrology and mineralogy of Deep Spring Lake, Inyo County, California: U.S. Geological Survey Professional Paper 502-A, 56 p.

Jensen, J. H. F., Kuijpers, A., and Troelstra, S. R., 1986, A mid-Brunhes climatic event: Long-term changes in global atmosphere and ocean circulation: Science, v. 232, p. 615-622.

King, J. E., and Saunders, J. J., 1986, Geochelone in Illinois, and the Illinoian-Sangamonian vegetation of the type region: Quaternary Research, v. 25, p. 89-99.

Knopf, A., 1918, A geologic reconnaissance of the Inyo Range and the eastern slope of the southeastern Sierra Nevada, California, with a section on the stratigraphy of the Inyo Range by Edwin Kirk: U.S. Geological Survey Professional Paper 110, 130 p.

Lajoie, K. R., 1968, Quaternary stratigraphy and geologic history of Mono Basin, eastern California [Ph.D. thesis]: Berkeley, California, California University, 271 p.

Lal, D., and Peters, B., 1967, Cosmic ray produced radioactivity on the earth in Flugge, S., gen. ed., Sitte, K., ed., Handbook der Physik, v. 46/2: Berlin, Springer-Verlag, p. 551-612.

Lawrence, D. B., and Lawrence, E. G., 1961, Response of enclosed lakes to current glaciopluvial climatic conditions in middle latitude western North America: Annals of the New York Academy of Science, v. 95, article 1, p. 341-350.

Leavy, B. D., Phillips, F. M., Elmore, D., Kubik, P. W., and Gladney, E., 1987, Measurement of cosmogenic $^{36}Cl/Cl$ in young volcanic rocks: An application of acceleration mass spectrometry in geochronology: North-Holland, Amsterdam, Nuclear Instruments and Methods in Physics Research B29, p. 246-250.

Lee, C. H., 1912, Water resources of a part of Owens Valley, California: U.S. Geological Survey Water-Supply Paper 294, 135 p.

Li, C. C., 1964, Introduction to experimental statistics: New York, New York, McGraw-Hill Book Company, Chap. 9, p. 75-78.

Liddicoat, J. C., Opdyke, N. D., and Smith, G. I., 1980, Palaeomagnetic polarity in a 930-m core from Searles Valley, California: Nature, v. 286, no. 5768, p. 22-25.

Matthes, F. E., 1924, Evidence of two glacial stages in the Sierra Nevada (abstract): Geological Society of America Bulletin, v. 35, p. 69-70.

-----1929, Multiple glaciation in the Sierra Nevada: Science, v. 70, p. 75-76.

Matthews, R. A., Burnett, J. L., compilers, 1965, Geological Map of California, Fresno Sheet, Olaf P. Jenkins edition: California Division of Mines and Geology, scale, 1:250,000.

Mifflin, M. D., and Wheat, M. M., 1979, Pluvial lakes and estimated pluvial climates of Nevada: Nevada Bureau of Mines and Geology Bulletin 94, 57 p.

Peng, T. H., Goddard, J. G., and Broecker, W. S., 1978, A direct comparison of C-14 and Th-230 ages at Searles Lake, California: Quaternary Research, v. 9, p. 319-329.

Phillips, F. M., Smith, G. I., Bentley, H. W., Elmore, D., and Gove, H. E., 1983, ^{36}Cl dating of saline sediments: Preliminary results from Searles Lake, California: Science, v. 222, p. 925-927.

Phillips, F. M., Leavy, B. D., Jannik, N. O., Elmore, D., and Kubik, P. W., 1986a, The accumulation of cosmogenic chlorine-36 in rocks: A method for surface exposure dating: Science, v. 231, p. 41-43.

Phillips, F. M., Peeters, L. A., Tansey, M. K., and Davis, S. T., 1986b, Paleoclimatic inferences from an isotopic investigation of groundwater in the central San Juan Basin, New Mexico: Quaternary Research, v. 26, p. 179-193.

Putnam, W. C., 1950, Moraine and shoreline relationships at Mono Lake, California: Geological Society of America Bulletin, v. 61, p. 115-122.

Roederer, J. C., 1986, ICSU gives green light to IGBP: Eos, v. 67, p. 777-781.

Rubin, M., and Berthold, S. M., 1961, U.S. Geological Survey radiocarbon dates VI: Radiocarbon, v. 3, p. 86-98.

Ruddiman, W. F., and Wright, H. E. Jr., 1987, North America and adjacent oceans during the last deglaciation, in The Geology of America, v. K-3, Introduction, (chapter 1): The Geological Society of America, p. 1-12.

Russell, I. C., 1889, Quaternary history of Mono Valley, California: Eighth Annual Report, U.S. Geological Survey, part I, p. 261-394.

Sharp, R. P., 1969, Semiquantitative differentiation of glacial moraines near Convict Lake, Sierra Nevada, California: Journal of Geology, v. 77, p. 68-91.

Sharp, R. P., and Birman, J. H., 1963, Additions to the classical sequence of Pleistocene glaciations, Sierra Nevada, California: Geological Society of America Bulletin, v. 74, p. 1079-1086.

Smith, G. I., 1962, Subsurface stratigraphy of late Quaternary deposits, Searles Lake, California - A summary, article 82 of Short papers in geology and hydrology: U.S. Geological Survey Professional Paper 450-C, p. C65-C69.

-----1964, Geology and volcanic petrology of the Lava Mountains, San Bernardino County, California: U.S Geological Survey Professional Paper 457, 97 p.

-----1968, Late Quaternary geologic and climatic history of Searles Lake, southeast California, in Morrison, R. B., and Wright, H. E. Jr., eds., Means of correlation of Quaternary successions: Salt Lake City, Utah, University of Utah Press, v. 8, p. 293-310.

-----1976, Origin of lithium and other components in the Searles Lake evaporites, California, in Vine, J. D., ed., Lithium resources and requirements by the year 2000: U.S. Geological Survey Professional Paper 1005, p. 92-103.

-----1979, Subsurface stratigraphy and geochemistry of late Quaternary evaporites, Searles Lake, California, with a section on Radiocarbon ages of stratigraphic units, by M. Stuiver and G. I. Smith: U.S. Geological Survey Professional Paper 1043, 130 p.

-----1984, Paleohydrologic regimes in the southwestern Great Basin, 0-3.2 my ago, compared with other long records of "global" climates: Quaternary Research, v. 22, p. 1-17.

Smith, G. I., and Haines, D. V., 1964, Character and distribution of nonclastic minerals in the Searles Lake evaporite deposit, California: U.S. Geological Survey Bulletin 1181-P, p. P1-P58.

Smith, G. I., and Pratt, W. P., 1957, Core logs from Owens, China, Searles, and Panamint Basins, California: U.S. Geologic Survey Bulletin 1045-A, 62 p.

Smith, G. I. and Street-Perrott, F. A., 1983, Pluvial lakes of the western United States, in Wright, H. E. Jr., gen ed., Porter, S. C., ed., Late-Quaternary Environments of the United States: Minneapolis, Minnesota, University of Minnesota Press, v. 1, chap. 10, p. 190-212.

Smith, G. I., Troxel, B. W., Gray, C. H., Jr., and von Huene, R., 1968, Geologic reconnaissance of the Slate Range, San Bernardino and Inyo Counties, California: California Division of Mines and Geology Special Report 96, 33 p.

Smith, G. I., Barczak, V. J., Molton, G. F., and Liddicoat, J. C., 1983, Core KM-3, a surface-to-bedrock record of late Cenozoic sedimentation in Searles Valley, California: U.S. Geological Survey Professional Paper 1256, 23 p.

Smith, R. S. U., 1976, Late-Quaternary pluvial and tectonic history of Panamint Valley, Inyo and San Bernardino counties, California [Ph.D. thesis]: Pasadena, California, California Institute of Technology, 300 p.

Snyder, C. T., and Langbein, W. B., 1962, The Pleistocene Lake in Spring Valley, Nevada, and its climatic implications: Journal of Geophysical Research, v. 67, p. 2385-2394.

Sorey, M. L., Lewis, R. E., and Olmsted, P. H., 1978, The hydrothermal system of Long Valley caldera, California: U. S. Geological Survey Professional Paper 1044-A, 60 p.

Spaulding, W. G., Leopold, E. B., and Van Devender, T. R., 1983, Late Wisconsin paleoecology of the American Southwest, in Wright, H. E. Jr., gen ed., Porter, S. C., ed., Late Quaternary environments of the United States: Minneapolis, Minnesota, University of Minnesota Press, v. 1, p. 259-293.

Strand, R. G., compiler, 1967, Geologic Map of California, Mariposa Sheet, Olaf P. Jenkins edition: California Division of Mines and Geology, scale, 1:250,000.

Street, F. A., 1980, The relative importance of climate and hydrogeological factors in influencing lake-level fluctuations: Palaeoecol. Afr., v. 12, p. 137-158.

Street-Perrott, F. A., and Harrison, S. P., 1985, Lake levels and climate reconstruction, in Hecht, A. D., ed., Paleoclimate analysis and modeling: New York, New York, John Wiley, Chap. 7, p. 291-340.

Stuiver, M., 1964, Carbon isotopic distribution and correlated chronology of Searles Lake sediments: American Journal of Science, v. 262, no. 3, p. 377-392.

Stuiver, M., and Smith, G. I., 1979, Radiocarbon ages of stratigraphic units, in Smith, G. I., Subsurface stratigraphy and geochemistry of late Quaternary evaporites, Searles Lake, California: U.S. Geological Survey Professional Paper 1043, p. 68-73.

Szestay, K., 1974, Water balance and water level fluctuations of lakes: Hydrol. Sci. Bull., v. 19, p. 73-84.

Van Devender, T. R., and Spaulding, W. G., 1979, Development of vegetation and climate in the southwestern United States: Science, v. 204, p. 701-710.

Wahrhaftig, C., and Birman, J. H., 1965, The Quaternary of the Pacific Mountain system in California, in Wright, H. E., and Frey, D. G., eds., The Quaternary of the United States: Princeton, New Jersey, Princeton University Press, p. 299-340.

Watts, R. G., and Hayden, Md. E., 1984, A possible explanation of differences between pre and post-Jaramillo ice sheet growth, in Berger, A., Imbrie, J., Hans, J., Kukla, G., and Saltzmen, B., eds., Milankovitch and climate: Dordrecht, Holland, Reidel, part 2, p. 599-604.

Whitney, J. D., 1865, Geology: Geological Survey of California, v. 1, p. 450-455.

Williams, S. F., Thunell, R. C., Tappa, E., Rio, D., and Raffi, I., 1988, Chronology of the Pleistocene oxygen isotope record: 0-1.88 m.y. B.P.: Palaeogeography, Palaeooclimatology, Palaeoecology: Amsterdam, The Netherlands, Elsevier Science Publishers B.V., v. 64, p. 221-240.

Winograd, I. J., Szabo, B. J., Coplen, T. B., Riggs, A. C., and Kolesar, P. T., 1985, Two-million-year record of deuterium depletion in Great Basin ground waters: Science, v. 227, p. 519-522.

Yokoyama, Y., Reyss, J. L., and Guichard, F., 1977, Production of radionuclides by cosmic rays at mountain altitudes: Earth Planetary Science Letters, v. 36, p. 44-50.